The Performance of a Carbon-Dioxide Plume Geothermal Energy Storage System

A DISSERTATION
SUBMITTED TO THE FACULTY OF
UNIVERSITY OF MINNESOTA
BY

Mark R. Fleming

IN PARTIAL FULFILLMENT OF THE REQUIREMENTS
FOR THE DEGREE OF
DOCTOR OF PHILOSOPHY

Thomas H. Kuehn, Advisor

February 2019

Acknowledgements

During my first semester as a graduate student at the University of Minnesota, I was recruited by my advisor, **Professor Thomas Kuehn**, to work on the CO_2-Plume Geothermal (CPG) project, a novel technology which combines Carbon Capture and Storage (CCS) and geothermal energy. As a new member of the research group, I was faced with the task of getting up to speed on the diverse research conducted by our group, which was led by **Professor Martin Saar** (the Principle Investigator) and included researchers from the departments of mechanical engineering, earth sciences, applied economics, and public policy at the University of Minnesota; eventually expanding to included researches from The Ohio State and ETH Zurich. Over time, I was able to become a contributing member of the group, thanks to Professors Kuehn and Saar; who provided me with guidance, honest feedback, immense patience, support, and funding; I was fortunate to receive funding from a **National Science Foundation** (NSF) grant, for which I am grateful. It is only with their support that I have been able to achieve my degree.

I am further indebted to the additional members of my research group who have enabled me to competently complete my work. To **Jeffrey Bielicki** and **Jonathan Ogland-Hand** who have provided feedback on numerous drafts and educated me on many of the non-engineering concepts related to CPG; and **Nagasree Garapati** and **Jimmy Randolph** who taught me how to use the simulation software required for my research. Lastly, but most importantly, to **Benjamin Adams,** who began as a fellow doctoral student and is now a post-doctoral research advisor to me, for providing feedback on every chapter of this dissertation (multiple times) and for the guidance and motivation that has enabled me to compete this large undertaking.

Outside my research position, I split my Teaching Assistant positions between ME 4031w Basic Measurement Lab, taught by **Peter Bruggeman** and ME 4131w Thermal Environmental Engineering Lab taught by **Uwe Kortshagen** and **Thomas Kuehn**. Each of the courses taught students how to conduct experimental measurements, perform an uncertainty analysis and how to write reports in three of the most important and dreaded undergraduate engineering topics. Additionally, both Professor Kortshagen and Bruggeman allowed me the opportunity to work directly with revising course material to ensure that students achieved the learning objectives without increasing the workload. I am especially grateful to professor Kortshagen, who provided me the opportunity to develop the course syllabus and schedule, run the course Moodle webpage, improve the lab manuals, and deliver course lectures. While challenging, these experiences have proven to be some of the most rewarding in my academic career.

As a TA preparing for the labs in these courses, I was constantly reminded of the saying "prepare for the best, plan for the worst". This was particularly true during the renovation of the Mechanical Engineering building; where the equipment for these labs was moved

and assembled in new locations each term. This resulted in many unique challenges that needed to be addressed; including reconstructing the lab equipment, ensuring that the room had been approved for occupancy, and determining auxiliary measurements to replace measurements which were unobtainable due equipment being damaged or lost during the renovation. While these provided a unique challenge to the TA's, allowing for unique lab experiences and the occasional demonstration how lab experiments do not always work the way you expect.

I would like to thank **Zongxuan Sun** for allowing me to join the Mechanical Engineering Department's Graduate Safety Team. The Graduate Safety Team was responsible for the development of three new training sessions: the Chemical, Machine, and Computation/Office Safety sessions for the Annual Departmental Safety Training which mandatory for all graduate students, faculty, and staff to attend at the beginning of each academic year. As a member of the graduate safety team, I aided the development of these new training sessions, specifically developing and presenting the material for the Mental Health and the Computation/Office sessions. I have been encouraged by the advances that the Mechanical Engineering Department has taken in the recent years.

Lastly, I would like to thank my wife, **Bridget Fleming**, and my parents, **Richard and Susan Fleming**, for their unwavering support throughout this entire process and for proof reading this dissertation. Without their support, understanding, patience, and sacrifices this would not have been possible. Thank you for all that you have done.

Dedication

I dedicate this thesis to my loving **wife**, my supportive **parents**, and to the rest of my family who have supported me throughout this endeavor.

Abstract

CO_2-Plume Geothermal (CPG) is a system that can produce electricity from low-temperature heat from the subsurface of the earth, effectively combining geothermal energy and carbon capture and geologic storage; two technologies that have the potential to significantly reduce the amount of CO_2 emitted into the atmosphere and limit the impacts of climate change. This system is different from other geothermal concepts as 1) the system uses CO_2 as the heat extraction fluid in the subsurface reservoir, 2) the system does not rely shallow-natural hydrothermal locations or engineered (i.e. enhanced or fractured) reservoirs, instead using naturally permeably sedimentary basins, and 3) CPG systems utilize low-temperature resources which are currently undeveloped for geothermal energy. Therefore, CPG has significant potential to expand the geographic region where geothermal energy can operate, while providing an end used for captured CO_2.

This research demonstrates how the unique properties of the CPG system allow the system to be modified to operate as an energy storage system, which can increase the penetration of variable wind and solar resources on the grid, by using an additional shallow reservoir to separate the components that generate and consume power. To operate, the system generates power by extracting CO_2 from the deeper-hotter reservoir and generates power in the turbine before the CO_2 is slightly cooled and injected into the shallow reservoir, making use of the thermosiphon effect, where the thermal expansion of CO_2 results in a density difference in each vertical well that can circulate CO_2 without the need for pumps. To store power, the CO_2 can be produced from the shallow reservoir, cooled and compressed, and then reinjected into the deep reservoir where it is heated.
This research began by establishing the feasibility of the CPGES cycle for a single reservoir configuration and a mass flow rate near the optimum energy generation condition, demonstrating the effects of the intermittent injection and production of CO_2 on the transient reservoir pressures and the power generated and consumed by the system over the first 10 years of operation (Chapter 2). The results demonstrated that the system was at a quasi-steady state condition at 10 years, and that the system could generate more energy to the grid than it consumed, providing both net energy generation of and energy storage. Using historical electrical price data, it was found that the CPGES system could use price arbitrage to be competitive with a CPG system, for the same geothermal heat extraction rate. Work was then expanded to illustrate how the CPGES system can operate over a range of time scales, with the cycle duration ranging from diurnal to seasonal (Chapter 3), and over a range of duty cycles (Chapter 5), demonstrating the versatility of this system. The CPGES system was compared to the CPG system for a range of geologic conditions, and it was determined that the trade-off of the flexible energy storage system was a reduction in the net energy generated per cycle (Chapter 4 & 5). However, these energy losses could be alleviated by operating the CPG and CPGES systems concurrently in the CPG+CPGES system. The addition of the second reservoir required for the energy storage operation increases the capital cost of the system, however, the increased cost of this flexible system

could be alleviated by the value that the system adds to the grid as the amount of variable renewable energy increases (Chapter 5). Lastly, the effect of the co-production of water in solution with the CO_2 is considered and found to increase the generation capacity of the CPG system, a result of the higher production temperature despite the reduced CO_2 mass flow rate (Chapter 6).

Overall, this research has demonstrated how the CPG system can be modified to operate as an energy storage system. The impact of this work is to establish the flexibility of the CPG technology and demonstrate that captured carbon can be used to increase the penetration of renewable energy technologies onto the grid, thereby further mitigating the emission of CO_2 into the atmosphere. This will enable CPG to be integrated into future renewable energy portfolios.

Table of Contents

List of Tables

List of Figures

List of Acronyms

Term	Definition
CBECCS	**Bio-energy carbon capture and storage** The combination of Bio-energy and carbon capture and storage technology.
CAES	**Compressed Air Energy Storage** A form of energy storage which uses a large storage vessel to store air at high pressure for later release using a gas turbine.
CCES	**Compressed CO_2 Energy Storage** A separate CO_2 geothermal energy storage system that uses multiple-reservoirs to provide energy storage. This system is different from our proposed CPGES system as it uses surface heating to generate power.
CCS	**Carbon Capture and Storage** A process for that prevents CO_2 from being emitted into the atmosphere by separating CO_2 from other emissions at the source and then permanently storing the CO_2 in the subsurface.
CCUS	**Carbon Capture Utilization and Storage** A carbon capture and storage system which uses the stored CO_2 for another process, such as geothermal energy or oil/gas recovery.
CO_2-BES	**CO_2 Bulk Energy Storage** A multi-fluid geothermal energy storage system which uses CO_2 to displace and pressurize brine for geothermal heat extraction.
CO_2-EGS	**CO_2-Enhanced Geothermal System** An enhanced geothermal system which uses CO_2 as the subsurface heat extraction fluid.
CPG	**CO_2-Plume Geothermal** A geothermal power system that uses CO_2 as the subsurface heat extraction fluid in sedimentary basins.
CPGES	**CO_2-Plume Geothermal Energy Storage** An extinction of the CO_2-Plume geothermal technology that allows the geothermal system to provide energy storage. The performance of this energy storage system is the primary focus of this dissertation.
EES	**Engineering Equation Solver** A program that numerically solves equations and includes thermodynamic properties of many known fluids.
EGS	**Enhanced (Engineered) Geothermal System**

	A type of geothermal energy that artificially creates a geothermal reservoir by fracturing a high temperature, low permeability formation, which was previously inaccessible to traditional geothermal systems.
EOR	**Enhanced Oil Recovery** A method to extract oil from a reservoir by injecting a gas to increase the pressure and displace the oil. The displaced oil is then recovered and produced from the reservoir.
IEA	**International Energy Agency** An agency that evaluates and advises on worldwide energy generation.
IPCC	**Intergovernmental Panel on Climate Change** An organization focused on assessing and modeling the global climate.
LMP	**Locational Marginal Price** A metric that assesses the wholesale cost of electricity for a given location.
MISO	**Midwest Independent Service Operator** An independent service operator that provides transmission and monitoring of the electrical grid and energy market in the Midwest of the United States.
PHES	**Pumped Hydro Energy Storage** A form of energy storage which operates by moving water between reservoirs at different elevations.
TOUGH2	**Transport Of Unsaturated Groundwater and Heat** Series of codes from Lawrence Berkeley National Laboratory for the simulation of the subsurface flow of heat and fluids
VRE	**Variable Renewable Energy** Renewable energy technologies that are not dispatchable, and the availability of the energy source is outside the control of the grid operator. Examples include wind and solar.

Chapter 1: Forward and Literature Review

Limiting human-induced climate change is currently one of the greatest social, political, and scientific challenges of our modern society. Human activity has resulted in a substantial increase in the atmospheric concentration of carbon dioxide (CO_2) in the atmosphere, driving global climate change. Carbon dioxide is emitted into the atmosphere as a byproduct of combustion, which is used to produce heat or power in the transportation, manufacturing, and electricity generation industries since the industrial revolution. In the atmosphere, carbon dioxide is a greenhouse gas, which absorbs infrared heat emitted from the earth, preventing the heat from being emitted into space, warming the atmosphere. The cumulative effect of this prolonged emission of carbon dioxide into the atmosphere is an increase in the atmospheric concentration of carbon dioxide, which increases the greenhouse effect, trapping more heat, raising the global atmospheric temperature. This global warming has significant environmental effects, with decreased air quality, rising sea levels, melting ice caps, and changing weather patterns. Left unabated, these effects will intensify and permanently change the planet. To limit the impact of the global climate change, the emission of carbon dioxide (and other greenhouse gases) must be reduced, and eventually eliminated, requiring significant change.

In the electricity generation sector, renewable energy sources, such as geothermal power, can be used to generate electricity without emitting carbon dioxide into the atmosphere. Geothermal energy utilizes the heat found in hot rocks in the subsurface to generate power. To extract energy from the subsurface, a cold fluid is generally injected and circulated

through a reservoir, where it is heated by rock. The heated fluid is then extracted and brought to the surface to generate heat or electricity.

In this dissertation, research on the performance of an innovative geothermal system, termed Carbon Dioxide Plume Geothermal (CPG), and its capabilities to operate as an energy storage system are presented. This new technology is different from existing geothermal systems, as the system synergistically operates a geothermal power system and Carbon Capture and Storage (CCS), in what is known as a Carbon Capture Utilization and Storage (CCUS) system; using CO_2 as the primary working fluid to extract heat from the subsurface. To facilitate the storage of CO_2 in the subsurface CPG uses naturally permeable sedimentary basins; expanding the geo-spatial region where geothermal power system can operate, as sedimentary basins underlay large portions of the United States, where traditional hydrothermal geothermal resources are not readily available. Traditional geothermal systems are usually limited to specific geologic regions, where high temperature fluid, generally in excess of 150°C (~300°F), is readily available at shallow depths, in existing or artificially fractured rock structures. In the United States, these regions are generally located along the western coastal region, which is generally referred to as the ring of fire. CPG systems are not limited to these regions, as the system can operate using “low-temperature” geothermal resources, or reservoirs with temperatures less than 150°C. This allows CPG to expand the region where geothermal systems can be built to the Midwest and the South, where natural permeable sedimentary basins are located.

The development of the CPG system provides dispatchable power that can increase the penetration of renewable wind and solar energy systems. Currently, wind and solar systems are the preferred renewable resources, due to the maturity of the technology and the low capital costs. However, these resources can generate only variable or non-dispatchable power, as these systems require wind or direct sunlight to operate. The large-scale implementation of these resources can be challenging; periods of power generation may not correlate with demand, resulting in periods of excess generation of power where the energy is wasted or a generation deficit, which requires additional power facilities to be brought online to compensate. Currently, in the United States, the penetration of wind and solar are low, and the abundance of non-renewable baseload sources, such as coal, natural gas, and nuclear power, can compensate and be dispatched when the variable power systems are offline. However, as the penetration of these renewable sources increases, displacing existing baseload fossil fuel systems, managing this variability using clean energy is challenging. This can be achieved through the use of dispatchable renewable systems or a renewable based energy storage system. Currently, only geothermal energy, hydroelectric and pumped hydroelectric energy storage (PHES), and bio-energy coupled with carbon capture and storage (BECCS) are capable of providing clean dispatchable power, which is required to support the variable generation. However, the recent development of theses energy sources has been limited; as environmental effects limit the development of new hydroelectric systems, CCS is not currently widely used with bio-energy sources, and geothermal energy is typically limited to regions with high sub-surface

temperatures. The usage of BECCS is likely to expand, as the CCS technology matures; however, the expanded usage of traditional geothermal energy is challenging.

While dispatchable power systems can supplement variable renewables, they only address periods of generation deficit and not the periods of over-generation of power that can occur; however, energy storage systems can provide both. Energy storage systems are ideal to support variable renewables, as it can store the excess energy that is generated and then dispatch this energy back to the grid when it is needed. Currently, there are two large scale energy storage systems that can provide bulk energy storage that is required for renewable integration, namely, pumped hydroelectric energy storage (PHES), and compressed air energy storage systems (CAES). Other types of energy storage exist, such as battery and flywheel systems, however, currently these systems cannot provide the large-scale energy storage required. While PHES and CAES can provide large scale energy storage, the increased development of these systems has challenges. PHES, like hydroelectric systems, are limited by environmental regulations, and CAES relies on the combustion of fuel, thereby emitting CO_2 into the atmosphere, to generate power, reducing the clean energy benefit of the renewable energy sources that it is supporting.

The CPG system can be modified to operate as an energy storage system, supplementing variable renewables with a renewable energy storage system. Previous research has only demonstrated the effectiveness of the CPG at generating power [1,2], and the operation of the system as an ancillary service providing energy storage has not been considered, and thus is the primary focus of this dissertation.

1.1 Overview of Thesis

This thesis is comprised of six individual chapters, including published and soon-to-be published papers, with each chapter providing specific research into a fundamental question on the operation of the CPG system as an energy storage system, termed CO_2-Plume Geothermal Energy Storage (CPGES).

Chapter 1: Background, motivation, and literature review

Chapter 2: CPGES: Single base case with transient reservoir performance

Fleming, M. R., Adams, B. M., Kuehn, T. H., Bielicki, J. M., & Saar, M. O. Earth Battery: A High-Efficiency, Large-Scale Subsurface Energy Storage System, Using Carbon Dioxide Plume Geothermal Energy. Unpublished Working Paper.

Chapter 3: Diurnal vs Seasonal Energy Storage

Fleming, M. R., Adams, B. M., Randolph, J. B., Ogland-Hand, J. D., Kuehn, T. H., Buscheck, T. A., Bielicki, J. M., Saar, M. O. (2018). High Efficiency and Large-scale Subsurface Energy Storage with CO_2. In 43rd Workshop on Geothermal Reservoir Engineering. Palo Alto, California. Retrieved from https://pangea.stanford.edu/ERE/pdf/IGAstandard/SGW/2018/Fleming.pdf

Chapter 4: CPGES Parameter Study

Fleming, M. R., Adams, B. M., Kuehn, T. H., Bielicki, J. M., & Saar, M. O. Parametric study of a Large-Scale Energy Storage System using Carbon Dioxide Plume Geothermal Energy. Unpublished Working Paper.

Chapter 5: CPGES Operational Configurations

Fleming, M. R., Adams, B. M., Kuehn, T. H., Bielicki, J. M., & Saar, M. O. The Performance of a CO_2-Plume Geothermal Energy Storage System using a Low-Temperature High-Permeability Sedimentary Reservoir. In Preparation.

Chapter 6: Vertical Well Solubility

Fleming, M. R., Adams, B. M., Kuehn, T. H., Bielicki, J. M., & Saar, M. O. The Increase in Power Generation due to Water Precipitation in CO_2 Plume Geothermal (CPG) Power Plants. In Preparation.

The remainder of this section is devoted to providing the background necessary to demonstrate why CO_2 Plume Geothermal research is essential. For this reason, I overview the development of renewable energy systems, Carbon Capture and Storage, and current geothermal technologies, with a focus on previous research on CO_2-Geothermal systems.

1.2 The BIG PICTURE

Since the industrial revolution in the 19th century, human activity has resulted in an increase in the global mean temperature, and in 2017 the temperature increase above pre-industrial levels was approximately 1°C [3]. The increase in the global mean temperature correlates with the rise in concentration of CO_2 in the atmosphere [3–5], shown in Figure 1-1. For example, from 1980 to December 2017 the global mean concentration of CO_2 rose from 338.8 ppm to 406.77 ppm [6], corresponding to a global mean temperature rise of 0.79 °C [7,8]. Without corrective action, atmospheric concentrations of CO_2 will continue to rise, and the global mean temperature rise will exceed 2°C before 2050. To limit the global mean temperature rise to less than 2°C from pre-industrial levels, the International Panel on Climate Change (IPCC) has estimated an atmospheric concentration of CO_2 to 450 ppm has a 50% chance achieving this target [5], allowing for an estimated 1000 Gt of CO_2 to be emitted after 2011 [4]. These estimates have been recently refined, allowing for an estimated 570 Gt and 1320 Gt of CO_2 to be emitted post-2017 to achieve the 1.5°C and 2.0°C warming cases respectively [3,9]. This indicates that to limit global climate change CO_2 emissions must be reduced and eventually eliminated, resulting in a carbon neutral state. To achieve this state, significant changes across all economic sectors are required.

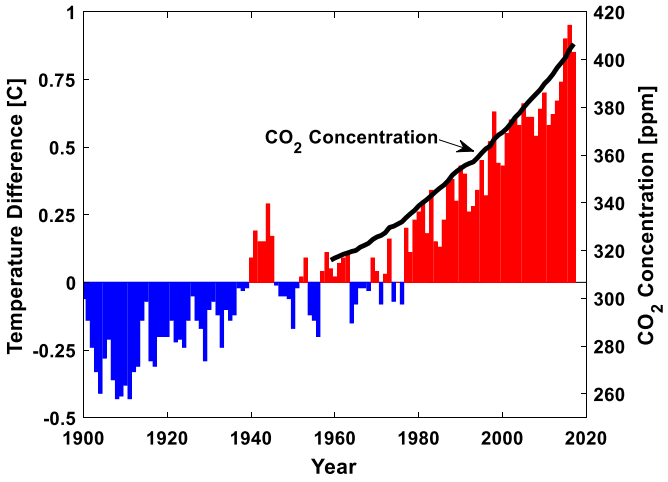

Figure 1-1: The temperature deviation from the 1951-1980 average temperature and the global CO_2 concentration at Mauna Loa, Hawaii. Data is sourced from [6,7].

The emission of CO_2 is attributed to several main sectors: electricity and heat production, industry, transportation, buildings, and agriculture forestry and other land use (AFOLU). Of these sectors, electricity generation is the largest source of CO_2 emissions, accounting for 25% of the total emitted CO_2 in 2010, with agriculture 24%, industry 21%, and transport 14% [4,5]. The total energy sector contribution is 35%, accounting for secondary processes required to generate energy, such as fuel extraction and refining. To prevent climate change and achieve a carbon neutral state, a reduction in the CO_2 emissions is required for all sectors. The de-carbonization of the energy generation sector is critical to the viability of this endeavor [3], shown in Figure 1-2, where electricity has the largest reduction in emissions.

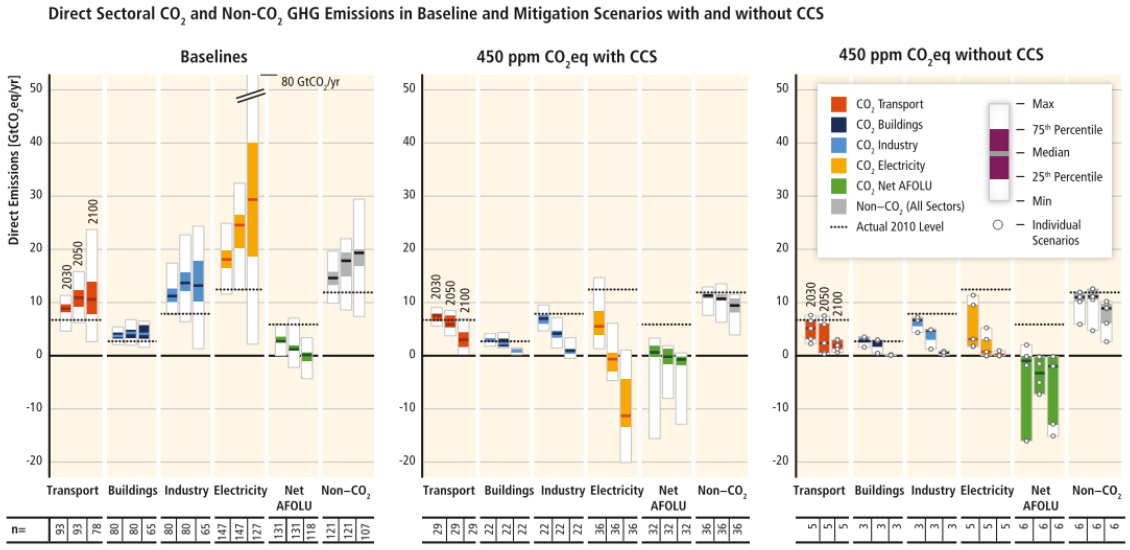

Figure 1-2: CO_2 emissions for each sector for the baseline and reduced CO_2 emissions scenarios. Figure is sourced from Figure SPM.7 of the IPCC Report: Climate Change 2014 Mitigation of Climate Change [5] **published by Cambridge University Press and reused in accordance to the IPCC copyright (Appendix: Copyright Reuse Permissions).**

1.3 Decarbonizing the Electricity Sector

To decarbonize the energy sector, existing technologies can be further developed and deployed. These technologies include Carbon Capture and Storage (CCS) and renewable energy sources, specifically wind, solar, geothermal, and biofuels [5,10]. The increased penetration of these renewable resources into the energy grid will displace fossil fuel energy generation with cleaner, low carbon energy sources, reducing the amount of CO_2 emitted. The International Energy Agency (IEA) scenario to decarbonized energy solutions estimated that renewable energy sources could provide up to 40% of the primary energy demand in 2040, displacing fossil fuel power sources, incentivized by new policies [11]. For example, the European Union has the Renewable Energy Directive that requires 20% of the energy generation to be from renewables in 2020, with each individual nation

achieving a minimum of 10% renewable; and a 50% reduction in greenhouse gas emissions by 2050 [12]. In the United States, individual states have set renewable goals, with California requiring 50% and Hawaii requiring 100% renewable energy by 2045 [13,14]. In Minnesota, the Renewable Energy Standard requires utilities to have 20% renewable energy sources by 2020, and 25% by 2025 [15].

Figure 1-3 illustrates that while wind and solar energy have grown in the United States over the past decade, geothermal energy has not seen significant growth since the late-1980s. The growth of geothermal has been limited as a result of the development of the known hot shallow hydrothermal resources, the lack of incentives to continue geothermal development, and the elevated startup capital costs of exploration and accessing deeper hotter resources. While challenges exist to the future development of geothermal, it is possible to expand the geothermal capacity by 100 GW or more by 2050 using new technologies [16]. These developments in geothermal energy are discussed in detail, in section 1.6.

The recent growth in renewable energy is shown in Figure 1-3. Since 2000, the primary increase in renewable energy has been in wind, bioenergy, and to a lesser extent, solar. In 2016, the growth of these renewables increased the total energy generated by renewables by 66% from the 2000 levels, and accounted for 12% of the total energy generated in the United States [17]. While the increased development of wind, bioenergy, and solar energy has increased the renewable penetration on the electricity grid, the majority of the grid is still dominated by fossil fuel sources, including coal, natural gas, and crude oil, resulting

in the emission of CO_2 into the atmosphere. For example, in 2010, when renewables accounted for 11% of the total energy generated in the United States; the United States energy sector emitted 2.27 Gt-yr^{-1} into the atmosphere [18], or approximately 5% of the global CO_2 emitted (6% of the total greenhouse gas). This indicates that further action is required to efficiently decarbonize energy generation.

A drawback of the development of wind and solar renewable energy sources is that these resources are considered variable renewable energy (VRE) and are not dispatchable resources; meaning that these sources are only available when their resource is available and cannot be controlled by a system operator. This results in the resource energy production to be well below the rated capacity. For example, in 2016, wind produced only 34.5% of its rated capacity (Capacity Factor), while solar photovoltaic was limited to 25.1%, whereas dispatchable resources such as geothermal and nuclear power have capacity factors of 74.2% and 92.5% [19]. The variability of both wind and solar energies are impacted by the weather, which is inherently unpredictable. This unpredictability (variability) in these resources has a substantial impact on energy markets and the electric grid, particularly as the penetration of variable renewable energies increases [20]. Some of these effects have already been observed in regions with high penetration of VRE, with negative electricity market prices resulting from the over generation of energy [21]. As the high penetration of VRE becomes more widespread, these effects will increase and change the nature of energy markets, decreasing the value of VRE and increasing the value of ancillary services, requiring markets to move beyond levelized cost of electricity (LCOE)

(i.e. capital cost over the generation capacity) and consider the performance and contribution of each system to the energy grid [20,22]. In particular, this will benefit dispatchable energy systems and energy storage systems, which can generate energy when VRE are unavailable. Currently, the electricity grid is supported by secondary power systems, known as peaking power plants, which generate power for only short periods when the demand is large. Typically, these peaking power plants use natural gas; however, to reduce CO_2 emissions these plants will need to be replaced by clean, carbon neutral power systems. Energy storage systems have been considered as the ideal solution to support the integration of VRE onto the grid [20,23–26], as energy storage systems can consume power during periods of excess generation and then later dispatch this energy back to the grid when there is a generation deficit; and allowing for the increased penetration of renewable energy without supplementing the need for fossil fuel power. The details of energy storage are discussed in detail in section 1.5.

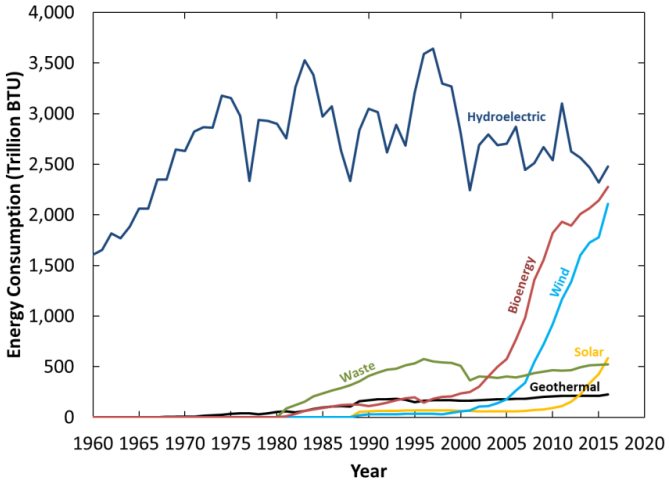

Figure 1-3: Energy consumption for each renewable resource in the United States. Data is sourced from [27]**.**

In addition to the development of low carbon renewable energy sources, existing fossil fuel energy sources (as well as other large point sources of CO_2) can be retrofitted to capture CO_2 from the flue gas before it is emitted into the atmosphere, as part of the Carbon Capture and Storage process (CCS) [10,28–30]. The implementation of CCS will reduce the carbon footprint of existing power plants, enabling the existing energy infrastructure to provide clean energy. Currently, CCS is the only available technology which is capable of decarbonizing existing fossil fuel power systems. Currently, no single technology is capable of providing the required reduction in CO_2 emissions; however, by employing multiple technologies the required reduction in CO_2 emission can be achieved, and most models predict that the 450 ppm goal cannot be achieved without CCS [5].

1.4 Carbon Capture and Storage

The development of Carbon Capture and Storage (CCS) is vital to the de-carbonization of the energy sector, and the development of the CO_2-Plume Geothermal (CPG) system, that is the primary focus of this dissertation. Thus, a review of the current state of this technology is provided.

Carbon Capture and Storage (CCS) is a process that involves capturing CO_2 at a point source, compressing, transporting, and then permanently storing the CO_2. CCS is an important anthropogenic CO_2 mitigation technology, as it is currently the only mitigation technology which can reduce or eliminate CO_2 emissions from fossil fuel power plants. In addition, CCS can mitigate emissions from other larger point sources of CO_2, including petroleum refineries and large industrial facilities [10,31].

There are two main types of carbon storage that have been proposed; geologic and ocean storage. For the purposes of this paper, we focus the discussion on geological CO_2 storage; as oceanic storage, while providing vast storage potential, considerably larger than geologic storage, cannot permanently contain the CO_2, slowly releasing CO_2 into the atmosphere over time, and has significant environmental effects, including the acidification of the oceans, and the increased mortality of organisms near the injection site [10]. The geologic storage of CO_2 utilizes natural subsurface formations to permanently store the CO_2. The geologic formations typically considered for CCS include oil and gas reservoirs and deep saline aquifers; as these reservoirs provide sufficient storage capacity for CO_2, estimated to be 2379 Gt CO_2 in North America [32], and have high natural permeabilities. In the subsurface the long-term storage of CO_2 is achieved by several trapping mechanisms:

Structural Trapping – CO_2 trapped beneath a sealing layer, a low-permeability caprock, that prevents the vertical leakage of CO_2, which is naturally buoyant at the reservoir conditions [32–34].

Residual Trapping – CO_2 is trapped in the pore space between rock grains due to capillary forces [32].

Solubility Trapping – CO_2 dissolves into the native brine and remains in solution with the brine [32,35].

Mineral Trapping – CO_2 reacts with the brine and rock structure to form carbonate minerals [32,36,37].

These trapping mechanisms ensure that the CO_2 remains in the subsurface and is not released back into the atmosphere.

1.4.1 Current State of Carbon Capture and Storage

CCS is a developing technology that has had several successful demonstration projects, however, it has not been adapted for large-scale deployment [38]. In 2017, there were 17 operating CCS projects, however, the majority of these (13) are associated with Enhanced Oil Recovery (EOR) [39], where CO_2 is injected into the reservoir to displace the native fluids, increasing the amount of oil extracted, operating as a Carbon Capture Utilization and Storage (CCUS) system. The remaining four projects; 1) Snøhvit CO_2 Storage, 2) Quest, 3) Illinois Industrial Carbon Capture and Storage, and 4) Sleipner CO_2 Storage, are dedicated CO_2 storage sites. Other notable CCS projects include the In Salah project [40], the Illinois Basin Decatur Project, and Weyburn-Midale project [41–43] which are no longer actively injecting/storing CO_2, but are actively monitored to demonstrate the long term stability and containment of the CO_2 in the reservoir. The sites are used to determine the large-scale viability of CCS.

These current and past CCS projects have demonstrated the feasibility and challenges associated with geologic storage of CO_2. While these projects have demonstrated the feasibility of CCS, not all CCS projects have been successful [44], as challenges exist. These challenges to CCS are primarily related to the project economics, specifically the transportation infrastructure, regulatory and legal issues, and the subsurface evaluation to ensure permanent storage (i.e. reservoir overpressurization and CO_2 leakage) [45]. These current economic challenges can be overcome with stricter emission regulations and

economic incentives [46], particularly, increasing the cost for emitting CO_2, as this leads to an increase in the development and implementation of renewable energy sources and CCS for fossil fuel plants [47]. Overcoming these challenges will allow CCS to be scaled up to store the gigatons of CO_2 required for large scale CO_2 mitigation.

The development of CCS is limited not only by technological and geological conditions, but also on the public perception of CCS [48]. In countries such as the United States, public opinion plays an important role in public policies and can influence the development and implementation of CCS projects. Public opinion often varies, based on a number of perceived technological and social factors, including benefits, risks, costs, public knowledge, and trust in related industries [48]. Risks associated with CCS is not a deterrent on the societal level, however, this can provide a major obstacle to development on the local level [49]. In general, CCS is a relatively new concept; there are several public misconceptions about the purpose and effects. For example, some people overestimate the impact renewable energy can have on lowering atmospheric CO_2 levels and view CCS as a technology designed to limit renewable energy implementation. Overcoming these social misconceptions about CCS is important for the long-term success of carbon capture.

CCS is needed, in addition to clean energy technologies, to achieve the required reduction in emissions to achieve sustainable environmental goals. No single technology will be able to achieve the required CO_2 reductions, and CCS must be used in addition to the development and implementation of clean energy sources.

1.5 Energy Storage Systems

The projected growth of variable renewable energy generation and the expected instability in the electric grid has resulted in an increased focus on the integration of large scale energy storage systems into the grid. These systems are considered the ideal technology to enable the growth of variable renewables, as they can reduce the curtailment of renewables by storing energy during periods of excess generation, and they can dispatch the energy back to the grid when there is a generation shortage, without the need for ramping up a carbon emitting fossil fuel peaking power plant [23,26,50–52]. Without energy storage integration variable renewable penetration is expected to be limited to less than 30% [53], though actual penetration limits will vary based local grid characteristics.

1.5.1 Energy Storage Services

While the increase in variable renewables has increased the discussion of grid scale energy storage, the integration of energy storage systems can provide a variety of services and benefits to the energy grid [50]. These include:

Bulk Energy Storage: Storage and generation of large amounts of energy over extended periods, increasing the grid capacity, allowing for the use of price arbitrage and peak shaving (i.e. dispatching energy when demand is high to reduce generation assets).

Ancillary Services: The ability to support the grid infrastructure by serving as a backup or regulation system. Examples include: providing reserve power to the grid to compensate for generation losses; operating as voltage/frequency support to ensure energy transmission is within specified tolerances; black start services to enable grid services to be restored in the case of a blackout; and load following.

Transmission Deferral: Delayed transmission of energy though the grid to avoid congested transmission lines during periods of peak usage.

To provide this range of grid services, a variety of energy storage technologies are considered. These technologies include batteries, fly-wheels, pumped-hydroelectric, and compressed air energy storage systems. The proposed energy storage system discussed in this dissertation is envisioned to be scaled up to operate as a large-scale bulk energy storage system, in a similar capacity to the existing technologies of pumped hydroelectric and compressed air energy storage systems. Therefore, a brief overview of these technologies is provided.

1.5.2 Pumped Hydroelectric Energy Storage

Pumped Hydroelectric Energy Storage Systems operate using two water reservoirs at different elevations. The system stores energy as gravitational potential energy in the water, consuming power to pump the water from the lower reservoir to the upper reservoir [54–56]. To produce power, the water is transferred from the upper reservoir to the lower reservoir, where the energy is extracted by a hydraulic turbine as the fluid flows between the reservoirs, recovering 70-85% of the stored energy. Pumped hydroelectric systems have been extensively developed, with a 20 GW capacity in the United States, and 127 GW worldwide [55,57]. However, further developments of these systems are limited, due to the environmental impacts of their large surface reservoirs.

1.5.3 Compressed Air Energy Storage

A compressed air energy storage system utilizes a gas turbine power plant that is coupled with a large-volume, high-pressure storage vessel, typically a subsurface cavern, to enable

the system to offset periods of energy generation and power consumption. To store energy, air is compressed and then diverted into the storage vessel. To produce power, the high-pressure air is released, heated using fossil fuels, and then expanded in a turbine [58]. In this system, the use of an intermittent Brayton power cycle allows the energy generated to the grid to be greater than the energy consumed from the grid, due to the addition of heat. Despite this, the development of compressed air energy storage systems has been limited by the ability to locate and develop suitable subsurface storage vessels [59]; as a result there are only two, first-generation, large-scale compressed air energy storage systems operating, providing a combined capacity of 430 MW [58,60,61]. However, research and development on compressed air energy storage systems is ongoing and additional projects have been proposed [58,60,61].

1.5.4 Geothermal Energy Storage Systems

Other large-scale geothermal energy storage systems have been proposed and are discussed in section 1.9 in the context of geothermal energy systems.

1.6 Geothermal Energy

Geothermal energy is a renewable resource that uses heat contained within the body of the earth to generate power or produce heat. Geothermal energy is an abundant resource, with an estimated 12.6×10^{24} MJ of total energy stored within the earth, primarily generated from the decay of radioactive isotopes [16,62]. Currently, only a small fraction of this energy is utilized to produce power; however, there is significant potential for development, and unlike other renewable resources, specifically wind and solar, geothermal resource is dispatchable, as the heat from the earth is always available.

The earth is comprised of several layers: the solid inner core, outer liquid core, mantle, and the thin crust. The inner core is comprised of iron, and has a temperature that exceeds 4000°C [62,63]; however, some sources report this temperature may exceed 5000°C [64,65]. The surface of the earth has an average temperature of 15°C, resulting in a thermal gradient, and a continuous heat flux from the core to the surface. In the crust, heat is transferred primarily through conduction, resulting in a temperature gradient, with temperature increasing with depth. The average continental geothermal temperature gradient is approximately 28-31°C/km [16,65,66], and typical geothermal gradients are reported between 20-35°C/km [63], however, this value can vary based on local geologic conditions. In select regions, special geologic conditions can result in large temperature gradients, in excess of 70°C/km [67], with high temperatures occurring near the surface. These high temperature resources are ideal sites for the development of geothermal power systems.

The heat extracted from the subsurface can be used to generate power, provide direct heating, or in some cases both. The selection of power generation or direct use heating is typically based on the resource temperature, with low temperature resources being used for direct use applications and high temperatures used for power generation [65,68]. For the purposes of discussion, the remaining overview is focused solely geothermal power systems, as this is the primary focus of the dissertation, and does not discuss direct use geothermal systems, such as geothermal heat pumps.

To produce power from the heat in the subsurface, geothermal systems operate using a concept known as a heat engine. A heat engine operates by moving thermal energy from a high-temperature thermal source, to a low-temperature thermal sink, producing useful energy in the process. The thermal efficiency of this energy conversion depends on the resource temperature, with higher temperature resources resulting in greater efficiencies. For this reason, geothermal power systems typically extract heat from resources that have temperatures that exceed 150°C [69]. However, while these temperatures are considered high temperature or high enthalpy geothermal systems, the efficiency of these geothermal systems are low compared to other baseload systems, such as gas turbine engines, that can achieve turbine inlet temperatures up to 1600°C [70]. While the efficiency of the geothermal power systems is lower than other fossil fuel systems, it alone has not prevented the development of geothermal energy, as the earth is a free-renewable source of heat (fuel), does not emit CO_2 into the atmosphere, and is available throughout the world. However, while geothermal energy is abundant, the economics of accessing this energy is challenging, particularly at great depth, and not all geothermal resources are economically viable for development at current technology levels.

In the current energy market, only shallow, high-temperature, easily accessible hydrothermal resources have been economically viable, which has limited the distribution of geothermal power plants to specific locations. New geothermal energy developments are limited by the significant capital investment costs required to evaluate and drill the wells required to access the subsurface resources. This has resulted in the stagnation in the

development of geothermal energy once the shallow, high temperature hydrothermal resources were developed, shown in Figure 1-3. However, the economics of geothermal energy is likely to improve due to the increased focus on CO_2 emissions that may result in legislation taxing CO_2 emissions and/or requiring carbon capture and storage, increasing the costs of fossil fuels plants and stimulating the growth of renewables, particularly baseload renewables to ensure the reliability of the electrical grid.

1.7 Current Status of Geothermal Technology

In 2014, the United States had a total capacity of 3.1 GW provided by 197 geothermal units with a worldwide capacity of 12 GW, provided by 573 geothermal units [65]. The geothermal energy capacity is limited compared to other renewable resources, such as wind, which as of 2016 has an installed worldwide capacity of 486.8 GW, with 82.2 GW in the United States [71]. Most commercially developed geothermal power installations are in geologically active regions, where abnormally large subsurface temperature gradients exist. In the United States, these regions occur in California, Nevada, Idaho, and Utah, and this corresponds to the locations of operating geothermal power plants [72].

1.7.1 Types of Geothermal Resources

While all geothermal systems extract heat from the subsurface, there are several types of geothermal resources that could be sufficiently developed to provide commercial stage geothermal power. These resources are broadly classified as hydrothermal, enhanced geothermal systems (EGS), and low temperature geothermal systems [65]. To date, nearly all geothermal developments have been of hydrothermal resources, however, these resources only represent a small fraction of the accessible geothermal energy. To realize

the full potential of geothermal power, these unutilized geothermal resources must be developed.

1.7.2 Conventional Geothermal (Hydrothermal)

Most geothermal sources are classified as hydrothermal systems; or a system which circulates water. To be considered a viable hydrothermal source a resource must contain water, a permeable reservoir, and overlaying impervious caprock, a large heat source, and a water recharge mechanism [65]. Naturally occurring sources are ideal for geothermal energy, as a system can simply extract the heated fluid to produce power and then reinject the cooler fluid back into the subsurface. However, for these sources to be economically viable, the resource temperature must be greater than 150°C and must occur at shallow depths to reduce drilling complexity and costs (i.e. < 2 km).

1.7.3 Low Temperature

Low temperature geothermal encompasses all resources less than 150°C, including low temperature hydrothermal resources. These resources are considered to be a separate category and they include the majority of known resources, over 60%, in the United States. They have traditionally not been considered for geothermal power application due to their low thermal efficiency and large specific costs [65]. Though, with proper incentives and technology development, these systems are feasible, as demonstrated by the Chena Hot Springs Power Plant that has a resource temperature of 74°C [73].

Additionally, these low temperature reservoirs typically include sedimentary basins, which are a target for CCS and the proposed CO_2-Plume Geothermal systems (Section 1.8.2).

Therefore, the CO_2-Geothermal Energy Storage system presented in this dissertation can be considered a low temperature geothermal system.

1.7.4 Enhanced Geothermal Systems

Enhanced Geothermal Systems (EGS) evolved from the concept of Hot Dry Rock Geothermal, which originated at Los Alamos National Laboratory in 1973 [74,75] as a method to access deep high-temperature geothermal resources that were previously inaccessible due to low rock permeabilities or an absence fluid in the formation. EGS systems can operate in these formations by "enhancing" the permeability of the rock structure by hydraulically fracturing the rock in the reservoir. The resulting fracture network allows cold water to be injected and circulated in the reservoir to extract heat [75]. The heated fluid is then extracted from the facture network at the production well and brought to the surface to generate power.

The development of EGS can significantly expand geothermal energy generation. Unlike traditional geothermal systems, which are limited to select high temperature regions, EGS can be deployed nearly anywhere, as the required resource temperatures can be achieved at deeper depths, due to the thermal gradient. In the United States it is estimated that 100 GW of EGS could be added in the next 50 years [16]. However, despite being proposed and initially demonstrated in 1973, EGS has not become commercially viable, due to geologic uncertainties and the large capital costs, particularly due to drilling the wells. Since the initial Fenton Hill project started in 1973, other EGS projects have been undertaken, including sites at: The Geysers, USA; Desert Peak, USA; Soultz, France; Landau, Germany; Hijiori, Japan; Habanero, Australia; and Basel, Switzerland. Of these,

only four remain active and have a combined generation capacity of 14.2 MW [76,77]. While some of these projects have established the potential of EGS, other projects never produced power due to reservoir complications and socio-political resistance. Reservoir stimulation was unsuccessful in connecting the injection and production wells at the Hijiori and Orgachi plants, limiting the power generation [77]. In Basel, the EGS project was canceled after hydraulically fracturing in the reservoir induced seismic events [78], which resulted in significant social-political resistance to the development of EGS [79]. Despite these setbacks, EGS is closer to commercialization due to ongoing research and developments in technology [67]. Recently, the U.S. Department of Energy sponsored the Frontier Observatory for Research in Geothermal Energy (FORGE) project, which aims to develop an EGS site to accelerate the development of EGS technologies [80].

1.7.5 Geothermal Energy Conversion Systems

To generate power, geothermal power plants must convert the geothermal heat into electricity at the surface. This is generally achieved using variations of the basic Rankine cycle. In general, there are three primary geothermal power systems: dry steam, flash-steam, and binary power plants. Each cycle is configured based on the thermodynamic properties of the produced fluid, described in detail below.

1.7.5.1 Dry Steam Geothermal

The first type of geothermal power plant is the dry steam configuration. In this system, dry steam (i.e. superheated water vapor) is produced at the surface from the geothermal reservoir. The produced steam is filtered to remove contaminants and directly passed through a steam turbine to produce power [63,65]. After the turbine, the exhaust can be

cooled and condensed, extracting additional heat from the fluid. The condensed fluid can be reinjected into the geothermal reservoir, where it can be reheated extracting additional heat from the subsurface.

Locations where dry steam geothermal systems can operate, are limited, as the resource temperature required to produce dry steam is significant and is generally not found near the surface. To operate a dry steam plant, produced fluid temperatures greater than 180°C are required [68]. While the geothermal resources for these types of plants are limited, these systems account for a large fraction of the overall geothermal energy production due to the large amounts of power that these systems can generate, resulting from the relatively high production temperature. In 2014, dry steam geothermal accounted for 24% of geothermal capacity, with 68 operational plants [65].

1.7.5.2 Flash Geothermal Cycle

Most geothermal reservoirs produce a mixture of steam and liquid brine at the surface, and a steam turbine, as used in the dry steam cycle, would be damaged if directly used on the produced fluid. To produce power, the steam is separated from the liquid and is passed through a steam turbine, similar to the dry system. However, in this configuration, the heat from the liquid is wasted, and limited power is produced by the steam, especially when steam concentrations are low. To increase the amount of power generated, the produced mixture is expanded in an expansion valve, decreasing the pressure, causing a fraction of the liquid to flash, and transition to steam [68]. The steam is then separated from the liquid and fed through a steam turbine. In this configuration, the flashing process produces additional steam, which can be used to produce additional power.

Power plants can operate using a single-flash, double-flash, or triple-flash cycle. Multi-flash cycles operate by performing multiple flash separations and turbine expansions in series, increasing the amount of energy produced relative to a single-flash cycle. For example, a double-flash cycle is able to produce 15-20% more power than a single flash cycle [65]. Each additional flashing stage increases the amount of energy that can be extracted, but also increases the plant complexity, as the additional flashing processes require additional system components, also increasing capital costs.

Single-flash geothermal systems are widely used, and as of 2014, 185 systems were operating accounting 43% of the geothermal power production [65]. The same year, double-flash systems accounted for 9.4% of all geothermal plants, with 54 operational plants. Only four operational plants utilize the triple-flash system, however, these plants average 75 MW, generating considerably more power than a double-flash system, which averages only 35 MW [65].

1.7.5.3 Binary Geothermal Cycle

Not all geothermal resources produce fluids at temperatures greater than 150 °C, which is required to operate the flash-steam plant. While it is theoretically possible to produce power using a flash system for lower temperatures, the system efficiency and economics become prohibitive as the resource temperature decreases. Power can still be produced from these lower temperature resources; however, a secondary working fluid is required.

For lower temperature resources, a binary cycle, where the produced fluid is not directly used as the working fluid, can be used. In a binary cycle, a heat exchanger is used to transfer heat from the produced fluid to a secondary fluid, which is used as the working fluid. The

secondary fluid has a lower boiling point than water and produces power using a turbine in a closed loop Organic Rankine Cycle (ORC). Binary geothermal plants have efficiencies of 10-13%, which is considerably lower than other power cycles, due to the low resource temperature [65]. In 2014, binary cycle units accounted for 35.4% of the installed geothermal units, but accounted for only 10.4% of the overall geothermal capacity [65].

1.7.5.4 Advanced Geothermal Cycles

To increase the performance and utilization of geothermal energy, hybrid geothermal systems have been designed. These hybrid systems combine geothermal energy with another energy source to increase the utilization efficiency of each process. Examples of these systems include Fossil Fuel-Geothermal and Solar-Geothermal systems [65], where the heat from the auxiliary source can be used to increase the temperature of the geothermal fluid, increasing the power generated. For Fossil Fuel Geothermal, it is also possible to operate the geothermal system as a pre-heater a fossil-fuel system, decreasing the amount of fossil fuel required by the plant.

Additionally, to improve the utilization of produced geothermal energy, the waste heat from a geothermal power cycle can be used to provide direct use heating, in what is commonly known as a Combined Heat-Power Geothermal system.

1.8 CO_2 Geothermal Systems

Geothermal power traditionally uses water or brine (water with dissolved minerals) as the heat extraction fluid in the subsurface, as brine is traditionally found in formations suitable for traditional geothermal systems. However, the advent of carbon capture and storage as a pathway to mitigate global climate change has led the possibility of large volumes of CO_2

being stored in the subsurface, leading to the question, could this CO_2 be used for geothermal heat extraction. Potential benefits for each system are significant, particularly given that capital costs for both systems are large, mainly due to well and drilling costs, and combining geothermal energy and CCS into a single system could increase the feasibility for project development. Over the past two decades, two main versions of CO_2-Geothermal systems have been researched: CO_2 Enhanced Geothermal Systems (CO_2-EGS) and CO_2 Plume Geothermal (CPG) systems, discussed in detail below.

1.8.1 CO_2 Enhanced Geothermal Systems (CO_2-EGS)

CO_2 was proposed as a geologic working fluid for Enhanced Geothermal Systems (EGS) by Brown [81]. The use of CO_2 as a working fluid in geothermal systems has several advances over brine: 1) CO_2 has a lower kinematic viscosity than brine, thus a higher mobility in geothermal reservoirs, 2) CO_2 has a lower mineral solubility than brine, which limits the transport and precipitation of minerals throughout the system, decreasing pipe scaling, 3) CO_2 has a larger thermal expansion than brine, which results in the generation of a thermosiphon, and 4) the use of a thermosiphon allows the CO_2 to circulate without the need for a mechanical pump [1,2,81–83]. Pumping power in conventional geothermal power plants is a significant fraction of the gross power produced so eliminating the pumping requirement could significantly increase the net power delivered to the grid for the same resource temperature. In addition, the use of CO_2 in a geothermal system allows the CO_2 to be captured, stored, and used for energy production, acting as a carbon capture, storage, and utilization (CCUS) site.

Initial CO_2-EGS studies examined the effectiveness of CO_2 as a heat extraction fluid in the reservoir. Using simplified two dimensional fracture network models, it was shown that the heat extraction abilities of CO_2 were similar and perhaps superior to brine and the CO_2 mass flow rate could be considerably larger [84–86]. The reservoir simulations were then extended to include the reservoir thickness demonstrating the effect of the thermal expansion of CO_2 on the heat extraction. This three dimensional simulation determined that the thermal expansion of CO_2 resulted in an unequal heat extraction from the reservoir, with cooler denser CO_2 flowing along the bottom of the reservoir and the heated CO_2 buoyantly rising to the top [87]. It was concluded that to avoid early thermal breakthrough the production well should extract CO_2 only near the top of the reservoir, and not extend throughout the thickness of the reservoir.

Additional reservoir simulations examined the interaction between the CO_2 and the native brine and rock structure. The injection of CO_2 into the reservoir displaces the native brine, drying out the reservoir, resulting in the precipitation of primary minerals and formed carbonate minerals [37,88,89]. The precipitation of these materials near the injection well can decrease porosity and reduce the mobility of the CO_2 plume, however, co-injecting some water reduced mineral clogging, but also reduced the heat extraction [89].

After determining the effectiveness of CO_2 heat extraction in the reservoir, simulations were expanded to include the vertical wells and the surface power plant. Power plant models demonstrated that the electricity generation of CO_2-EGS was comparable with water based systems [90]. Additionally, the use of CO_2 eliminated the need for a circulation

pump, as the system was able to generate a thermosiphon; that uses the density difference in the injection and production wells, resulting from the thermal expansion of CO_2 in the reservoir, to circulate the fluid [90]. However, for CO_2-EGS to be competitive with brine based systems the vertical production well diameter must be increased for CO_2, which has a lower density and larger velocity in the well than brine, otherwise the frictional pressure losses in the well will substantially reduce the performance of CO_2-EGS [91]. From these models, Atrens et al. [91] determined that CO_2-EGS is preferable to brine based systems in low-permeability reservoirs, and shallow low temperature reservoirs, provided that the production wellbore is correctly sized.

While this research into CO_2-EGS demonstrated the potential of EGS to be combined with CCS technologies, the size of the artificial fracture networks for EGS systems are limited, and cannot store the volume of CO_2 required to mitigate climate change; which is the primary reason to consider CO_2-EGS [33,92]. This challenge, combined with the socio-political resistance to hydraulic fracturing [79], has led to another concept, termed CO_2-Plume Geothermal (CPG), which uses CO_2 as a working fluid in naturally permeable sedimentary basins [1,33,34,82,93–96].

1.8.2 Carbon-Dioxide Plume Geothermal

The CO_2-Plume Geothermal concept is a natural progression from the previously discussed CO_2-EGS technology, evolving the CO_2-Geothermal concept by reframing the combination of CCS and geothermal energy to eliminate several technology and socio-political obstacles that hindered the development of CO_2-EGS. The CO_2-Plume Geothermal system has several key differences that distinguish it from the previously

discussed CO_2-EGS configuration. Specifically, CPG does not require the reservoir to be "engineered", or fractured, and instead uses sedimentary basins that are naturally permeable [33,34,93,94,96]. This distinction is significant as hydraulic fracturing increases project uncertainty and risks, as fracture networks are random and may not result in a closed loop (i.e. the fracture don't connect the injection and production wells or fractures connect to an outside formation), and may induce seismic disturbances which has led to the cancelation of EGS projects due to socio-political resistance [78,79]. Additionally, the use of sedimentary basins benefits CPG, as these reservoirs are currently targets of CCS operations[10,97], providing a better synergy with CCS than CO_2-EGS [33,34,94,96]. Put simply, CPG reframes the problem that CO_2-EGS attempts to address, which was how CCS can be adapted for geothermal energy, and instead asks how geothermal energy can be adapted for CCS.

Initial research into CPG validated the heat extraction potential of CO_2 in permeable sedimentary reservoirs, and demonstrated that they produce more heat with higher CO_2 production temperatures for a longer period than a similar CO_2-EGS system [94], and similar brine-EGS and brine reservoir systems [96]. The effects of the permeability were evaluated on power generation for CPG, water, and brine systems, with CPG generating more power than water systems for permeabilities less than $5x10^{-14}$ m^2 [34], which was similar to findings of Atrens et al. for CO_2-EGS systems [91]. The synergistic value of the geothermal heat extraction on CCS was evaluated, and CPG increased the feasibility of CCS by offset approximately 10% of the carbon capture cost [33].

Two surface power plants were developed and evaluated for use with the CPG reservoir, a direct power cycle where CO_2 is directly expanded in a turbine (i.e. the CO_2 equivalent of the dry-steam cycle), and a binary cycle, where the heat is transferred to a secondary fluid to produce power using a simplified reservoir model (i.e. a binary cycle) [98]. The results of this simulation demonstrated that CPG has the capability to generate power from the heat extracted from the reservoir, and that for CPG applications the direct cycle was more efficient at generating power than the binary system. Adams et al. [1] further refined these models, accounting for friction losses in the adiabatic wellbore, realistic parasitic power consumption for the fans in the cooling towers, a circulation pump to augment the developed CO_2 thermosiphon [82], and a reservoir characterization estimating the reservoir pressure loss. The detailed thermodynamic model confirmed that CO_2 direct cycles generate more power than binary cycles, and CPG systems generate more power than an equivalent brine system for low and moderate permeabilities and temperatures. The availability of the geothermal resource additionally enables CPG to be more dispatchable than wind and solar [2]. This power system, defined by Adams et al. [1], is the most comprehensive power generation study completed for the CPG system and represents the state of the art in power conversion technology for CPG systems, and is shown in Figure 1-4.

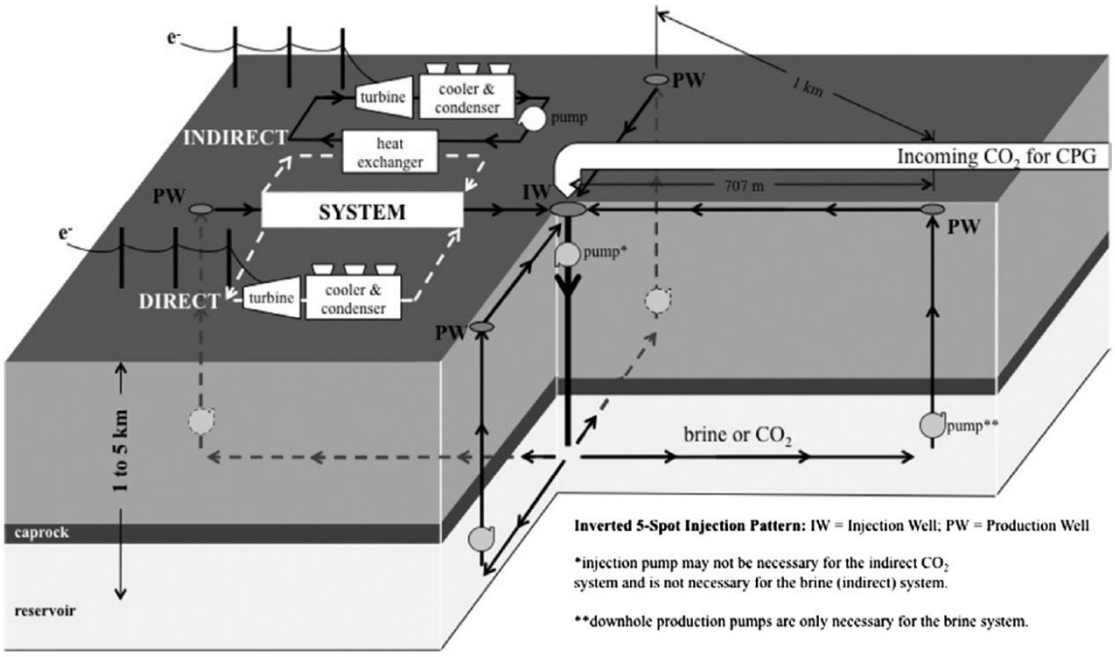

Figure 1-4: Layout of a CPG system using a 5-spot pattern. Both a direct cycle and an indirect cycle are indicated. Figure is sourced from Adams et al 2015 [1] **and reprinted with permission from Elsevier (Appendix: Copyright Reuse Permissions).**

Further research on CPG has enhanced the understanding of CO_2 heat extraction from the reservoir. Garapati et al. [83,99] simulated the performance of a radial-axisymmetric reservoir with a horizontal production well located beneath the caprock, and a vertical injection well located at the center. These simulations included the CO_2-brine interactions and the initial plume development, determining the minimum volume of initially injected CO_2 required to operate a CPG system, the lifetime of each reservoir, and the effects of stratified permeability within the reservoir. These simulations additionally demonstrated that in a CO_2-brine reservoir, the produced fluid will contain some brine in solution, but this fraction is typically within allowable limits for turbomachinery. However, this brine must be removed at the surface, as the reinjection of brine with the CO_2 increases reservoir

pressure losses. Finally, the thermal drawdown at the production well reservoir was characterized for variable reservoir thicknesses and production well radiuses, determining an optimum production well radius and mass flow rate for the lifespan of the reservoir [100].

A field test conducted at the Southeast Regional Carbon Sequestration Partnership (SECRAB) Cranfield site located in Cranfield, Mississippi demonstrated the viability of the recovery of CO_2 from the reservoir and the operation of a thermosiphon for 43 hours [101–103]. The reservoir is part of the Lower Tuscaloosa Formation and is highly permeable, and while the Cranfield site is not a saline reservoir, the site can be viewed as an analog to CO_2 injection into a saline reservoir [104].

1.9 CO_2 Geothermal Energy Storage Systems

While CO_2 geothermal systems can operate solely as dispatchable baseload power systems, research has demonstrated that they can operate as energy storage systems and both consume and generate power from the electrical grid to support the growth of other variable renewable systems. To date, three CO_2-Geothermal Energy Storage systems have been proposed: 1) CO_2-Bulk Energy Storage System (CO_2-BES), 2) Compressed CO_2 Energy Storage System (CCES), and 3) CO_2-Plume Geothermal Energy Storage System (CPGES).

1.9.1 CO_2-Bulk Energy Storage System

The CO_2-Bulk Energy Storage System is a complex multi-fluid geothermal system that uses the injection of CO_2 to pressurize, displace, and then produce heated brine for geothermal energy generation [105–107]. The geothermal reservoir consists of several concentric horizontal circular injection and production wells to circulate both CO_2 and

brine, shown in Figure 1-5. This well configuration is designed to create a hydraulic mound to store pressure in the CO_2 and create an artesian flow in the brine, generating power [106]. To consume power, the brine is pumped back into the reservoir to re-establish the hydraulic mound. Modelling demonstrated that with select mass flow rates, the system would establish a hydraulic mound, and brine extraction could generate significant power, in excess of 100 MW for the given reservoir configuration [105–108].

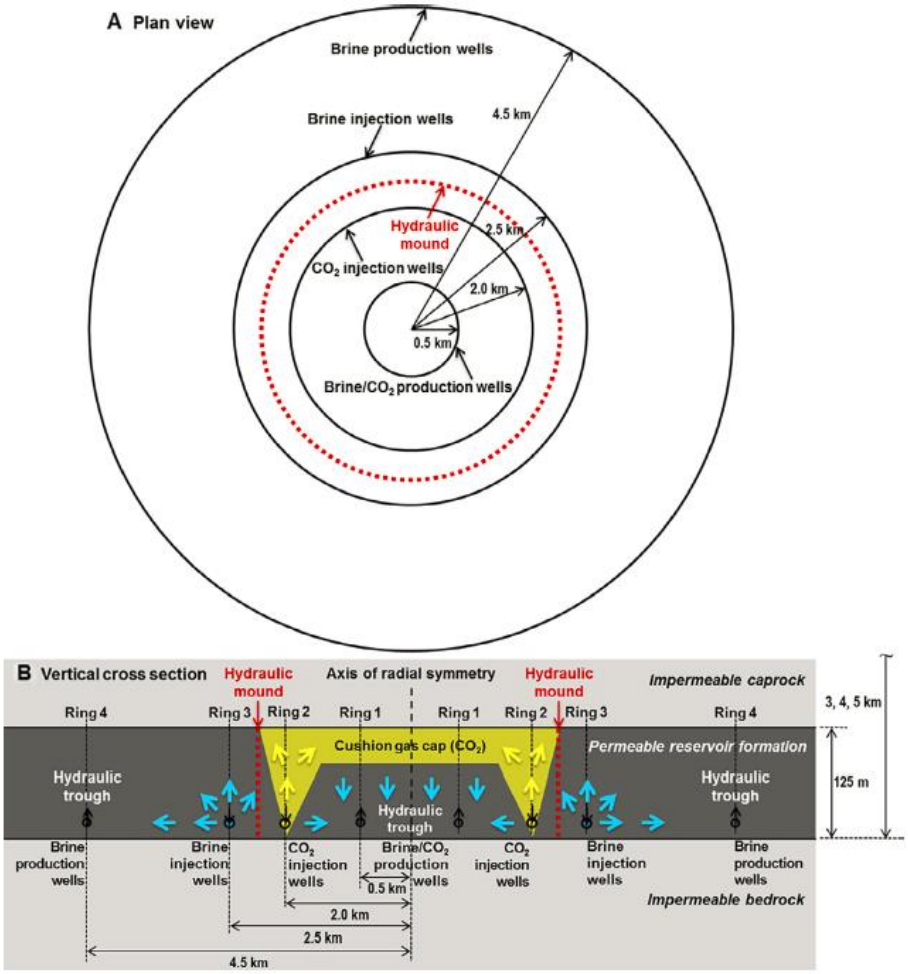

Figure 1-5: A cross section of the reservoir for the CO_2-Bulk Energy Storage system indicating the layout of the concentric injection and production wells. Figure is

sourced from Buscheck et al. 2016 [106] **and is reproduced with permission from Geological Society of America (Appendix: Copyright Reuse Permissions).**

1.9.2 Compressed CO_2 Energy Storage System

The Compressed CO_2 Energy Storage System (CCES) expands from the known Compressed Air Energy Storage System and utilizes a multi-level sedimentary reservoir to generate and then store energy using a supercritical CO_2 Brayton cycle, shown in Figure 1-6. The CCES system has two modes: a generation and consumption mode. In the generation mode, CO_2 is extracted from the subsurface and heated at the surface, using heat recovered after the turbine and an external fuel source, and then expanded in a turbine. Most of the waste heat is recovered and used in the pre-heat process and then the CO_2 is injected into the shallow reservoir. This generation process is similar to the Compressed Air Energy Storage system, as most of the generated power is a result of the heat addition at the surface, provided by an external heat source. To consume power, the CO_2 is recovered in the shallow reservoir and then compressed into the deeper reservoir. They found that the system operated with round trip efficiencies (i.e. power out over sum of the compression power and adjusted heat added) of approximately 63%. However, accounting for the full amount of heat addition this value is likely to be closer to 50%. Overall, the system operated with energetic efficiencies near 50%. System performance is limited by the large power consumption by the compressors, which generally exceeded the turbine generation capacity, even with heat addition. The overall efficiencies, however, are maintained by the large heat recovery system in the generation mode. Modeling however, neglects the vertical wells, which can have an significant impact on the performance of the cycle [1,91]. This, combined with the inoperable heat recovery system, which transfers

heat against the temperature difference, shown by state 7 in Figure 1-6d, may significantly impact the findings. Additionally, surface heating of a CO_2-Geothermal cycle, as demonstrated in CCES, operates with a lower efficiency than a secondary power system alone for high turbine inlet temperatures [109]. None the less, this provides valuable insight into multi-level CO_2 energy storage.

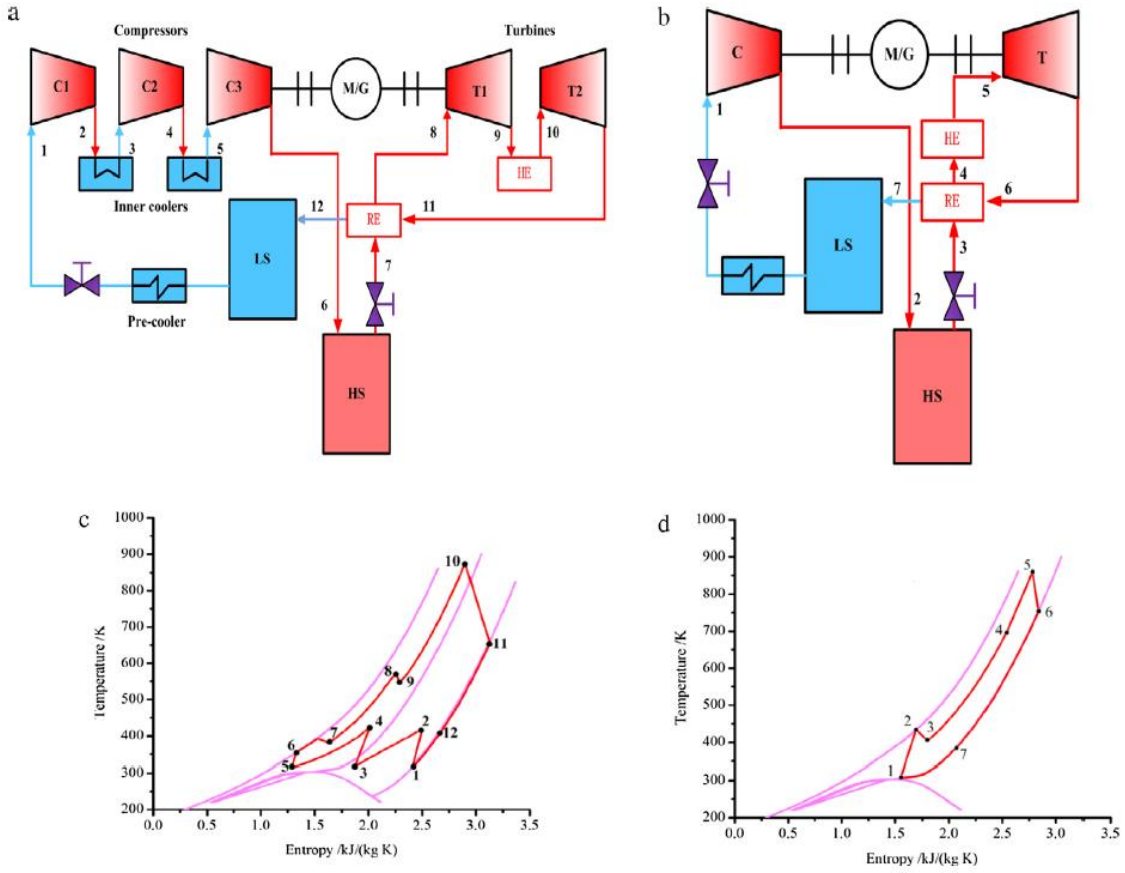

Figure 1-6: A schematic for the proposed Compressed CO_2 Energy Storage System. System components include the compressor (C), the turbine (T), the high-pressure reservoir (HS), the low pressure reservoir (LS), the surface heat addition (HE), and the reheat heat exchanger (RE). Image was sourced from Liu et al 2016 [110]**, and reused with permission from Elsevier (Appendix: Copyright Reuse Permissions).**

1.9.3 CO_2-Plume Geothermal Energy Storage System (CPGES)

The CO_2-Plume Geothermal Energy Storage system is an extension of the CPG power system, and operates by adding a second shallower reservoir which enables the system to operate as an intermittent Rankine cycle. This system is different from the previous CCES systems, as the CPGES system operates using a supercritical Rankine cycle using only geothermal energy to produce power, whereas, the CCES system used a Brayton cycle with auxiliary heating on the surface. The design and performance of the CPGES system is the primary focus for the remainder of this dissertation. The purpose of this work is to provide insight on how the CPG system can be a flexible power generation and storage facility to supplement the growth for variable renewable energy sources, and limit climate change, thereby increasing the versatility of the CPG system.

Chapter 2: Simulation of a Transient CO_2-Plume Geothermal Energy Storage System

Earth Battery: A High-Efficiency, Large-Scale Subsurface Energy Storage System, Using Carbon Dioxide Plume Geothermal Energy

Mark R. Fleming[1], Benjamin M. Adams[2], Thomas H. Kuehn[1], Jeffrey M. Bielicki[3,4], Martin O. Saar[2,5]

[1]Department of Mechanical Engineering, University of Minnesota, USA
[2]Geothermal Energy and Geofluids Group, Department of Earth Sciences, ETH-Zürich, Switzerland
[3]Department of Civil, Environmental, and Geodetic Engineering, The Ohio State University, USA
[4]John Glenn College of Public Affairs, The Ohio State University, USA
[5]Department of Earth Sciences, University of Minnesota, USA

Synopsis

A Carbon Dioxide Plume Geothermal (CPG) energy system has been modified into a large-scale energy storage system (CPGES) by including a second geothermal reservoir at a shallower depth, some surface plant modifications, and operating the system as an intermittent Rankine cycle. The shallow reservoir serves to store CO_2 at a lower pressure and temperature than the deep reservoir between the energy production and energy storage processes. Circular injection wells are used in both reservoirs to provide more surface area than the use of vertical wells and reduce detrimental pressure drops. A CPGES system has been simulated with 16 hours of power production and 8 hours of energy storage per day. Results show that more energy can be provided than consumed after initial startup transients, the ratio of energy produced to energy consumed per day was found to be 2.92 after 10 years of operation. The additional energy is provided by the deep geothermal reservoir. Daily revenue of a CPGES system can become larger than an equivalent continuously operating CPG system when the time of day electrical prices are sufficiently high between daytime and night time and all the produced power can be sold.

2.1 Introduction

Fossil energy (oil, natural gas, coal) based power generation has been identified by the Intergovernmental Panel on Climate Change (IPCC) as a significant source of carbon dioxide (CO_2) emissions to the atmosphere [5]. The IPCC has furthermore estimated that limiting atmospheric CO_2 concentrations to a maximum of 450 ppm results in a 50% chance of preventing a global mean temperature increase by more than 2°C [5], as agreed upon by the United Nations Framework Convention on Climate Change in the Paris Agreement [111]. To achieve this goal, an estimated 1000 Gt of CO_2 can be emitted after 2011 [4], requiring the reduction, and eventual elimination of CO_2 emissions. In the electricity sector, which comprises 25% of the global CO_2 emissions [5], the utilization of clean, CO_2-emission-free energy sources, or coupling CO_2-emitting energy sources, such as fossil energy, with CO_2 capture and geologic storage (CCS), is critical to reduce, and eventually cease, CO_2 emissions to the atmosphere [5,10].

In the United States, state legislation has set goals that require the expanded use of renewable energy sources. For example, in California, legislation passed in 2015, requires public utilities to generate 33% of their electricity from renewable energy sources by the end of 2020 and 50% by the end of 2030 [13]. In 2015, Hawaii updated its clean energy initiative, passing a house bill that requires utilization of 100% renewable energy by 2045 [14]. In 2015, renewable energy utilization accounted for 9.45% of the total energy used in the United States [27]. However, expanded utilization of renewable energy, particularly of wind and solar, increases the complexity of grid management due to the variable energy supplied from these sources [112,113].

Renewable energy sources, such as wind and solar, can only produce variable power, as these energies are naturally only intermittently available. Therefore, to ensure on-demand power supply at any time, excess power, that may be generated when it is not needed, requires energy storage for later use when power demand is high. Without the storage of intermittently available solar and wind energy, their integration into the electrical power grid, while maintaining grid reliability, is challenging [112,113]. Therefore, large-scale energy storage systems are key to the widespread development and implementation of wind- and solar-based power supply [56,114].

An alternative to storing excess solar and wind energy for later use is to install dispatchable backup power. However, this alternative to actual excess energy storage comes at the expense of utilizing fossil energy, as typically natural gas turbines are employed [50], which, again, results in CO_2 emissions. Therefore, this commonly deployed backup power approach does not constitute a favorable solution.

Both excess energy storage and energy backup systems are capable of supplementing renewable energy resources [50,58,115,116], allowing continuous power supply, even when the renewable energy resource is unavailable [50,115]. Without this ability to provide power reliably at all times, solar and wind energy are unlikely capable of completely replacing baseload power plants, such as fossil energy or nuclear power plants. To note, the only renewable-energy-based power generation systems that are commonly considered to provide baseload power, are those that use either bio energy or geothermal energy [117].

Here, we investigate excess energy storage that utilizes supercritical carbon dioxide (CO_2) as the subsurface energy storage medium, which, compared to other excess energy storage approaches, has the following three main advantages: 1) It is large scale in space, utilizing subsurface saline aquifers, potentially enabling excess energy storage for a significant portion of the power grid; 2) It is large scale in time, capable of storing energy for hours to seasons; and 3) It is highly efficient, due to a) its capability to store both heat and pressure energy in the form of supercritical CO_2 and b) its potential to take up geothermal energy during the underground storage of the supercritical CO_2. Under favorable conditions, the geothermal energy input can more than make up for parasitic power requirements to store and retrieve the energy, essentially resulting in a CO_2-based geothermal power plant [1,93,96] with add-on energy storage.

2.1.1 Background on Energy Storage

Energy storage systems have two operation modes: a charge period, and a discharge period. The charge period consumes electrical power from the power grid, while the discharge period releases the stored energy from the energy storage system back to the power grid. The timescales of the charge and discharge operations vary depending on the type of the energy storage system. For example, so-called peak-shaving energy systems store excess energy during peak power production and supply it later from storage, when intermittently available energy resources are not able to provide power. Currently, relatively large-scale, energy storage systems, capable of peak-shaving, include pumped hydroelectric energy storage (PHES) and compressed air energy storage (CAES).

PHES stores energy using two surface-water reservoirs that are vertically offset. Energy is stored by pumping water from the low elevation reservoir to the one at higher elevation. In this system, energy is stored as gravitational potential energy of the water, resulting in a low energy density [54–56]. The stored energy can be converted to electricity by reversing this process (i.e. letting the water drop from the upper to the lower reservoir) and converting the energy to power using a hydraulic turbine. Pumped hydroelectric is a mature technology which operates at a typical energy storage efficiency of 70-85% [54,55], meaning that 70-85% of the energy required to operate the PHES system is later retrieved. Relatively recently, pumped hydroelectric had a capacity of 20 GW in the United States, 1.8 GW in Switzerland , and a worldwide capacity of 127 GW [55,57]. Pumped hydroelectric can store energy over long periods of time, with only minor losses. However, most economically viable sites worldwide have already been developed [55]; others pose environmental challenges, hindering development.

Compressed air energy storage (CAES) operates as an intermittent Brayton cycle [58], by separating the air compression and expansion processes. When excess electricity is available to be stored, the system compresses the air, consuming or storing energy in the process. The high-pressure air is stored in caverns underground. When energy is needed, the high-pressure air is released from storage, heated, expanded in a turbine, and then vented back to the atmosphere [58]. In contrast to PHES, CAES requires additional (heat) energy input during the energy production to operate efficiently, and this heat typically comes from fossil fuels. The deployment of CAES systems has been limited in comparison

to PHES. Currently, only two, first-generation, large-scale CAES systems exist, a 321 MW plant in Huntorf, Germany, and a 110 MW plant in McIntosh Alabama [58]. The McIntosh and Huntorf plants operate with an overall energy efficiency of 54% and 42%, respectively [58]. Currently several CAES sites are under development [58,61].

The CO_2-based geothermal energy systems, such as the one mentioned at the end of the introduction, can also serve as particularly high-efficiency and large-scale (in both space and time) energy storage systems, as discussed in detail throughout the remainder of this paper. In essence, such CO_2-Plume Geothermal (CPG) systems fall somewhere on a continuum between pure energy storage and pure CO_2-based geothermal power generation, depending on subsurface energy storage depth, geothermal conditions (reservoir temperature and heat-input rates), reservoir permeabilities, and system operating conditions (e.g., energy storage versus energy retrieval durations). We refer to this technology as "Earth Battery," which emphasizes that the main purpose of this form of energy storage is large-scale electric power storage (albeit in the form of heat and/or pressure energy), although it can also be used for heat storage and production.

The Earth Battery, or CPG system, requires large amounts of CO_2, which can come from the CO_2 capture process at fossil-fueled power plants, cement manufacturers, biofuel refineries, or any other CO_2-emitting technology, which is increasingly implemented to reduce global warming [5]. To keep the CO_2 from the atmosphere, it needs to be stored permanently, which typically requires underground, i.e., geologic, storage of the CO_2, ideally in its supercritical phase to ensure high density, in deep saline, and thus unusable,

aquifers or partially depleted oil/gas fields. This process is referred to as Carbon, or CO_2, Capture and (geologic) Storage (CCS) [10]. The CCS reservoir is a permeable reservoir overlain by a low-permeability caprock, which prevents upward leakage of the CO_2. In addition to this so-called structural trapping mechanisms, the CO_2 can also be stored due to capillary forces, binding the CO_2 in small pores between grains, dissolution into the underlying brine [35], and eventually carbonate mineral formation [36,37].

CO_2 injected underground, for example, as a result of CCS operations, may be utilized as a working fluid in Enhanced Geothermal Systems (EGS) [81,87,90,91] and in CO_2-Plume Geothermal (CPG) systems [1,82,83,118], thereby constituting a Carbon Capture Utilization and Storage (CCUS) system. However, as the artificially generated, by hydraulic stimulation, EGS reservoir sizes are rather small, only minimal amounts of CO_2 can actually be stored in such CO_2-EGS systems [34,96]. In contrast, CPG uses naturally permeable sedimentary basin formations that are overlain by low-permeability caprocks, resulting in significant CO_2 storage capacities [34,96]. The effectiveness of CO_2 as a heat and pressure energy extraction fluid, from a subsurface CPG reservoir, is documented in [33,34,83,94,96,119]. Furthermore, numerical models of the power generation by a theoretical CPG system demonstrated the effectiveness of a thermosiphon [82] and system performance relative to brine-based geothermal energy systems [1]. This CO_2 thermosiphon utilizes the density difference between the injection and production wells to reduce or eliminate pumping power requirements [91].

In a standard CPG system, CO_2 is continuously circulated between a subsurface reservoir and a surface power plant to constantly produce baseload electrical power [1,82]. In general, the ability of geothermal power plants to produce baseload power distinguishes them from most other renewable energy sources, such as wind and solar, which are capable of producing intermittent only power – one exception being Bio Energy (BE) [117], which, however, produces CO_2 emissions, unless it is coupled with CCS, resulting in what is commonly referred to as BECCS [28]. However, geothermal power plants may, depending on geologic and power system conditions, instead be run at different power generation rates, i.e., intermittently, to provide (more) power to the electricity grid during times of peak power demand. An example of such a Subsurface Energy Storage (SES) system is the one introduced here, which is a modified CPG system, i.e., a CPG Energy Storage (CPGES) system. CPGES is related to, but still significantly different from the other Earth Battery system we have introduced in Buscheck et al. [106,107], and the Compressed CO_2 Energy Storage concept, discussed by Liu et al. [110]. In contrast to Buscheck et al. [106,107], our concept here uses only CO_2, and no water or brine, and employs two geothermal reservoirs at different depths. The deeper reservoir has greater temperatures and pore-fluid pressures, due to the geothermal temperature gradient and the increased fluid column, respectively. The CPGES system adds a shallow reservoir to the standard CPG system that acts as a "storage tank" for lower-pressure, lower-temperature CO_2, enabling the CPGES system to operate as an intermittent power supply system, i.e., as an intermittent Rankine cycle. The CPGES system operates using only the energy stored from

the grid and geothermal energy, which is significantly different from the Compressed CO_2 energy storage system, which uses a supercritical CO_2 Brayton cycle and requires substantial heat addition at the surface. This multi-reservoir approach facilitates power production and consumption at different times, dispatching power when needed and charging the system when low-cost power is available.

The objective of this discussion is to quantify the performance of a CPG electricity generation system that is modified to operate as an energy storage system, i.e., a CPGES system. We demonstrate this system for a small-scale pilot plant to illustrate the fundamental mechanics of the operation of the system. We compare the energy performance of this system to the closest existing technologies for large-scale energy storage, Compressed Air Energy Storage (CAES) and Pumped Hydroelectric Energy Storage (PHES). We also consider time-of-day electricity pricing (in the USA) that would make this option economically viable.

2.2 Method

2.2.1 System Overview

A CO_2-Plume Geothermal (CPG) system consists of CO_2 injection and production wells, a permeable sedimentary reservoir overlain by a low-permeability caprock, sufficient reservoir temperature, and a surface power plant that converts the heat and pressure energy from the reservoir to electrical power. If only heat is desired, a heat exchanger to another working fluid suffices. In the direct system considered here where no secondary fluid is used in the power plant at the Earth's surface, the supercritical CO_2 ($scCO_2$) is heated in the reservoir, produced to the surface through a production well, expanded through a

turbine, cooled to a condensed liquid, compressed, and reinjected through a well back into the reservoir [1,34,82,83,96]. CPG systems may ideally be developed at a CO_2 storage site or at a naturally occurring underground CO_2 deposit [33].

The CPGES system is similar to the CPG system, but operates by moving CO_2 between two reservoirs at different depths, where the deeper reservoir exhibits higher temperature and pore-fluid pressure as outlined before. Figure 2-2 shows that the CPGES system operates in two different modes for the power generation and power consumption processes:

1) Power Generation Mode: CO_2 production from the deep reservoir, electric and/or thermal power generation, and injection of the CO_2 into the shallow reservoir.

2) Energy Storage Mode: CO_2 production from the shallow reservoir and injection into the deep reservoir, consuming power.

During power generation, the system produces geothermally heated CO_2 from the deeper reservoir and expands the CO_2 in a turbine to generate power. When the fluid exits the turbine, it is in a low-pressure, high-energy state. This state is not suitable for CO_2 injection into the deeper reservoir as significant compression is required, however, it may be stored temporarily near the surface in a shallow reservoir. The shallow reservoir allows for storage of the CO_2 at hydrostatic fluid pressure with minimal parasitic power consumption.

During energy storage (i.e., power consumption) mode, CO_2 is removed from the shallow reservoir and brought to the surface, where it is cooled, compressed, and injected into the deeper reservoir. The cooling and compression processes consume energy.

Because the fluid in the deep reservoir is heated by a geothermal energy source, the net electrical energy produced can be greater than the net electrical energy consumed by the system. This can result in a net positive energy contribution to the electric power grid, depending on geologic, geothermal, and system operation (energy storage duration) parameters.

2.2.2 CPGES numerical modeling

The CPGES system is divided into two sub-systems: 1) the two reservoirs and 2) the remaining components, which include the vertical wells, the turbine, the cooling towers and fans, the throttling valves, and the pump. The reservoirs are numerically simulated using TOUGH2 [120], with the ECO2N equation of state module [121]. The remaining components are simulated employing Engineering Equation Solver (EES) [122]. We couple the models for the reservoirs and the other components with MATLAB [123].

2.2.2.1 Reservoir numerical modeling (TOUGH2-ECO2N)

Following the approach presented by Garapati et al. [83], both reservoirs are numerically modeled employing a three-dimensional, axisymmetric geometry. Both reservoirs have a porosity of 10%, are 300 meters thick, and are overlain by low-permeability caprocks. The respective reservoir temperatures are given by their depth, a standard continental-crust geothermal gradient of 35^{o}C/km, and a mean annual surface temperature of 15^{o}C. Additionally, we model the heat flux through the top and bottom reservoir boundaries as semi-analytic conduction heat transfer [120], representing the surrounding rock. The reservoirs are initially filled with brine with an NaCl saturation of 20%. Reservoir

parameters are consistent with the base case presented by Adams et al. [1,82] and are summarized in Table 2-1.

Table 2-1: Reservoir physical properties for the numerical simulation.

Reservoir Parameters/Conditions	
General Parameters	
Horizontal Permeability	5.0×10^{-14} m^2
Vertical Permeability	2.5×10^{-14} m^2
Thermal Conductivity	2.1 W/m/°C
Porosity	10%
NaCl Concentration	20%
Geothermal Gradient	35 °C/km
Surface Temperature	15 °C
Reservoir Thickness	300 m
Rock Density	2650 kg/m^3
Rock Specific Heat	1000 J/kg/°C
Simulated Radius	100 km
Initial Conditions	Hydrostatic equilibrium, pore space occupied by brine
Deep Reservoir	
Mean Reservoir Depth	2.5 km
Mean Reservoir Temperature	102.5 °C
Injection Well Radius	200 m
Production Well Radius	707 m
Number of grid cells, vertical	42
Number of grid cells, horizontal	117
Shallow Reservoir	
Mean Reservoir Depth	1.5 km
Mean Reservoir Temperature	67.5 °C
Well Radius	400 m
Number of grid cells, vertical	34
Number of grid cells, horizontal	121

2.2.2.1.1 Deep Reservoir

As shown in Figure 2-2, during the energy storage operation, power is consumed to inject cold, but still supercritical, CO_2 ($scCO_2$), with its critical point being at only 31.04 °C, into the deep reservoir at the deep horizontal, circular injection well. Due to the mobility and

buoyancy of the $scCO_2$, the CO_2 plume expands vertically and radially away from the injection location, overrides the higher-density brine, and is geothermally heated as it moves through the hot geothermal reservoir. Vertical movement ceases at the top of the reservoir, due to the overlaying, low- to virtually zero-permeability caprock. During the power generation mode, the geothermally heated CO_2 is extracted at a horizontal, circular production well, located just beneath the caprock (Figure 2-2), as also shown in Garapati et al. [83].

The deep injection well is located at a radius of 200 meters directly above the low-permeability rock at the bottom of the reservoir (Figure 2-2), although it should be noted that, due to the buoyancy of the $scCO_2$, such a basal, low-permeability rock or layer is not required. This injection well configuration differs from that used in previous CPG power system studies that used a vertical injection well, including in Garapati et al. [83] who used a horizontal, circular production well, but a vertical injection well. We consider a horizontal, circular injection well to increase the injection well length, compared to a vertical well, thereby reducing the injection pressure, other factors remaining the same, which is desirable [95]. The location of the injection well at the bottom of the reservoir allows the CO_2, which is naturally buoyant at the reservoir conditions, to extract heat via convection over the entire thickness of the reservoir. The circular, horizontal production well is located at a radius of 707 meters directly beneath the top-bounding caprock, where this radius is chosen for better comparison with previous CPG results, in particular those reported by Randolph and Saar [33], Adams et al. [1], and Garapati et al. [83,119].

The CPGES system requires the deep, hot reservoir to contain a CO_2 plume, which must be developed prior to starting CO_2 circulation. In this study, we prime the deep reservoir by injecting CO_2 for 2.5 years, during which time the developing CO_2 plume displaces some of the native brine. The CO_2 injection rate increases linearly from 0 to 250 kg/s during the first year, then remains constant at 250 kg/s for the remaining 1.5 years, similar to Garapati et al. [83]. This results in the total injection of 15.78 Mt of CO_2 and CO_2-plume breakthrough at the production well, where the CO_2 saturation at the production well is 30% (Figure 2-2). As demonstrated by Garapati et al. [83,119] CO_2 saturations in the production well are significantly higher than even in the reservoir immediately surrounding the production well inlet, due to the high mobility (low kinematic viscosity) of the supercritical CO_2, which is preferentially entering the production well, compared to brine. This tends to result in CO_2 saturation values in the production well significantly above 90%, often very close to 100%, , as demonstrated by Garapati et al. [83,119].

2.2.2.1.2 Shallow Reservoir

The shallow reservoir is used differently and, thus, has a different well configuration than that of the deep reservoir (Figure 2-2). The shallow reservoir is located at a depth of 1.5 km and has a single horizontal, circular well located at the top of the reservoir directly beneath the caprock. The well has a radius of 400 meters and operates both as a CO_2 injection and a CO_2 production well (i.e., as a so-called “Huff and Puff” system).

The use of a single injection/extraction well allows efficient injection and recovery of CO_2. During the power generation mode, CO_2, produced from the deep reservoir is passed through the turbine (where it is expanded and thus cooled), and injected into the shallow

reservoir, where it partially displaces the pre-existing CO_2 and the brine near the well, forming or maintaining a "pocket" of CO_2 around the well. During the energy storage mode, when power is consumed to extract CO_2 from the shallow reservoir, high CO_2 concentrations near the well minimize brine entrainment, thereby maximizing the likelihood that the produced fluid is only CO_2.

As with the deep reservoir, the shallow reservoir must be primed by injecting sufficient CO_2 to ensure that the fluid extracted during the energy storage phase is only CO_2. Therefore, we prime the shallow reservoir by injecting CO_2 at a rate that linearly increases from 0 to 100 kg/s over the first two weeks and then remains constant at 100 kg/s for another ten weeks, resulting in a total injected CO_2 mass of 0.67 Mt (Figure 2-2).

During our early numerical analyses of CPGES system performance, the CO_2 plume in the shallow reservoir dispersed over multiple energy storage and discharge cycles, depleting the CO_2 pocket around the well, as the CO_2 rose to form a thin layer beneath the caprock. The decreased CO_2 saturation values near the combined injection-production well increased CO_2 injection and decreased CO_2 production pressures, increasing the parasitic power consumption of the system. This problem can be mitigated by injecting slightly more (5% in our simulations) CO_2 into the shallow reservoir than extracted from it during each cycle. Our approach uses the deep reservoir, which contains a substantially larger amount of CO_2, as a CO_2 source to maintain the required CO_2 injection/withdrawal mismatch in the shallow reservoir, enabling the system to operate for decades without requiring external makeup CO_2.

Figure 2-1 shows the CO_2 saturation in the shallow reservoir at the end of ten years when 5% more CO_2 has been injected than removed each cycle. The 5% excess CO_2 injection is sufficient to maintain a high CO_2 concentration near the injection well. The observed growth of the CO_2 plume, both horizontally and vertically (Figure 2-1 and Figure 2-2), indicate that a lower excess injection fraction can be used to maintain the CO_2 concentration near the well. This will slow the growth of the CO_2 plume in the shallow reservoir, which will minimally impact the performance of the reservoir. However, reducing the excess injection fraction will increase the mass flow rate during the production phase, increasing the power consumed.

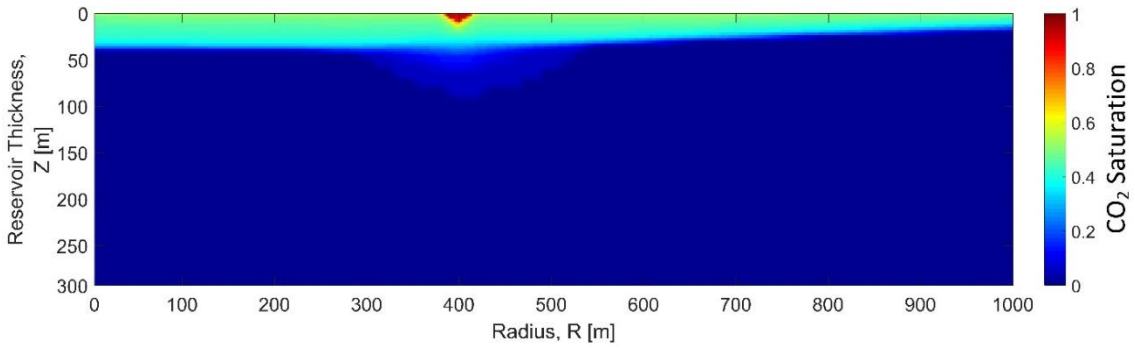

Figure 2-1: The shallow reservoir CO_2 saturation distribution with 5% extra CO_2 delivered each cycle. The CO_2 plume expands horizontally beneath the caprock due to the buoyancy of the CO_2, maintaining a high concentration near the well (located at the top of the reservoir at a radius of 400 meters).

2.2.2.2 Reservoir Heat Transfer

The heat extraction from the reservoir for each power-generation-energy-storage cycle, $Q_{reservoir}$, is defined by the product of the total circulated CO_2 mass, m_{CO2}, and the mean enthalpy difference, h_1-h_{10}, between the production and the injection wells, i.e.,

$$Q_{reservoir} = m_{CO2}(h_1 - h_{10}). \quad (2\text{-}1)$$

Each state point is defined in Figure 2-2. The fluid states at each well are given by the reservoir conditions. The circulated mass of CO_2 is defined as the amount of mass of CO_2 produced from the deep reservoir during the power generation mode.

In the shallow reservoir, the CO_2 injection temperature is nearly equal to that of the reservoir, so we assume isothermal conditions, i.e., we neglect heat transfer between the CO_2 and the rock within the shallow reservoir. In addition, heat transfer between the surrounding rock and the shallow reservoir well is essentially eliminated due to the single-well "Huff and Puff" approach. After several injection/production cycles, the reservoir near the well is thermally depleted and does not change the fluid temperature, justifying the assumption of isothermal conditions.

2.2.3 Power Plant Modeling

The main components of the direct CO_2-system plant are vertical wells, a turbine, cooling towers, throttling valves, and a pump. This configuration is illustrated in Figure 2-2, while Figure 2-3 shows the corresponding state points on a temperature-entropy, T-s, diagram, with the working fluid in the surface power plant also being the pure CO_2 that is produced from the reservoir. The parameters assigned to each component are consistent with Adams et al. [1,82] and are given in Table 2-2.

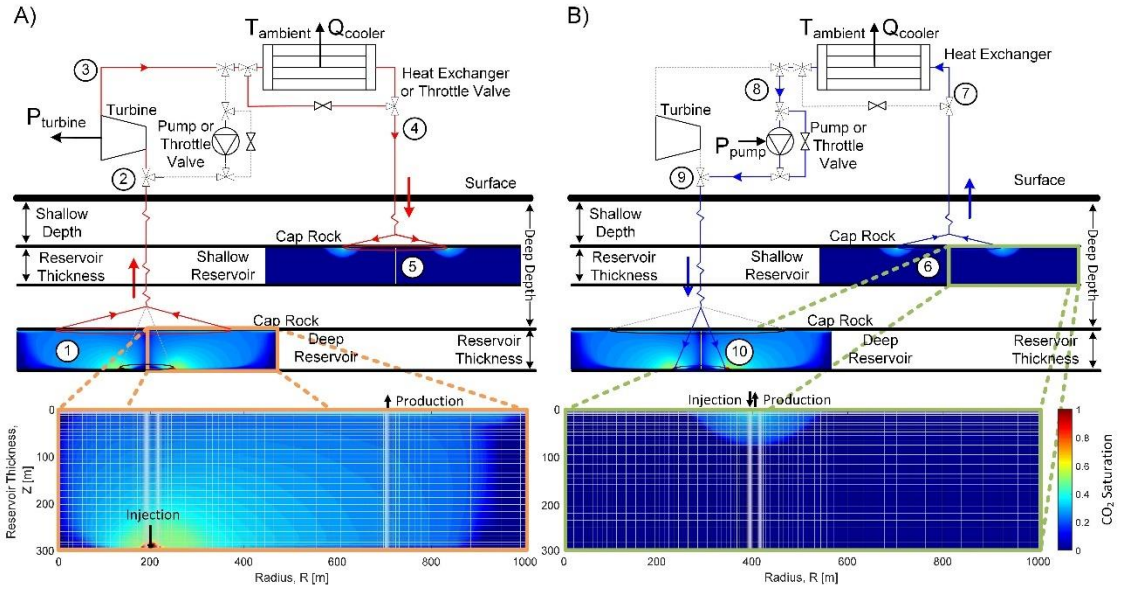

Figure 2-2: Schematic of the two operational modes of a CPGES system. In the production mode (A), power is generated by producing hot CO_2 from the deep reservoir, extracting thermal energy at the surface in an expansion device (turbine), and injecting the cooled CO_2 into the shallow reservoir. During the energy storage mode (B), power is consumed by extracting the CO_2 from the shallow reservoir, cooling and compressing it at the surface prior to injecting it into the deeper reservoir. CO_2 saturation in the shallow and in the deep reservoirs after the initial charging period, with the computational grid overlay are illustrated below the system schematic. The shallow reservoir exhibits limited CO_2 plume development, as only enough CO_2 is injected to displace the brine near the well. The deep reservoir exhibits significant CO_2 plume development so that the CO_2 reaches the production well, as required. The numerical grid is refined near the injection and production wells, near the caprocks, and, in case of the deep reservoir, near the baserock. The numerical grid spacing is increased logarithmically in the horizontal direction beyond 1 km, to the model boundary at 100 km, to reduce computational costs.

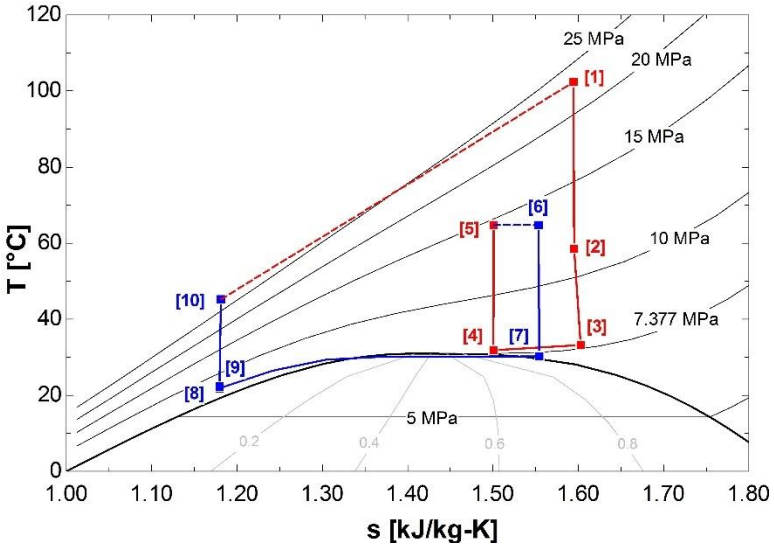

Figure 2-3: Temperature-entropy, T-s, diagram for CO_2, showing state points for a complete CPGES power generation (red: 1-5) and energy storage (blue: 6-10) cycle. The difference between State Point 5 and 6 is due to the transient pressure conditions at the well in the shallow reservoir, resulting from changing CO_2 mass flow rates and the temporal separation between the power generation and the energy storage modes. The CO_2 in the generation mode remains supercritical throughout the cycle, whereas, the storage mode may operate in the sub-critical region, particularly during the cooling operation.

Table 2-2: Plant parameters

System Parameters	
Ambient Temperature	15 °C
Daily Power Generation Duration	16 hours
Mass Flow Rate during Power Generation	200 kg/s
Daily Energy Storage Duration	8 hours
Mass Flow Rate during Energy Storage	380 kg/s
Well Internal Diameter	0.41 m
Turbine Efficiency	78%
Isentropic Pump Efficiency	90%

2.2.3.1 Energy Generation

The production process begins by extracting hot CO_2 from the deep reservoir at State 1 (Figure 2-3) through the deep horizontal production well. Four vertical wells connect the

deep horizontal well to the surface and the CO_2 rises buoyantly, i.e., without requiring pumping, and while adiabatically expanding, to the surface, reaching State 2. Four vertical wells are used to reduce the frictional losses, and maintain parity with previous 5-spot CPG models. To simulate the vertical wells, we employ the vertical CO_2 well model from Adams et al. [1,82], where we numerically integrate over the well length beginning at the deep reservoir, simultaneously solving the continuity, energy balance, and momentum equations. The frictional pressure losses are modeled using the Darcy-Weisbach relation, assuming a pipe surface roughness of 55 μm [124]. The model assumes an adiabatic, steady-state operation and does not include transients that occur during the transitions between the power generation and the energy storage modes. Supercritical CO_2 ($scCO_2$) properties are given in Span and Wagner [125].

At the surface, the $scCO_2$ is expanded to State 3 in the turbine to produce power (Figure 2-3). The turbine power output is determined as the product of the $scCO_2$ mass flow rate and the enthalpy difference between the turbine inlet, h_2, and outlet, h_3,

$$\dot{E}_{turbine} = \dot{m}_{generation}(h_2 - h_3). \quad (2\text{-}2)$$

The turbine is assumed to have an isentropic efficiency of η_t=78%, consistent with the CPG model of Adams et al. [1,82]. The back pressure of the turbine is held constant at 7.5 MPa, keeping the $scCO_2$ as a supercritical fluid at State 3. This is necessary to prevent multi-phase flow within the injection well (State 4), where the liquid and vapor phases could separate.

The processes from State 3 to 4 are governed by the downhole reservoir pressure, required to inject the $scCO_2$ into the shallow reservoir (State 5). The reservoir pressure is determined from the reservoir simulation. Depending on the required injection pressure (State 5), the $scCO_2$ is either isobarically cooled in a cooling tower, or isenthalpically expanded in a throttling valve to State 4. The heat extraction rate for the cooling towers is obtained by the product of the $scCO_2$ mass flow rate and the enthalpy difference of the $scCO_2$ across them,

$$\dot{Q}_{cooler,generation} = \dot{m}_{generation}(h_3 - h_4). \quad (2\text{-}3)$$

The parasitic power requirement for the operation of the cooling tower fans is determined as a fraction of the heat extraction rate from the cooling towers, given as

$$\dot{E}_{cooler,generation} = \lambda_{generation}\dot{Q}_{cooling}, \quad (2\text{-}4)$$

where the parasitic loss fraction, λ, is defined in the supplemental information in Adams et al. [1] for cooling and condensing towers.

The resultant reservoir injection pressure is determined by the gravitational compression process (i.e., self-compression, not requiring an injection pump) in the injection well. The CO_2 is injected into the shallow reservoir and is stored there until the energy storage, requiring parasitic power, mode commences.

During the power generation mode, some of the $scCO_2$ stored in the deep reservoir rises buoyantly to the surface so that no power-consuming pump is needed, although the cooling tower fans do consume some minor power (typically <4% of the turbine output). The net electric power is continuously generated by the turbine and is sent to the power grid. The

net power produced during the power generation mode is defined as the difference between the turbine power output and the parasitic losses due to the operation of the cooling tower fans,

$$\dot{E}_{net,generation} = \dot{E}_{turbine} - \dot{E}_{cooling,generation}. \quad (2\text{-}5)$$

2.2.3.2 Energy Storage (Power Consumption)

The energy storage mode produces $scCO_2$ from the same four vertical wells coming from the horizontal, circular well in the shallow reservoir (the same wells used to inject $scCO_2$ into the shallow reservoir) and uses the same cooling towers, a throttling valve, a pump, and four vertical wells that feed CO_2 to the horizontal, circular injection well in the deep reservoir (which is different from the deep reservoir production well) as shown by the blue lines in Figure 2-2B.

The CO_2 is extracted from the shallow reservoir (State 6) through the horizontal, circular well and the connected four vertical wells and rises adiabatically to the surface (State 7). The temperature of the produced $scCO_2$ (State 7) is slightly cooler (e.g. within 2°C) than the injected temperature (State 4), resulting from the decrease in pressure between CO_2 injection and recovery in the shallow reservoir. At the surface, the fluid is isobarically cooled in a cooling tower, extracting the majority of the thermal energy from the CO_2 and reducing its density prior to injection into the deep reservoir. The power consumed to operate the cooling tower fans is the product of the $scCO_2$ mass flow rate, the parasitic loss fraction, and the enthalpy change,

$$\dot{E}_{cooler,storage} = \dot{m}_{storage}\lambda_{storage}(h_7 - h_8). \quad (2\text{-}6)$$

At State 8, the $scCO_2$ leaves the cooling tower at an assumed approach temperature of 7°C above the ambient air temperature (e.g. 15°C + 7°C = 22°C) [1]. Depending on the required injection pressure (State 10), defined by the TOUGH2 reservoir model, the CO_2 is either expanded in a throttling valve, or compressed by a pump to State 9. The power required to operate the pump is calculated from the product of the $scCO_2$ mass flow rate and its enthalpy difference across the pump,

$$\dot{E}_{pump} = \dot{m}_{storage}(h_9 - h_8). \quad (2\text{-}7)$$

The pump is modeled using an isentropic efficiency of 90%, consistent with previous studies [1,82] .

The CO_2 is then adiabatically injected into the deep reservoir, using four injection wells. The CO_2 is then geothermally heated in the deep reservoir as it flows buoyantly from the deep horizontal injection well to the shallower horizontal production well (State 1).

During the energy storage mode, the system consumes electrical power available as excess power on the grid, with no power being generated. The power consumed is defined as the sum of the pump and cooling tower fan power required during the energy storage phase,

$$\dot{E}_{storage} = \dot{E}_{pump} + \dot{E}_{cooling,storage}. \quad (2\text{-}8)$$

2.2.3.3 CPGES System Performance

We describe the characteristic behavior of the CPGES system in terms of the net energy produced, the system efficiency, and the energy storage ratio. The net energy is the amount of energy produced over a complete cycle, defined as,

$$E_{Net} = E_{net,generation} - E_{storage}, \quad (2\text{-}9)$$

where $E_{net,generation}$ is the net electrical energy generated by the system during the power generation mode and $E_{consumption}$ is the electrical energy consumed during the energy storage mode.

The efficiency of the system, η_{system}, is defined as the energy output of the system, $E_{turbine}$, over the sum of all energy input into the system during an entire cycle, including the geothermal heat energy, $Q_{reservoir}$, the pump energy, E_{pump}, and the cooling fan energy during both energy storage, $E_{cooling,storage}$, and energy generation, $E_{cooling,generation}$, i.e.,

$$\eta_{system} = \frac{E_{turbine}}{Q_{reservoir}+E_{pump}+E_{cooling,storage}+E_{cooling,generation}}. \quad (2\text{-}10)$$

Next, we quantify the energy storage performance of a CPGES system by calculating its energy storage ratio, χ, as

$$\chi = \frac{E_{net,generation}}{E_{storage}+Q_{purchased}}, \quad (2\text{-}11)$$

where $Q_{purchased}$ is any additional heating during the power generation mode. As we do not consider additional heating during the CPGES operations discussed here, $Q_{purchased}$ is zero. The lack of supplemental heating reduces the system energy storage ratio to the ratio of net electrical energy generated, $E_{net,generation}$, and consumed, $E_{consumed}$. This differs from the CAES system, which uses heating from purchased fuel sources. Auxiliary heating of geothermally preheated fluids (e.g., water, brine, $scCO_2$), before they enter the turbine in a direct geothermal power plant system, similar to Garapati et al. [126] and Liu et al. [110], is beyond the scope of this paper.

2.2.3.4 Economic Performance

We demonstrate the economic value of using the CPGES system using historical, localized marginal prices (LMP) obtained from Midcontinent Independent System Operator (MISO) [127]. The historical LMP values are averaged over one-hour time intervals at each LMP node, from 1/1/2015 through 12/31/2015. From this data, an average LMP profile is constructed for a representative day, given in Figure 2-9.

The LMP value varies throughout the day with electrical demand and typically is larger during the daytime hours and lower at night. In the morning, between 12:00 am and 6:00 am, the LMP is reduced due to the limited electrical demand; with the daily minimum LMP value of $16.81/MWh occurring at 3:00 am. The peak price occurs at 6:00 pm at $29.02/MWh. The average daytime (6:00 am to 10:00 pm) LMP value is $27.50/MWh and the average nighttime LMP is $19.00/MWh. The CPGES takes advantage of this difference in LMP values by producing energy during the 16-hour period of elevated prices and consuming energy during the 8-hour period, when the electricity price is the lowest.

The CPGES system revenue is determined by the product of the instantaneous LMP and the amount of energy the system produces or consumes versus time throughout the day. It is also assumed that all power produced is purchased at LMP values. The net daily profit of the system is determined by the total system revenue over the 24-hour period. The CPGES system is compared to equivalent CPG systems.

2.3 Results

The results are presented in two parts. First, we present how the system performs over the first six years of operation. Then we present the results of the diurnal cycle, illustrating

how the system performs due to the intermittent production and storage processes. System performance is presented in terms of the component power, net system power, energy storage ratio, and the reservoir pressures. All results assume that the system operates each day for 16 hours in the energy production mode, followed by 8 hours in the energy storage mode.

2.3.1 System Transients (Daily Average)

This section details how the system will perform over the first 10 years of operation. The system operation begins directly following the completion of the initial CO_2 injection.

At the end of the charging period, the deep reservoir has an over-pressurization of 10.54 MPa and 7.08 MPa at the injection and production wells, respectively, while the shallow reservoir has an over-pressurization of 4.43 MPa at the injection/production well.

When the charging period ends and the system operation begins, the pressures at each well decrease and approach a steady operating pressure. The time required to achieve an average pressure for the deep production well, deep injection well, and shallow well to within 1% of the final average pressure (at 10 years) were 2.2, 6.2, and 0.7 years, respectfully. The configuration of the shallow reservoir, in addition to the limited CO_2 plume, limit the initial over pressurization and allow the reservoir to achieve the steady operating pressure before the deeper reservoir.

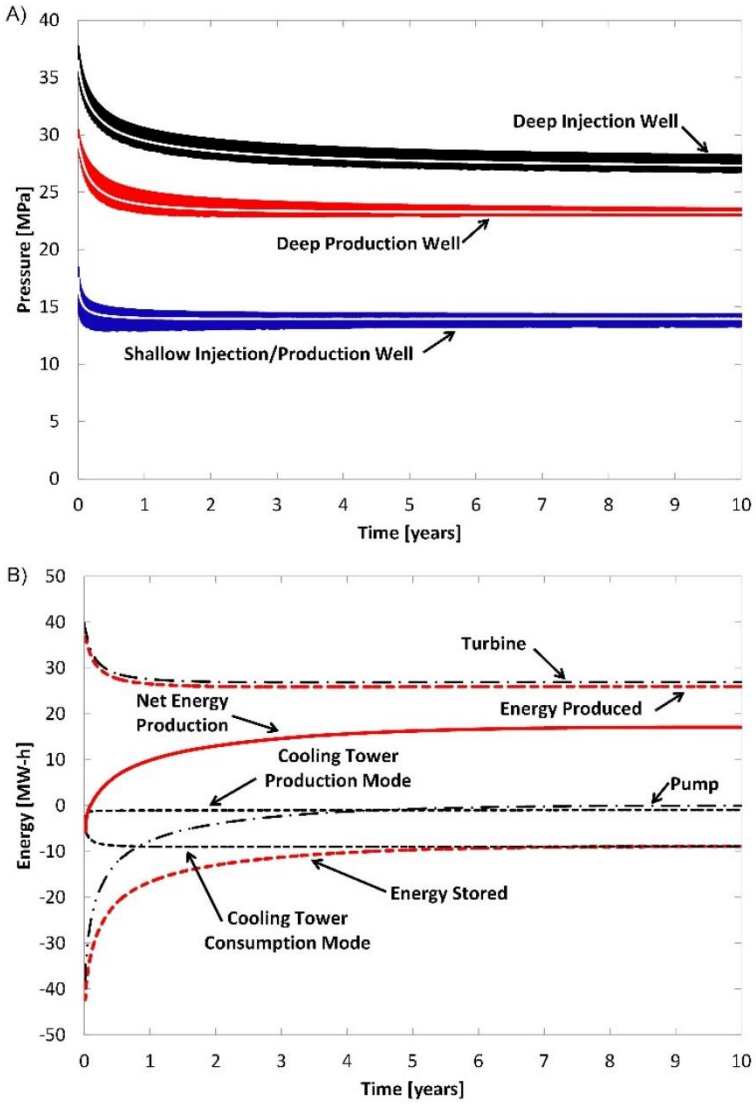

Figure 2-4: The resulting reservoir pressures (A) at the injection and production wells and the energy production and storage (B). The resulting variation in daily pressure is represented by the envelope thickness, and the average daily reservoir pressure is overlaid (white line). The energy contribution of each component is displayed in addition to the resulting energy production and consumption and the net daily system energy production.

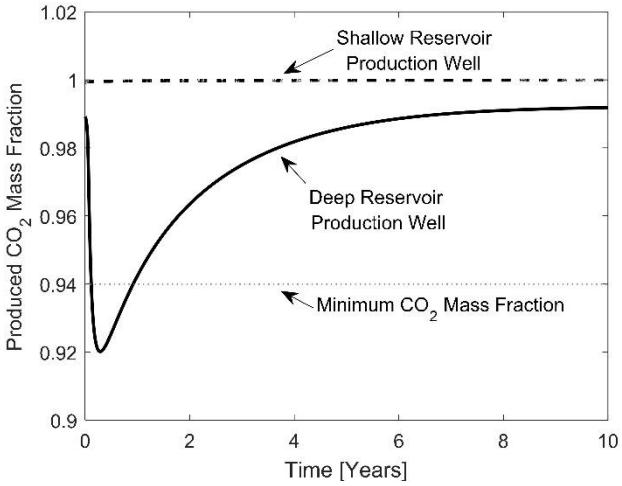

Figure 2-5: The CO_2 mass fraction of the produced fluid from the shallow and deep reservoir. The configuration of the shallow reservoir eliminates brine near the well, producing nearly pure CO_2 (i.e. > 99.7% mass ratio), whereas the deep reservoir experiences brine up-coning, particularly during the first year. The minimum accepted mass fraction of CO_2 is 94%, described in the text.

Figure 2-5 shows the produced mass fraction over time for each reservoir. The shallow reservoir configuration does not allow for the entrainment of brine in the produced fluid, having a minimum CO_2 mass fraction of 99.7%. The net injection of CO_2 during each cycle maintains the large CO_2 concentration near the well, and prevents brine from interacting with the produced fluid. The deep reservoir has a minimum CO_2 mass fraction of 91.9%, which is below the 94% approximation of Welch and Boyle [128] for specialized turbines, and may require the water to be separated at the surface upstream of the turbine, similar to geothermal systems using a flash cycle [65]. The mass fraction is less than the 94% approximation only during the first year of operation, indicating that use of a separator at the surface, may only be needed temporarily during the startup of the system.

At the beginning of the system operation, power generation and consumption are elevated relative to their steady values due to over-pressurization in the reservoirs. During this period, the system produces and consumes 41% and 372% more energy per day than at the steady operating conditions. The amount of energy produced and consumed decreases over time, as the pressure in the deep reservoir decreases. The daily energy production is steady after 1.5 years of operation, as the turbine and net daily energy production are within 1% of their respective 10 year values. In contrast, the energy consumption requires 7.7 years before achieving steady state, resulting from the over-pressurization at the deep reservoir injection well.

At the beginning of the system operation, the pump accounts for 90% of the total energy consumed, and is the primary source of energy consumption over the first 43 weeks. The pump is continuously run during the storage process for the first 80 weeks of system operation. After this point, the pump is used only when required by the system. After 7.5 years, the pump accounts for only 1% of the total energy consumed during the storage phase and after 9 years the pumping is insignificant (i.e. < 0.1%).

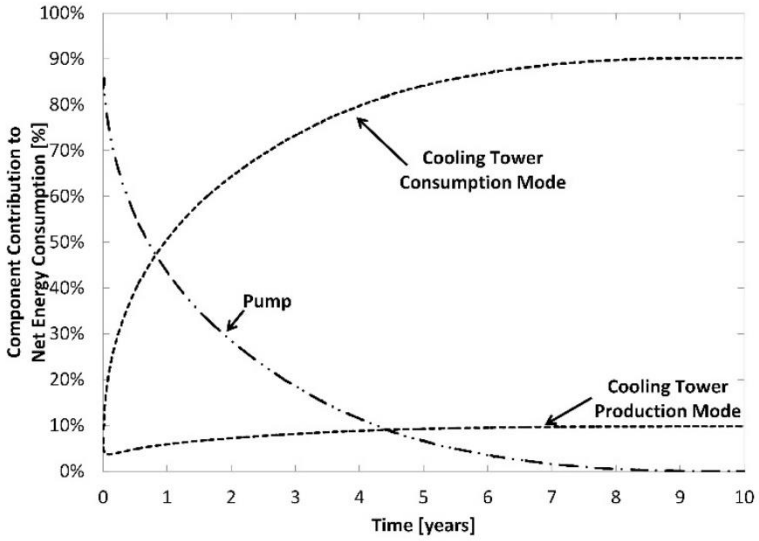

Figure 2-6: Power system component contribution to the overall energy consumption by the system. Initially, the pump is the primary consumptive element due to the elevated reservoir pressures. As the reservoir pressures become steady, the cooling tower fans (consumption) account for over 90% of the energy consumed. The production cooling tower fans account for less than 10% of the energy consumed.

For elevated reservoir pressures, the energy cost to compress the CO_2 is significant, and reduces the performance of the system. For our system, the initial large compression requirement could be mitigated by allowing the reservoir to rest after the initial CO_2 plume development; delaying the start of the CPGES system until the injection pressure diminishes, due to the dispersion of the CO_2 plume. Additionally, brine could be produced during the CO_2 plume development, using the over-pressurization of the reservoir to eliminate the need for downhole pumps [106].

The system is effective at separating power production from power consumption, although some power is consumed during energy production. In the generation mode, the cooling towers (production) consume only 4% of the total turbine energy produced, with the exception of the first three weeks, during which time they consume more energy due to the

elevated shallow reservoir pressure. This energy consumption, accounts for less than 9.8% of the total daily energy consumed by the cycle.

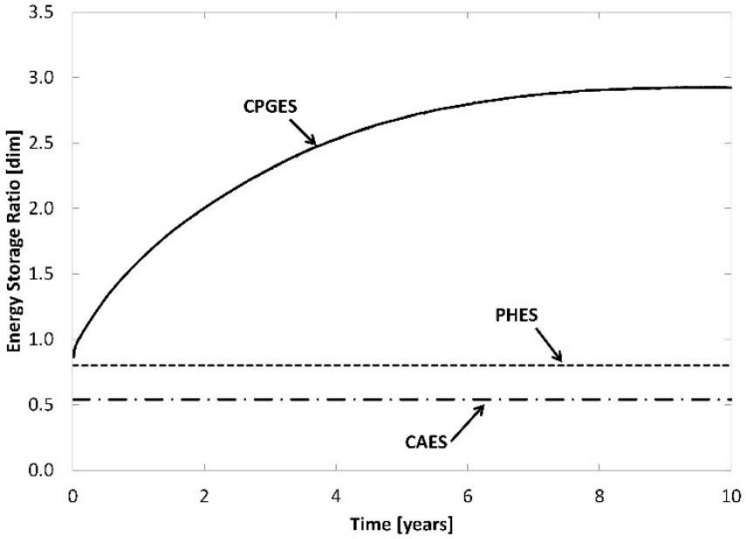

Figure 2-7: The energy storage ratio over the first 10 years of operation, compared with CAES and PHES. The system has a greater energy storage ratio than CAES and PHES, due to the geothermal heating in the deep reservoir. Results greater than one indicate that the system produces more electrical energy than it consumes. At 10 years the storage ratio is at a steady value of 2.92.

The decrease in both power production and power consumption over the first 10 years results in an increasing energy storage ratio (Figure 2-7). During the initial startup, the system consumes more energy than it produces, resulting in an energy storage ratio less than 1. This is caused by the large amount of power consumed by the pump during this initial time period. Over time, the energy storage ratio increases to a steady value of 2.92 mainly because the amount of power consumed by the pump decreases. The net electrical energy produced is larger than the electrical energy consumed. This net production of energy is a result of the geothermal energy added to the CO_2 in the deep reservoir that makes this system an intermittent heat engine.

2.3.2 Diurnal Cycle (Hourly Averages)

The system is able to time shift energy production and storage using a diurnal cycle. The results presented here, occur on a single day after 10 years of system operation.

The alternating generation and storage modes create a cyclical pressure variation, at each of the well locations, in the reservoirs due to the alternating mass flow conditions. The two system modes and the mass flow conditions can be seen in Figure 2-8a. The injection of CO_2 increases the pressure at each injection well, while the production of CO_2 decreases the pressure at each production well. In the deep reservoir, each well has a resting period, where CO_2 is neither injected nor produced. The resting phase counters the effects of the other phases, creating a cyclical pressure variation. This cycling of the reservoir well pressures, directly impacts the power electrical production and consumption of the system throughout the day (Figure 2-8).

In the energy production mode the net power varies as the reservoir pressure changes (Figure 2-8). The turbine power output is a function of the pressure difference across the turbine, and the turbine inlet pressure is related to the pressure of the fluid at the production well in the deep reservoir. Over the course of the 16-hour operation, the turbine power decreases slightly from 1.73 MW to 1.68 MW, corresponding with a decrease in pressure in the deep production well from 23.47 MPa to 23.04 MPa.

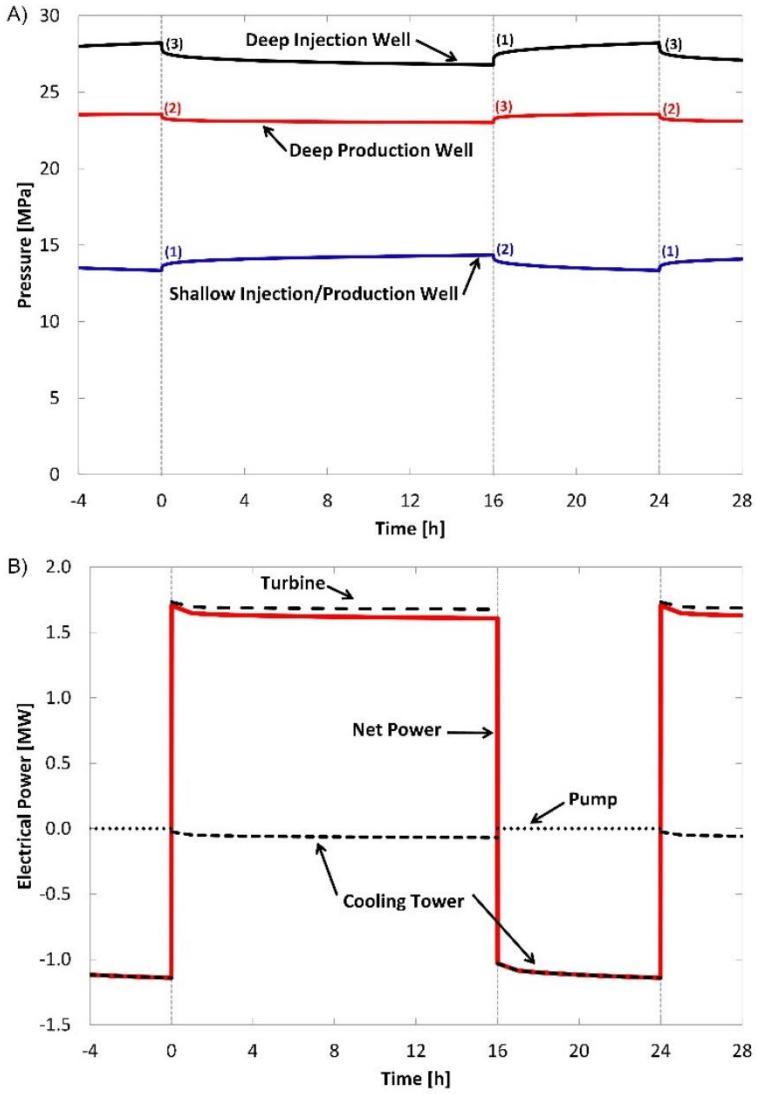

Figure 2-8: Reservoir pressure values during system operation for the representative diurnal cycle (A) and the net and component power output (B). The diurnal cycle illustrated shows a representative day, occurring 10 years after the system began operating. The pressure transients result from the mass flow conditions: (1) injection of CO_2, (2) production of CO_2, and (3) the resting period.

The power consumed during the production mode is limited to the cooling tower fans, which varies based on the pressure in the shallow reservoir, where an increase in pressure must be accompanied by an increase in the amount of cooling. For example, during the

16-hour production period, the pressure in the shallow reservoir increases from 13.45 MPa to 14.35 MPa, resulting in an increase in power consumption from 25.79 kW to 69.13 kW for the cooling tower fans.

Figure 2-8 shows the net power output decreases from 1.71 MW to 1.61 MW over the 16-hour production period. This decrease is a combination of decreasing turbine power and an increase in parasitic losses from the cooling tower. A single 16-hour production period results in 25.99 MW-h of energy. The turbine produces 26.95 MW-h of energy while the cooling towers consume 0.97 MW-h.

The power consumed in the storage mode is determined by the pressures in the shallow and deep reservoirs. The power required by the cooling tower is determined by the pressure in the shallow reservoir, where a decrease in pressure results in an increase in consumed power. Over the eight-hour storage mode, the amount of power required to operate the cooling tower fans increases from 1.03 MW to 1.14 MW, as the shallow reservoir pressure decreases from 14.35 MPa to 13.45 MPa. During the eight-hour energy consumption process, the system consumes 8.89 MW-h of electricity. For the given diurnal cycle, power is consumed by only the cooling tower fans; the pump does not operate and is replaced by an expansion valve. This occurs when the gravitational compression in the vertical well is sufficient to achieve the minimum required injection pressure.

Over a single cycle, the system uses the available geothermal energy to produce 17.10 MW-h of net energy with an energy storage ratio of 2.92 and an overall system efficiency of 6.45%. The cooling tower rejects 408.89 MW-h of waste heat throughout the cycle,

compared to the 25.99 MW-h of electric energy generated by the turbine. The system has a low thermal efficiency due to the low resource temperature, which results in a majority of the energy extracted from the deep reservoir being rejected through the cooling towers, similar to results of Adams et al. [1,82]. The intermittent injection and production of CO_2 from the reservoirs and the resulting pressure transients do not result in major variations in the power produced, with the net power decreasing at an average rate of 6.15 kw/h over the operation of the generation mode. The power consumed during the storage phase increases throughout the mode, at a rate of 13.85 kw/h. These results indicate that the system is capable of producing and consuming power consistently from the electrical grid for a diurnal cycle, allowing the system to provide stable energy storage for the grid. The stability of the power generation and consumption indicate that the system is capable of operating as an energy storage system over long periods of time and could operate with cycle duration's on the order of weeks, months, and possibly even seasonally.

2.3.3 Economics of CPG Energy Storage

Using the diurnal cycle discussed in Section 2.3.2 , along with the average LMP curve, the net daily profit is optimized by varying the time of day during which generation and storage modes occur. For a system with 16-hour production and 8-hour consumption, the maximum profit occurs when the production operation begins at 6:00 am and the storage operation begins at 10:00 pm, the resulting system revenue is shown in Figure 2-9.

Using the locational marginal price (LMP), the economic benefit of a CPG energy storage system is defined by comparing to the system baseline, that produces the same net energy per day as the CPGES system but produces power continuously throughout the day (i.e.

the system produces 0.71 MW continuously for 24 hours). The CPGES system has a 29.41% increase in daily income over the baseline system, illustrating the economic benefit of temporal arbitrage for the CPGES system.

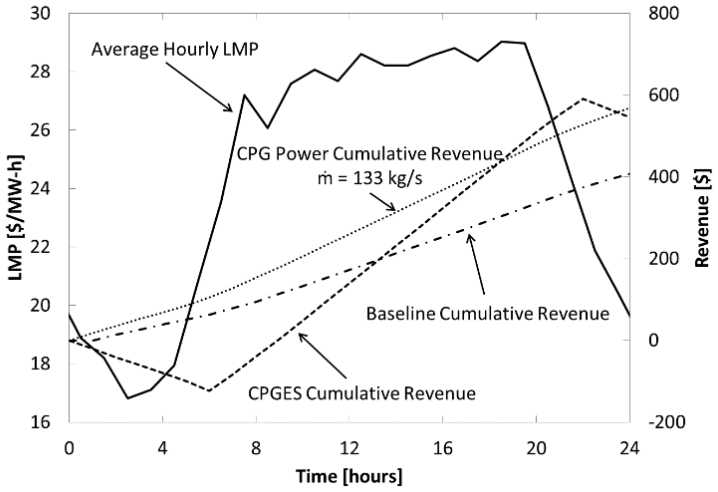

Figure 2-9: The average hourly localized marginalized price (LMP) from MISO for 2015 with the corresponding CPGES system cumulative revenue for the representative day shown in Figure 2-8. The system consumes electricity from 10:00pm to 6:00am and produces power from 6:00am to 10:00pm. The CPGES system was slightly outperformed by an equivalent CPG system, both in terms of net energy production and net revenue.

The CPGES system produced less cumulative daily revenue than an equivalent continuously operating CPG power system would, with the same reservoir parameters and well configuration in the deep reservoir. The CPG power system operates with a continuous mass flow rate of 133 kg/s, the same daily circulation rate that the CPGES system uses. After 10 years of operation, the CPG system produces 0.96 MW of power. This results in a 3.97% decrease in profit from the CPG system, indicating that the CPG

system performs slightly better economically than the CPGES system under the given market conditions.

To determine where the CPGES systems daily revenue outperforms the CPG system, the LMP data are simplified into average high and low LMP values, where the average high value occurs between 6:00am and 10:00pm. From these conditions the average high-low price differential where the CPGES system out performs the CPG system is determined.

The CPGES system out-performs the CPG power system when the average high LMP is 55.94% larger than the average low LMP value (Figure 2-10), indicating that the CPGES system is able to capitalize on the variation in LMP in these cases. This ratio remains constant within the range of expected average low LMP values. The LMP values presented in Figure 2-9 result in an average high and low LMP of $27.50 per MW-h and $19.00 per MW-h, respectively. This produces an average high LMP which is 47.8% larger than the average low LMP, slightly less than the 56.94% required to outperform the CPG system. To match the performance of the CPG system in this case, the average high LMP must be $29.263 per MW-h.

The power output of the CPGES system can be directly compared to the power produced by a CPG system using a LMP ratio of 1. The CPGES system incurs additional system losses when separating the operation of power production and consumption phases. These losses result in a 25.8% decrease in the amount of energy produced by the system. The decrease in energy production is a result of the alterations from the CPG system to operate as an intermittent system. The main contributions to the decrease in energy output are

associated with an elevated turbine back pressure compared to the CPG power system, the additional cooling required as a result of the elevated back pressure, and the addition of the shallow reservoir.

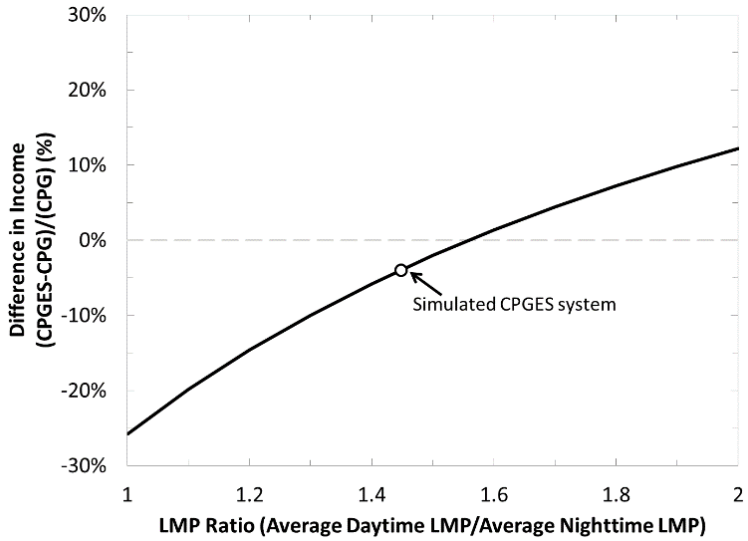

Figure 2-10: Difference in income between a CPGES system and a continuously operating CPG system under the same conditions versus daily average high and low electrical prices. Positive values represent conditions where the CPGES produces a greater daily revenue than the CPG system. The CPGES system preforms better in markets with larger variations in prices, using temporal price arbitrage.

2.4 Conclusions

A CPG system with two geologic reservoirs at different depths can be operated as an energy storage system that time shifts the periods of power generation and power consumption. Our modeling and simulation of a CPGES system allow for the following conclusions:

The CPGES system is able to separate power production and consumption periods operating as an intermittent Rankine Cycle, allowing the system to be used as a large-scale energy storage system. After ten years of operation, the 16-hour production mode of the system simulated here produces 26.0 MW-h. Minimal power consumption occurs during

the production period, where 3.6% of the gross turbine power is consumed by the cooling tower fans. The eight-hour power storage mode consumes 8.89 MW-h, resulting in a daily net energy production of 17.1 MW-h.

A CPGES system can deliver net electrical energy to the grid over a diurnal cycle (i.e. $\chi > 1$). The system simulated here began to provide net energy after five weeks of operation. After ten years of operation, the system provides 17.1 MW-h of energy over a single diurnal cycle with an energy storage ratio of 2.92, meaning the system produces more energy to the grid than it consumes. The system operates as an intermittent Rankine cycle, which produces net electrical power using a geothermal heat source. This process is similar to a CAES system that uses an intermittent Brayton cycle to provide power, however, the CPGES system uses a geothermal heat source rather than fossil fuels.

The initial injection of CO_2 over-pressurizes the deep reservoir which initially increases power consumption and decreases the energy storage ratio of the system. The initial injection of CO_2 is required to develop a plume and displace the native brine near the production well prior to the system operation, and results in a maximum over-pressurization of 12.18 MPa. Initially, the system operates with an energy storage ratio of 0.87 due to the additional pumping power required.

Reservoir management is required to maintain continuous operation of the CPGES system. Over time, the usable amount of CO_2 in each reservoir decreases due to advection and diffusion. Losses in the shallow reservoir are more critical and can be overcome by retaining a fraction of the injected CO_2. By retaining 5% of the injected CO_2, the CO_2

plume grew in the shallow reservoir and sufficient downhole pressures were maintained. This is an effective method to maintain sufficient CO_2 in the shallow reservoir; however, 5% was found to be more than necessary.

The CPGES system can be economically competitive with an equivalent CPG power system in terms of daily revenue. In this study, a CPGES system produces 74.20 % of the daily energy of an equivalent continuously operating CPG power system, and has a 3.97% decrease in the daily revenue from the CPG systems revenue, using temporal price arbitrage. This CPGES system will generate more revenue than the equivalent CPG power system when the average daytime (6:00 a.m. to 10:00 p.m.) price is 55.94% larger than the average night time price, indicating the benefit of operating the CPGES system in regions where large variations in hourly electrical prices occur.

Chapter 3: CPGES Diurnal vs. Seasonal Energy Storage

Published in Stanford Geothermal Workshop and reproduced with permission (Appendix: Copyright Reuse Permissions).

Fleming, M. R., Adams, B. M., Randolph, J. B., Ogland-Hand, J. D., Kuehn, T. H., Buscheck, T. A., Bielicki, J. M., Saar, M. O. (2018). High Efficiency and Large-scale Subsurface Energy Storage with CO_2. In 43rd Workshop on Geothermal Reservoir Engineering. Palo Alto, California. Retrieved from https://pangea.stanford.edu/ERE/pdf/IGAstandard/SGW/2018/Fleming.pdf

High Efficiency and Large-scale Subsurface Energy Storage with CO_2

Mark R. Fleming[1], Benjamin M. Adams[2], Jimmy B. Randolph[1,3], Jonathan D. Ogland-Hand[4], Thomas H. Kuehn[1], Thomas A. Buscheck[3], Jeffrey M. Bielicki[4], Martin O. Saar*[1,2]

[1]The University of Minnesota, Minneapolis, MN, USA; [2]ETH-Zurich, Zurich Switzerland; [3]TerraCOH Inc., Minneapolis, MN, USA; [4]The Ohio State University, Columbus, OH, USA; [5]Lawrence Livermore National Laboratory, Livermore, CA, USA.

Keywords: geothermal energy, multi-level geothermal systems, sedimentary basin, carbon dioxide, electricity generation, energy storage, power plot, CPG

Synopsis

Storing large amounts of intermittently-produced solar or wind power for later, when there is a lack of sunlight or wind, is one of society's biggest challenges when attempting to decarbonize energy systems. Traditional energy storage technologies tend to suffer from relatively low efficiencies, severe environmental concerns, and limited scale both in capacity and time.

Subsurface energy storage can solve the drawbacks of many other energy storage approaches, as it can be large scale in capacity and time, environmentally benign, and highly efficient. When CO_2 is used as the (pressure) energy storage medium in reservoirs underneath caprocks at depths of at least ~1 km (to ensure the CO_2 is in its supercritical state), the energy generated after the energy storage operation can be greater than the energy stored. This is possible if reservoir temperatures and CO_2 storage durations combine to result in more geothermal energy input into the CO_2, at depth, than what the CO_2 pumps

at the surface (and other machinery) consume. Such subsurface energy storage is typically also large scale in capacity (due to typical reservoir sizes, potentially enabling storing excess power from a substantial portion of the power grid) and in time (even enabling seasonal energy storage).

Here, we present subsurface electricity energy storage with supercritical carbon dioxide (CO_2) called CO_2-Plume Geothermal Energy Storage (CPGES) and discuss the system's performance, as well as its advantages and disadvantages, compared to other energy storage options. Our investigated system consists of a deep and a shallow reservoir, where excess electricity from the grid is stored by producing CO_2 from the shallow reservoir and injecting it into the deep reservoir, storing the energy in the form of pressure and heat. When energy is needed, the geothermally heated CO_2 is produced from the deep reservoir and injected into the shallow reservoir, passing through a power generation system along the way. Thus, the shallow reservoir takes the place of a storage tank at the surface. The shallow reservoir well system is a huff-and-puff system to store the CO_2 with as few heat and pressure losses as possible, whereas the deep reservoir has an injection and a production well, so the CO_2 can extract heat as it passes through.

We find that both the diurnal (daily) and seasonal (6 months) CPGES systems generate more electricity to the power grid than they store from it. The diurnal system has a ratio of generated electricity to stored electricity (called the Energy Storage Ratio) between 2.93 and 1.95. Similarly, the seasonal system has an energy storage ratio between 1.55 and 1.05,

depending on operational strategy. The energy storage ratio decreases with duration due to the pump power needed to overcome the increasing reservoir pressures as CO_2 is stored.

3.1 Introduction

The development of modern electricity systems that reduce the amount of carbon dioxide (CO_2) emitted into the atmosphere while producing steady, continuous power is one of society's biggest challenges. To limit the global mean temperature rise to 2°C, the Intergovernmental Panel on Climate Change (IPCC) has estimated that an atmospheric limit of 250 ppm of CO_2 results in a 50% chance of obtaining this temperature goal [5]. These regulations were agreed upon by a majority of nations in the Paris Agreement [111], allowing for an estimated 1000 GT of CO_2 to be emitted after 2011 [4]. This requires the immediate reduction, and eventual elimination of CO_2 emissions, to avoid exceeding this CO_2 emission limit. No single technology will provide the necessary reduction and elimination of CO_2 emissions; however, multiple technologies employed and integrated as a whole can provide the necessary reduction in CO_2 emissions. To reduce CO_2 emissions in the electricity sector, which accounts for 25% of the total CO_2 emissions, existing power plants can be retrofitted with CO_2 capture technologies and carbon-neutral power systems can replace existing generation [5,10].

To decarbonize existing power plants, CO_2 emissions can be captured, transported, typically via pipelines, to storage sites, and then injected into subsurface reservoirs, in a process referred to Carbon Capture and Storage (CCS). CCS reduces the emission of CO_2 into the atmosphere from sources such as fossil fuel power systems, cement factories, biofuel refineries, or from other large CO_2 point sources by permanently storing the CO_2

underground in deep saline aquifers or partially depleted oil/gas fields that can store large volumes of CO_2. The vertical leakage of the captured CO_2, which is naturally buoyant at the storage conditions, is contained by the overlying low-permeability caprock. In addition to structural trapping, CO_2 is stored in the reservoir due to capillary forces, dissolution into the underlying brine, and eventually the formation of carbonate minerals. Due to the depth of the storage formation, which is generally in excess of 800 meters to ensure supercritical CO_2 and maximize storage volumes, the average reservoir temperatures are greater than the temperature of the injected CO_2, and can be significantly greater, depending on the geothermal gradient, than the surface temperature, thus allowing the injected CO_2 to extract heat from the reservoir. This heat extraction process has led to the proposal of geothermal energy systems which can be combined with CCS, such as CO_2-Plume Geothermal (CPG), that directly uses the CO_2 as the heat extraction fluid, thereby operating as a Carbon Capture Utilization and Storage (CCUS) system, discussed in detail below.

In addition to CCS, renewable energy sources, such as wind and solar, can provide energy without fossil fuels, and their associated CO_2 emissions; however, these sources are variable power systems, capable of producing power only when the given resources are available. In 2016, wind had an annual capacity factor of 34.5%, while solar photovoltaic had a 25.1% capacity [19], due to the variability of their resources. The intermittent nature of these resources can provide challenges integrating these technologies into existing electrical grids by creating an excess or deficit in power generation, reducing the efficiency of the grid [112,113]. To provide baseload power, energy storage systems can be integrated

with the intermittent renewable sources to store excess power when it is generated, producing the energy at a later period when there is a demand for power [56,114]. With the expanded capacity of wind and solar, additional energy storage capacity is required to ensure electrical grid reliability. However, existing large-scale bulk energy storage systems, such as Pumped Hydroelectric and Compressed Air, may not have the ability to provide the expanded capacity that is required. Pumped Hydroelectric systems, have limited development opportunities resulting from environmental concerns regarding the development of the large surface storage reservoirs. Additionally, compressed air does not represent a sustainable long-term energy storage solution, as compressed air relies on auxiliary surface heating, typically from natural gas, to produce power, emitting CO_2 in the process. While these energy storage technologies have limitations, geothermal energy is widely available and can be accessed by CO_2-Plume Geothermal systems, which can be used to supplement wind and solar.

CO_2-Plume Geothermal (CPG) systems operate by producing hot CO_2, which is geothermally heated in natural high-permeability reservoirs, to the surface for power, or heat, generation [1,33,34,82,96]. The produced CO_2 is then reinjected into the reservoir, in a cold dense state, allowing the injected CO_2 to extract heat from the reservoir. CPG is different than CO_2-Enhanced Geothermal Systems (CO_2-EGS), which have previously been studied [81,87,90,91], as the CPG system uses natural high permeability sedimentary basins with a large storage volume, whereas CO_2-EGS requires artificially-generated, high-permeability reservoirs which are generally small and offer limited CO_2 storage capacity.

Operating a geothermal power system using CO_2 has several advantages, beyond the synergistic power production from a CCS site, including a low mineral solubility, high reservoir mobility (low kinematic viscosity), and a large density variation with temperature. A low mineral solubility is advantageous, as the produced fluid will contain minimal impurities and pipe scaling will be limited. A low kinematic viscosity increases the mobility of the CO_2 in the reservoir, allowing the fluid to move through the reservoir and extract heat, with reduced pressures losses. The larger variation in the density with temperature allows a geothermal system to operate as a thermosiphon, which is naturally occurring convective circulation of the CO_2 to the surface that reduces or eliminates the need for pumps. This is achieved by extracting hot, low-density CO_2 from the reservoir, cooling it at the surface, and then injecting cold, dense CO_2 into the reservoir, utilizing the density difference in each vertical well to create a pressure difference, thereby reducing or eliminating the need for circulation pumps in the system.

Here, we demonstrate how a CPG system can be modified to operate as a CO_2-Plume Geothermal Energy Storage (CPGES) system, storing energy over both diurnal and biannual periods, using a multi-reservoir approach, for a small demonstration-size plant, operating with CO_2-plume sizes consistent with previous work [1,82,83,119]. The CPGES system differs from previously proposed CO_2 based energy storage systems that include the CO_2-Bulk Energy Storage System (CO_2-BES) and the Compressed CO_2 systems. The CO_2-BES produces and stores energy using a multi-fluid approach using multiple concentric circular horizontal wells, where CO_2 is used as a cushion gas, displacing brine

and increasing the reservoir pressure to produce brine without downhole circulation pumps [106]. The compressed CO_2 system is similar the proposed CPGES system, using multiple reservoirs to time shift generation and consumption, however, the geothermal energy is used to pre-heat the fluid, with the majority of the heat added at the surface from a fuel source [110].

3.2 System Overview

The CPG system consists of injection and production wells, and a surface plant to convert the extracted heat into electrical power at the surface, and a permeable sedimentary reservoir that is overlain by a low-permeability caprock [33,34,96]. To produce power, the surface plant can directly expand the CO_2 in a turbine or operate it as a binary system in which the CO_2 is used to heat a secondary working fluid to produce power. However, the direct CPG system typically produces more power [1], and thus we consider only the direct CPG system here. In the direct system, CO_2 is extracted from the reservoir and produced at the surface in a vertical well. At the surface, CO_2 is directly expanded in a turbine, generating electrical energy, and is then subsequently cooled using wet cooling towers, increasing the density of the CO_2 for reinjection into the reservoir. After the cooling process, the CO_2 may be compressed using a circulation pump and then further compressed down the injection well to the reservoir. In the reservoir, the cold, dense CO_2 extracts heat as the CO_2 plume expands and moves away from the injection well. For the direct system, a circulation pump is not required to operate, as the system can operate using only a thermosiphon; however, a circulation pump increases the net power generation of the system [1,82].

The CPG system can be modified to operate as an energy storage system by adding a second shallow reservoir to store the CO_2 in an intermediate state after the turbine, but before the parasitic loads, separating the components that generate and consume power, illustrated in Figure 3-1. The CO_2-Plume Geothermal Energy Storage (CPGES) system operates using two modes:

1. **Power Generation**: Hot CO_2 is produced from the deep reservoir and brought to the surface in the vertical production well, and expanded in the turbine to produce power. After the turbine, the CO_2 is partially cooled only to the extent necessary to be stored in the shallow reservoir. With increased density, the CO_2 is injected into the shallow reservoir using only the gravitational compression in the vertical well. The shallow reservoir stores the CO_2 until the end of the generation mode.

2. **Energy Storage**: CO_2 is produced from the shallow reservoir and brought to the surface through the same vertical well, it is then cooled using cooling towers, compressed using a pump, and injected back into the deep reservoir through the vertical injection well.

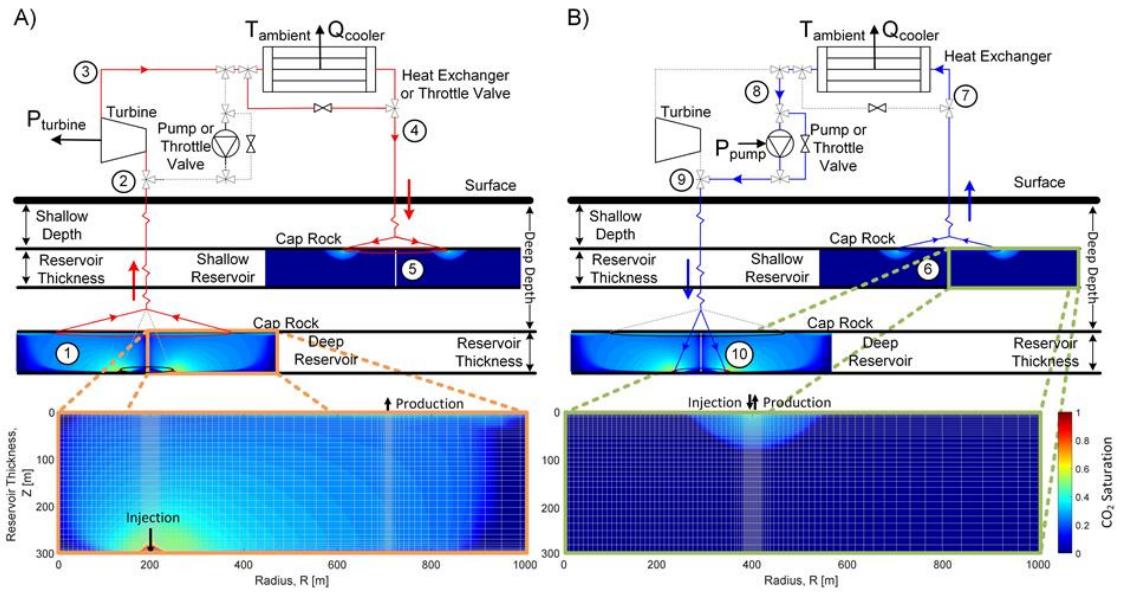

Figure 3-1: The CPGES system operates using two modes: A) Power generation where the system produces net power to the electrical grid and B) Energy Storage where the system consumes electrical power to cool and compress the CO_2. Power is produced by extracting CO_2 from the shallow reservoir to the surface, expanded in a turbine to produce power, partially cooled, and injected into a shallow, storage reservoir. To consume power the system extracts CO_2 from the shallow reservoir and produces it at the surface, where it is cooled and compressed before it is injected back into the deeper reservoir where the CO_2 is heated, extracting energy from the reservoir. The operation of each reservoir in the system is different and requires each reservoir to operate with an independent configuration. The shallow reservoir operates using a single well, that operates as both the injection and production well. The deeper reservoir, the thermal source for the system, operates with two horizontal-circular wells, allowing heat to be extracted from a significant portion of the reservoir. The CO_2 plume in each reservoir, with the computational grid overlaid, is displayed below the system diagram. The deep reservoir requires a significant CO_2 plume for operation, where the shallow reservoir operates using limited CO_2.

The CPGES system, like the CPG system, is a Rankine power cycle fueled by geothermal heat. As the CPGES system is a power cycle, the system generates more net energy to the grid than it consumes from the grid, due to the addition of the geothermal heat from the deep reservoir. Similarly, compressed air energy storage systems also generate more power to the grid than they consume, but they do this by combusting fossil fuel, emitting CO_2.

Thus, the CPGES system operates using geothermal energy, producing net power to the grid without CO_2 emissions.

3.3 System Modeling

We simulate the CPGES system using two separate models: the subsurface geologic reservoirs and a surface power plant. The subsurface reservoirs are simulated using TOUGH2 [120] with the ECO2N [121] equation of state and the surface power plant is modeled using Engineering Equation Solver (EES) [122]. We use two storage cycles: a diurnal cycle with power generation occurring for 16 hours and energy storage occurring for the remaining 8 hours, and a seasonal storage model, with a continuous power generation period followed by a continuous energy storage period, each operating for 3 months.

Table 3-1: Simulated physical properties for the numerical simulation.

Simulated Parameter/Value			
General Properties		Deep Reservoir	
Horizontal Permeability	5.0×10^{-14} m^2	Mean Reservoir Depth	2.5 km
Vertical Permeability	2.5×10^{-14} m^2	Mean Reservoir Temperature	102.5 °C
Thermal Conductivity	2.1 W/m/°C	Injection Well Radius	200 m
Porosity	10%	Production Well Radius	707 m
NaCl Concentration	20%	Number of grid cells, vertical	42
Geothermal Gradient	35 °C/km	Number of grid cells, horizontal	117
Surface Wet Bulb Temperature	15 °C		
Reservoir Thickness	300 m	Shallow Reservoir	
Rock Density	2650 kg/m^3	Mean Reservoir Depth	1.5 km
Rock Specific Heat	1000 J/kg/°C	Mean Reservoir Temperature	67.5 °C
Simulated Radius	100 km	Well Radius	400 m
Initial Conditions	Hydrostatic equilibrium, pore space occupied by brine	Number of grid cells, vertical	34
		Number of grid cells, horizontal	121

3.3.1 Reservoir Modeling

We numerically simulate each reservoir employing a three-dimensional, axisymmetric geometry, illustrated in Figure 3-1. Each model is bounded by an impermeable caprock above and bedrock below. To avoid radial boundary effects, the models are simulated out

to a radius of 100 km, similar to prior reservoir models [83]. Modeled reservoir properties are given in Table 3-1.

3.3.1.1 Deep Reservoir

The deep reservoir is the thermal source of the CPGES system, providing the heat that is converted to electricity at the surface, shown in Figure 3-1. To extract heat, CO_2 is injected in a cold, supercritical state at the injection well during the energy storage mode. The circular injection well is located at the bottom of the reservoir, just above the base rock with a radius of 200 meters from the center of the reservoir. Unlike previous models, a horizontal injection well is used instead of a vertical well to increase the CO_2 injection area, thereby reducing the pressure losses. The increased well length is particularly critical for the diurnal cycle simulated here, where the injection mass flow rate is twice as high as the produced mass flow rate. The injection well is located at the bottom of the reservoir to allow the buoyant CO_2 to sweep a majority of the reservoir rock before being removed. As the CO_2 moves away from the injection well, it extracts heat from the rock, buoyantly rising until it is captured beneath the caprock. During the generation mode, CO_2 is produced from the reservoir through a horizontal-circular production well that is located directly beneath the caprock at the top of the reservoir, at a radius of 707 meters from the center of the reservoir. The radius of the production well corresponds with previous CPG simulations [1,82,83].

The deep reservoir is initially filled with brine and is primed with CO_2 for 2.5 years. The injection rate is increased linearly over the first year from zero to 250 kg/s. For the next year and one-half, the injection rate remains constant at 250 kg/s. During this priming

period, 15.78 Mt of CO_2 is injected, with a final CO_2 gas saturation more than 30% at the production well. This results in a CO_2 mass fraction near the production well greater than 94% when production begins. After the development period, the intermittent operation of the generation and storage modes begins.

3.3.1.2 Shallow Reservoir

The shallow reservoir is used to store CO_2 produced during the generation mode, which is different from the deep reservoir, which is used to extract heat from the subsurface. In the shallow reservoir, a single well, which functions for both injection and production of CO_2, referred to as a "Huff and Puff" method, was selected to minimize the amount of CO_2 required to operate the reservoir and reduce the amount of CO_2 that is lost into the reservoir, due to advection and diffusion of the CO_2 plume. The single circular well is located at the top of the reservoir directly beneath the caprock at a radius of 400 meters from the center of the reservoir. The placement of the well at the top limits the vertical movement of the buoyant CO_2, allowing only horizontal expansion of the CO_2 plume and CO_2 diffusion into the brine, thereby retaining the majority of the CO_2 plume near the well.

Similar to the deep reservoir, the shallow reservoir is initially filled with brine and requires the CO_2 plume to be developed prior to the operation of the CPGES system. CO_2 is injected over 12 weeks by linearly increasing the injection rate from zero to 100 kg/s over the first two weeks and then sustaining this rate for the remaining 10 weeks, resulting in 0.76 Mt of CO_2. This plume development was needed to limit the amount of brine produced during the storage mode. As the CPGES system operates, some of the CO_2 plume will disperse

into the brine. Thus, the shallow reservoir retains 5% of the injected CO_2 from each cycle to maintain the plume.

3.3.2 Surface Modeling

The surface model includes the vertical wells, turbine, pump, throttling valves, and cooling towers. The surface model is numerically coupled with the reservoir model at the injection and production wells by the reservoir pressures from the TOUGH2 models.

The vertical well model has been previously documented [1] and is briefly summarized here. The vertical well is numerically integrated over 100-meter elements, solving the continuity, energy balance, and momentum equations for CO_2, neglecting the kinematic effects in the energy equation. Each element is assumed to be adiabatic [129], and pipe friction is modeled using the Darcy-Weisbach relation, assuming a surface roughness of 55 μm [130]. To reduce pressure losses, each horizontal well is connected to the surface by four vertical wells.

At the surface, CO_2 is expanded in a turbine to produce power, given as,

$$\dot{E}_{turbine} = \dot{m}_{generation}(h_2 - h_3), \tag{3-1}$$

where $\dot{m}_{generation}$, $\dot{E}_{turbine}$, and h are the mass flow rate during the generation mode, the power produced by the turbine, and the enthalpy of the fluid, respectively. Enthalpy state points are defined in Figure 3-1. The turbine outlet enthalpy, h3, is calculated with an isentropic efficiency of 78%, consistent with previous CPG models [1,82]. The turbine back pressure is maintained at 7.5 MPa so the produced CO_2 remains in a supercritical state to prevent multiphase CO_2 from entering the vertical well at state point 4.

The circulation pump, which is used during the storage mode, consumes power, defined as,

$$\dot{E}_{pump} = \dot{m}_{storage}(h_9 - h_8), \tag{3-2}$$

where $\dot{E}_{pump}$, $\dot{m}_{storage}$, and h are the pumping power, the mass flow rate during the storage mode, and the enthalpy, respectively. The circulation pump outlet enthalpy, h_9, is calculated using an isentropic efficiency of 90%.

The CO_2 is cooled at the surface using cooling towers.

$$\dot{Q}_{cooler,generation} = \dot{m}_{generation}(h_3 - h_4), \tag{3-3}$$

$$\dot{Q}_{cooler,storage} = \dot{m}_{storage}(h_7 - h_8), \tag{3-4}$$

where $\dot{Q}_{cooler,generation}$, $\dot{Q}_{cooler,storage}$, $\dot{m}_{generation}$, $\dot{m}_{storage}$, and h represent the heat transfer rate during the generation and storage modes, the mass flow rate during the generation and storage mode, and the enthalpy of the CO_2, respectively. The cooling towers must consume power to operate the cooling tower fans. We model this parasitic power consumption as a fraction of the heat transfer rate in the cooling tower, defined as,

$$\dot{E}_{cooler,generation} = \lambda_{generation}\dot{Q}_{cooler,generation}, \tag{3-5}$$

$$\dot{E}_{cooler,storage} = \lambda_{storage}\dot{Q}_{cooler,storage}, \tag{3-6}$$

Where $\dot{E}_{cooler}$ and λ are the cooling tower power consumption and the cooling tower loss fraction, respectively. The cooling tower loss fraction is a function of the cooling tower approach temperature and the ambient wet bulb temperature, and is defined in Adams et al. (2015) for both cooling and condensing towers.

The surface throttling valve, which can replace the cooling tower in the generation mode or the pump in the storage mode, is modeled as an isenthalpic process.

3.3.3 System Performance

The net power that is produced during the generation mode is defined as the difference between the turbine power generated and the generation cooling tower consumption, given as,

$$\dot{E}_{net,generation} = \dot{E}_{turbine} - \dot{E}_{cooling,generation}, \tag{3-7}$$

where $\dot{E}_{net,generation}$ is the net power that is produced during the generation mode. The net energy produced during the generation mode is the integral of the net power generated over the duration of the generation mode, defined as,

$$E_{generation} = \int_0^{t_{generation}} \dot{E}_{net,generation} dt, \tag{3-8}$$

where $E_{generation}$ and $t_{generation}$ are the net energy generated by the system during the generation mode and the duration of the generation mode, respectively.

Similarly, the net power consumed during the storage phase is defined as the sum of the power consumed by the cooling towers and the pump, defined as,

$$\dot{E}_{storage} = \dot{E}_{pump} + \dot{E}_{cooling,storage}, \tag{3-9}$$

where $\dot{E}_{storage}$ is the total power consumed during the storage mode. The net energy consumed by the system during the storage phase is found by integrating the total power consumed over the duration of the storage mode, given as,

$$E_{storage} = \int_0^{t_{storage}} \dot{E}_{storage} dt, \tag{3-10}$$

where $E_{storage}$ and $t_{storage}$ are the net energy consumed during the storage phase and the duration of the storage mode, respectively.

The net energy that is produced by the system is defined as the difference between the generated energy during the generation mode and the energy consumed during the storage mode, given as,

$$E_{Net} = E_{net,generation} - E_{storage}, \tag{3-11}$$

where E_{Net} is the net energy that is produced by the system over a complete generation and storage cycle.

We define the energy storage performance of the CPGES system using the energy storage ratio as the ratio of the net energy generated during the production mode divided by the net power consumed during the storage mode,

$$\chi = \frac{E_{net,generation}}{E_{storage}+Q_{\,purchased}}, \tag{3-12}$$

where χ and $Q_{\,purchased}$ are the Energy Storage Ratio and the additional surface heating during the power generation mode, if used. The CPGES system does not require additional surface heating to increase the temperature of the fluid prior to entering the turbine. This differs from compressed air energy storage systems, which do require additional heat, typically from purchased fossil fuels, to produce power during the generation mode.

3.4 Results

We demonstrate how the CPGES system will operate for a diurnal cycle and a biannual cycle. The performance of the system is characterized in terms of the reservoir pressures,

component power, net system power, and the energy storage ratio, summarized in Table 3-2.

The following results occur after ten years of system operation. The diurnal cycle results represent values occurring for a single 24-hour period (i.e. year 10.0000 to 10.0027). Similarly, the seasonal cycle results represent values occurring for a 6-month period after ten years of operation (i.e. year 10.0 to 10.5).

Table 3-2: Summary of the key performance characteristics of the CPGES system.

Generation Time	Storage Time	Generation Mass Flow Rate (kg/s)	Storage Mass Flow Rate (kg/s)	Generation Average Net Power (MW)	Storage Average Net Power (MW)	Energy Storage Ratio (MW-h/MW-h)
16 hours	8 hours	200	380	1.63	1.11	2.93
16 hours	8 hours	300	570	2.29	2.33	1.95
3 months	3 months	200	190	1.50	0.99	1.55
3 months	3 months	300	285	1.97	1.87	1.05

Several trends are immediately apparent in these results: the energy storage ratio decreases with increased mass flow rate; the average generation and storage power increase with mass flow rate, and increasing the overall cycle period (i.e. from one day to six months) decreasing the energy storage ratio. However, in all cases, the energy storage ratio of the system is still greater than unity. Below, we discuss these results in detail.

3.4.1 Diurnal Cycle

The CPGES system can operate on a diurnal cycle, producing and consuming power during a 24-hour period. To simulate a diurnal cycle, the system generates power for 16 hours and stores power for 8 hours. These time periods correlate with periods where the cost of electricity are elevated and reduced [127]. The storage mass flow rate, listed in Table 3-2, is selected to retrieve 95% of the CO_2 stored in the shallow reservoir back into the deep reservoir. This process continuously deposits small amounts of CO_2 into the shallow

reservoir to maintain high CO_2 saturation near the well, making up for CO_2 that has diffused away into the reservoir.

Figure 3-2 shows the varying reservoir pressures over a 24 hour period (Figure 3-2A and 3.2B) and the corresponding power generation and storage (Figure 3-2C and 3.2D). Figure 3-2A and 3.2C show results for a 200 kg/s generation mass flow rate and Figure 3-2B and 3.2D show results for a 300 kg/s generation mass flow rate.

Figure 3-2A shows that the injection of CO_2 into each reservoir increases the pressure at each injection well downhole, while the production of CO_2 from each reservoir decreases the pressure at each production well downhole. In the deep reservoir, only one of the wells is active during each mode, while the other is stopped. Despite there being no flow in a production or injection well at various times, the stopped well downhole pressure will vary, based on the activity from the other well. Over a complete cycle, the downhole pressure at the deep reservoir varies from 23.01 MPa to 23.57 MPa, and 22.24 MPa to 23.46 MPa for the production well, and 26.78 to 28.22 and 26.94 MPa to 28.98 MPa for the injection well, while the shallow reservoir varies from 13.34 MPa to 14.35 MPa, and 13.19 MPa to 14.63 MPa for generation mass flow rates 200 kg/s and 300 kg/s, respectively.

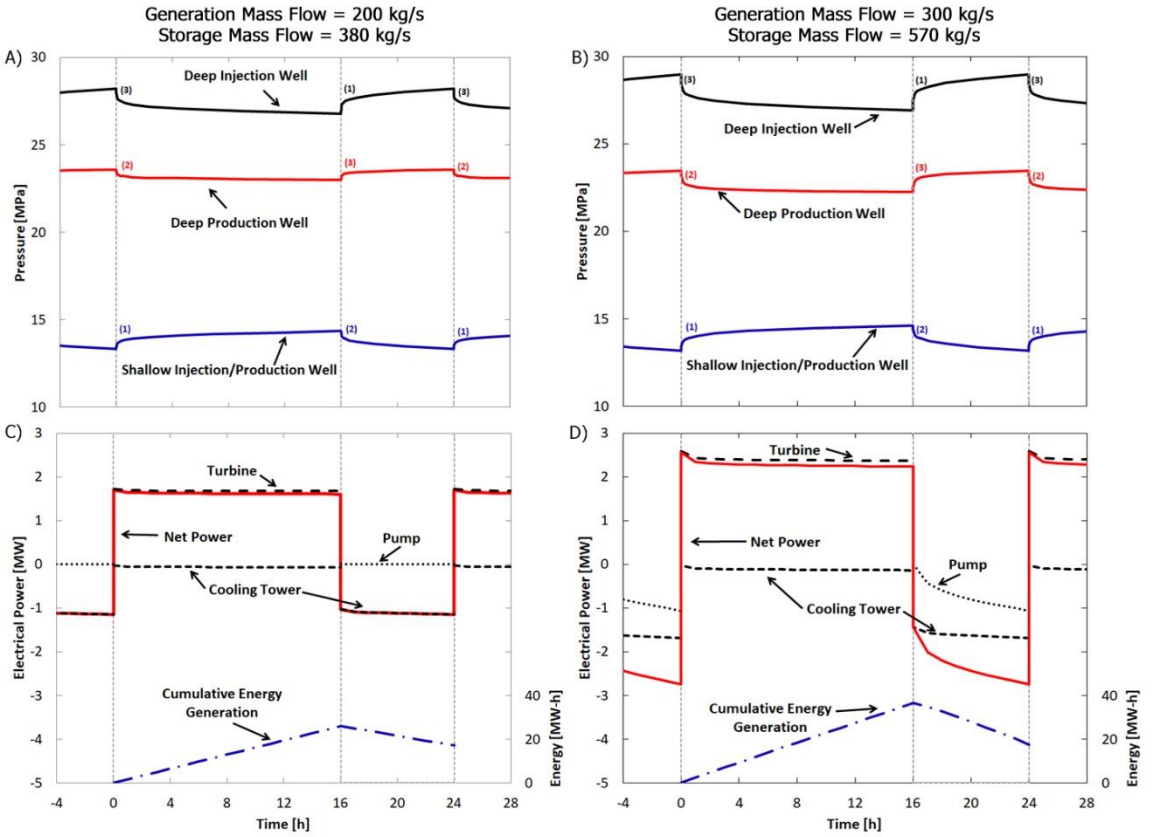

Figure 3-2: The transient reservoir pressure (A, B) and power (C, D) performance of the CPGES system for a single diurnal cycle after ten years of intermittent operation for the 200 kg/s (A, C) and 300 kg/s (B, D) mass flow rate cases. The pressure transients result from the mass flow conditions: (1) injection of CO_2, (2) production of CO_2, and (3) the resting period where no CO_2 is injected or produced. The power production and consumption are directly impacted by the reservoir conditions, varying with the reservoir pressures. The system operates in the generation mode for the first 16 hours, followed by the energy storage mode for 8 hours.

Figure 3-2C and 3.2D show that the system produces steady power during the generation mode, despite the variation in the reservoir pressures in Figure 3-2A and 3.2B. The net power produced varies from 1.71 MW to 1.61 MW for the 200 kg/s generation case (Figure 3-2C) and 2.57 MW to 2.24 MW for the 300 kg/s generation case (Figure 3-2D). In both cases, over 60% of the variation in the net power generated occurred within the first hour

of operation, due to the large variation in pressure at each well during this time, thus the system generates consistent power for the remaining 15 hours of the generation period.

Alternatively, the power consumed during the storage period is steady only for the 380 kg/s storage case (Figure 3-2C) but continuously increases for the 570 kg/s storage case (Figure 3-2D). This difference is a result of operating the pump, which is required in the 570 kg/s case. For the storage mass flow rate of 380 kg/s, the pump is not required during the storage mode, and the power is consumed by the cooling towers, which increase from 1.03 MW to 1.14 MW over the 8 hours of the storage mode. In the case with the 570 kg/s storage mass flow rate, pumping is required and the power stored increases from 1.43 MW to 2.74 MW over the duration of the mode, with the cooling towers increasing from 1.43 MW to 1.68 MW while the pump increases from 0 MW to 1.06 MW. Thus, the majority of the storage power increase is caused by the required pumping.

Normally, the injection temperature of the CO_2 is used to control the downhole pressure. As the injection temperature decreases, the density increases, and therefore the downhole pressure, which is the product of density, gravitational constant, and reservoir depth, also increases. However, the injection temperature is limited by the sum of the ambient temperature and the approach temperature, thereby limiting this pressure rise that can be achieved by gravitational compression. Thus, for this 570 kg/s case (Figure 3-2D), the pump is used to increase the injection pressure beyond what can be achieved by gravitational compression alone. Over the duration of the storage mode, the downhole

injection pressure increases as CO_2 is injected, therefore pump power will always rise when pumping is required in the storage mode.

The net energy produced during the generation mode increases from 25.99 MW-h to 36.47 MW-h when the generation mass flow rate increases from 200 kg/s to 300 kg/s, while the amount of energy consumed during the storage mode increases from 8.89 MW-h to 18.85 MW-h. Despite these differences, both cases have similar net daily energy generation, with the 200kg/s and 300 kg/s cases producing 17.1 MW-h and 17.6 MW-h, respectively. The resulting energy storage ratios are 2.93 and 1.95 for the 200 kg/s and 300 kg/s generation cases, respectively. The system operates with an energy storage ratio greater than one, meaning the energy generated by the system was greater than the energy that was stored. This occurs because the system operates both as a geothermal electricity plant and as an energy storage plant. Thus, the additional power generated is produced from the geothermal heat input from the deep reservoir.

The similar daily generation values of 17.1 MW-h and 17.6 MW-h are due to the 112% increase in pumping required from the 200 kg/s to the 300 kg/s generation case, while the power generation increases by only 40%. For further increases in mass flow rate, it is expected that the power consumed by the pump will increase at a greater rate than the power generated, resulting in an “optimal” mass flow rate at the peak of net daily energy generation, similar to the CPG system [1]. For this configuration, this maximum net daily energy occurs at a mass flow rate between the 200 kg/s and 300 kg/s generation cases.

While the net daily energy generation can be maximized, the system may be operated to maximize different quantities. For example, the magnitude of energy generated and stored will continue to increase with increasing mass flow rates, despite a decreasing net energy produced. Thus, if the prices of electricity during storage and generation modes are sufficiently extreme, the system may be operated at higher mass flowrates, decreasing overall net energy produced, but maximizing revenue.

3.4.2 Seasonal Cycle

The period of storage for a CPGES system is not limited to a 24-hour period. CPGES may be used to store energy for weeks or months when electricity is expensive and later generate when prices decline. Therefore, to illustrate the variable-term energy storage potential of the CPGES system, we demonstrate the operation of a system at the long-term extreme, a biannual or seasonal cycle. This seasonal system operates using the same parameters and configuration as the diurnal cycle; however, we simulate continuous generation for 3-months followed by continuous storage for 3-months.

Figure 3-3 shows the variation in reservoir pressures for the 200 kg/s (Figure 3-3A) and the 300 kg/s (Figure 3-3B) generation mass flow rates. The instantaneous electric power and cumulative energy generated are shown for the 200 kg/s (Figure 3-3C) and 300 kg/s (Figure 3-3D) generation mass flow rates. The duty cycle of this seasonal system is 50%, unlike the 67% duty cycle of the diurnal system; thus, the storage mass flow rate is only 95% of the generation flow rate.

Figure 3-3A and 3.3B show that the variation in the downhole pressure at each well is greater than for the diurnal cycle, due to the larger volume of CO_2 that is injected or

removed from each reservoir. For example, in the 200 kg/s generation mass flow rate case (Figure 3-3A), the pressure varies between 21.3 MPa and 25.5 MPa for the deep production well, compared to 23.0 MPa and 23.6 MPa in the diurnal cycle. Similarly, in the 300 kg/s generation mass flow rate case (Figure 3-3B) the downhole pressure varies between 18.8 MPa and 26.8 MPa, compared to 22.4 and 23.5 MPa in the diurnal cycle. This large variation in pressure causes a corresponding variation in the power generation or consumption in each case.

Figure 3-3C and 3.3D show that the instantaneous power generation decreases over the course of the generation period from 1.97 MW to 1.46 MW for a mass flow rate of 200 kg/s (Figure 3-3C), and 3.21 MW to 0.95 MW for a 300 kg/s mass flow (Figure 3-3D). This decrease in power generation occurs as a result of two factors: a decrease in turbine power due to the pressure drawdown of the deep reservoir at the production well, and an increase in the cooling tower power, due to a downhole pressure rise in the shallow reservoir. Over the course of the generation mode, the system generates 3.34 GW-h and 4.31 GW-h of energy for the 200 kg/s and 300 kg/s generation cases, respectively. When considered over 3 months of operation, this system generates on average 1.54 MW and 1.57 MW for the 200 kg/s and 300 kg/s cycles, respectively, which are lower than the diurnal cycle values of 1.63 MW and 2.29 MW.

The seasonal cycle differs from the diurnal cycle primarily due to the increased pumping and cooling tower loads during the storage mode, shown as the negative electric power values in Figure 3-3C and 3.3D. The amount of power that the system stores increases from

0.33 MW to 1.76 MW between the start and end of the 200 kg/s case, and similarly increases from 0.47 MW to 3.53 MW between the start and end of the 300 kg/s case, storing 2.15 GW-h and 4.09 GW-h over the entire cycle. When considered over the 3 months of operation, this amounts to an average of 0.99 MW and 1.87 MW for the 200 kg/s and 300 kg/s cycles, respectively, which are less than the diurnal cycle average values of 1.11 MW and 2.33 MW. However, due to the variation in the generation duty cycle and the associated change in storage mass flow rate, the seasonal system operates with higher energy consumption per cycle period than the diurnal, even though the instantaneous power generation is lower than the diurnal cycle.

When the total generation energies are divided by the total storage energies, the seasonal cycle has energy storage ratios of 1.55 and 1.05, for the 200 kg/s and 300 kg/s cases, respectively. These energy storage ratios are significantly lower than the diurnal cycle values of 2.93 and 1.95, due to the increase in the storage energy consumption, the decrease in the generation energy output, and variation in the duty cycle. For example, by the end of the 300 kg/s cycle, the power consumed by the cooling tower exceeded 46% of the total turbine power.

In these seasonal cases, the elevated downhole deep injection well pressure requires larger pump power than the diurnal cases. Over the duration of the three-month storage period, the pump consumes 1.2 GW-h for the 200 kg/s case and 2.67 GW-h for the 300 kg/s case, or 26% and 44%, respectively, of the total energy generated by the turbine. In contrast, the pump consumes 0% and 15% of the total power generated by the turbine the diurnal phase.

Thus, the pump operation is a key factor that decreases the energy storage ratio in the seasonal cycle.

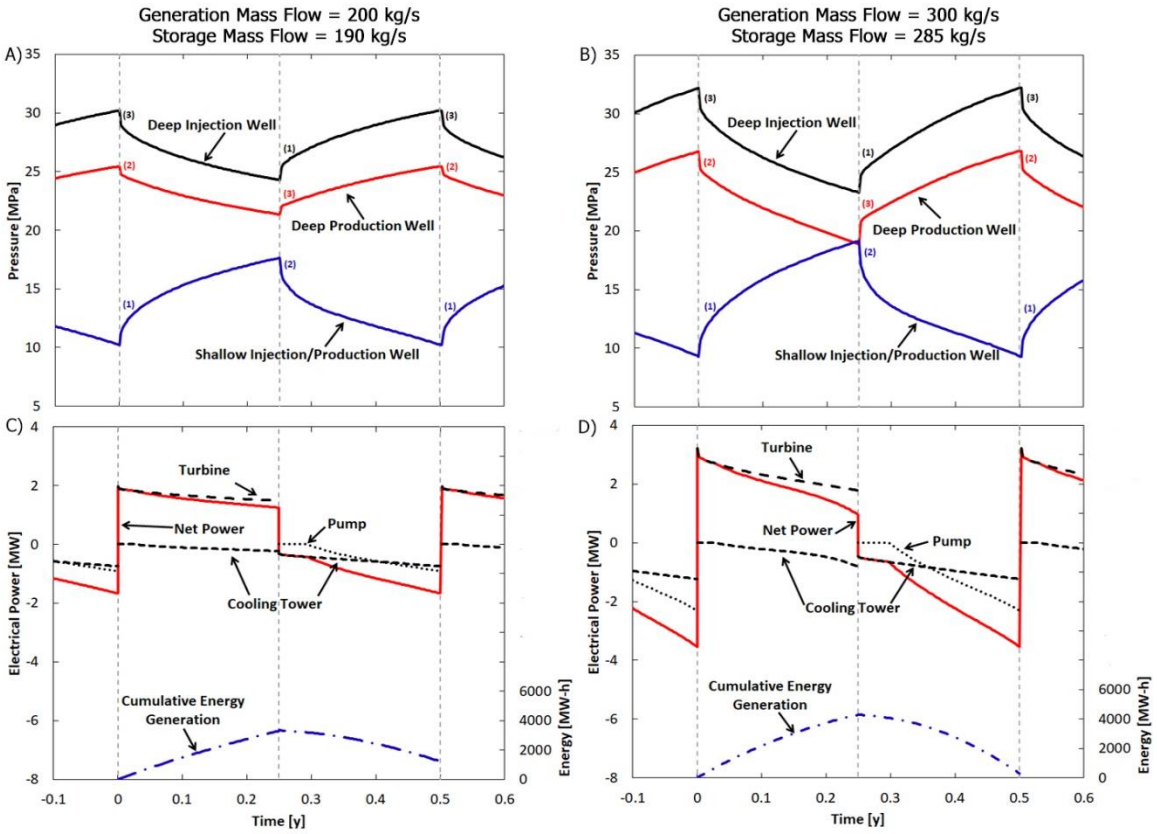

Figure 3-3: The pressure (A, B) and power (C, D) performance of the CPGES system for the long-term storage cycle for a single cycle for the 200 kg/s (A, C) and 300 kg/s (B, D) mass flow rates. The system is illustrated after 10 years of energy storage operation. The pressure transients result from the mass flow conditions: (1) injection of CO_2, (2) production of CO_2, and (3) the resting period where no CO_2 is injected or produced. The power transients result from the variation in the reservoir pressures at each well, which results from the intermittent injection and/or production of CO_2 in the reservoir.

While the elevated storage-phase power (i.e. cooling tower and pump) accounts for most of the decrease in energy storage ratios of the seasonal system, the non-zero cooling tower power during the generation phase also contributes to this decrease. The energy storage

ratio of the CPGES system can be greater than zero because the components which generate the power (i.e. turbine) can be temporally offset from the components which consume power (i.e. cooling towers and pumps). When some power consumption is needed during the generation mode, as occurs in the 300 kg/s case (Figure 3-3D), this reduces the decoupling of generation and consumption components, decreasing the energy storage ratio. One option that could be used to reduce the generation phase cooling tower power consumption would be a significantly larger well radius in the shallow reservoir. The large radius would increase the accessible volume which would decrease the reservoir pressure, reduce the required pre-injection cooling, and ultimately increase the energy storage ratio.

3.5 Implications

The CPGES system can operate over a range of energy storage cycle durations, as demonstrated here in terms of a diurnal and biannual (seasonal) cycles, which illustrate a range of cycle durations that are more than sufficient to provide full storage support to variable renewable sources, thereby allowing for increased renewable energy penetration into the electrical grid. While the pressure transients affect the power generation and storage over the course of the cycle, the ultimate limitation of the cycle duration is the size of the CO_2 plume in the reservoir; and, given the large volume of CO_2 that is required to mitigate climate change, the operation of the system could be substantially longer than the simulated cycle times. This ability to operate over extended cycle durations, is an advantage that CPGES has over existing storage systems, such as compressed air, which can generate power over only limited periods, typically a few hours, before the system must be recharged.

The CPGES system operates using only geothermal resources, requiring no additional fuel sources at the surface, while providing permanent subsurface storage for CO_2. This allows the CPGES system to supplement variable renewable sources using renewable energy to provide baseload power that is not achieved using existing energy management practices, which generally use fossil fuels, typically natural gas, to supplement wind and solar sources, which increases the carbon cost of operating these systems to provide baseload power. Furthermore, beyond providing renewable energy, the CPGES system has the synergistic effect of reducing the environmental impact of nearby CO_2 sources by permanently capturing CO_2 at the surface, thereby reducing the amount of CO_2 emitted into the atmosphere.

The amount of power that can be produced can be increased by operating over a larger subsurface area, scaling up the power production and consumption, similar to the approach applied to the CPG system [118].

3.6 Conclusion

A CPG system can be modified to operate as an energy storage system, CPGES, to temporally separate the power generation and power consumption components in a power cycle. System modeling of CPGES allows for the following conclusions:

A second, shallow reservoir can be added to the CPG system to separate power generation and energy storage. The second reservoir stores the CO_2 in an intermediate state after it is expanded in the turbine before the parasitic cooling and pump loads. Later, the CO_2 is re-extracted where it is cooled and compressed, consuming power before it is injected into

the deep reservoir. Thus, the shallow reservoir allows the turbine to be separated from the consumptive elements of the power cycle, accommodating for intermittent operation.

The shallow reservoir can operate with a single well that operates as both the production and injection well for the system. The shallow reservoir operates as an intermediate storage vessel for the CO_2 between the generation and storage modes. The injected CO_2 must be stored adiabatically and then later recovered for the energy storage process to function. A single horizontal circular injection well placed directly beneath the caprock and a continuous sequestration of 5% of the CO_2 allowed a majority of the injected CO_2 to be recovered with minimal brine entrainment.

The energy storage system produces net positive energy to the grid. The system operates with an energy storage ratio greater than one for both the diurnal and seasonal cases. The diurnal case can operate with an energy storage ratio of 2.93, meaning it produces almost three times more power during the generation phase than it stores in the storage phase. The system is able to produce significantly more power than it stores due to the geothermal heat from the deep reservoir. The seasonal energy storage system simulated here operates with an energy storage ratio of 1.55, which is lower than the diurnal cycle value of 2.93, a result of the larger pressure oscillations in the reservoir. The minimum calculated energy storage ratio was 1.05 for the 300 kg/s seasonal storage case, due to larger than optimal mass flowrates in the generation period; however, this system still generated more electric output than it stored.

The system can operate over a range of cycle durations, providing a robust energy storage solution. The system was demonstrated operating on both a diurnal and a biannual cycle, while still producing net energy to the grid. Thus, the system is not limited to a given cycle length and can operate over several different cycle durations that may be required to supplement variable renewable sources and/or maximize profitability.

Chapter 4: CPGES Parametric Study

Parametric study of a Large-Scale Energy Storage System using Carbon Dioxide Plume Geothermal Energy

Mark R. Fleming[1], Benjamin M. Adams[2], Thomas H. Kuehn[1], Jeffrey M. Bielicki[3,4], Martin O. Saar[2,5]

[1]Department of Mechanical Engineering, University of Minnesota, USA
[2]Geothermal Energy and Geofluids Group, Department of Earth Sciences, ETH-Zürich, Switzerland
[3]Department of Civil, Environmental, and Geodetic Engineering, The Ohio State University, USA
[4]John Glenn College of Public Affairs, The Ohio State University, USA
[5]Department of Earth Sciences, University of Minnesota, USA

4.1 Introduction

We model a single-demonstration scale CPGES system in terms of the power and energy generated/consumed during each mode and over the course of the entire cycle, and the energy storage ratio. We then compare the system to an equivalent CPG plant, operating with the same reservoir configuration.

4.2 Method

A CO_2-Plume Geothermal (CPG) system uses CO_2 as a working fluid in a permeable sedimentary reservoir [1,33,34,82,83,94–96,119,126]. The CPG system consists of a reservoir, vertical injection and production wells, and a surface plant that converts the thermal energy to electrical power. Alternative surface configurations produce heat, using a heat exchanger and a secondary fluid, however, this is beyond the scope of this paper. A detailed overview of the direct CPG cycle is discussed below, in Section 4.2.1 . The CO_2-Plume Geothermal Energy Storage (CPGES) system operates by separating the components that produce and consume power of a CPG system (Rankine cycle) and operating them at separate times as discussed in Section 2.2.

4.2.1 The Direct CPG System

The direct CPG system is defined in Adams et al. [1,82] and illustrated in Figure 4-1. CO_2 is produced from the reservoir at the production well (State 1) and adiabatically expands as the fluid moves vertically to the surface (State 2). At the surface, the CO_2 expands in the turbine to produce power (State 3). The CO_2 is cooled and condensed (State 4) using a cooling tower to reject heat to the ambient air temperature, with an approach temperature of 7°C [1]. The cooling process increases the density of the fluid, resulting in a subcooled liquid at State 4. The CO_2 is compressed in a pump at the surface (State 5) prior to the gravitational compression in the adiabatic vertical injection wells and is reinjected into the reservoir (State 6). In some cases, depending on the reservoir characteristics, a throttling valve is used in place of the pump. The CPG system operates in a continuous loop, constantly producing power.

4.2.2 The CPGES System

The CPGES system operates by separating the components that produce and consume power of a CPG system, operating them at separate times. In a CPG system, power is produced by extracting hot supercritical CO_2 from a subsurface reservoir and expanding the fluid in a turbine at the surface. Power is consumed by cooling towers and pumps required to cool and compress the CO_2 for reinjection into the reservoir. The CPGES system is able to separate these components by adding an additional shallow reservoir, after the turbine, to store the low-pressure CO_2 (Figure 4-1) before the CO_2 is cooled and compressed. The system operates in two modes:

1) **Power Generation**: Hot CO_2 is extracted from the deep reservoir, expanded in the turbine to produce power, and injected into the shallow reservoir. Depending on the configuration, some cooling may be necessary prior to the injection of CO_2 into the shallow reservoir, this increases the density of the CO_2 which allows the system to inject the CO_2 using only gravitational compression, without the need for surface pumping.

2) **Power Consumption**: CO_2 is produced from the shallow reservoir, cooled and compressed on the surface by a cooling tower and pump before the CO_2 is injected into the deep reservoir.

The placement of the shallow reservoir before the cooling and pumping process maximizes the power output during the power generation mode, by temporally shifting the power consumption to the later energy storage mode. In this configuration, the deep reservoir is the thermal source of the system and the shallow reservoir is used as a "storage tank" to hold the CO_2 in an intermediate state between the generation and storage modes.

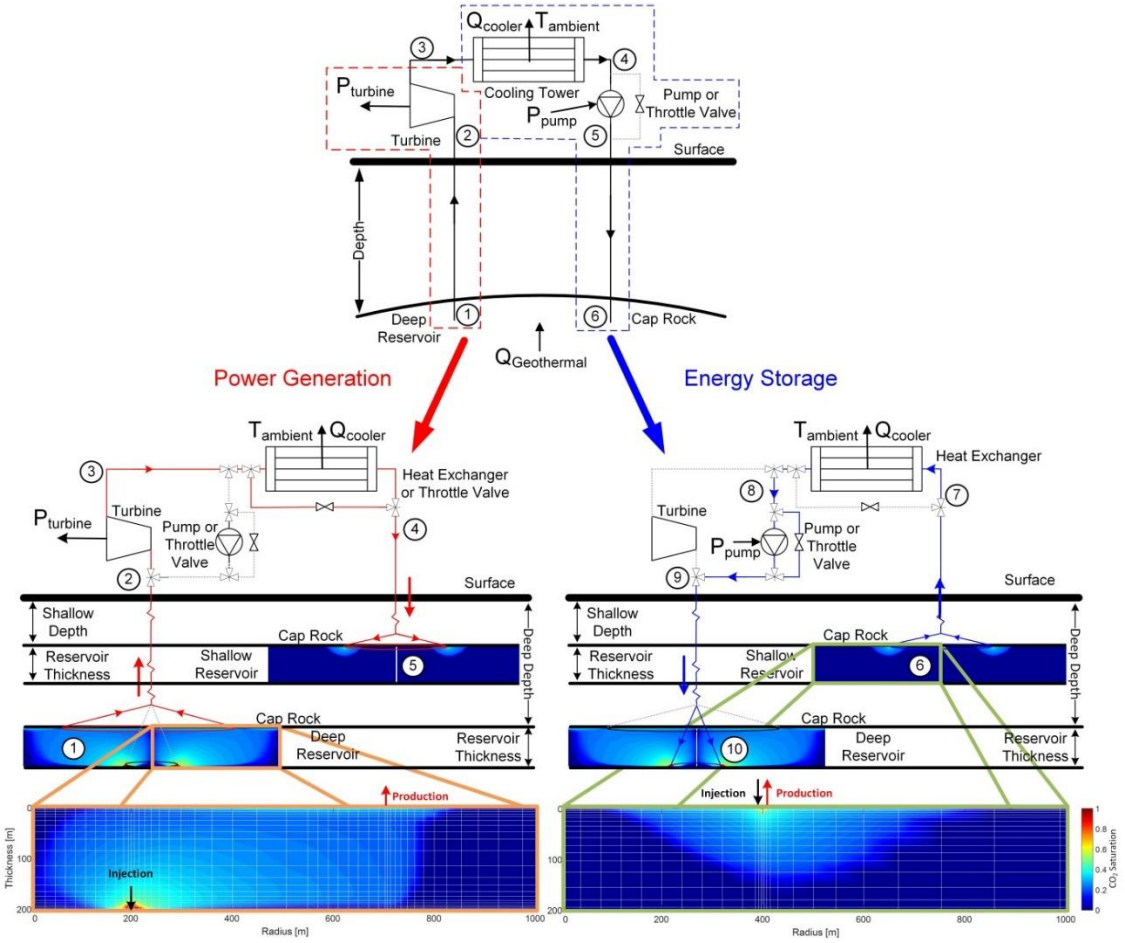

Figure 4-1: The energy production and consumption elements of the CPG system are separated with the addition of a shallow reservoir to operate as an energy storage system (CPGES) using two separate modes: 1) the power generation mode (RED) and 2) the energy storage mode (BLUE). The horizontal well configurations for the deep (left) and shallow (right) reservoirs are illustrated with the CO_2 plume at the beginning of the operation of the CPGES system for the two reservoirs with the corresponding computational grid overlaid. Beyond the production wells, the radial grid spacing increases logarithmically to the computational boundary [83].

In the generation mode, the CPGES system operates by producing CO_2 from the deep reservoir at the production well (State 1). The CO_2 adiabatically expands in the vertical well to the surface (State 2). At the surface, the CO_2 is expanded in the turbine to produce electric power. After the turbine (State 3), the CO_2 is partially cooled by the cooling towers

(State 4) and then injected into the shallow reservoir (State 5) using gravitational compression in the vertical well. The gravitational compression process is determined by the density of the CO_2 at the surface, at the top of the injection well, which is controlled by the amount of cooling at the surface. The CO_2 is stored in the shallow reservoir until the end of the generation mode.

In the storage mode, CO_2 is extracted from the shallow reservoir (State 6) and produced at the surface (State 7) using the same vertical well. At the surface, the CO_2 is cooled and condensed to the minimum achievable temperature by using the cooling towers (State 8), rejecting heat to the ambient surface temperature and is then compressed by the pump (State 9) before the CO_2 is injected into the deep reservoir through the injection well (State 10). The injected CO_2 is geothermally heated by the rock structure as it migrates from the injection well to the production well (State 1).

To demonstrate the operation of the CPGES system we simulate the CPGES system operating on a diurnal cycle with a 16-hour generation mode and an 8-hour storage mode. This duty cycle was selected to follow the diurnal variation in the locational marginal pricing (LMP) for the Midwest Independent Service Operator (MISO) in 2015 [127], demonstrating how the system will perform when it is operated using arbitrage as economic strategy.

4.2.3 Numerical Modeling

The CPG and CPGES systems are simulated using two software packages. The subsurface reservoirs are simulated in TOUGH2 [120] with the ECO2N equation of state module [121], and the surface power plant and the vertical wells are simulated in Engineering

Equation Solver (EES) [122]. EES is a simultaneous equation solver with built-in thermodynamic properties, including the properties of CO_2 [125].

Table 4-1: Nomenclature

Variable	Parameter
h	Enthalpy [MJ/kg]
$\dot{m}$	Mass Flow Rate [kg/s]
$\dot{W}$	Power [MW]
W	Energy [MW-h]
$\dot{Q}$	Heat Rejection Rate [MW]
Q	Heat [MW-h]
ρ	Density [kg/m^3]
P	Pressure [kPa]
T	Temperature [°C]
z	Thickness [m]
f	Friction factor
V	Velocity [m/s]
λ	Parasitic loss fraction
g	Gravitational Constant [m/s^2]
η	Efficiency [Dim]
χ	Energy Storage Ratio
Z	Reservoir depth [m]
T_{grad}	Geothermal Temperature Gradient [°C/km]
κ	Permeability [m_2]
φ	Porosity [dim]

In each trial, the storage mode operates using 98% of the mass of CO_2 used during the generation mode. The remaining 2% is retained in the shallow reservoir to maintain the plume.

To reduce the computation time for each trial, the reservoir simulations are de-coupled from the surface model. The de-coupled model operates by first characterizing the performance of the subsurface reservoirs at each horizontal well using TOUGH2 (section 2.3.1 and 2.3.2), and then the resulting subsurface characterization equations are the

implemented in the surface power system (section 2.3.3), eliminating the need to directly simulate the subsurface reservoirs for each power plant configuration.

4.2.3.1 Reservoir Model Parameters

The CPGES system uses two independent reservoirs located at separate depths, with different well configurations illustrated in Figure 4-1. Each reservoir is simulated as a three-dimensional axisymmetric cylindrical reservoir, similar to Garapati et al. [83]. The reservoir interstitial space are initially filled with brine, 20 wt% NaCl. The initial reservoir temperatures are determined as the product of the reservoir depth and the geothermal temperature gradient, in addition to the ambient surface temperature, which is taken to be 15°C [83]. The initial reservoir pressure is modeled as the hydrostatic pressure (10 kPa/km) at the given depth. Each reservoir is bounded by low-permeability caprock (above) and low-permeability baserock (below), preventing leakage of CO_2 into the surrounding formations. Heat flux through the reservoir boundaries is modeled using semi-analytic heat conduction [120].

We vary the following reservoir parameters:

(i) **Permeability**: The horizontal permeability ranges from $2.5\times10^{-14} \leq k_x \leq 10\times10^{-14}$ m^2, corresponding with an expected range of permeabilities. For example, the Mt. Simon Sandstone in the Illinois Basin has documented horizontal permeabilities as low as 1×10^{-12} m^2, with an average horizontal permeability of 2.6×10^{-14} m^2 [41]. Additionally, we limit the lower permeability range to decrease convergence issues, particularly at higher mass flow rates utilized in the study.

(ii) **Permeability Anisotropy**: The ratio of the horizontal to vertical permeability (k_x/k_z), varies from $2 \leq k_x/k_z \leq 10$. Previous CPG reservoir simulations considered an anisotropy values of 1 [33,34,94,96],2 [83,119], and 5 [95].

(iii) **Porosity**: We consider porosity values from 10% to 20%, which is consistent with values reported from the Illinois basin, where the effective porosity varied from 8.72% to 21.8% [41].

(iv) **Geothermal temperature gradient**: The geothermal temperature gradient varied from 25 °C/km to 50 °C/km, similar to the values used in the Adams et al. [1] study in which the gradient from 20°C/km to 50°C/km. The surface temperature was set at 15°C for the determination of reservoir temperatures [1,83]. The average North American continental heat flux is 65 mW-m^{-2} [16,66] leading to an approximate temperature gradient of 28-31 °C/km.

(v) **Mass Flow Rate**: The generation mode mass flow rate of CO_2 was varied from 100-900 kg/s, which corresponds to a circulation rate of 5.76 to 51.84 ktonnes per day, for a 16-hour production operation. The mass flow rate is constant within each trial, and varies only between trials. The storage mode mass flow rate varies with the generation mass flow rate to return 98% of the mass of CO_2 produced back into the deep reservoir, with 2% remaining in the shallow reservoir to account for CO_2 plume losses.

(vi) **Reservoir depth(s)**: The depth of the deep reservoir varied from 2.5 to 4.5 km, while the shallow reservoir depth varied between 1.0 and 1.5 km. The shallow

reservoir depths are selected to maintain the supercritical state in the reservoir (> 1km) and while only using reservoir depths that are unsuitable for power generation (<1.5 km) [1].

To characterize the reservoir performance, a design of experiments approach was utilized, resulting in 242 trials for the deep reservoir and 241 trials for the shallow reservoir, discussed below. The pressures and produced CO_2 mass fraction were recorded for each trial.

4.2.3.1.1 Deep Reservoir

The deep reservoir is the thermal source of the system. The injection well for the deep reservoir is a horizontal, axisymmetric, circular well located at a radius of 200 meters from the center. We use a horizontal injection well in place of the vertical injection well used in previous CPG models [33,34,83,94,96,126] to reduce pressure losses near the well in the reservoir, by increasing the injection well length. The injection well is situated just above the low-permeability rock at the bottom of the reservoir. The deep reservoir production well is a horizontal well, similar to that used by Garapati et al. [83,119], situated directly beneath the caprock at a radius of 707 meters, consistent with prior CPG system models [1,33,34,82,94,96]. The combination of these well locations maximizes the volume of the reservoir rock that is swept by the CO_2 plume, and thus the heat extraction volume, as the buoyant CO_2 rises and expands away from the injection well. The vertical mobility of the CO_2 is limited by the low-permeability caprock at the top of the reservoir, which prevents upward leakage of CO_2, trapping the CO_2 in the reservoir, which leads to the formation of a CO_2 rich pocket just beneath the caprock. The horizontal production well is located just

beneath the caprock in this CO_2 rich region, to increase the volume of CO_2 extracted from the reservoir, and reduce the production of brine.

The reservoir is initially filled with brine and CO_2 is injected, displacing the native brine. This plume is developed by injection of pure CO_2 at a rate of 1.58 Mt-yr^{-1}, with no production. Development occurs until the production well has a 35% CO_2 saturation, or a minimum of 5 years injection time to ensure that the CO_2 plume is sufficient to begin extracting CO_2 and operate for extended durations without the need for additional CO_2 injection. Once the plume has developed, normal operation begins. To reduce computational time, the intermittent operation is simulated for only a one-week period, 10 years after normal operation begins. The previous 10 years are simulated as continuous injection and production into the reservoir.

We use this same reservoir configuration to simulate the CPG system. However, unlike the CPGES system, the system operates continuously by simultaneously injecting and producing equal amounts of CO_2. We simulate this system out to 10 years, to allow for a direct comparison to the CPGES system.

4.2.3.1.2 Shallow Reservoir

The shallow reservoir has a different operation than the deep reservoir; it functions as the storage vessel for the CO_2 between the power production and consumption modes. The well configuration and operation are separate from the deep reservoir. To facilitate the operation of the reservoir for short-term CO_2 storage between modes, a single horizontal circular well is used as both the injection and production well. This single, bi-directional

well is located at the top of the reservoir directly beneath the caprock at a radius of 200 meters.

For this system, CO_2 is injected into the reservoir during the energy production mode for temporary storage in the reservoir. The CO_2 is recovered and extracted from the reservoir during the energy consumption mode. The single well configuration minimizes CO_2 losses in the reservoir, due to advection and diffusion, by limiting the CO_2-brine interaction to the region near the well. The CO_2 does not have any vertical mobility in the reservoir, as the buoyant effects are minimized through the placement of the well directly beneath the caprock on top.

Prior to the system operation, CO_2 is injected into the shallow reservoir to develop a plume/pocket of CO_2 surrounding the horizontal well. The reservoir is charged with 3.55 Mt of CO_2 over 2.5 years to ensure that the CO_2 plume is maintained near the injection well throughout the operation of the system, preventing the upconing of brine during the storage mode, when CO_2 is extracted from the reservoir.

CO_2 is lost from the plume over time, as it diffuses horizontally in a thin layer beneath the caprock. To account for these losses, additional makeup CO_2 is added to the shallow reservoir to maintain the CO_2 pocket, ensuring that CO_2 is the primary component (i.e. > 94% mass fraction) of the fluid extracted from the reservoir during the storage mode. The additional CO_2 is added to the shallow reservoir by retaining 2% of the injected CO_2 during each cycle, which results in transfer of some of the CO_2 from the deep reservoir to the shallow reservoir over time.

4.2.3.2 Reservoir Characterization

To model the reservoir performance in the decoupled power plant model, we develop characteristic models for the average injection and production well pressures for each mode using the individual reservoir simulations, discussed previously.

To characterize the reservoir, we assume that the system operates using the mean pressure loss in the deep reservoir and the maximum pressure loss in the shallow reservoir for each simulation. Specifically, we assume that the system operates with the maximum injection pressure and the minimum production pressure in the shallow reservoir, and the mean injection and production pressures in the deep reservoir, and thus will provide a conservative evaluation of the performance of the power system. We use the maximum pressure difference in the shallow reservoir to account for the pressure variation in the huff and puff design (i.e. $(P_5\text{-}P_6)_{max}$), as the mean pressure underestimates the huff and puff performance. We first determine the mean pressure for the deep production well and maximum pressure for the shallow injection well during the generation mode, and the mean pressure in the deep injection well and the minimum pressure in the shallow production well during the storage mode for each trial.

We characterize the pressure differences in each reservoir for all the trials using a one-dimensional radial Darcy equation, with additional terms representative of our parameter space, specifically the permeability, permeability anisotropy, depth, geothermal temperature gradient, and the mass flow rate, shown in Table 4-2. We exclude the porosity, which was found to not significantly impact the pressure difference. To predict the magnitude of injection and production pressures, which are required for the surface power

model, two pressure differences are required for each reservoir: 1) between the injection and production pressure, and 2) between the injection and the hydrostatic reservoir pressure (P_D and P_S for the deep and shallow reservoirs). In each case, additional terms are included in the Darcy equation to increase regression accuracy. The resulting regression equations are given in Table 4-2.

Table 4-2 presents the results of the regression analysis, specifically the slope (α) and the intercept (β) coefficients. The intercept is non-zero, due to the pressure difference that results from the initial CO_2 plume development (injection of CO_2) and the displacement of the brine. This non-zero offset also indicates that CO_2 plume is continually expanding, with a bulk movement of CO_2 away from the injection well.

Table 4-2: The resulting regression equations for the pressure differences in each reservoir.

	Equation	Slope (α)	Intercept (β)
Deep Reservoir	$P_{10} - P_1 = \alpha \frac{\dot{m}}{\kappa_h T_r} ln\left(\frac{k_h}{k_v} + e - 1\right) 10^{-12} + \beta$	$0.213 \left[\frac{MPa\ m\ K}{TPa\ s}\right]$	2.463 [MPa]
	$P_{10} - P_D = \alpha \frac{\dot{m}}{\kappa_h T_r} ln\left(\frac{k_h}{k_v} + e - 1\right) 10^{-12} + \beta$	$0.099 \left[\frac{TPa\ m\ K}{TPa\ s}\right]$	1.538 [MPa]
Shallow Reservoir	$P_5 - P_6 = \alpha \frac{\dot{m}}{\kappa_h} \ln\left(\frac{k_h}{k_v} + e - 1\right) 10^{-15} + \beta$	$0.221 \left[\frac{MPa\ m}{PPa\ s}\right]$	0.194 [MPa]
	$P_5 - P_s = \alpha \frac{\dot{m}}{\kappa_h Z_s} 10^{-12} + \beta$	$0.122 \left[\frac{MPa\ m^2}{TPa\ s}\right]$	0.325 [MPa]
CPG Reservoir	$P_6 - P_1 = \alpha \frac{\dot{m}}{\kappa_h T_r} ln\left(\frac{k_h}{k_v} + e - 1\right) 10^{-12} + \beta$	$0.510 \left[\frac{MPa\ m}{TPa\ s}\right]$	2.296 [MPa]
	$P_6 - P_D = \alpha \frac{\dot{m}}{\kappa_h T_r} ln\left(\frac{k_h}{k_v} + e - 1\right) 10^{-12} + \beta$	$0.084 \left[\frac{MPa\ m\ K}{TPa\ s}\right]$	1.343 [MPa]

4.2.3.3 Power Plant Model

The surface power plant consists of a turbine, cooling towers, a pump, throttling valves, and the vertical wells. For the configuration presented in this paper, each horizontal well is connected to the surface by four vertical wells to reduce pressure losses. The system configuration and the two operational modes are illustrated in Figure 4-1. The CPGES system directly expands the produced CO_2 in a turbine without a secondary working fluid, similar to the CPG system.

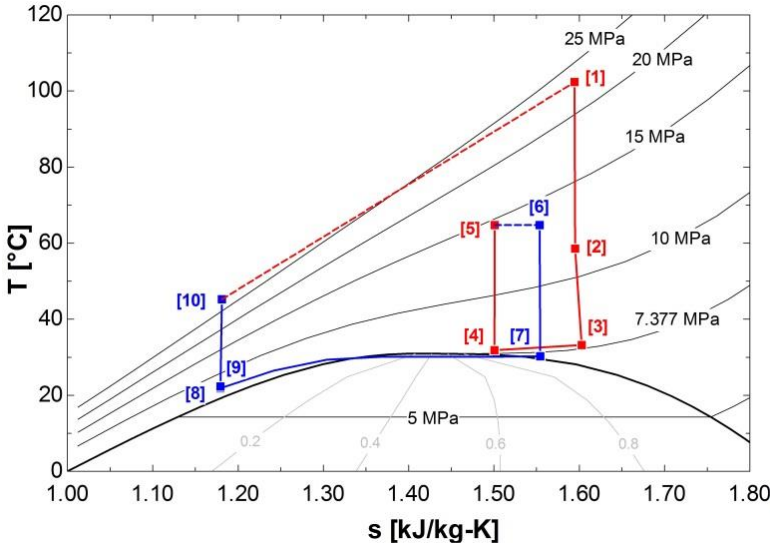

Figure 4-2: An example T-s diagram for the CPGES system. States 1-5 are for the generation mode, and States 5-10 are for the consumption mode. Heat is added from the deep reservoir from state 10 to state 1. The pressure changes in the shallow reservoir from state 5 to 6 in an isothermal process as a result of the injection and production of CO_2.

The turbine is the only power generator in the system and operates during power generation mode in the CPGES system. The power produced from the turbine, $\dot{W}_{turbine}$, is defined as the product of the mass flow rate during the generation mode and the enthalpy difference between the turbine inlet and outlet,

$$\dot{W}_{turbine} = \dot{m}(h_a - h_b). \quad (4\text{-}1)$$

where the inlet and outlet enthalpies are h_a and h_b. The inlet and outlet state point of each component for the CPG and CPGES system are detailed in Table 4-3. Consistent with prior CPG models, the turbine has an isentropic efficiency of 78% [1,82]. Additionally, we fix the turbine back pressure for the CPGES system at 7.5 MPa to maintain supercritical CO_2 at the turbine outlet, whereas the backpressure on the CPG system is set at the saturation pressure for the cooling tower outlet temperature, which is 7°C above the ambient temperature (i.e. we model a 7°C approach temperature for the cooling towers). While setting the backpressure at 7.5 MPa reduces the CPGES power output compared to CPG system, it is necessary to keep the fluid in the supercritical state to prevent multi-phase CO_2 in the shallow reservoir injection well.

The CPG and CPGES systems reject heat to the ambient conditions using the cooling towers. The heat rejected from the cooling towers is defined as the product of the mass flow rate for the operational mode and the enthalpy difference between the inlet and outlet conditions,

$$\dot{Q}_{Cooling} = \dot{m}(h_a - h_b). \quad (4\text{-}2)$$

The operation of the wet cooling towers, in particular the cooling tower fan, consume power. This parasitic power consumption is modeled as a fraction of the total heat rejected from the cooling towers,

$$\dot{W}_{cooler} = \lambda \dot{Q}_{cooling} \quad (4\text{-}3)$$

where the parasitic cooling fraction, λ, is defined for wet cooling towers in Adams et al. [1], and is a function of the ambient temperature, the approach temperature, and the temperature difference across the cooling tower. The cooling towers in the CPGES consumption mode and for the CPG system operate with an approach temperature of 7°C, which was determined to be the optimal condition in prior CPG systems [1].

To compress the CO_2 from the surface to the reservoir pressures, the system relies on gravitational compression in the vertical well, which we discuss in terms of modeling below. In situations where the gravitational compression is insufficient to increase the pressure to the necessary reservoir pressures, pumping is required. The pump is modeled as the product of the mass flow rate and the enthalpy difference across the pump, which is given as,

$$\dot{W}_{pump} = \dot{m}(h_a - h_b). \tag{4-4}$$

The pump is assumed to have an isentropic efficiency of 90%, consistent with the CPG model of Adams et al. [1]. Pumping is not always required, and for certain configurations the pump and/or generation cooling tower can be replaced with throttling valves (Figure 4-1). Throttling valves are assumed to produce an isenthalpic process.

4.2.3.3.1 Vertical Well Model

The vertical well model used in these simulations, is documented in Adams et al. [1,82]. Each vertical well is numerically integrated over 100-meter segments, balancing computational time and accuracy. Across each segment, the continuity equation, momentum and energy balances are applied assuming pure CO_2. The vertical wells are assumed to be adiabatic, and the change in kinetic energy is neglected in the energy balance

[1,82]. Well frictional losses are modeled using the Darcy-Weisbach relation. A well with a 0.41 meter diameter is used, as smaller diameter wells have significant pressure losses, which reduce the net power generation of the system [1,91].

Table 4-3: CPG and CPGES system components with the designated state points. The state points are defined in Figure 1.

Component	Schematic	Component Power (W)	State Points (a-b)	
			CPG	CPGES
Turbine	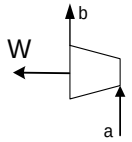	$\dot{W}_{turbine}$	2-3	2-3
Pump	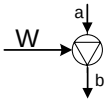	$\dot{W}_{pump}$	4-5	8-9
Cooling Towers	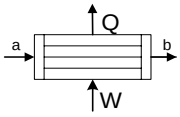	$\dot{W}_{cooler}$	3-4	3-4 7-8
Throttling Valve[1]			4-5	3-4 8-9
Vertical Wells			1-2 5-6	1-2 4-5 6-7
Reservoir(s)			5-1	5-6 10-1

[1]Throttling valves are used in place of cooling towers and pumps under certain conditions

4.2.3.3.2 System Performance

The performance of the system is characterized by the power produced during the generation mode, the power consumed during the consumption mode, the system efficiency, and the energy storage ratio.

During the generation mode net power is generated, $\dot{W}_{net,generation}$, and is defined as the difference between the gross turbine power output and the cooling tower fan requirements (generation mode), given as,

$$\dot{W}_{net,generation} = \dot{W}_{turbine} - \dot{W}_{cooling,generation}. \quad (4\text{-}5)$$

Similarly, the net power consumed during the storage mode, $\dot{W}_{consumption}$, is defined as the sum of the power consumed by the pump and the cooling tower fans.

$$\dot{W}_{consumption} = \dot{W}_{pump} + \dot{W}_{cooling,storage}. \quad (4\text{-}6)$$

The net energy produced during a single diurnal cycle, $W_{net,system}$, is the difference between the energy produced during the generation mode and the energy consumed during the storage mode, defined as,

$$W_{net,system} = \int \left(\dot{W}_{net,generation} - \dot{W}_{consumption}\right) dt. \quad (4\text{-}7)$$

The efficiency of the system is defined as the energy produced from the turbine over the sum of the energy entering the system, including the heat from the geothermal reservoir over a 24-hour period, given as,

$$\eta_{system} = \frac{W_{turbine}}{Q_{reservoir} + W_{pump} + W_{cooling,storage} + W_{cooling,generation}}. \quad (4\text{-}8)$$

The performance of the energy storage system is quantified by the energy storage ratio, χ, defined as,

$$\chi = \frac{W_{net,generation}}{W_{consumption} + Q_{purchased}}. \quad (4\text{-}9)$$

Here, $Q_{purchased}$ is auxiliary heating at the surface from a purchased fuel source. The CPGES system does not require auxiliary heating at the surface prior to the turbine, thus $Q_{purchased}$ is zero here; it is included to contrast a CPGES system with systems which require heat

addition to operate, such as compressed air energy storage. Reservoir heat addition is neglected in this equation, as its marginal cost is very low. Auxiliary heating of geothermal CO_2 is discussed in Garapati et al. [126] and Liu et al. [110], and is beyond the scope of this paper.

4.3 Results and Discussion

We discuss the modeling results in terms of the CPGES system performance in terms of the energy storage ratio and energy generation, and compare the net daily energy generation of the CPGES system relative to a CPG system.

Table 4-4: Base Case Parameters

BASE CASE PARAMETERS	
Horizontal Permeability (k_h)	6.25×10^{-14} m^2
Permeability Anisotropy (k_h/k_v)	6
Ambient Web Bulb Temperature ($T_{ambient}$)	10°C
Porosity (ϕ)	0.15
Deep Reservoir Depth (D_d)	3.5 km
Shallow Reservoir Depth (D_s)	1.25 km
Temperature Gradient ($T_{gradient}$)	37.5 °C/km

4.3.1 System Performance

We characterize the performance of the CPGES system in terms of the electricity generation and storage using the following parameters: the net power generation, net power stored, the energy storage ratio, and the net daily energy generation, which are defined in section 4.2.3.3 . In addition, we document the reservoir pressures, to verify the operation of the reservoir. As previously mentioned in section 4.2.3.1 , we consider a number of reservoir parameters, including the porosity, permeability, permeability anisotropy, geothermal temperature gradient, reservoir depths, and the mass flow rate of CO_2. In

addition to the reservoir parameters, we also consider the ambient wet bulb temperature, which we vary between 5°C to 20°C.

4.3.1.1 Optimized Energy Generation

For a given plant configuration, the performance of the system varies, depending on the mass flow rate, shown in Figure 4-3. Variations in the mass flow rate influence the reservoir and well pressure losses, the power produced by the turbine, and the power consumed by the cooling tower fans and the pump. Unlike the other plant parameters, which are fixed for a given site, the mass flow rate can be controlled by a system operator using pumps and valves at the surface [1]. In the CPG system, the mass flow is varied to optimize the instantaneous net power output; however, because the CPGES operates as an energy storage system, the instantaneous net power output cannot be maximized, instead, we optimize the net daily energy generation.

Figure 4-3 illustrates the relationship between mass flow rate and net energy generation. As the mass flow rate increases the net power produced during the generation mode increases, as does the net power consumed during the storage mode. At low mass flow rates, the pump is not required; however, at larger mass flow rates, frictional losses in the reservoir and the pipes increase, and the pump is required (i.e. generation mass flow rates greater than 225 kg/s). While the pump consumes additional energy, the system has a net benefit from the additional mass flow rate through the turbine, and thus the additional power it generates for the given case. However, the rate that the energy consumption increases with mass flow rate is greater than the turbine power once the pump is active,

and thus the net energy generation reaches a maximum. While the net energy has an optimum mass flow rate, the generation mode energy increases beyond the maximized net energy flow rate, due to the separation of the components that generate and consume power. For instance, at the maximum energy generation flow rate of 250 kg/s the generation mode delivers 1.99 MW, while the maximum power generated is 3.55 MW at a mass flow rate of 675 kg/s, however, the net energy generation decreases from 17.1 MW-h to -48.8 MW-h. This indicates that the tradeoff of the increased power generation is a decrease in the net energy generation. Therefore, we consider the maximized net energy condition as the design point for the CPGES system.

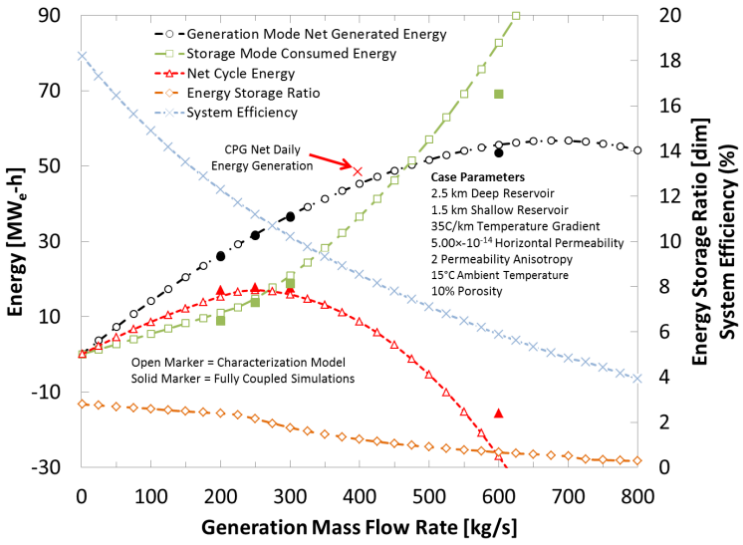

Figure 4-3: Optimization of daily energy generation by varying the mass flow rate. The system efficiency and the energy storage ratio are maximized at low mass flow rates, independent from the net energy generation. We include results from the fully coupled simulations, which are represented by solid markers.

Maximized net energy generation does not correlate with the maximum energy storage ratio or the maximum system efficiency as these parameters are maximized when the

system operates with the minimum mass flow rate (1 kg/s), as frictional losses in the wells and from the reservoir are minimized. For the presented case (Figure 4-3), the energy storage ratio and the system efficiency maximum values are 2.80 and 18.20 respectively while the net energy generation is 0.095 MW-h per day, whereas, when the energy generation is optimized (250 kg/s generation) at 17.1 MW-h per day these values decrease to 2.16 and 11.20%.

For all remaining combinations of system parameters presented, the mass flowrate is not considered as an independent variable, as the mass flow rate is used to maximize the net daily energy generation. We select the net daily energy generation as the maximized condition (as opposed to the energy storage ratio and the system efficiency), as it is the only parameter that has a maximum value at a non-zero mass flow rate. We preform the optimization of the net power generation in EES

Additionally, we verified our characterization model with fully coupled system models (i.e. where each reservoir is directly simulated and paired with the power model, accounting for the pressure transients), specifically at mass flow rates of 200, 250, 300 kg/s, and 600 kg/s as illustrated in Figure 4-3. The characterization model slightly underestimates the net energy of the fully coupled models, by 10%, 3%, and 16% for the 200 kg/s, 250 kg/s, and 300 kg/s mass flow rates, respectively. This is expected, as the characterization model assumes the system operates at the minimum or maximum pressure at each well for the entirety of each of operation, which, as previously discussed, decreasing the power generation and increasing the power consumed, and thus decreasing the predicted energy

generation. This is verified in our comparison, which resulted in an overestimation of the power consumed by 25%, 7%, and 11% for the 200 kg/s, 250 k/s, and 300 kg/s cases respectfully. However, while the energy consumption was overestimated, the energy generated in the generation mode was also overestimated by 2% for each case. The deviation between the fully coupled model and the characterization model is larger for the 600 kg/s case, with the characterization model overestimating the energy consumption by 20% and the energy generation by 4%, resulting in a 11.47 MW-h underestimate in the net energy, a result of the overestimate of the pumping power at large mass flow rates due to the reservoir pressure model. However, given that we have defined the maximum net energy generation case as the design point, we do not expect the system to operate with net energy consumption, due to the excessive amount of pumping, as demonstrated in the 600 kg/s. Thus, we verify the characterization model within the expected operation range of the system.

4.3.1.2 System Performance

We consider the effects of the input parameters on the net daily energy generation and the energy storage ratio. We then compare the CPGES system to two CPG modes utilizing identical deep reservoirs:

1) Equivalent Daily CO_2 Circulation Rate: The CPG system extracts the same mass of CO_2 per day, and thus heat, from the deep reservoir, as the CPGES system. For the 16-hour generation cycle in the CPGES system, the mass flow rate of the CPG system is 2/3 of the generation CPGES generation mass flow rate.

2) Optimized CPG: The mass flow rate of the CPG system is selected to optimize the net power/energy generation.

4.3.1.2.1 Shallow Reservoir Depth

The addition of the shallow reservoir to a CPG system allows the system to operate as an energy storage system (i.e. a CPGES system), and the depth of the shallow reservoir effects the net energy generation, the energy storage ratio, and the amount of cooling that occurs during the generation mode. Deeper depths increase the net energy generation and the energy storage ratio, but also increase the amount of power consumed during the generation mode, shown in Figure 4-4. The system increases the net energy generation by decreasing the specific energy consumption over a complete cycle, which is a result of the increased cooling load in the generation mode. In the generation mode, the cooling towers are used to control the density of the CO_2 at the wellhead, and thus the gravitational compression in the vertical well; this allows the system to inject CO_2 into the shallow reservoir without the need for circulation pumps. When the depth of the shallow reservoir increases, the pressure difference between surface (7.5 MPa) and the downhole reservoir pressure (i.e. $\sim\rho_w g d_s$) increases, and thus additional cooling in the generation mode is required to increase the gravitational compression (i.e. $\sim\rho_{CO2} g d_s$) to inject the CO_2 into the shallow reservoir. The increased cooling load in the generation mode distributes the cooling tower parasitic power consumption over each mode, decreasing the specific parasitic power consumption, as the parasitic loss fraction in the generation mode is lower than the parasitic loss fraction in the storage mode due to the elevated approach temperature in the generation mode.

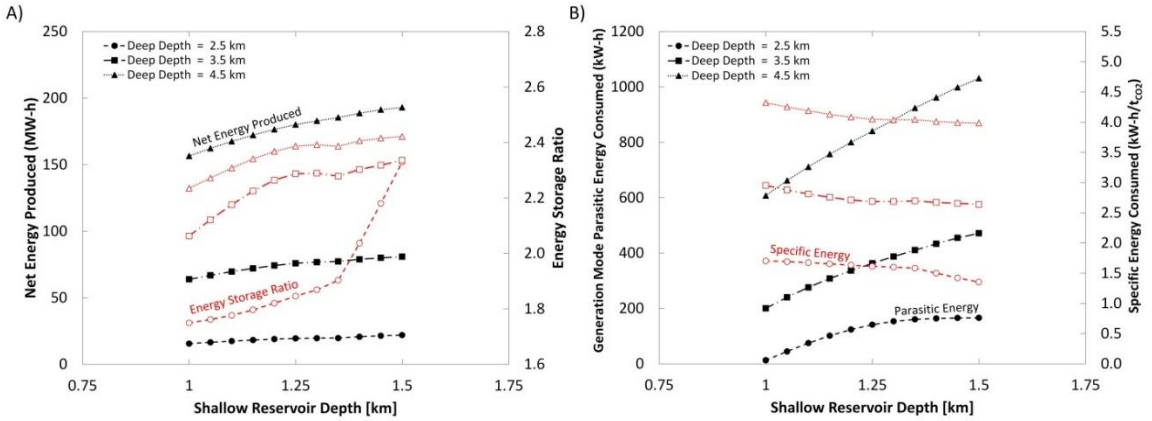

Figure 4-4: The parasitic energy consumed during the generation mode, and the energy storage ratio as a function of the shallow reservoir depth, for the base case conditions.

The energy storage ratio increases when the CPGES system operates with increased parasitic power consumption in the generation mode, illustrated in Figure 4-4. As the depth of the shallow reservoir increases, and thus as parasitic power in the generation mode increases, the energy consumption during the storage mode decreases, all other factors being equal. This decrease in the power consumed during the energy storage mode, increases the energy storage ratio, as the energy consumed during the storage mode is in the denominator (Equation 10). Thus, as the energy consumed during the storage mode decreases, the energy storage ratio will increase. For instance, in the base case when the shallow reservoir depth was incresed from 1.0 km to 1.5 km, the energy consumed in the generation mode increased from 3.20 MW-h to 7.54 MW-h, resulting in a increase in the energy storage ratio from 2.06 to 2.34, shown in Figure 4-4. Therefore as the depth of the shallow reservoir, and the energy consumed in the generation mode, increase, the energy storage ratio will increase. This indicates that while the energy storage ratio demonstrates

the ability of the system to time shift energy, a large energy storage ratio is not ideal for the CPGES system, as the CPG system operates with a theoretical infinite energy storage ratio due to the concurrent generation and consumption of power during generation. In practice, these excessive large energy storage ratios are avoided, due to the limited depth of the shallow reservoir, allowing the system to time shift the generation and consumption of power.

4.3.1.2.2 Reservoir and Ambient Temperatures

The net daily energy generation and the energy storage ratio increase as the temperature difference between the deep reservoir (heat source) and the ambient temperature (heat sink) increases, shown in Figure 4-8, as the CPGES system operates as an intermittent heat engine. The net daily energy increases as the ambient wet bulb temperature (heat engine thermal sink) decreases, illustrated in Figure 4-8B. In the CPGES system, a lower ambient temperature has two effects: 1) it increases the heat rejected through the cooling towers, and thus the amount of power consumed by the cooling towers, and 2) it increases the density at the wellhead of the deep injection well (State 8), thereby increasing the gravitational compression and reducing the pumping load. For instance, the pumping specific enthalpy consumption decreases from 4.53 kJ/kg to 1.75 kJ/kg, while the cooling tower specific energy consumption increases from 6.14 kJ/kg to 7.10 kJ/kg, resulting in a decrease in the total specific energy consumption by 1.82 kJ/kg as the ambient wet bulb temperature decreases from 15°C to 5°C, for the 37.5C/km geothermal temperature gradient. These specific energy consumptions result in a net daily energy generation of 70.35 MW-h for the 15°C case and 91.32 MW-h for the 5°C case, thus lower ambient

temperatures increase the performance of the CPGES system. It is worth noting that we treat the ambient temperature as an independent variable, however, in a real system, the mean wet bulb temperature will vary with the geographical position and will vary in time due to seasonal effects, and thus performance will vary as the system operates over a range of ambient temperatures.

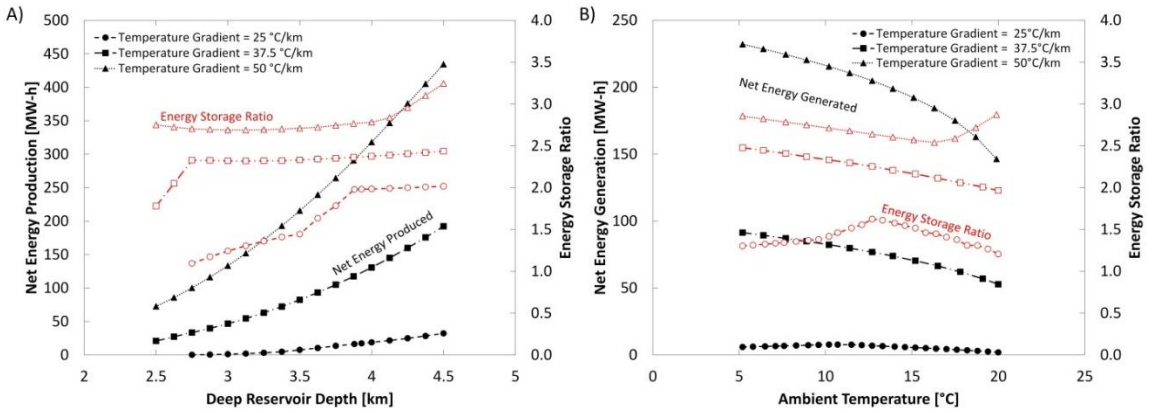

Figure 4-5: The net energy generation and energy storage ratios dependence on the reservoir and ambient temperatures by varying A) the deep reservoir depth and the temperature gradient, and B) the temperature gradient and the ambient temperature. The discontinuities in the energy storage ratio occur as the system transitions from throttling to cooling in the generation mode, and pumping begins in the storage mode.

The net daily energy generation increases as the deep reservoir depth and temperature gradient, and thus the resource temperature, increase, shown in Figure 4-8A. The lowest geothermal temperature gradient (25°C/km) is unable to generate net energy for depths less than 3.25 km, and only exceeds the minimum 37.5°C/km case (20.88 MW-h) at depths greater than 4.125 km, indicating that low geothermal temperature gradients limit the performance of the system. The lowest temperature that produces net daily energy in Figure 4-8A is 83.8°C, generating 0.13 MW-h, while the largest temperature of 240°C generates

434 MW-h. The energy storage ratio also increases as the depth and geothermal temperature gradient, and thus the reservoir temperature, increases, particularly for temperatures less than 115°C. For temperatures greater than 115°C, the energy storage ratio generally does not vary with the deep reservoir depth, but only with the geothermal temperature gradient. This indicates that while the system can generate more energy with deeper reservoirs, the energy generated and consumed are proportional for given geothermal temperature gradient and reservoir temperatures greater than 115°C, shown by the nearly constant net energy production fraction in Figure 4-6. The nearly constant net energy generation faction indicates that while the energy generated and thermodynamic efficiency of the system increase with the resource temperature, the parasitic loss fraction of the system is consistent at 40-50% of the gross turbine output. The losses for the CPGES system, while large, are similar to parasitic losses in the Soda Lake geothermal facility [65], and are larger than the reported parasitic loss fraction of 32% for the CPG system [1] due to the additional components in the system. For temperatures less than 115°C, the net generation fraction decreases, as the parasitic loss fraction from the cooling tower in the storage mode increase; a result of the limited gross turbine energy generated at low resource temperatures as a large fraction of the heat extracted from the deep reservoir cannot be used to generate power and is rejected to the atmosphere. Additionally, at these low temperatures, the system does not require pumping, and operates using only a thermosiphon to circulate the fluid between the reservoirs.

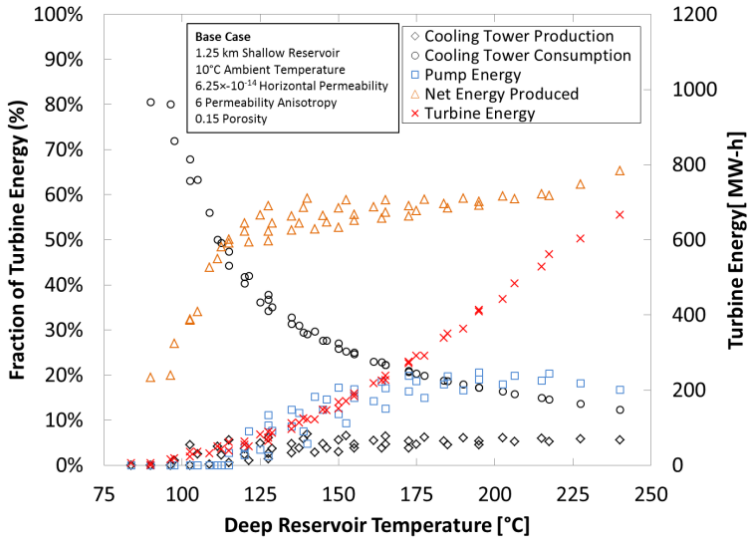

Figure 4-6: Parasitic energy losses for each component relative to the gross energy produced by the turbine. The deep reservoir temperature is varied by varying the temperature gradient and the deep reservoir depth.

4.3.1.2.3 Pressure losses

In the CPGES system, we consider two pressure losses; the reservoir pressure loss and pipe frictional loss, with the reservoir pressure loss typically accounting for over 95% of the total pressure loss (at the maximum daily net energy flowrate); with a minimum observed loss fraction of 72% in cases with high permeability and deep, hot reservoirs. These reservoir pressure loss fractions are larger than those observed in previous CO_2 geothermal studies; which demonstrated that friction losses in small diameter pipes significantly decreased the energy generation potential [1,82,91]. The increased reservoir pressure loss fraction for the CPGES system is a result of the addition of the shallow reservoir and the intermittent injection and production of CO_2, which increases the reservoir pressure loss by a factor of 2.21 when compared to the CPG system, shown in Figure 4-7, and the

reduced pressure losses in the wells due to the selection of a 0.41 meter diameter wellbore [1].

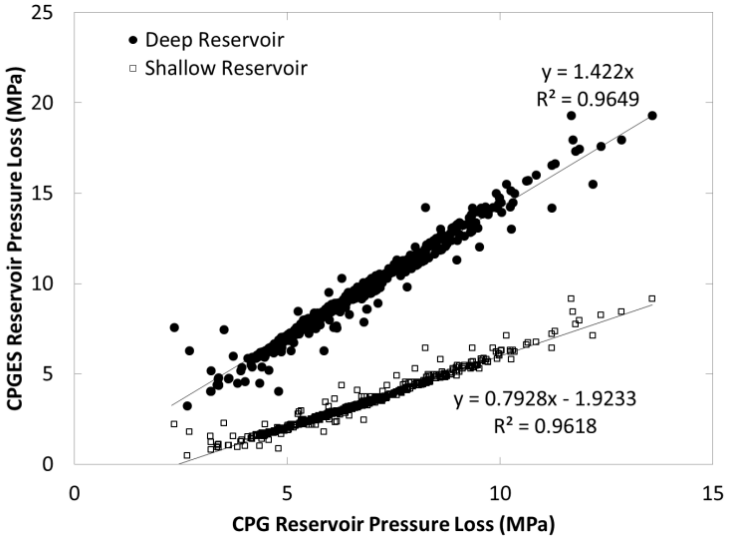

Figure 4-7: The CPGES reservoir pressure loss as a function of the CPG reservoir pressure loss for the same daily circulation of CO_2 for each system.

The reservoir pressure loss, which is dependent on the reservoir permeability and permeability anisotropy, effects the energy generation from the system through the mass flow rate, shown in Figure 4-8. The performance of the CPGES system is shown in Figure 4-8A as a function of the effective permeability, where the effective permeability is a combination of the horizontal permeability and the permeability anisotropy (i.e. $\kappa_e = \frac{\kappa_h}{\ln\left(\frac{k_h}{k_v}+e-1\right)}$). The net energy generation increases with increasing permeability and decreasing anisotropy, as expected. In the given reservoir configuration, the permeability anisotropy decreases the effective permeability by increasing the horizontal dispersion of the CO_2 in the reservoir, limiting the vertical mobility of the CO_2, which increases the pressure difference required for the CO_2 to rise across the 200-meter thickness of the

reservoir. While the net energy varies with the effective permeability, the effective permeability has a limited impact on the energy storage ratio (Figure 4-8B), varying from 2.25 to 2.50 over the range of permeabilities tested. This indicates that the permeability impacts the net energy generated by the system through mass flow rate, effecting the energy generation and storage equally, and it does not impact the ability of the system to time shift energy generation and consumption.

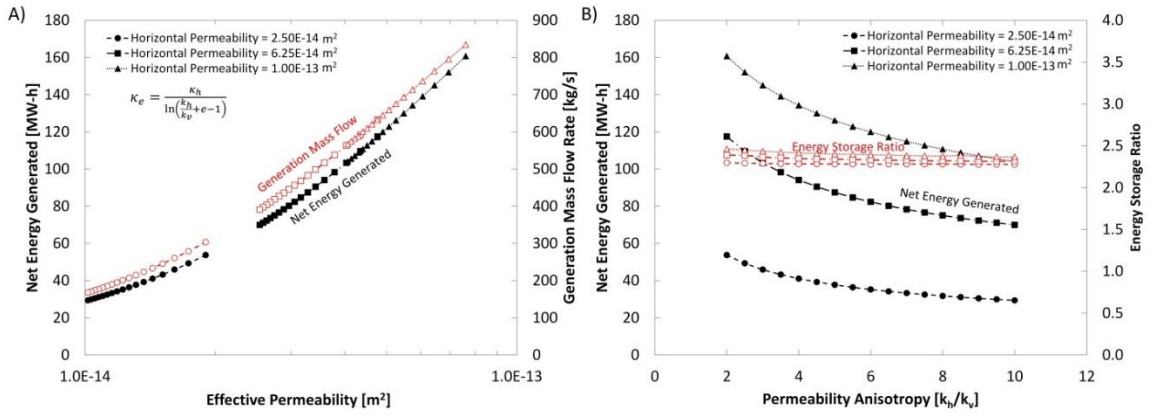

Figure 4-8: Net daily energy generation and energy storage ratio dependence on: A) the horizontal permeability and the permeability anisotropy, C) the deep reservoir depth and temperature gradient, D) the temperature gradient and ambient temperature.

4.3.1.2.4 Combined Effect

Figure 4-9 illustrates how the permeability, the deep reservoir temperature, and the shallow reservoir depth impact the net daily energy generation, with the net daily energy increasing as the reservoir temperature, permeability, and shallow reservoir depth increase. The effects of the shallow reservoir depth and the reservoir permeabilities are more pronounced at higher reservoir temperatures.

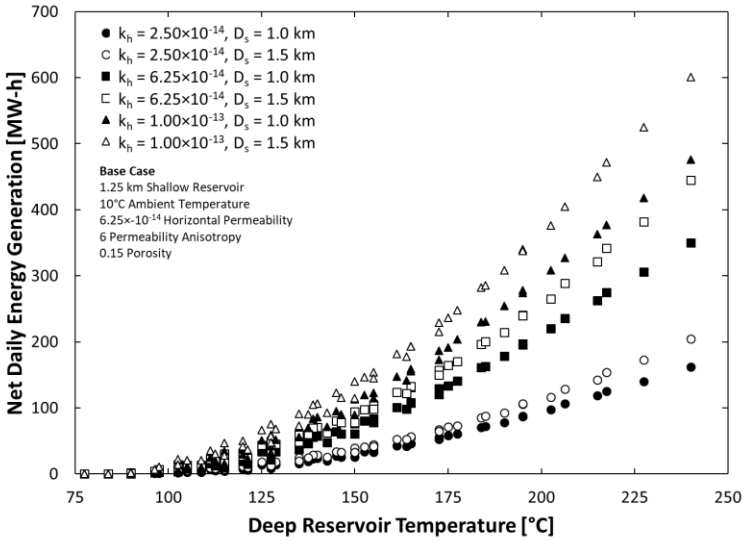

Figure 4-9: Net energy produced as a function of the reservoir temperature for varying permeabilities and shallow reservoir depths for a subset of the parameter space. Net energy generation increases with the deep reservoir temperature, increased reservoir permeability, and shallow reservoir depth.

4.3.1.3 Generation Mode Energy Consumption

The operation of the CPGES system as an energy storage system is defined by the capacity to decouple the turbine generation from the parasitic cooling and pumping loads. This is achieved in the CPGES system with the addition of the shallow reservoir to store the CO_2 after the turbine is used to generate power; however, to inject the CO_2 into the shallow reservoir the density of the CO_2 is increased by cooling (for most cases), requiring power consumption during the generation mode, decreasing the net power generation and the temporal separation of the generation and consumptive elements. Here, the amount of cooling during the generation mode is directly related to the CO_2 density change on the surface, and thus the cooling will be directly impacted by parameters that vary the density of the CO_2 after the turbine (State 3), and the density at the top of the shallow injection

well (State 4), specifically, the geothermal temperature gradient, the shallow reservoir depth and the permeability.

The amount of cooling required during the generation mode increases as the geothermal temperature gradient and the shallow reservoir depth, increase, shown in Figure 4-10A. Here, larger temperature gradients decrease the density of the CO_2 in the reservoir, and thus at the surface at State 3, while increased shallow reservoir depths increase gravitational compression in the injection well, and thus the density of the CO_2 at the top of the injection well at State 4; increasing the amount of cooling in the generation mode.

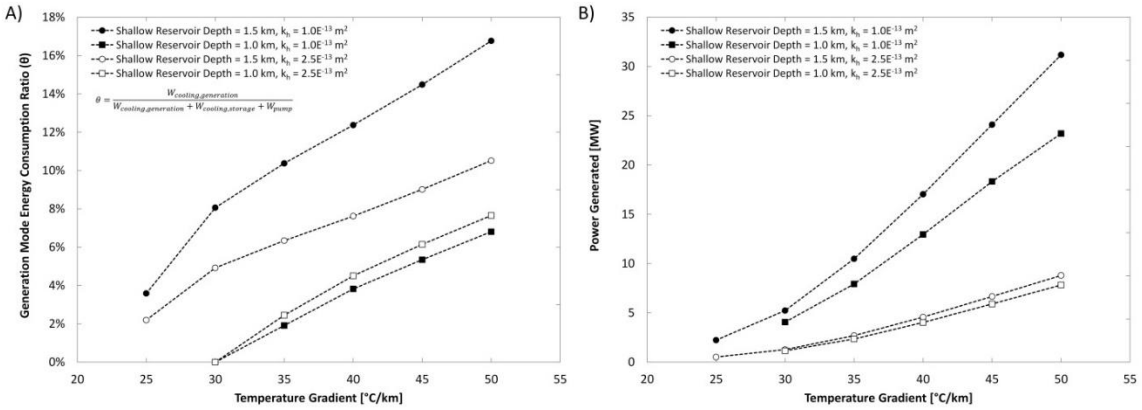

Figure 4-10: A) The percentage of the power consumption that occurs during the generation mode and B) the net power generated during the generation mode. Increases in the thermal gradient and shallow reservoir depth increase the amount of energy consumed during the generation mode, reducing the effectiveness of the system to separate the power consumptive elements from the generation mode.

While increased shallow reservoir depths and geothermal gradients increase the fraction of the total energy that is consumed in the generation mode, they also increase the net power that is generated, in Figure 4-10B. This indicates that while these parameters increase the power consumption during the generation mode, the turbine generates additional power to

counteract this effect. Thus, the system can sustain some parasitic losses in the generation mode and operate as an energy storage system.

4.3.1.4 Reservoir Pressures

The injection and production pressures for the deep reservoir for the CPGES system are shown in Figure 4-11. In the deep reservoir the injection overpressure and the production drawdown pressure are equivalent and symmetric about the hydrostatic pressure. Thus, the maximum overpressure of the reservoir is half the pressure difference between the injection and production well. As previously stated, the CPG and CPGES systems do not artificially fracture the reservoir, thus the injection pressure for these systems must be maintained below the fracture limit of the rock.

The CPGES system operates below the estimated fracture pressure in all cases, indicating that steady operation of the system does not risk fracturing the reservoir. The fracture pressure gradient is estimated to be two times the hydrostatic pressure [131], though this may vary based on the specific regional geophysical properties. The maximum calculated injection pressure ratio for the steady operation of the system are 1.23 and 1.46 for the deep and shallow injection wells, which are 62% and 73% of the calculated fracture limit. The deep reservoir operates below the estimated pressure gradient for extending an existing fracture estimated by the Hubbert and Willis method [132], which is 1.42 times the hydrostatic pressure, however, the shallow reservoir exceeds this limit, indicating that if a pre-existing fracture was present in the shallow reservoir, the operation of the CPGES system could, under select cases, extend the fracture. In the entire parameter space considered, only four shallow reservoir pressure ratios exceeded this limit, most notable

the subset of cases containing the combination of the 4.5 km deep reservoir, 1.0 km shallow reservoir, 50 °C/km geothermal temperature gradient, and $2.5x10^{-14}$ m^2 permeability. While the steady state operation of the system operates with injection pressures below the fracture limit, the initial plume development period, where the overpressure is likely to be maximum, is not simulated for each trial. While it is possible that the development of the CO_2 plume in the reservoir could exceed the fracture limit, the overpressure can be limited by employing an operational strategy while developing the reservoir, such as active reservoir management, which controls the injection mass flow rate and the production of brine from the reservoir [133–136], limiting the reservoir overpressure; however, this is beyond the scope of this study.

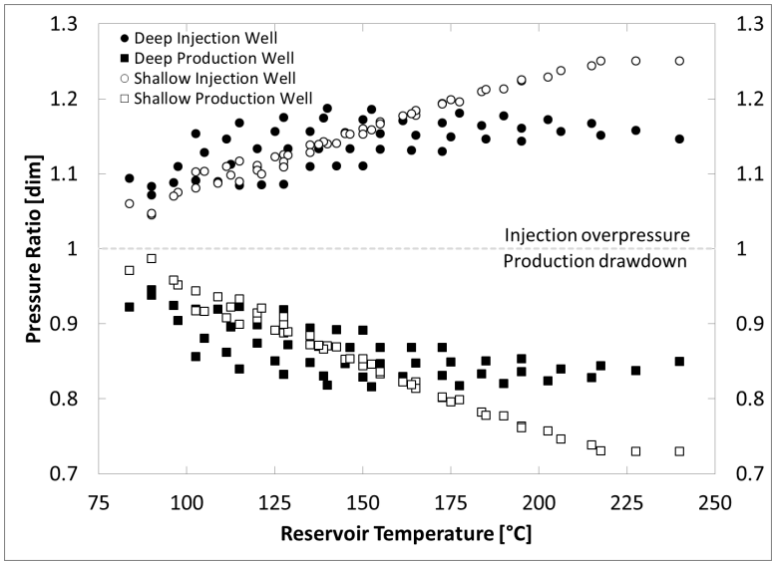

Figure 4-11: The injection overpressure and production drawdown pressures for the shallow and deep reservoirs in the CPGES system for the base case system, with varied deep reservoir depths and geothermal temperature gradients. The pressures are normalized by the hydrostatic pressure (ambient reservoir pressure). The limit for the injection pressure ratio is 2.02 [131].

4.3.1.5 Comparison between CPG and CPGES

We evaluate and compare the net daily energy and net power generation of the CPGES and the CPG systems. Traditionally, such a comparison between an energy storage system and a power generation system would be of little value as each system provides unique characteristics to the energy grid; however, given that the CPGES system is an extension of the CPG technology, we choose to compare the systems to demonstrate the trade-off of the energy storage operation.

4.3.1.5.1 Energy Generation

The CPGES system generates less net daily energy than the CPG system, shown in Figure 4-12. The CPG system operates continuously throughout the day whereas a CPGES system generates electricity for only 16-hours aday. Therefore, for a given parameter set and constant daily circulation rate, we'd expect the net energy production of the CPG system to be 50% greater than the CPGES system. Figure 4-12 shows that a CPG system produces 58% (1/0.63) more net electricity than a CPGES system for a constant daily circulation rate, as we predicted. However, while this shows the comparison between equivalent reservoir heat extraction rates, the CPG system will be independently optimized to produce the most power, which on average generates 288% (1/0.35) more net electricity than a CPGES system. The decrease in energy generation for CPGES results from the increased reservoir pressure losses due to the intermittent injection and production of CO_2 and the additional shallow reservoir, previously shown in Figure 4-7, as well as the elevated turbine backpressure required to maintain the CO_2 in a supercritical state during the generation mode, which for an ambient temperature of 15°C is ~1.5 MPa larger than the CPG turbine

backpressure. This demonstrates the drawback of operating the CPGES system as an energy storage system as decreased net energy generation.

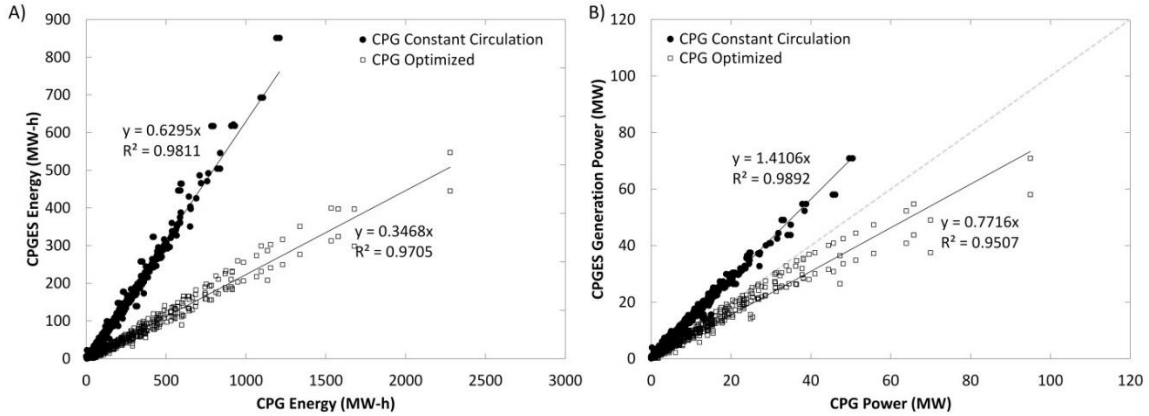

Figure 4-12: The A) net daily energy and the B) power generation of a CPGES system relative to the CPG system for the two cases: 1) the equivalent CO_2 circulation rate and 2) the energy maximized CPG system. The CPG system will always generate more energy than the CPGES system, as the CPGES system sacrifices net energy generation for ancillary energy storage capacity. The CPGES system generates more power than the CPG system for the same reservoir heat extraction, however, when each system is independently operated, the losses in the CPGES system limit the power generation and allow the CPG system to generate more power.

The advantage of the CPGES system is that it can produce more power than the CPG system, given the same reservoir heat extraction rate, during the 16-hour generation mode, shown in Figure 4-12B. For the same daily circulation rate, the CPGES system generates 41% more power than the CPG system, as the CPGES system operates with a 50% larger mass flow rate than the CPG system during the generation mode. The increased power generation during the generation mode is ideal for the CPGES system, as it allows the system to take advantage of price arbitrage, selling power when demanded, and thus price, is high, and consuming power when electricity costs are low.

In this paper the CPG system is optimized for the net power generation, the CPGES system generally operates with lower power generation than the CPG system, generating on average 77% of the power of the CPG system. Here, the decreased power generation for the CPGES system is a result of the optimization of the net daily energy for the CPGES system, which significantly limits the mass flow rate, and thus power generation, due to the increased turbine back pressure and the increased reservoir pressure losses. This limits the effectiveness of the price arbitrage economic model for the CPGES system, unless the system is able generate a revenue during the storage mode by consuming power during periods of negative electricity prices [137,138], due to the excess generation of energy, typically resulting from the increased penetration of variable wind and solar power systems.

Overall, this indicates that for the given CPGES system, optimizing the system for net energy generation, like the CPG power system, does not optimize the performance of the CPGES system, as the restricted mass flow rate limits the power generation of the system. To increase the power generation of the system, the system can operate at a higher mass flow rate, increasing the power generation, but decreasing the net energy generation, as previously shown in Figure 4-3. Alternative operating conditions could include a zero-net daily energy condition, where the system energy generated during the generation mode is equal to the energy consumed in the storage mode, or an optimized power generation in the generation mode. However, the economic operation of the system at either of these conditions could be challenging, as the system would rely on price arbitrage and negative

electricity prices, conditions which are rare in the current energy market, due to the low cost of natural gas. Future work may consider these operational conditions, as well as shorter duty cycles, which would increase the power generated.

4.4 Conclusion

The CPG system can be modified to operate as an energy storage system using two geologic reservoirs at different depths. Our modelling of the CPGES system allows for the following conclusions:

Shallow reservoirs, which are not suitable for energy production, can be used to store CO_2 allowing the system to operate as an energy storage system. The shallow reservoir operates as a storage tank, where produced CO_2 can be temporarily stored before it is further cooled and injected back into the deep reservoir. This temporary storage of CO_2 allows the components which generate power (turbine) to be separated from those that consume power (cooling towers, pumps). Thus, the system can 'store' electricity from the grid. Additionally, the depth of the shallow reservoir affects the performance of the system, with deep shallow reservoirs increasing the net daily energy generation and energy storage ratio, while also increasing the cooling required in the generation mode.

The CPGES system is able to operate with an energy storage ratio greater than one, generating net positive energy to the grid. The CPGES system functions as an energy storage system by operating as an intermittent Rankine cycle, generating net energy due to the heat extraction from the deep reservoir. The net energy generated by the system increases as the effective permeability and the temperature difference between the deep reservoir and the ambient temperature increases.

The injection pressures for the operation of the CPGES system is below the calculated fracture limit, indicating that the system does not risk fracturing the reservoir. The CPGES system operates using the natural permeability of the reservoir, unlike EGS systems which need the permeability of the reservoir to be artificially increased, thus the injection pressure for the operation of the system must remain below the fracture limit for the reservoir. All simulated cases are below the fracture limit, where the maximum injection pressure ratios for each reservoir are 1.23 and 1.46 for the deep and shallow reservoirs, which are 62% and 73% of the calculated fracture limit. The development of the CO_2 plume for each system model is not simulated, and it is assumed that the plume development is achieved using active reservoir management to ensure that the development injection pressure does not exceed the fracture limit.

The operation of the CPG system as an energy storage system increases the power generation relative to the CPG system, at the expense net energy generation, for the same daily CO_2 circulation rate. On average the CPGES system generates 41% more power than the equivalent CPG system due to the increased mass flow rate during the generation mode, and the reduced concurrent consumption of power; but, the addition of the second, shallow reservoir, the additional vertical wells, and the elevated turbine backpressure decreases the net daily energy generation capacity by 37% relative to the CPG system. However, when the CPG system is independently optimized, the CPGES system generates 33% less power, and 65% less daily net energy. This indicates that the CPGES system should not be optimized for the net energy generation, similar to the CPG, but at a mass flow rate that

increases the power generation, or should be operated with a shorter duty cycle (i.e. generation mode).

Chapter 5: CPGES Power and Economics

The Performance of a CO_2-Plume Geothermal Energy Storage System using a Low-Temperature High-Permeability Sedimentary Reservoir

Mark R. Fleming[1], Benjamin M. Adams[2], Thomas H. Kuehn[1], Jeffrey M. Bielicki[3,4], Martin O. Saar[2,5]

[1]Department of Mechanical Engineering, University of Minnesota, USA
[2]Geothermal Energy and Geofluids Group, Department of Earth Sciences, ETH-Zürich, Switzerland
[3]Department of Civil, Environmental, and Geodetic Engineering, The Ohio State University, USA
[4]John Glenn College of Public Affairs, The Ohio State University, USA
[5]Department of Earth Sciences, University of Minnesota, USA

5.1 Introduction

Geothermal energy is an abundant renewable resource that can provide baseload power. The earth's surface is estimated to contain $540x10^7$ EJ of energy [67], which is available for geothermal energy production. In the United States, it is estimated that over 100 GW can be developed by 2050 [16]. The current installed geothermal capacity is 3.52 GW, concentrated primarily in California and Nevada in regions with high geothermal temperature gradients [72]. To achieve 100 GW by 2050, geothermal systems must be expanded to a wider geographic region to utilize undeveloped geothermal resources, which include shallow, low temperature and deep, high-temperature resources. Enhanced Geothermal Systems(EGS) can be utilized to extract heat from deep high temperature and low-permeability reservoirs [16,67,139]; however, EGS requires fracturing [67], which can be controversial and limits EGS projects [140]. Shallow, low-temperature geothermal resources (i.e. <150°C) can be used to produce power using a binary cycle [65]. These low-temperature resources can also be utilized by CO_2-Plume Geothermal (CPG) systems, that

use CO_2 as the heat extraction fluid as part of a Carbon Capture, Utilization, and Storage (CCUS) system [1,33,34,82,83,93,96,119].

CO_2 was initially proposed as a working fluid in EGS systems by Brown [81]. CO_2 has three primary advantages over brine: (1) CO_2 has a larger density variation with temperature, that allows the system to generate a thermosiphon in the wells, reducing or eliminating the need for circulation pumps [1,81,90,91,129], (2) CO_2 has a lower kinematic viscosity, which reduces the pressure losses through the rock in the reservoir, [84,87], and (3) CO_2 has a lower mineral solubility, that will reduce pipe scaling [81]. CO_2 was found to be superior to brine for EGS systems in terms of heat extraction and operation using a thermosiphon [86,90,91]. However, CO_2-EGS has a limited CO_2 storage potential, due to the limited volume of the fractured reservoir [34,96]. In contrast, a CPG system uses sedimentary basin formations that have large CO_2 storage potential, and are the target for Carbon Capture and Storage (CCS) efforts [10,141]. Previous studies have demonstrated the effectiveness of CPG systems at extracting heat and pressure energy from the subsurface reservoirs [33,34,83,94,96,119], power production driven by a thermosiphon [82], and benefits of using CO_2 over brine in sedimentary basins [1].

CCS can work in synergy with a CPG system by developing the necessary subsurface plume. Thus, CPG will benefit from the implementation of CCS, which is a solution to mitigate CO_2 emissions from existing fossil fuel power plants and limit the effects of global climate change [10,142,143]. The emission of CO_2 into the atmosphere, and subsequent rise in the atmospheric concentration of CO_2 has been correlated with the increase in the

mean global temperature by the Intergovernmental Panel on Climate Change (IPCC) [5]. The IPCC set a limit for atmospheric CO_2 of 450 ppm, which has a 50% chance of limiting the mean global temperature rise to 2°C [5], which was agreed upon by a majority of world nations in the Paris Agreement [111]. To avoid exceeding this defined limit an estimated carbon budget of 1000 Gt of CO_2 can be emitted after 2011 [4], which requires a reduction and eventual elimination of CO_2 emissions. In particular for electricity generation and heat production, which accounts for 25% of the total CO_2 emitted into the atmosphere [5], carbon capture and storage can be implemented on existing fossil fuel plants and clean renewable energy sources can be expanded [3,10].

The electrical power industry has developed energy portfolios which include renewable energy sources, and in some cases are required by legislation to expand the utilization of renewable energy. In the United States, individual state legislation may set future renewable energy generation requirements. For example, California requires public utilities to provide 50% of generated electricity to be from renewable sources by 2045 [13], and Hawaii requires 100% renewable energy by 2045 [14]. The European Union has implemented the Renewable Energy Directive, which establishes that renewables contribute 20% of overall energy production, and individual member nations achieving at least 10% by 2020 [12]. The implementation of renewable energy sources typically favors wind and solar over geothermal as these systems are better known, mature technologies. However, wind and solar can produce only variable power, as the nature of the energy resource is inherently variable. This can increase the variability of the electrical grid [47].

Energy storage systems can be used in conjunction with variable renewable sources, such as wind and solar, to ensure consistent energy production and to maintain grid reliability [56,112–114]. Energy storage systems can supplement renewable resources by storing excess power when it is produced, and releasing it back to the grid when needed[50,58,115,116]. Without energy storage, baseload power plants, operated with fossil fuel or nuclear power, are unlikely to be completely replaced by wind and solar. However, geothermal energy, in addition to hydroelectric and bio-energy, can be utilized to produce baseload renewable power [117].

The direct CPG system where CO_2 is passed directly through a turbine and produces continuous power, can be modified to operate as a geothermal energy storage system, intermittently producing and consuming power to/from the electrical grid. This CPG Energy Storage (CPGES) configuration adds a second shallower geothermal reservoir that acts as a "storage tank" for the CO_2, allowing the system to produce and consume power from the electrical grid at different times, enabling the CPGES system to operate as an intermittent power system (i.e. intermittent Rankine cycle). The CPGES system is different from the previously proposed CO_2-Bulk Energy Storage (CO_2-BES) [106,107] system and the Compressed CO_2 Energy Storage system [110]. The CO_2-BES system uses a single reservoir multi-fluid approach, where CO_2 is injected into the reservoir as a cushion gas, increasing the reservoir pressure and displacing brine, using the reservoir overpressure to produce brine. The Compressed CO_2 Energy Storage system uses a multi-reservoir approach, similar to the proposed CPGES system, however, the system uses geothermal

heat to pre-heat the CO_2, with the majority of the heat being added at the surface by combusting fuel, operating as an intermittent supercritical Brayton cycle, whereas the CPGES system described here operates using only geothermal heat using a supercritical Rankine cycle. In addition, modeling of the Compressed CO_2 system neglects the vertical injection/production wells and does not couple the surface power plant model with a sub-surface model, which are both considered here in the CPGES system model.

Table 5-1: Nomenclature

Variable	Parameter
C	Cost [$]
CRF	Capital Recovery Factor
f	Friction factor
g	Gravitational Constant [m/s^2]
η	Efficiency [Dim]
h	Enthalpy [MJ/kg]
λ	Parasitic loss fraction
M	Daily Circulation Rate [kt/day]
$\dot{m}$	Mass Flow Rate [kg/s]
mf	Mass Fraction
P	Pressure [kPa]
$\dot{Q}$	Heat Rejection [MW]
ρ	Density [kg/m^3]
T	Temperature [°C]
t	Time [h]
TR	Tax Rate [%]
V	Velocity [m/s]
$\dot{W}$	Power [MW]
W	Energy [MW-h]
y	Payback Period [y]
z	Thickness [m]

We model a demonstration scale CPGES system in terms of the power and energy generated/consumed during each mode and over the course of an entire 24-hr cycle, varying the daily circulation rate and the duty cycle. We then compare the system to an equivalent CPG plant, operating with the same deep reservoir configuration. Finally, we

combine the CPG and the CPGES systems, operating each one concurrently, demonstrating the synergistic effects of the hybrid system.

5.2 Method

5.2.1 System Overview

We consider three independent CO_2 geothermal power systems, 1) the CPG system, 2) the CPGES system, and 3) the combined CPG+CPGES system, described in detail below.

5.2.1.1 CPG

The CPG system is comprised of a permeable sedimentary reservoir with a bounding caprock to contain the CO_2 within the reservoir, a surface plant to extract energy from the CO_2 and produce power, and vertical injection and production wells which connect the surface plant to the reservoir [33,34,96], shown in Figure 5-1. The direct CPG system operates by circulating CO_2 from a deep reservoir to the surface to extract energy, shown by the red lines in Figure 5-1. To produce power, CO_2 is extracted from the deep, hot storage reservoir (State 1) and brought to the surface through vertical wells (State 2). On the surface, the CO_2 is directly expanded in a turbine (State 4) producing electricity. Alternatively, a binary system, where the CO_2 is used to heat a secondary fluid to produce power can be used, however, the direct system has been shown to produce more power [1], thus we consider only the direct cycle. After the turbine, the CO_2 is cooled using a wet cooling tower before it is reinjected into the reservoir (State 5). This increases the density of the CO_2 for reinjection, as the CPG system makes use of gravitational compression, and thus a thermosiphon effect, in the vertical injection well. At the top of the well, a pump can be used to augment compression of the CO_2 (State 6) to ensure that the required downhole pressure is achieved (State 7). This pump is not always required, as the system can operate

using only the thermosiphon; however, use of a circulation pump generally increases the net power generation from the system [1,82].

5.2.1.2 CPGES

To operate as an energy storage system, the CPG system is augmented with a shallow geothermal reservoir, allowing the system to temporally separate the power generation elements (i.e. the turbine) from the elements that consume power (i.e. the cooling towers and the pump) as shown in Figure 5-1. The CPGES system operates using two modes:

1) **Power Generation:** The CO_2 is produced from the deep reservoir and brought to the surface in the production well and expanded in the high-pressure turbine (HPT) to produce power, as in a CPG system (States 1,2,3). After the HPT, the CO_2 is partially cooled in a cooling tower (State 8), increasing the density of the CO_2 only enough to utilize gravitational compression in the short vertical well to inject the CO_2 into the shallow reservoir (State 9). In the shallow reservoir the CO_2 is trapped and stored until the energy storage mode. During the power generation mode net power is generated to the grid from the turbine; however, some parasitic power consumption may be required to operate the cooling tower.
2) **Energy Storage:** The CO_2 stored in the shallow reservoir is recovered (State 10) and transported back to the surface in the short vertical well (State 11). It is then passed through the cooling towers, pump, and the vertical injection well (States 5, 6, 7) where it is cooled and compressed, similar to a CPG system. The throttling valve (State 11 to 4) is not required to operate the CPGES system; however, it is

required when the CPGES system is combined with the CPG system (CPG + CPGES system, discussed in detail below).

In the CPGES system described here, the shallow reservoir is utilized as a temporary storage vessel for CO_2, not for geothermal heat extraction, allowing the system to produce power with minimal power consumption during the production mode. A shallow reservoir is the ideal storage solution for a CPGES system, preferable to surface pressure vessel storage due to the high pressures of the CO_2, and the large capacity required. A surface storage solution would require significant cooling after the turbine. This would consume more power to operate the cooling tower fans and thus, reducing the ability to effectively time shift the energy consumption of the system. Additionally, the produced CO_2 may also include some brine, which can be produced from the reservoir as a liquid or in solution with the CO_2. When combined with the CO_2 it can form carbonic acid which can compromise the integrity of a surface storage vessel. The use of the shallow geothermal reservoir allows the system to avoid these issues as the injection of CO_2 into a shallow reservoir requires minimal cooling during the power production mode and the reservoir most likely contains some brine anyway. In this configuration, some cooling, and thus power consumption, is required to increase the density of the CO_2 prior to injection into the shallow reservoir; however, this cooling is ideally only a fraction of the overall cooling, with the majority occurring during the storage mode. The minimal cooling allows the system to use gravitational compression in the short vertical injection well to inject CO_2

into the shallow reservoir, without the need for pumping during the power production mode.

5.2.1.3 CPG+CPGES

In the previous descriptions, the CPG and CPGES systems were considered to be independent operations, with the system either being operated for net power generation (CPG) or energy storage (CPGES). In this mode, we combine them where the CPG system operates continuously and the CPGES system provides flexible energy generation or storage simultaneously.

To operate the combined CPG + CPGES systems, we add a low-pressure turbine (LPT) to the CPG line after the high-pressure turbine (HPT), and a throttling valve for the fluid extracted from the shallow reservoir shown in Figure 5-1. The low-pressure turbine is added to the CPG system to expand the CO_2 further as the back pressure from the high-pressure turbine is above the CO_2 saturation pressure at the given cooling tower outlet temperature (i.e. the sum of the ambient wet bulb temperature and the approach temperature) as the CPGES system requires a larger back pressure to account for the pressure losses in the shallow reservoir.

During the CPGES power production mode, the CPGES mass flow is diverted after the high pressure turbine to one of the cooling towers and sent to the shallow reservoir for storage (States 3, 8, 9), while the CPG mass flow is further expanded in the low-pressure turbine, to produce more power, before it is cooled, compressed, and re-injected back into the deep reservoir (States 3, 4, 5, 6, 7). In this mode, both systems extract CO_2 from the

deep reservoir using the same production wells and both systems produce power using the high-pressure turbine (States 1, 2, 3).

During the CPGES recharge mode, CO_2 is extracted from the shallow reservoir and mixed with the CO_2 leaving the low-pressure turbine. The surface pressure of the CO_2 produced from the shallow reservoir (State 11) is typically larger than the CPG low-pressure turbine backpressure; thus, the CPGES system has an added throttling valve which allows the pressure of each system to equilibrate prior to mixing. Similar to the generation mode, both systems operate using the same cooling tower, pump or throttling valve, and deep injection well in the recharge mode (States 4, 5, 6, 7).

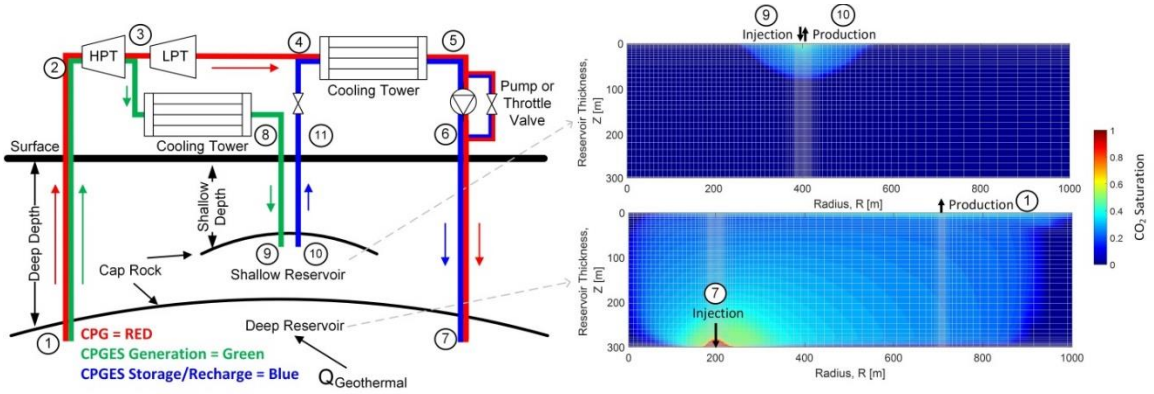

Figure 5-1: Overview of the CPG (red), CPGES generation (green) and storage (blue), and the combined CPG+CPGES (red + green + blue) system with the defined state points. The CPGES system operates in two modes: 1) Energy Generation: where CO_2 is produced from the deep reservoir (State 1), brought to the surface (state 2), expanded in a trubine (State 3), partually cooled (State 8), and the injected into the shallow reservoir (State 9), and 2) Energy Storage: where the CO_2 is extracted from the shallow reservoir (State 10) and produced to the surface (State 11), cooled (State 5) and compressed (State 6) before it is injected into into the deep reservoir (State 7); whereas the CPG systm operates continously (States 1-7). A detailed cycle analysis for each system is provided in the main text. Both the shallow (top) and deep (bottom) reservoir configurations are displayed with the initial CO_2 plume with the mesh grid overay.

5.2.2 System Modeling

We simulate the CPG, CPGES, and CPG+CPGES systems using two separate models: the subsurface reservoir model, and the surface power plant model. We model the subsurface reservoir using the TOUGH2 [120] with the ECO2N [121] equation of state module and model the surface power plant (including the vertical wells) using Engineering Equation Solver (EES) [122].

Table 5-2: Reservoir physical properties for the numerical simulation.

Simulated Parameter/Value			
General Properties		Deep Reservoir	
Horizontal Permeability	5.0×10^{-14} m^2	Mean Reservoir Depth	2.5 km
Vertical Permeability	5.0×10^{-14} m^2	Initial Reservoir Temperature	102.5 °C
Thermal Conductivity	2.1 W/m/°C	Injection Well Radius	200 m
Porosity	10%	Production Well Radius	707 m
NaCl Concentration	20%	Number of grid cells, vertical	42
Geothermal Gradient	35 °C/km	Number of grid cells, horizontal	117
Reservoir Thickness	300 m		
Rock Density	2650 kg/m^3	Shallow Reservoir	
Rock Specific Heat	1000 J/kg/°C	Mean Reservoir Depth	1.5 km
Simulated Radius	100 km	Initial Reservoir Temperature	67.5 °C
Initial Conditions	Hydrostatic equilibrium, pore space occupied by brine	Well Radius	400 m
		Number of grid cells, vertical	34
Boundary Condition Top/Bottom	No fluid flow, semi-analytic heat transfer	Number of grid cells, horizontal	121
Boundary Condition Lateral	No fluid or heat transfer		

5.2.2.1 Reservoir Modeling

We numerically simulate the CO_2 plume development and circulation in the reservoirs. Each reservoir is modeled using a three-dimensional, axisymmetric geometry using the reservoir parameters given in Table 5-2, illustrated in Figure 5-1. Each reservoir is simulated out to 100 km, consistent with previous models [83], to limit boundary effects on the pressure and the plume development. We apply a no fluid flow boundary condition on the top and bottom boundaries to simulate the bounding effects of the caprock above and the bedrock below, with the conductive heat flux across the boundary modeled using a semi-analytic solution [120].

5.2.2.1.1 Deep Reservoir

The deep reservoir is the primary reservoir for the system, with both the CPG and CPGES systems circulating CO_2 to extract heat. The deep reservoir operates with two horizontal wells, an injection well and a production well, shown in Figure 5-1. The injection well is located at the bottom of the reservoir, at a radius of 200 meters, unlike previous CPG simulations, which use a single vertical injection well [1,82,83,119,126]. We use the horizontal well for this configuration to reduce the over pressurization in the reservoir due to the injection of CO_2, as the horizontal well is longer, and for the same mass flow rate the mass flux will be lower, creating smaller pressure changes, reducing the pressure build up compared to the vertical injection well. The injection well is placed at the base of the reservoir to increase the area swept by the CO_2 plume in the reservoir, as the CO_2 is naturally buoyant at reservoir conditions, and thus will buoyantly rise to the top of the reservoir, extracting heat from the entire thickness of the reservoir. At the top of the reservoir, a layer of CO_2 is formed, as the CO_2 is contained beneath the caprock. The production well is located in this CO_2 rich layer, just beneath the caprock at a radius of 707 meters, consistent with previous CPG simulations [1,33,82,83,119], limiting the upconing of brine during the extraction of CO_2 from the reservoir.

The CO_2 plume that is used to circulate CO_2 in the deep reservoir is developed for 2.5 years prior to the operation of the system. The CO_2 plume is developed in the brine filled reservoir by injecting 15.78 Mt of CO_2 into the reservoir during the priming period, a volume which is sufficient enough to ensure the CO_2 breakthrough at the production well. At the end of the priming period, the CO_2 mass fraction at the production well is over 30%,

which results in a CO_2 mass fraction over 94% in the fluid extracted from the reservoir during the operation of the system, which is the approximated limit for specialized turbines [128].

5.2.2.1.2 Shallow Reservoir

The shallow reservoir is added to the CPGES system to separate the elements that generate and consume power. In this system, the shallow reservoir is used as a storage tank, storing the CO_2 that was produced during the generation mode. To function as a storage tank, injecting and then recovering the CO_2, the reservoir operates with a single horizontal well, which functions as an injection and production well. The use of a single well in the system limits the CO_2 plume losses, due to advection and diffusion, allowing most of the injected CO_2 to be recovered, during the storage mode, when CO_2 is extracted from the reservoir. The single well is located beneath the caprock, thereby limiting buoyant advection effects, at a radius of 400 meters. Similar to the deep horizontal injection well, the radius of the horizontal well in the shallow reservoir was selected to reduce the pressure transients in the shallow reservoir, due to the injection and production of CO_2.

Before the operation of the CPGES system, a CO_2 plume in the shallow reservoir is developed by injecting 0.67 Mt of CO_2 over 12 weeks. Unlike the deep reservoir, the plume in the shallow reservoir is not designed to facilitate the circulation of CO_2. But rather, displace the native brine from the horizontal well, forming a pocket of CO_2 around the well, allowing the reservoir to operate with a smaller CO_2 plume than the deep reservoir. This pocket of CO_2 has two main effects, first it displaces the brine, which has a larger kinematic viscosity than CO_2, which limits the variation in pressure due to the

injection and production of CO_2 during the storage operation, and secondly, the CO_2 pocket limits the amount of brine that is extracted from the reservoir during the storage mode.

While the reservoir is designed to operate with minimal CO_2 loses, diffusion and advection of the CO_2 in the reservoir occur, reducing the plume size over time. To account for these losses, the system supplements the CO_2 plume by retaining 98% of the injected CO_2 each cycle, transferring the CO_2 from the deep reservoir to the shallow reservoir.

5.2.2.2 Power System Modeling

The thermodynamic power system is comprised of the turbine, cooling towers, pump, throttling valve, and the vertical wells. The state points for the CPG, CPGES, CPG+CPGES systems are defined in Figure 5-1 and the main surface plant parameters are given in Table 5-3.

Table 5-3: Parameters used for the surface power plant simulations.

Parameter/Value	
Surface Wet Bulb Temperature	15 °C
Vertical Well Inner Diameter	0.41 m
Deep Reservoir Vertical Production Wells	4
Deep Reservoir Vertical Injection Wells	1
Shallow Reservoir Vertical Wells	2
Turbine Backpressure	7.5 MPa
Turbine Isentropic Efficiency	78%
Pump Isentropic Efficiency	90%
Cooling Tower Approach Temperature [a]	7°C

[a] when the temperature of the produced CO_2 is less than 22°C the approach temperature is reduced i.e. $T_{approach} = T_4 - 15$

We numerically simulate the vertical wells using the well model of Adams et al. [1], using a steady state finite volume approximation, with the vertical wells subdivided into 100-

meter elements. We numerically integrate across each element (i.e. from state i to state i+1), starting with the reservoir state, which is determined from the subsurface reservoir model, to the surface. Across each element, we solve the continuity, energy balance, and momentum equations, given as,

$$h_i + gz_i = h_{i+1} + gz_{i+1} \tag{5-1}$$

$$P_i + \rho_i g z_i = P_{i+1} + \rho_{i+1} g z_{i+1} - \Delta P_{loss} \tag{5-2}$$

$$\dot{m} = \rho_i A V_i = \rho_{i+1} A V_{i+1} \, . \tag{5-3}$$

We assume that that well is adiabatic, and neglect the kinematic effects as the energy change is insignificant in the overall energy balance [1,129]. We model the frictional pipe losses using the Darcy-Weisbach relation, given as,

$$\Delta P_{loss} = f \frac{L_{pipe}}{D} \rho \frac{V^2}{2} \, . \tag{5-4}$$

Where the friction factor is determined from the moody chart [144] using a surface roughness (ε) of 55 μm, based on bare Cr13 oil piping [124]. We model each well using a 0.41m diameter well, to limit the pressure losses in the well, which can be significant and reduce the performance the system when small diameter wells are used [1,91]. In the system configuration presented here, the CPG system operates with 5 vertical wells, four production wells and one injection well into the deep reservoir, similar to previous studies [1], while the CPGES system operates with seven vertical wells, the five CPG vertical wells in addition to two vertical injection/production wells into the shallow reservoir.

The CPG, CPGES, and CPG+CPGES systems produce power by directly expanding CO_2 in the turbine, modeled as,

$$\dot{W}_{CPG,turbine} = \dot{m}_{CPG}(h_2 - h_4), \tag{5-5}$$

$$\dot{W}_{CPGES,turbine} = \dot{m}_{CPGES,generation}(h_2 - h_3). \tag{5-6}$$

The turbine operates with an isentropic efficiency of 78%, which is consistent with previous CPG models [1,82]. We set the turbine backpressure for the CPGES system at 7.5 MPa (State 3), to account for additional pressure losses in the shallow reservoir and to maintain the CO_2 supercritical during the generation mode, preventing multiphase flow in the vertical injection well (State 8). The CPG system operates with a turbine backpressure of 5.4 MPa, the saturation pressure for the minimum CO_2 temperature, 22°C, which is the sum of the ambient wet bulb and the approach temperatures.

The cooling towers consume parasitic power to operate the fans which reject heat from the CO_2 to the surrounding atmosphere. We model the parasitic power consumption for the cooling towers as a fraction of the total heat rejection, given as,

$$\dot{W}_{CPG,cooler} = \lambda_{CPG}\dot{Q}_{CPG},. \tag{5-7}$$

$$\dot{W}_{CPGES,cooler,generaton} = \lambda_{CPGES,generation}\dot{Q}_{cooler,generation}, \tag{5-8}$$

$$\dot{W}_{CPGES,cooler,storage} = \lambda_{CPGES,storage}\dot{Q}_{cooler,storage}, \tag{5-9}$$

where, λ is the parasitic loss fraction, which is a function of the cooling tower approach temperature and the ambient wet bulb temperature, as defined in Adams et. al [1]. For each case, the heat rejection rate is defined as,

$$\dot{Q}_{CPG,cooler} = \dot{m}_{CPG}(h_4 - h_5), \tag{5-10}$$

$$\dot{Q}_{CPGES,cooler,generation} = \dot{m}_{CPGES,generation}(h_3 - h_8), \quad (5\text{-}11)$$

$$\dot{Q}_{CPGES,cooler,storage} = \dot{m}_{CPGES,storage}(h_4 - h_5). \quad (5\text{-}12)$$

The pump consumes power, given as,

$$\dot{W}_{CPG,pump} = \dot{m}_{CPG}(h_5 - h_6), \quad (5\text{-}13)$$

$$\dot{W}_{CPGES,pump} = \dot{m}_{CPGES}(h_5 - h_6), \quad (5\text{-}14)$$

The pump operates with an isentropic efficiency of 90%, consistent with previous CPG models [1]. In some instances, the pump can be replaced by a throttling valve, depending on the reservoir pressure, and the gravitational compression in the vertical well. Additionally, the CPG+CPGES system operates with a throttling valve in the storage process, to equilibrate the pressure at the surface before the cooling towers. In each case, the throttling is modeled as an isenthalpic process.

5.2.2.3 System Performance

We define the net power generation as the sum of the power from each specific component. For the CPG system, the net power is given as,

$$\dot{W}_{CPG,net} = \dot{W}_{CPG,turbine} + \dot{W}_{CPG,cooling} + \dot{W}_{CPG,pump}, \quad \textbf{(5-15)}$$

whereas the net power generation for the CPGES system is the sum of each component during the generation mode, given as,

$$\dot{W}_{CPGES,Generation} = \dot{W}_{CPGES,turbine} + \dot{W}_{CPGES,cooling,generation}. \quad (5\text{-}16)$$

Similarly, the net power that is consumed by the CPGES system during the storage mode is given as,

$$\dot{W}_{CPGES,storage} = \dot{W}_{CPGEES,cooling,storage} + \dot{W}_{CPGES,pump}. \quad (5\text{-}17)$$

The energy that the system generates or consumes is given as the integral of the power over the length of the operation, given as,

$$W_{CPG,net} = \int_0^{24\text{h}} \dot{W}_{CPG,net} dt, \quad (5\text{-}18)$$

$$W_{CPGES,generation} = \int_0^{t_{generation}} \dot{W}_{CPGES,generation} dt, \quad (5\text{-}19)$$

$$W_{CPGES,storage} = \int_{t_{generation}}^{24h} \dot{W}_{CPGES,storage} dt, \quad (5\text{-}20)$$

$$W_{CPGES,net} = W_{CPGES,generation} + W_{CPGES,storage}, \quad (5\text{-}21)$$

The CPG system operates continuously for 24 hours but the CPGES system generates energy only during the generation mode, and then consumes energy during the storage mode; the length of each mode is determined by the CPGES duty cycle. We define the duty cycles of the CPGES system as the length of the generation mode divided by the total cycle length, which is set at 24 hours for the diurnal cycle, given as,

$$Duty\ Cycle = \frac{t_{generation}}{24}. \quad (5\text{-}22)$$

To illustrate the effect of the duty cycle on the operation of the system, we selected 4 generation times; 16 hours, 12 hours, 8 hours, and 4 hours which we refer to as the 16-8, 12-12, 8-16, and 4-20 cycles, given in Table 5-4.

For the combined CPG+CPGES system, the power, and thus energy, that the system generates and consumes is the sum of the CPG and CPGES components. The utilization of the CPG and CPGES elements in the CPG+CPGES system is determined by the fraction of the total generation mode mass flow rate, or the mass flow rates of CO_2 extracted from the deep reservoir that is used for each, defined as,

$$mf_{CPG} = \frac{\dot{m}_{CPG}}{\dot{m}_{CPG}+\dot{m}_{CPGES,generation}}, \quad (5\text{-}23)$$

$$mf_{CPGES} = \frac{\dot{m}_{CPGES,generation}}{\dot{m}_{CPG}+\dot{m}_{CPGES,generation}}. \quad (5\text{-}24)$$

where the daily circulation rate for each element is defined as,

$$M_{CPG} = \int_0^{24h} \dot{m}_{CPG} dt, \quad (5\text{-}25)$$

$$M_{CPGES} = \int_0^{t_{generation}} \dot{m}_{CPGES,generation} dt. \quad (5\text{-}26)$$

To illustrate the performance of the CPG+CPGES system, we select a total of five CPGES mass fractions (mf_{CPGES}); 0%, 25%, 50%, 75%, and 100%, where the bounding cases (i.e. the 0% and 100% cases) are the operation of the CPG and CPGES systems in isolation.

Table 5-4: Duty cycles

Duty Cycle	Cycle Parameter	Cycle Characteristics
16-8	16-hour generation mode 8-hour storage mode	Peaking power consumption with extended power generation
12-12	12-hour generation mode 12-hour storage mode	Balanced power generation and consumption
8-16	8-hour generation mode 16-hour storage mode	Moderate peaking power generation with extended power consumption
4-20	4-hour generation 20-hour storage mode	Full peaking power generation with extended power consumption

5.2.2.4 Cost Modeling

We estimate the costs of the CPG, CPGES, and CPG+CPGES system using an economic model compiled from the Geothermal Energy Technology Evaluation Model (GETEM) [145] and the U.S. EPA Carbon Sequestration Technology Cost Analysis [146] to estimate the system costs. All cost estimates are provided in United States dollars.

We estimate the total turbine cost, which comprises the turbine and generator, using the GETEM model [145], adjusting for inflation; where total turbine cost scales with the power generated by the turbine, given as,

$$C_{turbine} = 12788\left(1000\,\dot{W}_{turbine}\right)^{0.6}. \tag{5-27}$$

We estimate the equipment costs by summing the costs of the three primary pieces of power equipment; the turbine-generator, pump, and cooling towers.

The cooling tower costs are estimated using the Baltimore Aircoil Company FXV closed loop cooling towers and the PC2 closed loop condensing towers [147], scaling with the heat rate rejected through the cooling tower, the temperature difference for the closed loop fluid ($T_{TC,\,range}$), and the approach temperature, modeled as,

$$C_{cooling\ tower} = \left(C_{cooling} + C_{condensing}\right)(3)\left(\frac{\dot{Q}_{cooling}+\dot{Q}_{condensing}}{1000}\right)^{-0.2}, \tag{5-28}$$

$$C_{cooling} = \left((0.0141\,T_{ambient} - 0.745)\,T_{TC,range} + \frac{(1470-34.4\,\dot{Q}_{cooling})}{T_{approach}}\right)\dot{Q}_{cooling}, \tag{5-29}$$

$$C_{condensing} = \left(\frac{(1010-18.5\,\dot{Q}_{condensing})}{T_{approach}}\right)\dot{Q}_{condensing}. \tag{5-30}$$

We estimate the circulation pump cost using the GETEM correlation [145], which scales the pump cost with power, given as,

$$C_{pump} = 3604\left(1000\,\dot{W}_{pump}\right)^{0.767}. \tag{5-31}$$

The total estimated equipment cost is the sum of the three primary components, the turbine-generator, pump, and cooling tower, given as,

$$C_{Equipment} = C_{turbine} + C_{pump} + C_{cooling\ tower}. \tag{5-32}$$

The total surface plant cost, or Engineering Procurement and Construction Cost (EPCC), which includes the costs of construction, materials, labor, secondary components, and other additional costs, scales with the total equipment costs, given as,

$$C_{EPCC} = C_{Equipment}(1 + x_{MCC} + x_{LCC} + x_{CMC} + x_{ST} + x_F)(1 + x_I), \quad (5\text{-}33)$$

where the component cost fractions are given in Table 5-5.

In addition to the surface power plant, we consider the costs of surface piping, the vertical well costs, and the reservoir development costs, which are obtained from U.S. EPA Carbon Sequestration Technology Cost Analysis [146]. For the given configuration, the surface piping costs $2.05M, and the vertical wells cost $10.72M for each 2.5km deep injection well, $10.37M for each 2.5 km deep production well, and $6.38M for each 1.5 km deep well, assuming a 100% well drilling success rate. The reservoir development cost for a single deep reservoir is estimated to be $2.47M, while the cost for the two-level CPGES system is $4.71M.

The total project capital cost (TPCC) is the sum of the EPCC, vertical well, surface pipe, and reservoir costs, with an added contingency cost. The total project capital cost includes a project and process contingency which account for unexpected costs, and variation in the system performance, modeled as,

$$C_{TPCC} = (x_{Pc2} + 1)\left((x_{pc1} + 1)(C_{EPCC} + C_{pipes} + C_{reservoir})\right) + C_{wells}. \quad (5\text{-}34)$$

Here, the well cost is not included in the contingency, as the quoted well cost includes the well contingency costs.

Table 5-5: Economic model parameters

Parameter	Cost Fraction
x_{MCC}	(0.39) Material Capital Cost
x_{LCC}	(0.81) Labor Construction Cost
x_{CMC}	(0.25) Construction Material Cost
x_{ST}	(0.05) Sales Tax
x_F	(0.05) Freight
x_I	(0.12) Indirect
x_{pc1}	(0.10) Process Contingency
x_{pc2}	(0.15) Project Contingency
x_d	(0.05) Discount Rate

We calculate the specific capital costs (SCC) of the system by dividing the TPCC by the power generation capacity of the system, given as,

$$SCC_{CPG} = {TPCC}/{\dot{W}_{CPG,net}}, \tag{5-35}$$

$$SCC_{CPGES} = {TPCC}/{\dot{W}_{CPGES,Generation}}. \tag{5-36}$$

For the CPG+CPGES system we use the same definition as the CPGES system, using the installed power capacity for the generation mode (maximum power generation) to define the specific capital cost.

CO_2 Tax Credits

The development of the greenfield CPG and CPGES systems requires captured CO_2 to be injected into the subsurface reservoirs to develop the CO_2 plume. Currently in the United States, the injection and geologic storage of CO_2 is eligible to receive a tax credit based on the mass of CO_2 stored, with the more resent revision to the tax code increasing the tax credit for sequestered CO_2 each year, from the current $20 per ton to $50 per ton in 2026 [148]. Based on these tax credits, the CPGES system, that requires 16.45 Mt of CO_2, would receive $329M to $822M, or approximately 1.6 to 3.9 times the total project capital cost

for our most expensive CPGES system. While the CPGES operator, the direct injector of the CO_2 into the subsurface, would directly receive these benefits, it is highly likely that these benefits would be transferred to the CO_2 source to provide incentive and offset the cost of capturing the CO_2, which can range from $21.5 per ton from natural gas to $83 for coal [149,150]. Therefore, in our economic model, we assume that the benefit from the CO_2 tax credit is used to offset the cost of the carbon capture.

5.3 Results and Discussion

We demonstrate how the CPG, CPGES, and CPG+CPGES systems will operate for the given reservoir configuration. Each system is characterized in terms of the net daily energy generation, average power generation and consumption (for energy storage configurations), and the specific capital cost, summarized in Table 5-6 for the CPG and CPGES system, and Table 5-7 for the CPG+CPGES system. The reported results for all cases are after 10 years of continuous operation, to avoid any initial transients due to the overpressure of the reservoir caused by the injection of CO_2 for the plume development. Some cases resulted in inoperable conditions and are not reported, notably at elevated CO_2 circulation rates, where the CO_2 extracted from the shallow reservoir is below the minimum temperature (i.e. the ambient wet bulb temperature plus the cooling tower approach temperature) due to the pressure variation in the shallow reservoir, and therefore could not be cooled by the system.

Several trends are immediately apparent in the data: the power generation in the CPGES system increases with increasing mass flow rate and decreasing duty cycle, the capital costs increase with increasing mass flow rates and decreasing duty cycles, and the CPGES

system can generate more power than the CPG system, but the CPG system generates more daily net energy and has a lower capital cost.

5.3.1 CPG Results

The amount of power, and thus energy, generated by the CPG system varies with the mass flow rate, shown in Figure 5-2. As the mass flow rate increases the turbine produces more power; however, the pressure losses within the reservoir and surface piping also increase, decreasing the pressure differential across the turbine, and increasing the amount of pumping required. This counteracts the turbine output gains resulting in a maximum net power, and thus energy, condition at a specific mass flow rate. As the CPG system is designed to generate and sell electricity continuously, we define the maximum net power condition as the design point for the CPG system, similar to Adams et al. [1]. For the system parameters considered here, the optimal mass flow rate is 450 kg/s (or 38.88 kt/day) resulting in 60.1 MW-h of energy generation (2.5 MW of continuous power production).

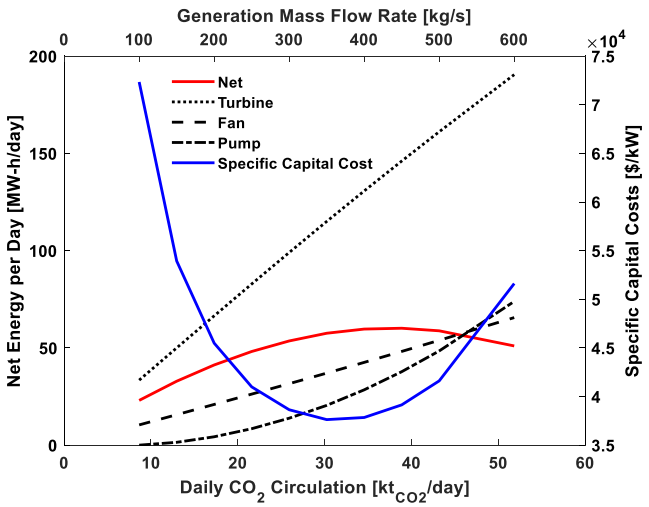

Figure 5-2: The daily energy generation and consumption for major system elements and the specific capital costs for the CPG system.

Table 5-6: Summary of the key power, energy, and economic performance parameters for the CPG and CPGES cases.

Configuration/Duty Cycle	Mass Flow Rate (kt/day)	Net Energy (MW-h/day)	Average Power Generated (MW)	Average Power Stored (MW)	Specific Capital Cost ($/kW$_e$)	Capital Cost (M$)
CPG	8.64	23.01	0.96	-	72,342	69.36
	12.96	32.87	1.37	-	53,937	73.88
	17.28	41.23	1.72	-	45,489	78.14
	21.60	48.15	2.01	-	40,994	82.25
	25.92	53.58	2.23	-	38,640	86.26
	30.24	57.53	2.40	-	37,627	90.20
	34.56	59.69	2.49	-	37,845	94.12
	38.88	60.10	2.50	-	39,142	98.02
	43.20	58.79	2.45	-	41,611	101.92
	51.84	51.02	2.13	-	51,616	109.72
16-8	5.76	7.13	0.80	-0.71	10,7124	85.92
	8.64	10.20	1.19	-1.10	77,298	92.02
	11.52	13.39	1.57	-1.45	61,620	96.70
	14.40	15.57	1.94	-1.91	52,385	101.46
	17.28	14.28	2.30	-2.79	46,778	107.37
	20.16	10.46	2.64	-3.94	42,664	112.67
	23.04	4.21	2.97	-5.35	39,761	118.02
	28.80	-18.77	3.48	-9.19	37,020	128.53
	34.56	-51.38	3.88	-14.02	38243	147.78
	40.32	-119.37	4.18	-23.06	49239	205.07
12-12	5.76	7.27	1.06	-0.46	77,984	83.00
	8.64	10.28	1.58	-0.71	55,879	87.98
	11.52	13.45	2.07	-0.94	44,241	91.58
	14.40	16.55	2.55	-1.16	37,216	94.75
	17.28	19.55	3.01	-1.37	32,492	97.59
	20.16	20.24	3.44	-1.75	29,402	101.10
	23.04	18.43	3.85	-2.30	27,171	104.36
	28.80	6.76	4.38	-3.78	25,221	110.19
	34.56	-14.24	4.71	-5.81	24,645	115.31
	40.32	-36.18	4.85	-7.77	25319	121.88
	46.08	-86.61	4.79	-11.84	29959	141.64
8-16	5.76	7.07	1.58	-0.35	52,254	82.67
	8.64	10.18	2.33	-0.52	37,219	86.60
	11.52	13.33	3.04	-0.68	29,482	89.51
	14.40	16.33	3.71	-0.83	24,839	92.05
	17.28	19.24	4.34	-0.96	21,762	94.13
	20.16	21.62	4.91	-1.10	19,650	96.19
	23.04	20.99	5.41	-1.38	18,242	98.29
	28.80	9.41	5.72	-2.24	17,889	101.48
	34.56	-12.25	5.46	-3.43	20,463	110.04
4-20	5.76	6.77	3.08	-0.28	27,323	84.06
	8.64	9.91	4.45	-0.39	19,902	88.23
	11.52	12.78	5.65	-0.49	16,539	93.07
	14.40	15.44	6.66	-0.55	14,852	98.31
	17.28	16.95	7.43	-0.63	14,119	104.10
	20.16	13.86	7.90	-0.87	14,173	110.77
	23.04	3.55	7.90	-1.37	15132	117.82

The economic performance of the system is demonstrated by the specific capital cost shown by Figure 5-2. The economic design point is indicated by the minimum specific capital cost. For the CPG system, the minimum specific capital cost condition occurs at a mass flow rate of 30.24 kt/day (350 kg/s) which is below the maximized energy condition (38.88 kt/day or 450 kg/s), indicating that the economic optimization produces less net power (and thus energy) than an energy-optimized system. For this case, the minimum specific capital cost mass flow rate yields 57.53 MW-h/day (2.40 MW), which is 96% of the optimized energy condition. This indicates that the benefit of the final 4% of the generation potential is outweighed by the additional component costs. Thus, the CPG system has at least two optimal mass flow rates, 1) for maximum net power generation, and 2) for minimum specific capital cost which has not been considered previously [1,82]. The minimum specific capital cost of the CPG system is $37,600 per kW, which is larger than current renewable energy sources. For example, wind and solar have specific capital cost's ranging from 1,100-10,000 $/kW [151]. However, this system represents a single CPG system operating using a low temperature (102°C) thermal source, which limits the power generation, compared with deeper, hotter reservoirs [1]. Additionally, the CPG system can be scaled, reducing the equipment costs, particularly the vertical well costs, while increasing the power generation [118].

5.3.2 CPGES Results

We operate the CPGES system for four duty cycles, specifically 16-8, 12-12, 8-16, and 4-20 (energy production hours-energy storage hours), varying the mass flow rate for each. We evaluate the performance of the system in terms of the net daily energy generation, the

energy and power dispatched during the generation mode, the energy and power consumed during the storage mode, and the capital cost.

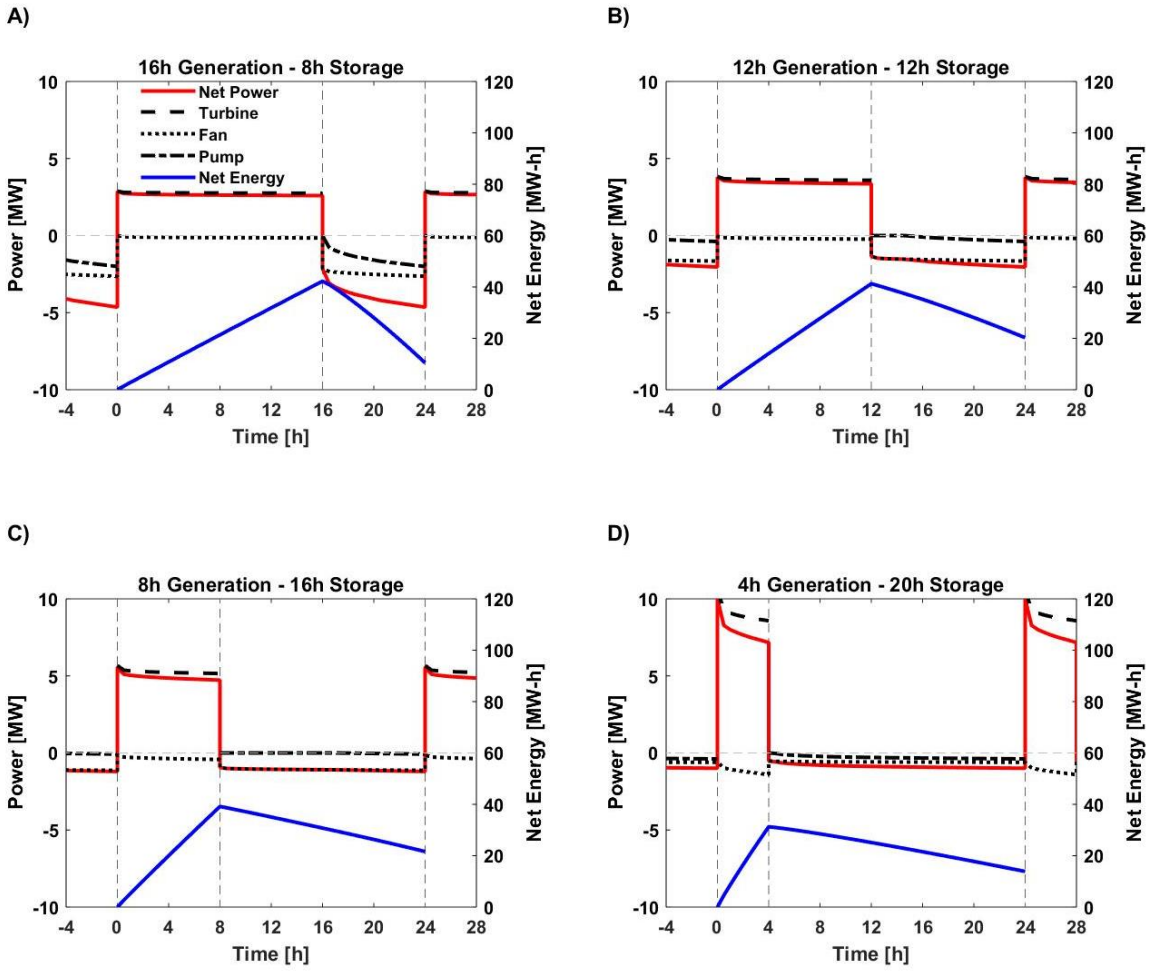

Figure 5-3: The power and cumulative energy generation profiles for the CPGES system with a daily circulation rate of 20.16 kt/day for the four duty cycles: A) 16-8, B) 12-12, C) 8-16, and D) 4-20. Positive net power indicates power delivered to the electrical grid and negative power indicates power consumption (storage). During the generation mode the cooling tower fans have parasitic power consumption, thus the net power generated during the generation mode is less than the gross turbine power. The cumulative energy generation profiles (blue lines) illustrate that the system is able to generate net energy per cycle while also functioning as an energy storage system.

Electricity Generation and Storage

The CPGES system can operate over a range of duty cycles, allowing the system to provide flexible support to the electrical grid, ranging from steady baseload power and short-burst storage for longer duty cycles to peaking power with a long steady recharge period for shorter duty cycles as shown in Figure 5-3. The selected duty cycles cover a range of possible operational configurations, with the 16-8 cycle demonstrating burst energy storage, the 12-12 cycle providing a balanced generation-storage operation, the 8-16 cycle providing moderate peaking power, and the 4-20 cycle operating as a full peaking power system.

Figure 5-3 shows the power profiles and cumulative energy generation for single diurnal cycles at a daily circulation rate of 20.16 kt/day for each, illustrating how the system operates as an energy storage system, with the system producing net power during the generation mode, and consuming power during the storage mode. The net power that is dispatched to the grid during the generation mode increases as the duty cycle decreases, a result of the shorter generation mode, with the 16-8 cycle generating 2.64 MW while the 4-20 system generates on average 7.90 MW, allowing the system to operate as a peaking power generation system. However, while the net power generation increases, so too does the power consumed by the cooling tower during the generation mode, decreasing the generation potential, shown in Figure 5-3D where the parasitic power in the generation mode is 20% of the turbine power, whereas other cases operate with less than 6%; a result of the pressure transients in the reservoirs, and the resulting over pressurization in the

shallow reservoir. Conversely, as the duty cycle decreases, the amount of power consumed in the storage mode decreases, with both the pump and cooling towers consuming less power, decreasing from 3.94 MW to 0.87 MW as the duty cycle decreases from 16-8 to 4-20, as the pressure losses in the injection well and the overpressure in the deep reservoir are reduced. The net effect of the variation in power generation and consumption with the duty cycle is that the net energy generated is maximized for the 8-16 duty cycle, shown by the cumulative energy generation profile (blue line in Figure 5-3), and discussed in detail below.

The performance of the CPGES system varies with the daily circulation mass flow rate and the duty cycle as shown in Figure 5-4. The CPGES system can generate positive net energy (per cycle) to the grid while operating as an energy storage system due to the addition of the geothermal heat, which is extracted from the deep reservoir. Without this heat, the net energy generated would decrease, and the system will consume net energy during each cycle. It is possible for the CPGES system that the net daily energy generation is less than zero, even with the addition of the geothermal heat, with a sufficiently large mass flow rate, as shown in Figure 5-4E. The daily net energy production of the CPGES system behaves similar to the CPG system, having a mass flow rate that maximizes net energy; however, the daily net energy generation for the CPGES system is significantly lower than the CPG system. The reduced energy output from the CPGES system is a result of the pressure losses from the additional components in the energy storage system, mainly the shallow reservoir and the additional vertical wells, and the elevated turbine backpressure

required to accommodate these additional pressure losses, which thereby reduces the generation potential of the system.

Figure 5-4E also shows that the largest daily net energy that the CPGES system can generate for the cycles simulated here is 21.62 MW-h/day, which occurs for the 8-16 duty cycle at a CO_2 circulation rate of 20.16 kt/day. This energy generation is significantly larger than the 16-8 and the 4-20 duty cycles which generate a maximum 15.57 and 16.95 MW-h/day respectively, and slightly larger than the balanced duty cycle (12-12) which generates 20.24 MW-h/day. This indicates that an optimal duty cycle for net energy generation is near the moderate peaking power case. The 8-16 duty cycle is the optimal daily net energy generation case, outperforming the balanced 12-12 cycle, due to the configuration of the CPGES system. The use of a single injection well into the deep reservoir causes increased pressure losses that increase the pumping required, particularly at elevated storage mode mass flow rates, that occur at elevated daily circulation rates and duty cycles, shown in Figure 5-4B,D. The effects of frictional pipe pressure losses on the daily net energy generation are prominent in the 16-8 case, that produces the most energy during the generation mode, but operates with the lowest daily net energy production, due to the elevated energy consumption in the storage mode. While the 8-16 cycle produces the largest daily net energy for the CPGES system, 21.62 MW-h, the CPG system produces 60.10 MW-h over the course of an entire day, demonstrating that while the CPGES system can generate net energy to the grid, the better configuration for net energy generation is the CPG system.

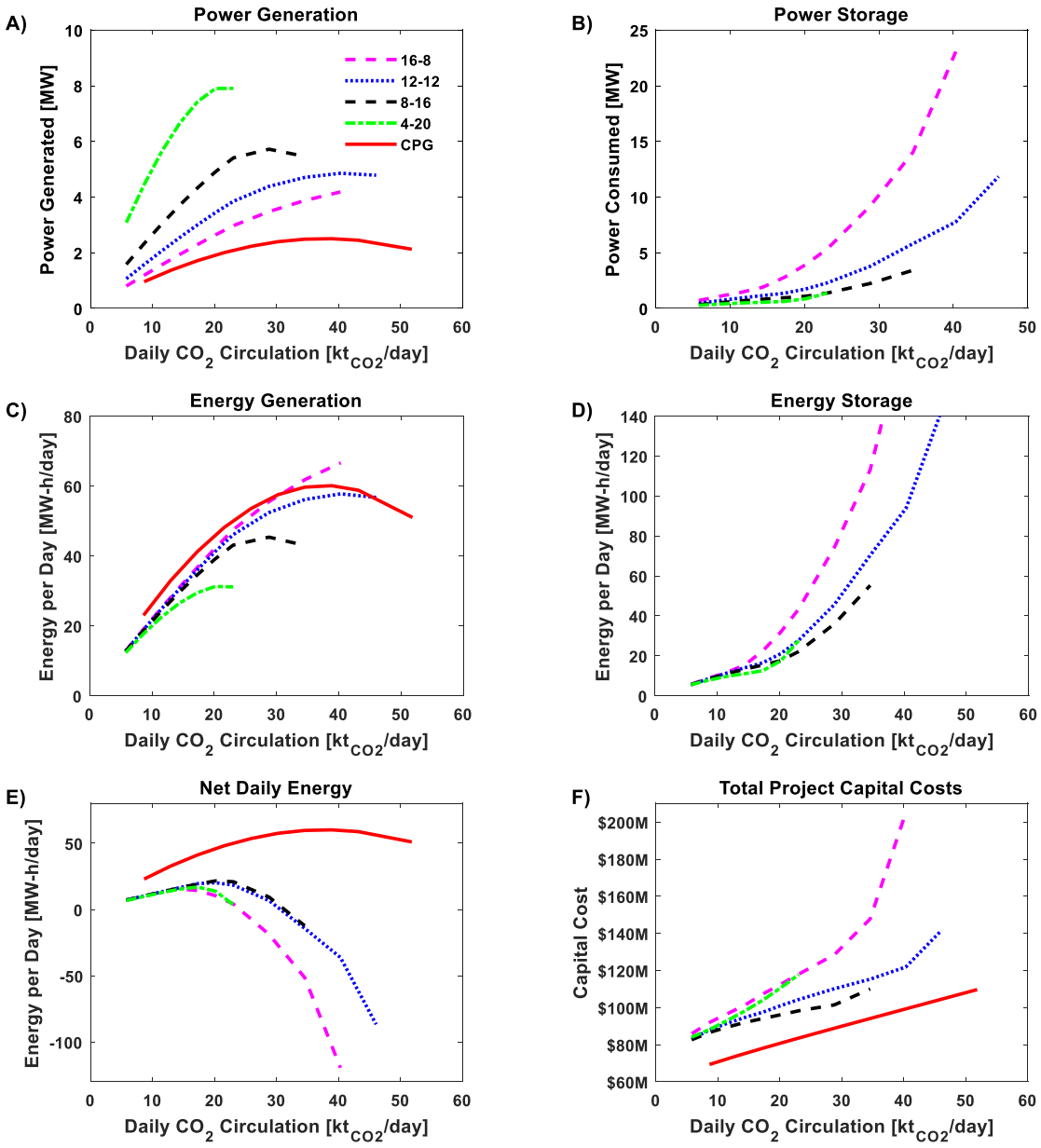

Figure 5-4: The performance of the CPGES relative to the CPG for A) the power generation, B) the power consumption during the storage mode, C) the energy generated during the generation mode, D) the energy consumed during the storage mode, E) the net daily energy generated, and F) the total project capital cost.

While the CPGES system generates less daily net energy than an equivalent CPG system, the amount of energy the CPGES system produces during the generation mode is slightly below the net daily output for the CPG system shown in Figure 5-4C. This illustrates the advantage of the CPGES system of time shifting the energy generation and allows the system to generate the same amount of energy as the CPG system. This energy generation, however, occurs during shorter generation modes, thus the CPGES system generates more power than the CPG system as shown in Figure 5-4A. For example, the 8-16 duty cycle with a circulation rate of 20.16 kt/day generates 4.91 MW of power, or 39.28 MW-h of energy, during the 8-hour generation mode and 21.62 MW-h of daily net energy, while the CPG system generates 2.01 MW of power, producing 45.84 MW-h of energy over the course of the day. The CPGES system produces more power than the CPG system due to the time shifting of the power consumptive elements to the storage mode, and the increased mass flow rate during the generation mode, for a given daily circulation rate. Figure 5-4A further demonstrates that shorter generation modes increase the power generation, with the 4-20 system generating the most power. However, while the CPGES system can generate more net power, it does so at the cost of daily net energy generation, shown in Figure 5-4E. This indicates that the benefit of the CPGES system is large non-continuous power/energy generation (peaking power/energy generation), but at the expense of net energy generation. The trade-off of operating as a peaking power generation system is that during the storage (recharge) mode the system consumes additional energy, shown in Figure 5-4D.

The length of the duty cycle alters the amount of energy that is generated and consumed during each mode as shown in Figure 5-4C-D. The larger duty cycles (i.e. longer generation times) generate the most energy per cycle, particularly at elevated daily circulation mass flow rates, and shorter generation modes produce less energy, resulting from the additional cooling required during the generation mode and the increased variability in the reservoir pressure at the injection and/or production wells. For example, the 16-8 system generates 42.24 MW-h of energy during the generation mode, while the 4-20 system produces 31.60 MW-h and the power consumed by the cooling tower fan during the generation mode increased from 2.03 MW-h to 4.63 MW-h for a daily circulation mass flow rate of 20.16 kt/day. This indicates that while the fan power increases during the generation mode as the duty cycle decreases, thereby reducing the generation capacity of the system, it accounts for only 25% of the variation in the energy generation. The remaining 75% is a result of the variability in the reservoir pressures, particularly near the deep production well, and thus the pressure differential across the turbine, a result in the variation in the generation and storage mass flow rates between duty cycles, for a fixed daily circulation rate. For example, at a daily circulation rate of 20.16 kt/day, the 16-8, 12-12, 8-16, and the 4-20 duty cycles operate with generation mass flow rates of 350 kg/s, 466.67kg/s, 700 kg/s, and 1400 kg/s, shown in Figure 5-7, while the storage modes operate with 686 kg/s, 457.33kg/s, 343 kg/s, and 274.4 kg/s, respectively. The increase in the generation mass flow rate from 350 kg/s to 1400 kg/s results in a 1.15 MPa reduction in the average pressure at the deep production well, and a 0.71 MPa increase in the pressure in the shallow injection well,

which accounts for 75% of the generation energy difference between the 16-8 and the 4-20 duty cycles.

System Costs

The total plant capital cost for the CPGES system is shown in Figure 5-4F versus mass flow rate. The capital cost for the CPGES system is greater than the CPG system due to the addition of the shallow reservoir, which incurs additional reservoir development costs, and includes the additional vertical injection/production well costs, resulting in the offset of $15.0M between the CPGES and CPG cases. Additionally, the capital cost of the CPGES system increases with increasing duty cycles, driven by the differences in the equipment size (i.e. turbine, cooling tower, and pump), which vary with the power generated or consumed by each component. The equipment cost breakdown, shown in Figure 5-5A, indicates that the cost of the cooling towers is significantly larger than the other equipment costs and has a larger variability between the different duty cycles, indicating that the system cost is sensitive to the cooling tower size. The impact of this is observed in Figure 5-4F with the 16-8 cycle, that has the largest heat rejection rate and thus the largest cooling towers. This has the largest capital cost, while the 8-16 system, with the lowest heat rejection rate has the lowest capital cost. It is worth noting that the 8-16 system has lower cooling tower costs than the 4-20 cycle, as the 4-20 cycle requires significant cooling during the generation mode, and results in the cooling towers being sized for the generation mode.

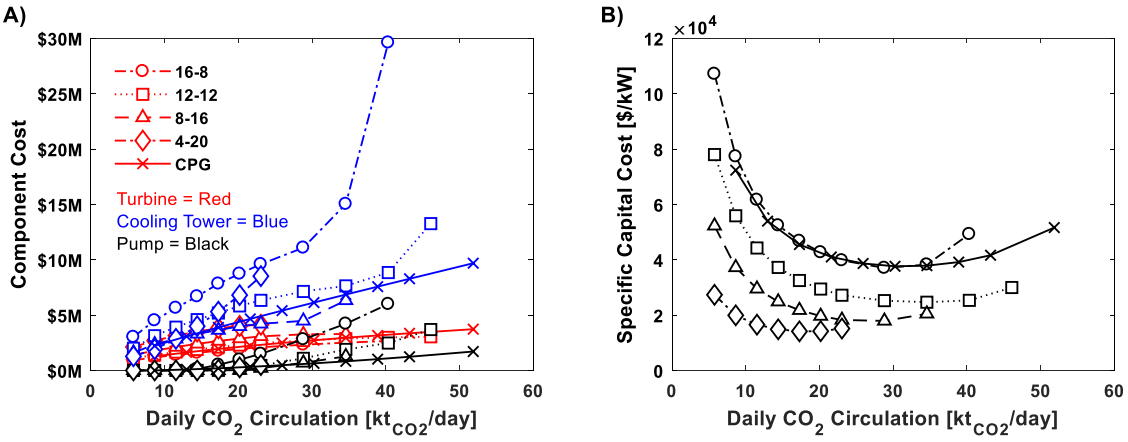

Figure 5-5: A) The cost breakdown of the primary surface equipment (turbine, cooling tower, and pump) and B) the specific capital costs for the CPG and CPGES systems.

While the cooling towers are the largest surface equipment cost, the largest expenditures for each system result from the drilling and placement of the vertical wells, shown in Figure 5-6. The CPGES system operates with a total of seven vertical wells, four deep production wells, two shallow injection/production wells, and a single deep injection well, costing an estimated $65M, or approximately half to two thirds the total capital cost. This indicates that the primary expense for CPGES is accessing the resource, at a fixed cost for the given configuration.

The specific capital cost for each duty cycle is shown in Figure 5-5B. Each duty cycle in CPGES system, like the CPG system, has an economic design point given demonstrated by the minimum specific capital cost. The economic design point changes for each duty cycle, as the power generation and system costs vary. For the CPGES system, the minimum economic condition occurs at the daily circulation rates which is equal to or greater than

the optimized daily energy generation conditions, shown in Figure 5-7. This differs from the CPG system, where the minimum specific capital cost occurs at a lower daily circulation rate, because the CPGES system can generate more power at mass flow rates above the maximum energy generation condition, indicating that the economic point varies with the power generation, and not the daily net energy. As a result, the economic condition occurs at or between the maximum power and maximum energy conditions, shown in Figure 5-7.

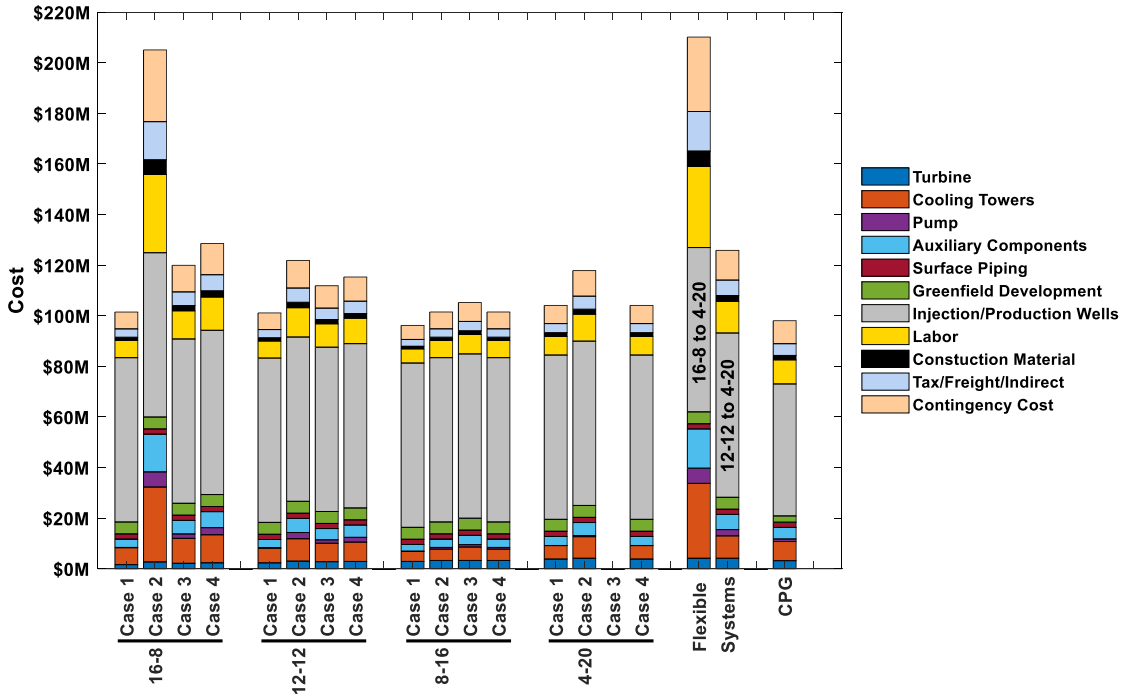

Figure 5-6: The cost breakdown for each of the select CPGES configurations, described in the main text, in addition to a flexible system that can operate over the entire range of duty cycles and daily circulation mass flow rates. For each case, the vertical well costs dominate the total capital costs. The pump cost is nearly negligible for most systems, with the surface equipment cost being dominated by the cooling towers. The flexible system and the case numbers are defined in the main text.

Cost of Flexible Energy Storage

In the presented cost estimates, we assume that the CPGES system is designed to operate at a specific duty cycle, in reality, the grid demands may require the system to be flexible and operate over a range of duty cycles. For this study, we define a flexible system using the same parameter space (Table 5-6), specifically between the 16-8 and the 4-20 duty cycles. We estimate the total capital cost of this system using the maximum turbine, pump, and cooling tower costs for the simulated CPGES configurations, propagating these through the cost model, resulting in a total project capital cost of $210.2M. This costs 114% more than the maximized power generation CPG system given in Figure 5-6; indicating that the cost of the flexible energy dispatch is approximately $112.2M. Including larger duty cycles significantly increases the cost, as the cost of including 16-8 duty cycle, the most expensive single duty cycle at $205.1M, due to the large cooling towers and pump, in the flexible energy system is $64.5, or 57.8% of the cost. While this cost of flexible energy dispatch may seem expensive, the adaptability of the system as an ancillary grid asset could offset these additional costs, particularly in grids with high penetration of variable wind and solar assists.

CPGES Design Points: Determining Power at Different Flowrates

While the CPGES system can operate over a range of daily circulation mass flow rates, we consider four primary operational configurations for each duty cycle as possible design points. This contrasts with the CPG system that has only two design point, the maximum

power (and thus daily energy generation) and the minimized specific capital cost. The CPGES system can be designed for the following four conditions:

1) **Case1: Optimized Daily Net Energy Generation:** The system is designed to generate the largest net energy to the grid over a complete cycle, similar to the design point for the CPG system, maximizing the energy that can be generated and sold to the grid.
2) **Case 2: Optimized Power Generation:** The system is designed to generate the most power during the generation mode, operating as a peaking power plant, which can dispatch peaking power when required.
3) **Case 3: Zero Daily Net Energy:** The system is designed with the net energy generated during the generation mode being equal to the net consumed during the storage mode, similar to an ideal battery, generating no net energy, only time-shifting power.
4) **Case 4: Minimum Specific Cost:** The system is designed to operate at the economic point where the cost of the power generation is a minimum.

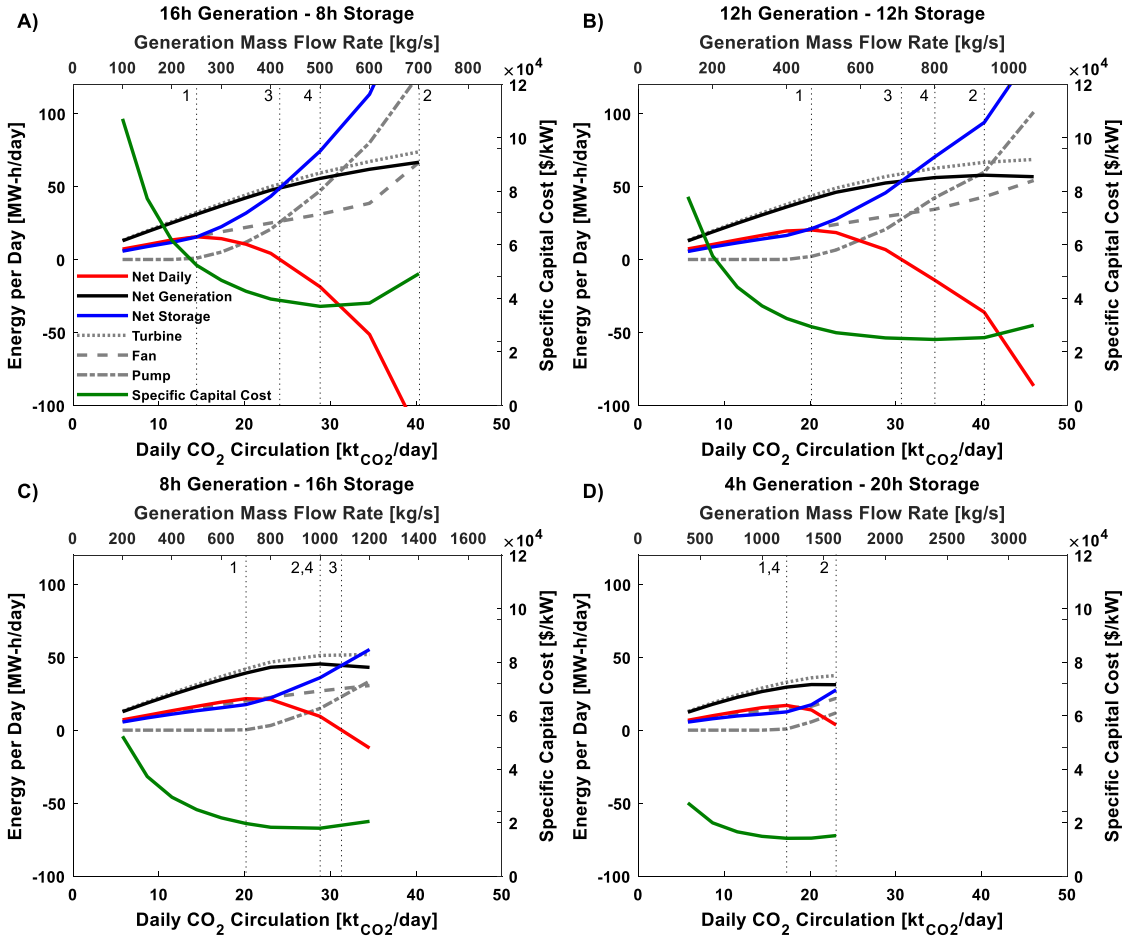

Figure 5-7: Component and net energy generation and consumption and component contribution for the CPGES system for the A) 16-8 case, B) 12-12 case, C) 8-16 case, and D) 4-20 case. The daily CO_2 circulation is marked for each of the following cases; 1) optimized daily net energy generation, 2) the optimized power generation, 3) zero daily net energy, and 4) the minimum specific capital cost.

The power generation and net daily energy generation for each configuration, as well as the power/energy maximized CPG system is shown in Figure 5-8. All the CPGES configurations, except the 16-8 maximum daily energy generation case, generate more power than the maximum power CPG configuration. The increased power capacity of the CPGES system is a critical criterion for the development of the system, as the increased

power generation demonstrates that the peaking power generation capabilities of the CPGES system cannot be replicated by a load following CPG system; and in highly variable energy markets, where the cost of electricity varies significantly throughout the day, the CPGES could be better equipped to use price arbitrage as an economic strategy. The exception to this is 16-8 maximum daily energy generation case, where the CPG system can generate more power than the CPGES system, as the extended 16-hour generation mode coupled with the additional system losses in the CPGES system limit the power generation in this configuration. For this case, the decrease in power generation for the CPGES system implies that the load following CPG system is preferred over the CPGES system; however, the CPGES system can still be economically viable under select conditions, namely, if the system consumes power while the price of electricity is negative, thereby generating a revenue during the storage mode. However, in the current market, periods of negative electricity prices are infrequent and would be unlikely to support this economic operation of the 16-8 CPGES system, as the limited penetration of variable wind and solar power currently limit periods of excess energy generation [137,138].

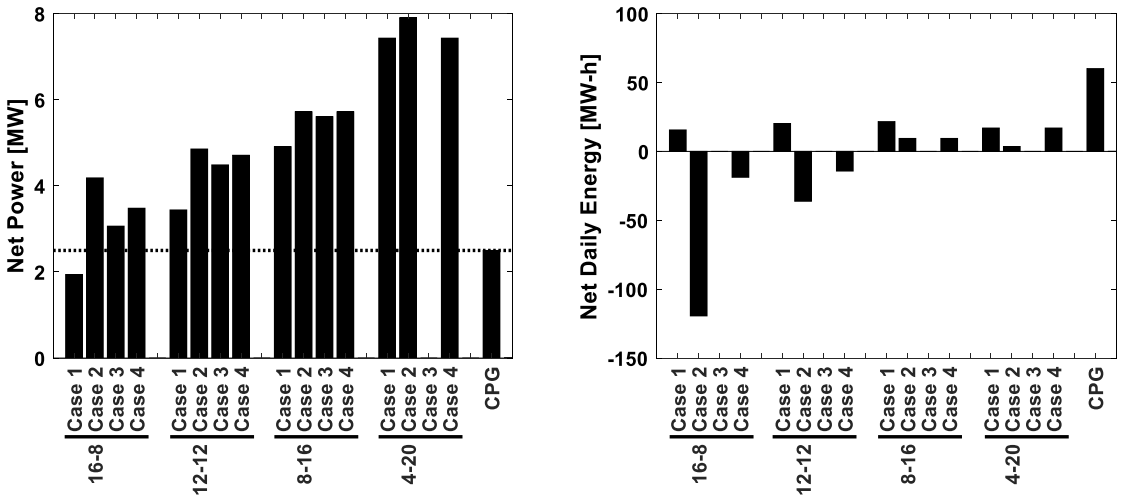

Figure 5-8: The performance of the CPGES system for the defined operating cases relative to the CPG design point (maximized power/energy generation) in terms of A) power generation, and B) daily net energy generation.

The selection of the design point for the system will depend on how the grid values the services that the energy storage system provides, and how the CPGES system is classified in the energy market. If the CPGES system is considered a generation asset and the market values the bulk daily energy generation, the system can be designed to operate at the optimized daily net energy condition, allowing the system to generate the largest amount of energy, and thus revenue, while providing energy storage. Alternatively, if the system is considered an auxiliary asset, such as a peaking power plant, where the availability to dispatch power is desired, the system can be compensated for the decrease in the daily net energy by the ability to produce increased power, as demonstrated by the optimized power generation, the zero-daily net energy, and the minimum specific cost cases. The optimized power generation, zero daily net energy, and economic configurations can be considered peaking power generation systems, as these configurations produce more power than the

maximized daily net energy generation cases and the maximized CPG system; with the selection of the operational case depending on the value of the daily net energy generation. For example, the optimized power generation cases for 16-8 and 12-12 cycles generate 4.18 MW and 4.79 MW of power, but operate with a negative daily net energy generation, specifically, -119.4 MW-h and -86.61 MW-h respectively, meaning the system consumes more energy than it generates, as shown in Figure 5-8. Alternatively, the daily zero-net energy cases have zero net generation while the economic condition generates -18.77 MW-h and -14.24MW-h daily net energy for the 16-8 and 12-12 cycles; however, the net power that is generated decreases by 1.12 MW and 0.36 MW and 0.70 MW and 0.14 MW from the optimized power generation configuration for the zero-net energy and economic configurations, respectfully. In these cases, the selection of the design point will depend on the services that the grid values. For the 8-16 cycles, the optimized power generation configuration and economic configuration occur at the same point, operating with a positive net power generation, 9.41 MW-h, while generating the most power, indicating that this configuration is preferred over the daily zero-net energy configuration in terms of both power and energy.

Currently, energy markets have little value of ancillary services, favoring net energy generation over flexible services. However, with the continued growth of variable renewable energy sources, particularly wind and solar, displacing baseload fossil fuel plants, the value of ancillary services is expected to increase. For example, in the United States, the Federal Energy Regulatory Commission (FERC) recently granted energy

storage system a pathway to participation in the capacity, energy, and ancillary services markets [152].

5.3.2.1 CPG+CPGES

We combine the CPG and CPGES elements and operate them concurrently, allowing the system to benefit from the continuous net energy generation from the CPG element and the peaking power generation from the CPGES element. We assume that the CPGES element operates on an 8-16 duty cycle, as this resulted in the largest energy generation for the CPGES operation, while providing peaking power generation. To quantify the performance of this combined system, we operate it over a range of daily CO_2 circulation rates and vary the operation from completely CPG to completely CPGES, by varying the daily mass fraction of CO_2 through each. Specifically, we consider 100% CPG, 75% CPG + 25% CPGES, 50% CPG + 50% CPGES, 25% CPG + 75% CPGES, and the 100% CPGES. We discuss the performance of each system in terms of the daily net energy generation, the generation mode energy delivered, the storage mode energy, the power generated and consumed, and the specific capital cost, summarized in Table 5-7. The results for the 100% CPG and 100% 8-16 CPGES systems are given in Table 5-6.

Table 5-7: The mass flow rates and the net power, energy, and economic results for the combined CPG+CPGES system.

Mass Distribution	CPG Mass Flow Rate (kg/s)	CPGES Generation Mode Mass Flow Rate (kg/s)	CO_2 Circulated (kt/day)	Peaking Power (MW)	Recharge Power (MW)	Daily Net Energy (MW-h/day)	Generation Mode Energy (MW-h/day)	Storage Mode Energy (MW-h/day)	Specific Capital Cost ($/MW)	Capital Cost ($M)
75% CPG +25 % CPGES	90.0	30.0	8.64	1.17	0.75	21.41	9.35	12.06	72646	84.93
	135.0	45.0	12.96	1.68	1.13	31.50	13.41	18.09	53236	89.23
	180.0	60.0	17.28	2.13	1.48	40.77	17.08	23.69	43730	93.35
	225.0	75.0	21.60	2.54	1.70	47.44	20.32	27.13	38453	97.66
	270.0	90.0	25.92	2.89	1.85	52.70	23.11	29.59	35227	101.76
	315.0	105.0	30.24	3.17	1.94	56.46	25.36	31.10	33329	105.65
	360.0	120.0	34.56	3.39	1.95	58.34	27.10	31.24	32364	109.61
	405.0	135.0	38.88	3.53	1.88	58.32	28.25	30.07	32159	113.55
	450.0	150.0	43.20	3.61	1.72	56.42	28.86	27.56	32582	117.53
	540.0	180.0	51.84	3.56	1.16	47.06	28.44	18.62	35304	125.50
50% CPG +50 % CPGES	75.0	75.0	8.64	1.45	0.53	20.04	11.63	8.41	58963	85.70
	112.5	112.5	12.96	2.10	0.81	29.73	16.78	12.95	42895	89.97
	150.0	150.0	17.28	2.71	1.00	37.73	21.70	16.03	34855	94.57
	187.5	187.5	21.60	3.26	1.11	43.90	26.09	17.81	30265	98.71
	225.0	225.0	25.92	3.77	1.13	48.25	30.15	18.11	27320	102.96
	262.5	262.5	30.24	4.22	1.08	51.09	33.73	17.36	25388	107.03
	300.0	300.0	34.56	4.61	0.94	52.00	36.85	15.15	24124	111.13
	337.5	337.5	38.88	4.93	0.71	50.86	39.48	11.38	23367	115.33
	375.0	375.0	43.20	5.17	0.40	47.85	41.38	6.46	23060	119.29
	450.0	450.0	51.84	5.42	-0.53	34.99	43.38	-8.40	23500	127.44
25% CPG +75 % CPGES	50.0	150.0	8.64	1.90	0.19	18.21	15.17	3.05	45538	86.34
	75.0	225.0	12.96	2.77	0.26	26.39	22.15	4.23	32918	91.15
	100.0	300.0	17.28	3.60	0.19	31.94	28.85	3.08	26666	96.18
	125.0	375.0	21.60	4.37	0.07	36.20	35.01	1.20	22980	100.56
	150.0	450.0	25.92	5.09	-0.13	38.75	40.74	-1.98	20582	104.81
	175.0	525.0	30.24	5.76	-0.43	39.29	46.10	-6.81	18946	109.17
	200.0	600.0	34.56	6.35	-0.80	38.15	50.85	-12.70	17808	113.20
	225.0	675.0	38.88	6.87	-1.27	34.83	55.06	-20.23	17028	117.19
	250.0	750.0	43.20	7.33	-1.84	29.35	58.69	-29.34	16512	121.14
	300.0	900.0	51.84	7.96	-3.30	11.23	63.80	-52.57	16155	128.83

The net power profile for the CPG+CPGES system varies between the 100% CPG and the 100% CPGES cases for a complete diurnal cycle as shown in Figure 5-9 for a fixed daily CO_2 circulation rate of 20.60 kt/day. The increased operation of the CPG element reduces the amount of power the system can time shift, reducing the amount of power that is

delivered during the generation mode and the power consumed during the recharge mode. For example, for a daily CO_2 circulation rate of 34.56 kt/day, the power delivered in the generation mode decreases from 6.35 MW to 4.61 MW for the 25% CPG+75% CPGES and 50% CPG+50% CPGES cases, respectively, while the power consumed by the system decreases from 0.80 MW to -0.94 MW, indicating the system generates power during the recharge mode. The reduced power consumption in the recharge mode is a result of the decreased power consumption from the CPGES element in addition to the supplemental energy generated by the turbine in the CPG system, which operates continuously through the entire cycle. This effect increases when the CPG portion increases, and with sufficient CPG operation, the CPG+CPGES system does not consume power during the recharge mode, operating as a peaking power plant in place of an energy storage system, as the system does not consume power. For the daily CO_2 circulation rate of 20.60 kt/day, power is only consumed in the recharge mode for the CPGES and 25% CPG +75% CPGES cases, thus the 50% CPG + 50% CPGES and the 75% CPG + 25% CPGES cases operate as a peaking power plant. While we only simulate the CPG+CPGES system for the 8-16 cycle, it is expected that similar results would be observed for other duty cycles.

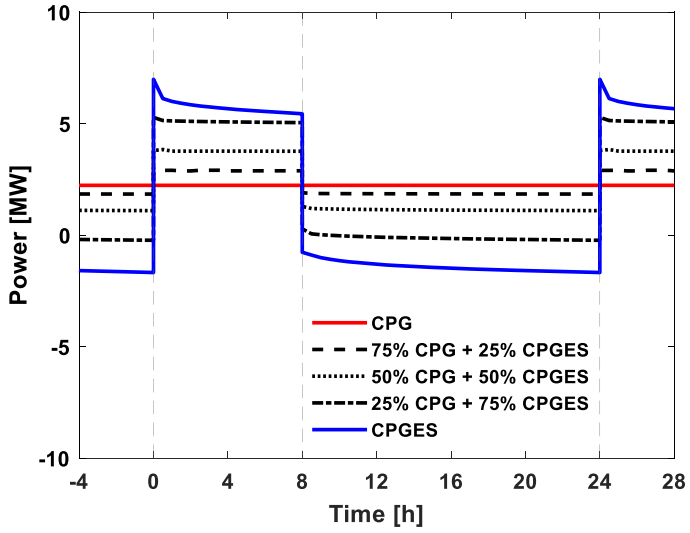

Figure 5-9: The net power generated and consumed over a complete diurnal cycle for the CPG+CPGES system, including the CPG and 8-16 CPGES systems alone for a daily CO_2 circulation rate of 20.60 kt/day.

The CPG+CPGES system combines net energy generation from the CPG system with peaking power generation from the CPGES system, as shown in Figure 5-10. The addition of the CPG element to the CPGES system increases the daily net energy that the system generates, shown in Figure 5-10B. For example, the maximum daily net energy generation for the CPGES system is 21.62 MW-h, while the 25% CPG + 75% CPGES generates 39.29 MW-h, an 82% increase. While the addition of the CPG element increases the daily net energy, it decreases the net power the system can generate, shown in Figure 5-10A. This indicates that the addition of the CPG element increases the net energy generated by the system but decreases the peaking power capacity. For example, changing from the 100% CPGES system to 25% CPG + 75% CPGES decreases the net power generated by 14%,

while the daily net energy generated increases by 73% for daily CO_2 circulation rates less than 30 kt/day.

The addition of the CPG element to the CPGES system increases the power generation capacity at larger mass flow rates, shown in Figure 5-10C for the 25% CPG + 75% CPGES configuration. The CPGES system provides the most power during the generation mode for daily CO_2 circulation rates below 30 kt/day. However, due to the large mass flow rates during peaking power generation, the overpressure in the shallow reservoir increases requiring more cooling, and thus power consumption, during the generation mode, reducing the net power dispatched to the grid. For circulation rates above 30 kt/day, the 25% CPG + 75% CPGES can generate more power, as the operation of the CPG element reduces the overpressure in the shallow reservoir due to the injection of CO_2, by circulating some of the CO_2 back into the deep reservoir, distributing the injection overpressure between multiple injection wells in multiple reservoirs. Consequently, this allows the CPG+CPGES system to operate with larger daily CO_2 circulation rates, and thus increased power and energy performance over the CPGES system, before the reservoir pressures become detrimental to the system performance. This allows the CPG+CPGES system to overcome some of the limitations of the CPGES system.

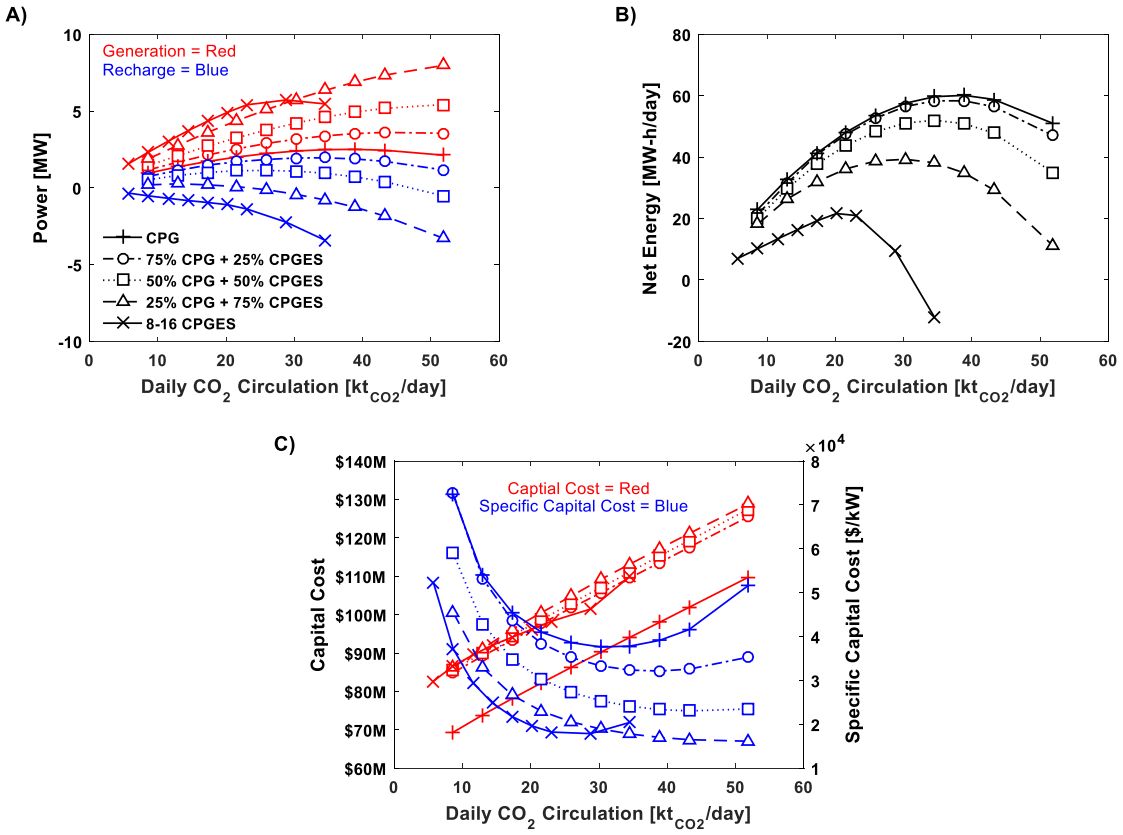

Figure 5-10: The performance of the CPG+CPGES system compared to the CPG and the 8-16 CPGES systems alone in terms of A) the power produced during the generation and recharge modes, B) the daily net energy generation, C) the total and specific capital costs.

Figure 5-10C shows the capital costs of the CPG, CPGES, and the combined CPG+CPGES systems. The capital costs for all the CPG+CPGES systems are similar to the capital cost for the 8-16 CPGES system, indicating that the operation of the CPG+CPGES system is preferential to the CPGES system alone, due to the increased energy generation, while maintaining the capacity for peaking power. The costs for the CPG+CPGES system are offset from the CPG system by a constant value, namely, the cost for the shallow reservoir

and the additional vertical wells. The cost of a flexible CPG+CPGES system that can vary between 100% CPG and 100% CPGES (for the 8-16 duty cycle) with a maximum daily CO_2 circulation rate of 51.84 kt/day, has a capital cost of $130.1M, which is only 1% larger than for the 25% CPG + 75% CPGES case at the given flow rate, indicating that designing for this point would allow the system to operate between the CPG and CPGES limits. Additionally, the cost of the CPG+CPGES system is 18% greater than the maximum cost of the 8-16 CPGES system, as the component cost for the CPG+CPGES system increases by $1.30M, $0.95M, and $3.53M for the turbine, pump, and the cooling towers, respectively; a result of the increased daily circulation rates, and thus heat extraction, in the CPG+CPGES system.

5.4 Conclusions

We demonstrate how a CPG system can be modified to operate as an energy storage system (CPGES), circulating CO_2 between two geothermal reservoirs. We model the CPGES and CPG systems using comparable reservoirs and surface plant configurations. The results of our simulations allow us to make the following conclusions:

T*he CPGES system is a flexible energy storage system that can operate over a range of duty cycles, allowing the system to function as a peaking power generation or peaking power consumption system, depending on the grid requirements.* The operation of the CPGES system is controlled by the duty cycle, with 4hr-20hr cycle operating as a peak generation system, generating up to 7.90MW in the generation mode, while the 16hr-8hr cycle demonstrates peak power consumption and storage, consuming up to 9.19 MW in the storage mode while only generating 3.48MW in the generation mode. While the system

can operate over the given range of duty cycles, the 8hr-16hr duty cycle is ideal as it has the largest energy generation of all the duty cycles considered and the lowest capital cost.

One benefit of the CPGES system is its increased power generation capacity over an equivalent CPG system, however, this also results in reduced daily net energy generation. The CPGES system can generate 5.72 MW and 7.90 MW of power during the generation mode for the 8-16 and the 4-20 duty cycles, respectively, significantly more than the 2.50 MW maximum of the CPG system. However, the maximum daily energy production for these cycles is 21.62 MW-h and 16.95 MW-h, which is lower than the 60.10 MW-h generated by the CPG system. This indicates that the CPGES system time shifts power/energy at the expense of daily net energy generation.

The CPGES system has a larger capital cost than an equivalent CPG system, due to the increased size of the surface equipment and the additional vertical wells to the shallow reservoir. The injection and production wells are the most expensive component of CPG and CPGES systems, costing $52.2M and $64.9M, respectively. This demonstrates that for the majority of the cases considered the primary factor in the cost difference between the CPGES and CPG systems is the addition of the second shallow reservoir.

The flexible power system costs 119% more than the cheapest CPGES system, and 114% more than the power maximized CPG system. The most expensive CPGES system considered is the flexible power configuration, which costs $210.2M, $112.2M more than the maximized CPG system. Here, the difference in the total project capital costs is due to the second reservoir and the additional wells which cost $15.0M, and the larger power

generation equipment which costs $39.73M, $18.65M of which is due to the large cooling towers and pumps required for the 16-8 duty cycle.

A CPG system can be combined and operated concurrently with a CPGES system to increase the power produced and daily net energy generation. The maximum power generated by the CPG+CPGES is 7.96 MW, 39% larger than the maximum power generated by the 16-8 CPGES system alone. The 25% CPG + 75% CPGES system generates more power than the 8-16 CPGES system at daily CO_2 circulation rates greater than 30 kt/day as the CPG+CPGES system reduces the overpressure in the shallow reservoir, the limiting factor in the 8-16 CPGES system, by circulating some of the CO_2 back to the deep reservoir. Additionally, the increased operation of the CPG element increases the daily net energy generated, with the 25% CPG + 75% CPGES system generating a maximum daily net energy of 39.29 MW-h, which is 82% more than the maximum daily net energy generated by the 16-8 CPGES system. This demonstrates that CPG+CPGES combines the peaking power generation of the CPGES system with the daily net energy generation of the CPG system and is preferable to the CPGES system alone.

Chapter 6: Increased Power Generation due to Co-production of Water in the Production Well

The Increase in Power Generation due to Water Precipitation in CO_2 Plume Geothermal (CPG) Power Plants

Mark R. Fleming[1], Benjamin M. Adams[2], Thomas H. Kuehn[1], Jeffrey M. Bielicki[3,4], Martin O. Saar[2,5]

[1]Department of Mechanical Engineering, University of Minnesota, USA
[2]Geothermal Energy and Geofluids Group, Department of Earth Sciences, ETH-Zürich, Switzerland
[3]Department of Civil, Environmental, and Geodetic Engineering, The Ohio State University, USA
[4]John Glenn College of Public Affairs, The Ohio State University, USA
[5]Department of Earth Sciences, University of Minnesota, USA

Synopsis

In Carbon Dioxide (CO_2) Plume Geothermal (CPG) systems, the CO_2 that enters the production well is saturated with H_2O from the geothermal reservoir. However, models thus far have only considered pure CO_2 in the production well and power generation equipment. The solubility of H_2O in CO_2 decreases as the CO_2 rises in the production well, causing H_2O precipitation from the CO_2 phase. We simulate wellhead pressures, temperatures, free-phase liquid water fractions and CPG power output for four different wellbore CO_2-H_2O solubility models: pure CO_2, two proposed wet CO_2 methods, and an existing T2Well CO_2 wellbore simulator. We show that wet CO_2 increases the power output by 15% to 25%, when exothermic water precipitation is considered.

6.1 Introduction

The emission of carbon dioxide (CO_2) into the atmosphere has been strongly correlated with the global rise of the Earth's mean (atmospheric) surface temperature, for example by the Intergovernmental Panel on Climate Change (IPCC), with the generation of electricity

and heat, using fossil fuels, contributing 25% of the total CO_2 emitted [5]. Clean renewable energy sources, such as wind, solar, bio-energy, and geothermal energy, have been developed and used to generate power with no or limited CO_2 emissions, thereby reducing the overall emission of CO_2 for electricity generation; however, of these sources, only geothermal and bio-energy systems are capable of providing continuous baseload power [117]. To further reduce the emission of CO_2 into the atmosphere, existing power plants can be augmented to capture produced CO_2 and store the captured CO_2 underground in geologic formations in a process that is referred to as carbon capture and (geologic) storage (CCS) [10,153,154]. CCS can permanently store captured CO_2 underground in saline reservoirs or (partially) depleted oil or gas reservoirs, which are overlain by a low- to virtually zero-permeability caprock, preventing the upwards leakage of CO_2 [10].

The CO_2 captured in a geologic formation can be used as a heat extraction fluid for geothermal systems, utilizing captured CO_2 instead of merely storing it, constituting a form of carbon capture utilization and storage (CCUS). Importantly, in this type of CCUS, after the CO_2 is produced from the geothermal reservoir and expanded in a turbine to generate electricity, the CO_2 is reinjected into the reservoir, so that all of the CO_2 is permanently stored underground. CO_2 was initially proposed as a geologic heat extraction fluid for Enhanced Geothermal Systems (EGS) by Brown [81], with subsequent studies illustrating in principle the effectiveness of CO_2-EGS [84,87,90,91]. Supercritical CO_2 (sCO_2) has several advantages over brine, including a significantly lower kinematic viscosity, i.e., greater fluid mobility, allowing much higher heat advection rates within reservoirs,

everything else being equal [1,81,82]. Furthermore, the density of sCO_2 has a much larger temperature dependence than brine, which, together with the high mobility of sCO_2, can generate a vigorously convecting thermosiphon that may reduce or even eliminate the need for operating fluid circulation pumps, as the density difference between the injection and production wells drives the CO_2 circulation [1,81,82,90,91]. Furthermore, CO_2, and even CO_2 dissolved in water, forming weak carbonic acid, has a low mineral solubility, even in carbonate reservoirs [155–157], limiting the leaching and transport of (dissolved) minerals from the rock, likely reducing subsequent scaling in pipes and turbomachinery [81], which is a significant challenge in brine based geothermal systems [158–161].

Another concept, CO_2 Plume Geothermal (CPG) utilizes CO_2 as a working fluid in naturally porous permeable sedimentary basins [33,93,96]. CPG differs from (CO_2-based) EGS [81,84,87], with the latter, per definition, requiring hydraulic stimulation (i.e. hydraulic fracturing or shearing) of a low-permeability formation to increase permeability [162], potentially causing significant socio-political resistance [79]. In contrast, CPG systems utilize naturally permeable reservoirs that do not require hydraulic stimulation. Additionally, naturally permeable reservoirs are typically quite large, enabling the storage of large amounts of CO_2, compared to artificially generated, fracture-based EGS reservoirs, which tend to be small in overall size and have small total porosities [34,96].

Prior research on CPG systems has focused on reservoir modeling and surface plant power production, using dry or pure CO_2. In analogy to previous CO_2-EGS models [84,87],these studies have employed a so-called inverted 5-spot well pattern within a 1 km^2 area

[1,33,82,96]. System modeling demonstrated that the CPG system produced more power than a brine-based geothermal system [1], generated a strong thermosiphon [82], and that the CPG system's power output is more dispatchable (i.e. capable of transmitting energy to the grid when it is needed to meet electricity demands) than variable renewable energy sources, specifically wind and solar [2].

Table 6-1: Nomenclature

Variables:			
A	Cross-sectional Area [m^2]	V	Bulk Velocity [m/s]
D	Diameter [m]	$\dot{W}$	Electric Power [kWe]
E	Energy [kJ]	x	Mole Fraction in the H_2O Rich Phase [dim]
$\dot{E}$	Energy Rate [kW]	X_i	Mole Fraction [dim]
f	Darcy Friction Factor [dim]	y	Mole fraction in the CO_2 Rich Phase [dim]
g	Gravitational Constant [m/s^2]	z	Elevation [m]
h	Specific Enthalpy [kJ/kg]	η	Efficiency [Dim]
h_m	Molar Specific Enthalpy [kJ/mol]	ρ	Density [kg/m^3]
L	Length [m]	φ	Mass Fraction [dim]
$\dot{m}$	Mass Flow rate [kg/s]	Subscripts	
M	Molar Mass [g/mol]	i	Well segment iteration
n_i	Moles of component [dim]	CO_2, Solution	CO_2 solution component of flow
P	Pressure [kPa]	H_2O,v	Water dissolved in CO_2
T	Temperature [C]	H_2O,L	Free, liquid water
		Total	Total component in any state

More recent reservoir models have used a radially axisymmetric system, using a vertical injection well at the center and a circular horizontal production well located at the top of the reservoir just under the caprock [83,119]. These radial models include multi-fluid

(CO_2-brine) algorithms that also simulate the displacement of brine by the CO_2 [83,119]. However, power production models continue to use dry CO_2 in the well and surface plant. Most prior research on CPG assumes that the subsurface working fluid that is extracted from the geothermal reservoir to be pure, dry CO_2, which is unlikely. A reservoir will initially be filled with water or, more likely, brine and, as CO_2 is injected into the reservoir, it will displace some but not all brine. Furthermore, a small amount of water will dissolve into the CO_2, while some CO_2 will dissolve into the water phase, forming (weak) carbonic acid near the interface to the CO_2 plume. We refer to the CO_2 that contains some dissolved water (H_2O) as "wet" CO_2.

The mutual solubility of CO_2-H_2O generally increases with pressure and temperature [163]. As a result, the maximum solubility during the CPG power production cycle is in the deep, geothermal reservoir. As the solution moves up the production well, both the pressure and the temperature decrease, reducing the solubility of H_2O in CO_2. As the CO_2 is likely saturated with H_2O when it enters the production well, some of the dissolved H_2O will come out of solution during the upwards movement, and associated pressure, temperature, and H_2O solubility reduction, resulting in free-phase (liquid) H_2O. This free-phase H_2O is then co-produced to the surface, along with the CO_2 phase. The co-produced H_2O may need to be separated from the CO_2 stream, as it can cause erosion of the turbine [164] and as re-injection of free-phase liquid H_2O can decrease the effective permeability of the reservoir near the injection well [83].

Consequently, the primary objective of this study is to determine the temperature, pressure, and mass fraction of liquid H_2O that may be produced at the wellhead, and its effect on the power production of CPG systems. To do so, we compare three different methods for calculating wellhead water content and compare them against the TOUGH2 [120] well simulator, T2Well [165]. Then, for each of these cases, we model the change in power production for a CPG system.

6.2 Methods

The wellhead temperature, pressure, and water mass fraction are calculated using three different wellbore models. The models differ in their approximation of the CO_2 component density, $\rho_{CO2,Solution}$, in the following ways:

(1) *Dry CO_2 Only:* The fluid in the well is assumed to be pure CO_2, where the CO_2 density, $\rho_{CO2,Solution}$, is obtained from Span and Wagner [125].

(2) *CO_2 Solution Proxy*: The fluid in the well is assumed to be a mixture of water-saturated CO_2 and liquid H_2O, where the CO_2 density, $\rho_{CO2,Solution}$, is assumed to be that of pure, dry CO_2 and obtained from Span and Wagner [125] and the free liquid H_2O density is obtained from steam tables [166].

(3) *Solution Density Approximation*: The fluid in the well is assumed to be a mixture of water-saturated CO_2 and liquid H_2O, where the CO_2 density, $\rho_{CO2,Solution}$, is found for the CO_2-H_2O solution from Spycher et al. [163,167] and the free liquid H_2O density is obtained from steam tables [166].

Each of these methods uses the mass-weighted average, shown in Equation 6.1, to calculate the bulk density of the fluid along the length of the well.

$$\rho_{bulk} = \rho_{CO2,Solution}\,\varphi_{CO2,Solution} + \rho_{H2OL}\,\varphi_{H2OL} \quad (6\text{-}1)$$

The nomenclature for the equations is provided in Table 6-1. In all cases, the liquid H_2O density, ρ_{H2OL}, is obtained from the state temperature and pressure using the steam tables. The wellbore fluid contains two components: CO_2 and free liquid H_2O, whose mass fractions sum to one ($\varphi_{CO2,Solution} + \varphi_{H2OL} = 1$). In the dry CO_2 case, pure CO_2 is assumed, and thus there is no water in the well, reducing the bulk density, ρ_{bulk}, to the density of pure CO_2.

The difference between *CO_2 Solution Proxy* and the *Solution Density Approximation* models is the way the density of the CO_2 component of the mixture ($\rho_{CO2\_Solution}$ in Equation 6-1) is calculated. The *CO_2 Solution Proxy* approximates the density of the CO_2 component as that of pure CO_2, while the *Solution Density Approximation* method obtains the density from a CO_2-H_2O solution model from Spycher et al. [163,167]. We did not use the *Solution Density Approximation* method outright to estimate the CO_2 solution density because the solution model from Spycher [163,167] has not been verified over the entire temperature and pressure range experienced in the well.

We employ an iterative procedure to calculate the well fluid properties as a function of the height above the reservoir. This procedure is based on a prior approach developed for dry CO_2 [1,82]. The well is divided into 100m vertical elements. Across each element, the exit

state (i+1) is calculated from the inlet state (i), where equations for the energy (Equation 6-2), momentum (Equation 6-3), and mass balance (Equation 6-4) are applied, i.e.

$$h_i + gz_i = h_{i+1} + gz_{i+1} \tag{6-2}$$

$$P_i + \rho_i g z_i = P_{i+1} + \rho_{i+1} g z_{i+1} - \Delta P_{loss} \tag{6-3}$$

$$\dot{m} = \rho_i A V_i = \rho_{i+1} A V_{i+1} \, . \tag{6-4}$$

The model assumes no heat transfer between the well and the surrounding rock and the kinetic energy is small and neglected [1,82,129]. The frictional pressure losses are determined from the Darcy-Weisbach relation,

$$\Delta P_{loss} = f \frac{L_{pipe}}{D} \rho \frac{V^2}{2} \, . \tag{6-5}$$

The friction factor is given by the Moody Chart [144] using bare Cr13 oil piping which has a surface roughness (ε) of 55 μm [124]. The dynamic fluid viscosity is assumed to be dominated by the viscosity of dry CO_2 and is modeled as the viscosity of dry CO_2 in all three models.

The well is numerically integrated from the downhole, reservoir state to the wellhead at the surface. We assume that the downhole reservoir pressure is modeled as the hydrostatic pressure and the downhole fluid temperature is the reservoir temperature, which is the product of the geothermal temperature gradient and reservoir depth added to the surface temperature of 15 °C. The numerical integration is performed using Engineering Equation Solver (EES) [122].

For the multi-fluid system, the energy balance (Equation 6-2) and continuity equation (Equation 6-4) are separately solved for each of the three components of this solution: CO_2,

H_2O in solution, and free H_2O. Each component is assumed to be in thermodynamic equilibrium within each element and is described in more detail in Section 2.1.

6.2.1 CO_2-H_2O Solution (Wet CO_2)

When CO_2 is injected into a brine reservoir, the mutual solubility of CO_2-H_2O has two effects: 1) CO_2 dissolves into the native brine and 2) H_2O dissolves and vaporizes into the CO_2 rich plume. The mutual solubility of the CO_2-H_2O system is defined by the phase and chemical equilibria Equations 6-6 and 6-7. These are the transition of aqueous phase CO_2 to gaseous phase (Equation 6-6), and the vaporization of water (Equation 6-7) [163,167–169], i.e.

$$CO_{2(g)} \rightleftharpoons CO_{2(aq)} \tag{6-6}$$

$$H_2O_{(l)} \rightleftharpoons H_2O_{(g)} \tag{6-7}$$

The solution properties of CO_2-H_2O mixtures for the pressures and temperatures encountered in geological CO_2 sequestration, and thus CPG systems, are defined by Spycher et al. [163]. This model was extended to include the mutual solubility of CO_2-H_2O and CO_2-H_2O-NaCl systems in Spycher et al. [163,167]. These CO_2-H_2O models cover the temperature range from 12-300 °C and pressure from 1-600 bar.

The CO_2 *Solution Pr*oxy and the *Solution Density Approximation* methods use Spycher et al. [163,167] to determine the solubility limit of H_2O in CO_2 solution ($y_{H2O,MAX}$). The *Solution Density Approximation* method further uses Spycher et al. [163,167] to determine the CO_2-H_2O solution density, $\rho_{CO2,Solution}$.

The CO_2-H_2O solution assumes that no NaCl is present. The presence of NaCl will decrease the amount of H_2O in solution, thus, the cases with no NaCl constitute an upper bound for the maximum H_2O content possible under typical geothermal reservoir pressure and temperature conditions.

6.2.1.1 CO_2-H_2O Solution Energy Balance

The dissolved H_2O is assumed to be saturated vapor at the pressure and temperature of the mixture, thus H_2O precipitation as free liquid will transfer a substantial amount of energy to the CO_2 as it condenses. The assumption that dissolved water in CO_2 may be treated as vapor is further justified in Section 2.1.3. This energy transfer has not been considered in previous wellbore models such as T2Well. Thus, we consider it here.

Equation 6-7 indicates that the H_2O will undergo a phase change when the H_2O leaves the saturated CO_2 [168]. When H_2O precipitates out of solution, the latent energy is released to the surrounding mixture. This is not the enthalpy of dissolution, which is an enthalpy change that occurs when two substances mix. We neglect the enthalpy of dissolution in our model and instead only employ the enthalpy of vaporization/condensation.

The CO_2 is assumed to be fully saturated with H_2O when the reservoir fluid enters the production well, with no free-phase H_2O or NaCl components present. Free-phase H_2O later develops as the fluid ascends within the well and the solubility of H_2O in CO_2 decreases and H_2O is forced out of solution, due to the decrease in temperature and pressure. The free H_2O phase is modeled as liquid H_2O at the given pressure and temperature. The energy, momentum, and continuity balances are repeated three times, for

each of the three components: (1) CO_2, (2) the H_2O dissolved in the CO_2, and (3) free-phase H_2O present around the CO_2

In Equations 6-8 to 6-11, the energy balance from Equation 6-2 is calculated separately for each component of the fluid: the CO_2 ($CO_{2,i}$), H_2O in solution ($H_2O_{v,i}$), and free liquid H_2O ($H_2O_{L,i}$). The H_2O in solution ($H_2O_{v,i}$) is assumed to be a saturated vapor at the bulk temperature. While the mass and energy of each water component across a vertical element can change (i.e. dissolved H_2O vapor becomes free phase liquid, increasing the mass of liquid water and reducing the mass of dissolved vapor), the overall energy of the fluid must remain constant (Equation 6-8),

$$0 = \Delta\dot{E}_{CO2} + \Delta\dot{E}_{H2Os} + \Delta\dot{E}_{H2OL} \tag{6-8}$$

$$\Delta\dot{E}_{CO2} = \dot{m}_{CO2\,i+1}(h_{CO2\,i+1} + gz_{i+1}) - \dot{m}_{CO2\,i}(h_{CO2} + gz_i) \tag{6-9}$$

$$\Delta\dot{E}_{H2Os} = \dot{m}_{H2Os\,i+1}(h_{H2Ov\,i+1} + gz_{i+1}) - \dot{m}_{H2O,s\,i}(h_{H2Ov\,i} + gz_i) \tag{6-10}$$

$$\Delta\dot{E}_{H2OL} = \dot{m}_{H2OL\,i+1}(h_{H2OL\,i+1} + gz_{i+1}) - \dot{m}_{H2OL\,i}(h_{H2OL\,i} + gz_i). \tag{6-11}$$

6.2.1.2 CO_2-H_2O Solution Mass Balance

The total mass flow rate is the sum of the mass flow rates for CO_2, H_2O in solution, and liquid H_2O (Equation 6-12). The total flow rate must be constant across segments (Equation 6-13).

$$\dot{m}_{Total,i} = \dot{m}_{CO2,i} + \dot{m}_{H2O,v,i} + \dot{m}_{H2O,L,i} \tag{6-12}$$

$$\dot{m}_{Total,i} = \dot{m}_{Total,i+1} = \rho_{bulk,i}\, A_{pipe} V_{bulk,i} \tag{6-13}$$

Additionally, the mass flow rates of CO_2 and H_2O must be conserved between vertical well segments (Equations 6-14 and 6-15). For example, a decrease of H_2O solubility in CO_2

across one well element results in an increase of free water and decrease of water in solution in the next segment; however, the total mass of water is conserved (Equation 6-15).

$$\dot{m}_{CO2,i+1} = \dot{m}_{CO2,i} \tag{6-14}$$

$$\dot{m}_{H2O,Total} = \dot{m}_{H2O,v,i} + \dot{m}_{H2O,L,i} = \dot{m}_{H2O,v,i+1} + \dot{m}_{H2O,L,i+1} \tag{6-15}$$

Lastly, as the CO_2 is assumed to be fully saturated with H_2O in each element, the mass flowrate of CO_2, and its dissolved water vapor, are determined using the solubility limit from Spycher et al. [163,167], converted from molar to mass units, in Equation 6-16.

$$y_{H2O,MAX,i} = \frac{\frac{m_{H2O,v,i}}{M_{H2O}}}{\frac{m_{CO2,i}}{M_{CO2}} + \frac{m_{H2O,v,i}}{M_{H2O}}} \tag{6-16}$$

6.2.1.3 Enthalpy Model Validation

A fundamental assumption of our model is that water is dissolved as vapor into CO_2 and therefore will release energy as it precipitates out as liquid water (Equation 6-7). An alternative modeling assumption would be that the water exists as liquid both in and out of solution and therefore little energy change would occur when the solubility changes. As our vapor-water assumption is the primary driver for our results, we now validate this enthalpy modeling assumption with existing data.

Validation of our model over our entire simulated range (25 to 50 MPa at 65 to 265°C) is not possible as limited published enthalpy of mixture values exist for CO_2-H_2O systems. However, Chen et al. [168] published experimentally determined enthalpy of mixture values for the CO_2-H_2O system from 225 to 325°C at 10.4 to 15 MPa which we compare our results against. Chen et al. [168] reported the change in enthalpy in terms of the specific

enthalpy of mixing, Δh_{mix} [kJ mol^{-1}], which is defined as the change in energy of a fixed number of moles of the mixture from its pure substances, divided by the total moles,

$$\Delta h_{mix} = \frac{E_{mixture} - E_{pure}}{n_{CO2} + n_{H2O}}. \quad (6\text{-}17)$$

Here the total energy of the pure substances is

$$E_{pure} = n_{CO2} h_{m,CO2} + n_{H2O} h_{m,H2O,L}. \quad (6\text{-}18)$$

Our model makes the assumption that the total energy of the mixture is the sum of CO_2, liquid water, and dissolved water vapor energies (Equations 6-8 to 6-12),

$$E_{mixture} = n_{CO2} h_{m,CO2} + n_{H2O,v} h_{m,H2O,v} + n_{H2O,L} h_{m,H2O,L}. \quad (6\text{-}19)$$

We assume that the mole fraction of aqueous CO_2 is negligible (i.e. $x_{CO2} < 2\%$) over the range of temperatures and pressures examined and that CO_2 has the same energy regardless of whether it is a solute or solvent (i.e. gaseous or aqueous). The number of moles of H_2O is the sum of moles in its different phases,

$$n_{H2O} = n_{H2O,L} + n_{H2O,v}. \quad (6\text{-}20)$$

Combing Equations 6-17 to 6-20 and eliminating terms, we get

$$\Delta h_{mix} = \frac{n_{H2O,v}}{n_{H2O} + n_{CO2}} \left(h_{H2O,v} - h_{H2O,l} \right). \quad (6\text{-}21)$$

For the CO_2-rich phase, the solubility of H_2O in the CO_2, y_{H2O}, is the moles of dissolved water, assumed here to be vapor, divided by the total moles of CO_2 and H_2O,

$$y_{H2O} = \frac{n_{H2O,v}}{n_{CO2}+n_{H2O,v}}. \quad (6\text{-}22)$$

The total mole fraction of CO_2 in the mixture, X_{CO2}, is

$$X_{CO2} = \frac{n_{CO2}}{n_{CO2}+n_{H2O}}. \quad (6\text{-}23)$$

Combining Equations 6-20 to 6-22 and assuming that CO_2 dissolution into H_2O is negligible ($x_{CO2} \approx 0$) yields

$$\Delta h_{mix} = X_{CO2}\ \frac{y_{H2O}}{1-y_{H2O}}\left(h_{H2Ov} - h_{H2O,L}\right). \quad (6\text{-}24)$$

A mixture of CO_2 and H_2O has two regions, one "CO_2 limited," where there is excess water and any CO_2 is fully saturated with H_2O (Region I), and one "H_2O limited," where there is excess CO_2 and the CO_2 contains H_2O at concentrations below its solubility limit (Region II). Figure 6-1A shows these two regions with data from Chen et al. [34] for a pressure of 12.4 MPa and a temperature of 250 °C. For a given pressure and temperature, the solubility limit of H_2O in the CO_2-rich phase, $y_{H2O,\,MAX}$, may be found using the solubility solution of Spycher et al. [163,167,169]. For the example of Figure 6-1A, the solubility limit is $y_{H2O,MAX} = 0.3866$.

At a CO_2 mole fraction of $X_{CO2} = 0$, the system is pure water. As the CO_2 fraction increases through Region I, added CO_2 is immediately saturated with water, vaporizing water in the process, thus increasing the enthalpy of mixing. Once the full saturation point is reached at $X_{CO2} = 1 - y_{H2O,MAX}$, all of the H_2O has been dissolved into the added CO_2 and there is no

excess water. This occurs at $X_{CO2} = 0.6134$ in Figure 6-1A. As the CO_2 fraction is increased into Region II, there is insufficient H_2O present to fully saturate the CO_2. Consequently, the fraction of H_2O in the CO_2, y_{H2O}, decreases below the saturation point, so that the amount of vaporized water decreases, decreasing the enthalpy of mixing.

Equations 6-25 and 6-26 show the enthalpy of mixing relations modified from Equation 6-23 for Regions I and II. In Region I, the CO_2 is always fully saturated with H_2O ($y_{H2O} = y_{H2O,MAX}$). In Region II, the H_2O in CO_2 is below the saturation limit. As we assume there is no CO_2 dissolved in H_2O ($x_{CO2} \approx 0$) and all the water enters the CO_2 solution, the CO_2 mole fraction is equal to one less the mole fraction of H_2O in CO_2 ($X_{CO2} = 1 - y_{H2O}$). Thus, Equation 6-23 further reduces to Equation 6-26 for Region II.

$$\Delta h_{mix} = X_{CO2} \frac{y_{H2O,MAX}}{1 - y_{H2O,MAX}} \left(h_{H2O,v} - h_{H2O,L}\right) \qquad \text{(Region I)} \qquad (6\text{-}25)$$

$$\Delta h_{mix} = (1 - X_{CO2}) \left(h_{H2O,v} - h_{H2OL}\right) \qquad \text{(Region II)} \qquad (6\text{-}26)$$

For a given pressure and temperature, the specific enthalpies of water, both liquid and vapor, are constant. In Region I, where $X_{CO2} \leq 1\text{-}y_{H2O,MAX}$, the CO_2 is fully saturated with water and therefore y_{H2O} is also constant and equal to $y_{H2O,MAX}$ (Equation 6-25). Thus, the mixture enthalpy, Δh_{mix}, increases linearly with the CO_2 mole fraction, X_{CO2}, in Region I. This relationship is shown in Figure 6-1A, where the slope of the line, 19.48 kJ mol^{-1}, is a result of the combination of the solubility limit ($y_{H2O,MAX} = 0.3866$) and the H_2O enthalpy difference, 30.9 kJ mol^{-1} (Equation 6-25), evaluated at a temperature of 250°C and a

pressure of 12.4 MPa. In this region, our model (Equation 6-25) strongly agrees with the experimental data from Chen et al. [168].

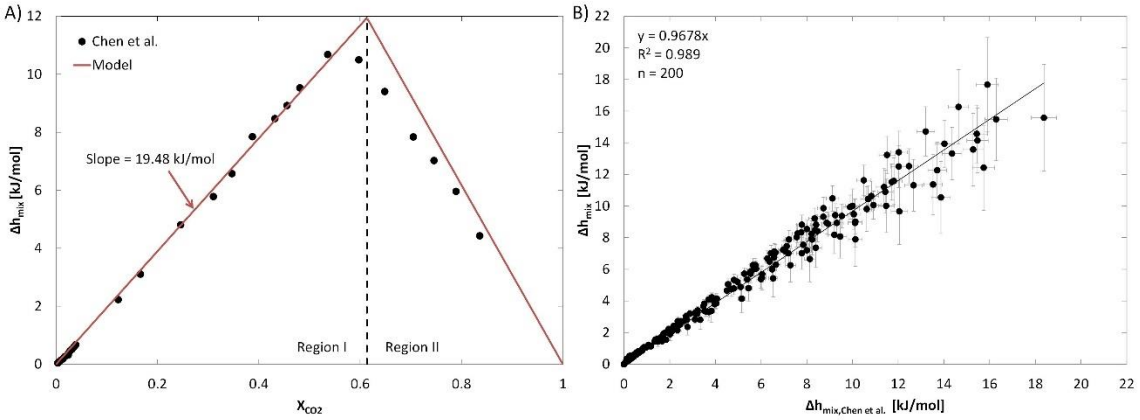

Figure 6-1: The correlation of our modelled enthalpy of mixing with the experimental data (Chen et al. [168]**) for A) a single pressure and temperature of 12.4 MPa and 250°C and B) the agreement between the modelled enthalpy of mixing and the calorimetric data. Modelled results show strong agreement with published values in the fully saturated region (Region I), however, the model overestimates the enthalpy of mixing in the sub-saturated region (Region II) due to modelling assumptions.**

In Region II, the mole fraction of water is insufficient to fully saturate the CO_2, and y_{H2O} decreases below the saturation limit, $y_{H2O,MAX}$. This relationship between the CO_2 fraction and the enthalpy of mixing is given by Equation 6-26, where the line slope is the negative difference of H_2O enthalpies (-30.9 kJ mol^{-1}). While the model fits the data quite well in Region I, it over estimates the enthalpy of mixing in Region II as not all the water enters the solution and some water remains as a liquid, which is not accounted for in our model. However, in the wellbore model used in this paper, we assume that the CO_2 is always fully saturated with H_2O, and therefore we are chiefly concerned with the data fit in Region I. Regardless, the enthalpy of mixing, Δh_{mix}, is fully explained by the multi-region model described here.

Figure 6-1B further shows the correlation between our enthalpy of mixing values (Equation 6-25) and those of Chen et al. [168] for all their Region I data (i.e. all temperatures and pressures). A correlation of $R^2 = 1$ and a slope of 1 would indicate a perfect agreement between the models. The resulting slope and coefficient of determination (R^2) are 0.9678 and 0.989, respectively, indicating that our model (Equations 6-16 to 6-23) accounts for 98.9% of the variation in the experimental enthalpy of mixing values, but underestimates the experimental enthalpy of mixing of Chen et al. [168] by ~3%. The variation in the experimental values and the model is accounted for in the uncertainty of the model, which has a mean uncertainty of 11%, which results from propagating the 5% uncertainty in the soluble H_2O mole fraction (y_{H2O}) reported in Spycher et al. [167] through Equation 6-25, indicated by the error bars in Figure 6-1B. Additionally, the 3% experimental variation reported in Chen et al. [168] are also indicated with horizontal error bars in Figure 6-1B. We have shown that the enthalpy of mixing may be approximated by heat of vaporization of water for a CO_2-H_2O solution and validated this assumption using available data from Chen et al. [168]. Therefore, the assumption that dissolved water in CO_2 may be modeled as saturated vapor is justified (Equation 6-10).

6.2.2 TOUGH2 Simulator Model

Our results are compared with those produced by TOUGH2 T2Well, which is a standard tool for wellbore flow simulation [165,170]. T2Well [165] uses the TOUGH2 [120] framework with the TOUGH2-ECO2N [121] equation of state module. The T2Well-ECO2N module incorporates the thermodynamic properties of the CO_2-H_2O-NaCl system, but the ECO2N module is limited to the temperature range of 12 to 110 °C, which is a

subset of the parameter space investigated here. Thus, the T2Well simulator results can only be compared to our results, where it is also valid.

The T2Well simulator differs from our model in three ways. First, it uses a transient drift-flux model (DFM) to simulate the flowrates and pressure losses of the two-phase flow of CO_2-H_2O mixtures [170]. The DFM uses empirical coefficients to separate the flow into liquid and gaseous phases with separate flow velocities for each phase. In contrast, our model assumes a single, homogenous flow with a single bulk density and velocity. As the fraction of liquid water is small for the cases considered here, the inclusion of the DFM modeling is not expected to produce appreciable differences from our bulk flow models. Second, unlike our approach, the ECO2N module does not include the change in fluid enthalpy as the water precipitates out of solution to free liquid water. Instead, the ECO2N module assumes that the CO_2 with H_2O in solution has the thermodynamic properties of dry CO_2. Third, the T2Well simulator numerically integrates using 10-meter elements along the axis of the well, whereas we use 100-meter elements. This difference is negligible because previous studies have found that 100 meter segments have less than 1% discretization error from much smaller values [82].

Thus, the T2Well simulator differs primarily from our simulations of water-saturated CO_2 in that it neglects the enthalpy of vaporization of the water vapor as it precipitates out of solution in the wellbore. Therefore, we expect the results of the T2Well model to agree only with our simulations for the dry CO_2 cases.

6.2.3 Power Plant Sensitivity Model

The surface power plant model determines the change in power produced from a direct CO_2-Plume Geothermal (CPG) system that uses water-saturated "wet" CO_2 instead of the pure "dry" CO_2 that we used within the power plant in our previous work [1,82]. Wet CO_2 will affect the power plant components due the change in two principal system parameters: 1) the temperature and pressure of the fluid at the wellhead and 2) the mass flowrate of CO_2 that passes through the turbine. In this power model, we assume that any produced liquid water will be separated from the wet CO_2 before the turbine, thereby reducing its mass flowrate (Figure 6-2). The energy required to remove the water is neglected. The water separator is assumed to be isobaric and isothermal.

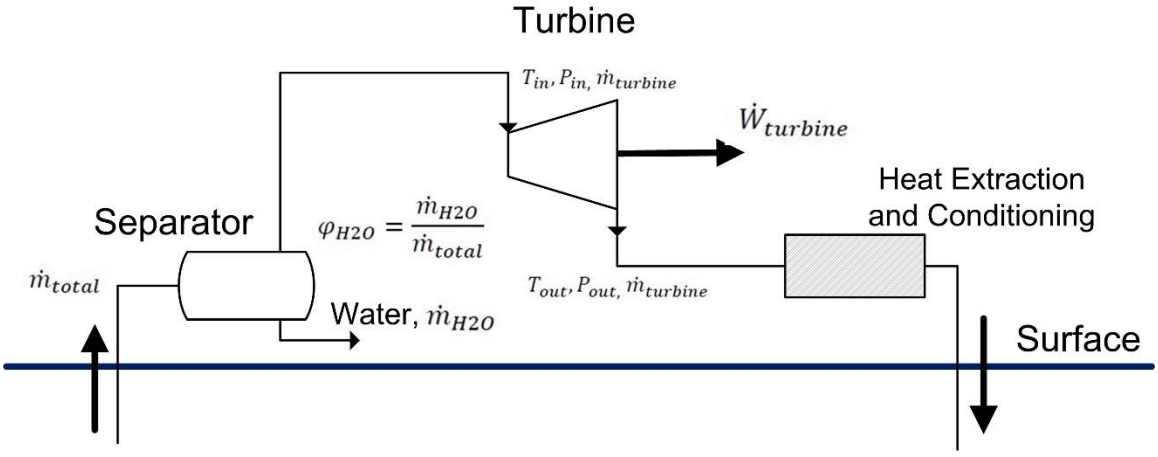

Figure 6-2: A potential schematic of the land-surface component of a CO_2-Plume Geothermal (CPG) power plant that includes liquid water separation at the surface, where $\dot{m}_{Total}$ is the total mass flow rate of the produced fluid and $\dot{m}_{CO2}$ and $\dot{m}_{H2O}$ are the mass flow rates of the CO_2 and liquid water, respectively. All other parameters are defined in the main text and in Table 6-1.

To estimate the effect of wet CO_2 on power production, the turbine power ($\dot{W}_{turbine}$) is numerically simulated using Engineering Equation Solver (EES) for each of the well

models (*Dry CO_2 Only*, *CO_2 Solution Proxy*, *Solution Density Approximation*, and *T2Well*) that were presented in Section 6.2 .0. Consistent with our earlier work, we assume a 78% isentropic turbine efficiency ($\eta = 0.78$) [1].

$$\eta = \frac{(h_{in} - h_{out})}{(h_{in} - h_{out,isentropic})} \tag{6-27}$$

The power produced by the turbine is the product of the mass flow rate and the difference between the enthalpy of the fluid at the turbine inlet and exit (Equation 6-28). The flow through the turbine is assumed to be pure CO_2.

$$\dot{W}_{turbine} = \dot{m}_{turbine}(h_{in} - h_{out}) \tag{6-28}$$

In the dry CO_2 case, the mass flow rate through the turbine is equal to the mass flow rate in the well and there is no need for a separator. When free liquid water is separated from the produced fluid, the mass flow rate through the turbine is reduced by the fraction of water that is removed from the produced fluid (φ_{H2O}),

$$\dot{m}_{turbine} = \dot{m}_{total}\left(1 - \varphi_{H2O}\right). \tag{6-29}$$

The turbine inlet enthalpy is found using the wellhead pressure and temperature, which changes when wet CO_2 is used. Thus, the fraction of turbine power change due to the wet CO_2, relative to the turbine power when using dry CO_2, is

$$\frac{\Delta\dot{W}}{\dot{W}} = \left(1 - \varphi_{H2O}\right)\frac{\left(h_{in,wet} - h_{out}\right)}{\left(h_{in,dry} - h_{out}\right)} - 1. \tag{6-30}$$

The turbine inlet enthalpy (h_{in}) is calculated from the temperature and pressure at the wellhead. The exit enthalpy (h_{out}) is calculated using the isentropic turbine efficiency. The isentropic outlet enthalpy ($h_{out,isentropic}$) is the enthalpy at the state defined by the inlet

entropy and an exit pressure equal to the saturation pressure of CO_2 at a temperature of 22°C (6.03 MPa), similar to Adams et al. [1].

6.3 Application and Results

The results are described in three parts: a single comparison case, a parametric study, and a power sensitivity analysis. A single case is used first to illustrate the differences between each of the well models. Then, the impact of well water content is found for a range of reservoir depths from 2.5 km to 5.0 km and for geothermal temperature gradients from 20 °C/km to 50 °C/km. Lastly, we employ a power sensitivity analysis to estimate the change in surface plant power generated due to water in the well.

6.3.1 Single Case Comparison

The comparison was conducted using values from the base case described in Adams et al. [1], where the total mass flow rate is 100 kg/s, the well depth to the reservoir is 2.5 km, and the assumed, typical geothermal temperature gradient is 35 °C/km. Thus, the downhole temperature is 102.5 °C and the pressure is 25 MPa. We assume a standard inner well diameter of 0.41 meters.

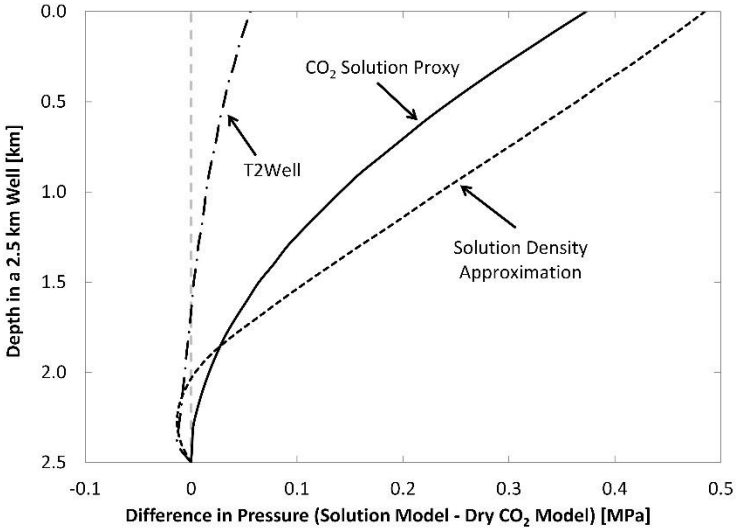

Figure 6-3: The difference in fluid pressure between each multi-fluid model and the dry CO_2 model for a 2.5km deep well with a geothermal temperature gradient of 35°C/km. A positive pressure change indicates the model predicts a greater well pressure than the dry CO_2 model.

Figure 6-3 shows the difference in pressure along the well between the *Dry CO_2 Only* model and the three wet CO_2-H_2O models (*CO_2 Solution Proxy, Solution Density Approximation, & T2Well*). All three wet CO_2 models predict higher wellhead pressures than the dry CO_2 model. The difference between the T2Well-ECO2N module and the dry CO_2 model is at most 0.06 MPa at the surface. Conversely, the *CO_2 Solution Proxy* and the *Solution Density Approximation* methods predict considerably higher surface pressures than the T2Well model, 0.36 MPa and 0.48 MPa, respectively.

The primary reason for the difference in pressure between the models is the fluid density that is used in each model. The pressure difference across each vertical element is determined primarily from the elevation change ($\Delta P = \rho g \Delta z$), as pressure losses (Equation 6-5) account for only ~1% of the pressure change. Therefore, as wet CO_2 tends

to have higher fluid temperatures, the bulk density of the CO_2 decreases, resulting in higher wellhead pressures relative to dry CO_2.

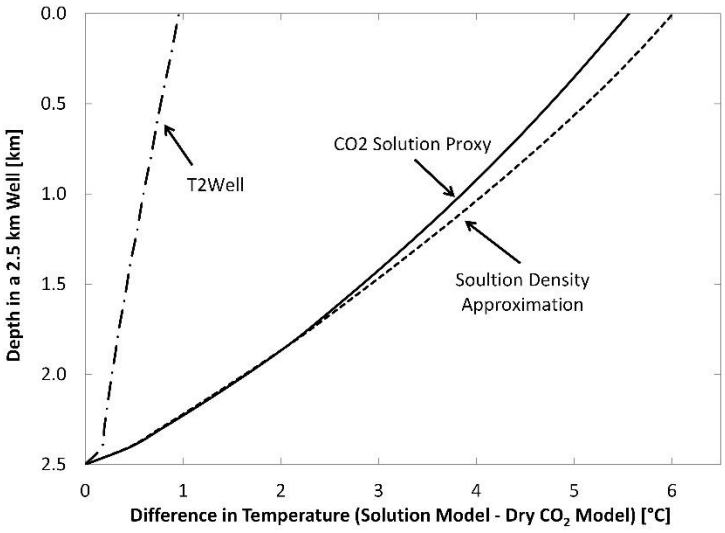

Figure 6-4: The temperature difference between each multi-fluid model and dry CO_2 as a function of depth. The wet CO_2 models predict elevated temperature over the dry CO_2 models, due to the thermodynamic effects of the H_2O in the well. The CO_2 solution proxy and the solution density approximation predict higher temperatures than T2Well and the dry CO_2 models, due to the inclusion of H_2O precipitation.

In the *CO_2 Solution Proxy* method, the density of the fluid is always less than the density of dry CO_2 throughout the well. In contrast, both the *Solution Density Approximation* method and T2Well occasionally result in higher fluid densities, because the densities are calculated from the CO_2-H_2O equation of state in these cases. Thus, the higher fluid density compared to dry CO_2, at the base of the production well, results in a negative pressure difference initially. However, the density becomes lower than that of dry CO_2 at depths less than ~2 km, so that the fluid pressure correspondingly increases.

Figure 6-4 shows the difference in temperature between the wet CO_2 models and dry CO_2. A positive "difference in temperature" indicates that the temperature in the well is greater

than using dry CO_2. All methods estimate wellhead temperatures that are higher than the estimated dry CO_2 model. Both the *CO_2 Solution Proxy* and the *Solution Density Approximation* methods estimate substantially larger increases (~6°C) in wellhead temperature compared to T2Well (~1°C).

The higher temperatures of the *CO_2 Solution Proxy* and the *Solution Density Approximation* methods are due to the enthalpy change of the precipitating H_2O. The precipitation of H_2O is due to the assumption that water is dissolved in CO_2 as vapor, thus reductions in solubility cause the condensation of water as it leaves the solution, which is an exothermic process, thereby increasing the fluid temperature. This increase in temperature causes the CO_2 to expand, reducing the CO_2 density. Over the length of the well, this effect increases the pressure of the fluid at the top of the well (Figure 6-3).

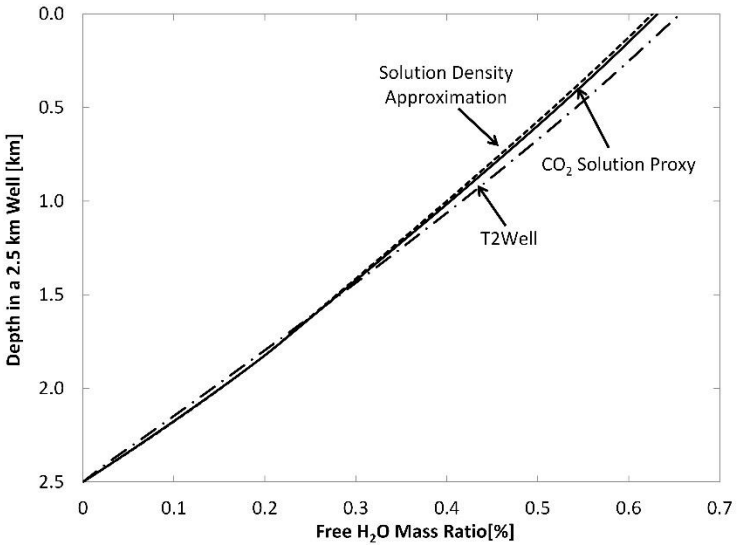

Figure 6-5: The mass ratio of free liquid H_2O increases with diminishing depth as the fluid pressure and temperature decrease. Differences between T2Well and the other models are the result of thermodynamic assumptions. The mass ratio is defined as $\dot{m}_{H2OL}/\dot{m}_{Total}$.

Figure 6-5 shows the percentage of free liquid water over the length of the well. At bottom-hole conditions, the CO_2 is assumed to be saturated with H_2O, with no free-phase H_2O. As the fluid ascends, the pressure and temperature decrease, which decreases the solubility of H_2O in CO_2, so that H_2O precipitates out of solution, forming free-phase water.

The three methods all have similar fractions of free water at the surface. However, unlike T2Well, the results from the *CO_2 Solution Proxy* and the *Solution Density Approximation* models have smaller and similar percentages of free H_2O because of the inclusion of enthalpy changes due to water precipitation. These two methods have elevated surface temperatures and pressures (Figure 6-3 and 6.4), which results in higher H_2O solubility and thus more H_2O remaining in solution.

6.3.2 Parameter Space

We estimate the wellhead temperature, pressure, and free H_2O phase mass fraction for combinations of three reservoir depths (2.5 km, 3.5 km, and 5 km) and three geothermal temperature gradients (20 °C/km, 35 °C/km, and 50 °C/km). The mass flow rate of water-saturated CO_2 at the production well inlet is assumed to be constant at 100 kg/s. The mean annual surface air temperature is set at 15°C and the well inner diameter is specified as 0.41 m. Table 6-2 shows the mass fraction of H_2O entering the production well from the reservoir and the free-phase liquid H_2O at the production well head. Table 6-3 presents the fluid pressures and temperatures at the production well inlet and at the wellhead.

Table 6-2: The mass fraction of water in solution with the CO_2 entering the production well and the fraction of free-phase liquid water at the wellhead.

		Reservoir H_2O Mass Ratio (%)			Wellhead Liquid H_2O Mass Ratio (%)		
Depth (km)	Temperature Gradient (°C/km)	CO_2 Solution Proxy	Solution Density Approximation	T2Well	CO_2 Solution Proxy	Solution Density Approximation	T2Well
2.5	20	0.42	0.42	0.42	0.28	0.28	0.31
2.5	35	0.93	0.93	0.9	0.63	0.63	0.65
2.5	50	2.09	2.09	-	1.04	1.08	-
3.5	20	0.69	0.69	0.69	0.49	0.47	0.52
3.5	35	2.15	2.15	-	1.31	1.36	-
3.5	50	5.63	5.63	-	1.93	2.02	-
5.0	20	1.44	1.44	-	1.03	1.03	-
5.0	35	5.97	5.97	-	2.57	2.71	-
5.0	50	19.01	19.01	-	3.72	3.98	-

Table 6-2 shows that the solubility of H_2O in CO_2 increases as the temperature and pressure of the fluid and reservoir increase. Therefore, the solubility of H_2O in CO_2 in the reservoir ranges from 0.42% in a 2.5 km deep reservoir and a geothermal temperature gradient of 20 °C/km (resulting in a reservoir temperature of 65 ^oC) to 19.01% in a 5.0 km deep reservoir and a geothermal gradient of 50 °C/km (giving a reservoir temperature of 265 ^oC) for the cases considered here.

The water fraction that enters the well in the *CO_2 Solution Proxy* and the *Solution Density Approximation* models are equivalent as both use the same solubility model. The T2Well model has the same constraint, however, the fraction of free-phase H_2O for the 2.5 km deep reservoir, 35 °C/km geothermal gradient case differs (0.93 versus 0.90) because T2Well only uses the low temperature solubility model (i.e., Spycher et al. [163]) for temperatures <100°C, whereas the *CO_2 Solution Proxy* and the *Solution Density Approximation* both use the appropriate high-temperature model for temperatures >100°C.

The fraction of liquid water produced at the wellhead varies between 0.28% and 3.98% for the bounding cases of a 2.5 km deep reservoir and a geothermal gradient of 20 °C/km and a 5.0 km deep reservoir and a geothermal gradient of 50 °C/km, respectively (Table 6-3). However, all but one case has wellhead liquid water fractions less than 3% (the 5.0 km deep and 265°C hot reservoir). In all cases, liquid H_2O is produced at the wellhead and the CO_2 is still fully saturated with H_2O.

Table 6-3: Temperature and pressure in the reservoir at the production well inlet and at the well head for each model.

				Pressure (MPa)				Temperature (°C)			
Depth (km)	Temperature Gradient (°C/km)	Reservoir Pressure (MPa)	Reservoir Temperature (°C)	Dry CO_2	CO_2 Solution Proxy	Solution Density Approximation	T2Well	Dry CO_2	CO_2 Solution Proxy	Solution Density Approximation	T2Well
2.5	20	25	65.0	7.62	7.85	8.25	7.72	31.4	32.7	34.1	31.2
2.5	35	25	102.5	12.28	12.64	12.75	12.34	61.4	66.8	67.3	62.8
2.5	50	25	140.0	15.29	15.61	15.17	-	100.7	113.9	112.7	-
3.5	20	35	85.0	10.68	11.11	11.6	10.8	43.2	46.7	48.1	44.3
3.5	35	35	137.5	16.9	17.62	16.92	-	89.1	104	102.3	-
3.5	50	35	190.0	20.77	21.31	20.27	-	144.1	170.6	169.3	-
5.0	20	50	115.0	15.43	16.46	16.52	-	62.1	72.1	72.2	-
5.0	35	50	190.0	23.97	25.2	23.39	-	132.5	165.9	164.2	-
5.0	50	50	265.0	29.09	29.86	25.99	-	211.1	257.4	256	-

Table 6-3 shows that the temperature of wet CO_2, produced at the wellhead is almost always higher than assuming dry CO_2. In only the T2Well 2.5 km deep reservoir, with a geothermal gradient of 20 °C/km, case is the temperature of produced, wet CO_2 lower than that of dry CO_2 and this is due to T2Well neglecting the increase in enthalpy due to H_2O precipitation. The temperature increase of wellhead wet CO_2 is larger for higher downhole temperatures and pressures. This is due to the larger water solubility in CO_2, entering the

well in the deep and hot reservoir cases, resulting in greater water precipitation in the wellbore and thus greater wellhead temperature increases, compared to dry CO_2.

The *Solution Density Approximation* model wellhead fluid pressures are often lower than those using dry CO_2. In contrast, the *CO_2 Solution Proxy* and T2Well fluid pressures tend to be higher than dry CO_2 wellhead pressures. This contrast is due to the generally larger fluid densities at a given temperature and pressure of the *Solution Density Approximation* than those of the *CO_2 Solution Proxy*. Increases in fluid density result in larger fluid pressure changes due to elevation changes ($\Delta P = \rho g \Delta z$) in the well, which results in a lower wellhead fluid pressure. This effect of fluid density on wellhead pressure is prominent in the 5 km deep reservoir and 50 °C/km geothermal gradient case, where the *CO_2 Solution Proxy* has a fluid density of 480.6 kg/m^3 and the *Solution Density Approximation* model yields a fluid density of 620 kg/m^3, which results in wellhead fluid pressures of 29.86 MPa and 25.99 MPa, respectively.

The wellhead fluid pressure for the *CO_2 Solution Proxy* is always greater than that of dry CO_2. The *CO_2 Solution Proxy* assumes that the CO_2 density is equivalent to that of dry CO_2. This results in a bulk fluid density (Equation 6-1) that is always equal to, or less than, the corresponding dry CO_2 density as a result of the temperature increase from the precipitation of H_2O. Thus, the *CO_2 Solution Proxy* model always predicts a larger wellhead fluid pressure than that using dry CO_2.

The mass fraction of H_2O in solution, given by Spycher et al. [163], has an uncertainty of 5%. When this error is propagated through our wellbore model, the resulting uncertainty

in pressure and temperature at the surface is less than 0.5%, and the uncertainty in the produced free-phase water at the surface is 5%, directly relating to the 5% uncertainty from Spycher et al. [163]. Furthermore, the uncertainty in the power produced by the turbine (Section 3.3) is less than 1.1% for all cases.

6.3.3 Power Sensitivity to Produced Water

The produced water fraction affects the power production of a direct CPG plant in two important ways. First, the produced free-phase water may need to be separated before any turbomachinery, depending on how much liquid water the turbine can handle along with the CO_2. It should be noted, however, that the presence of liquid water, together with supercritical CO_2, does not present as significant a challenge as liquid water in steam turbines, as the difference between liquid water and supercritical CO_2 density is, with a factor of approximately 2, much smaller than that between liquid water and steam (a factor of approximately 1000). Recent discussions with turbine manufacturers suggest that significantly larger mass fractions of liquid water in supercritical CO_2 than the ~6% reported by Garapati et al. [83] may be acceptable. Nonetheless, as water may still be removed from the produced fluid via gravitational separation, we investigate the consequences, including the reduced mass flowrate through the turbine. Second, the wet CO_2 alters the fluid state at the wellhead, while the turbine outlet pressure remains fixed, which affects the enthalpy difference across the turbine (Equation 6-28). Consequently, the turbine power output changes, as it is given by the product of the mass flowrate and the enthalpy drop across the turbine. We thus investigate in this section the change in power

generation due to the production of wet CO_2 and compare it to the case where dry CO_2 is produced from the reservoir, as is commonly assumed.

Table 6-4 shows the change in the power output from dry to wet CO_2 for the *CO_2 Solution Proxy*, the *Solution Density Approximation*, and T2Well simulations assuming liquid water is removed prior to the turbine. The produced water fraction values from Table 6-2 are used in Equations 6-27 to 6-30 to determine the power change.

Table 6-4: Turbine power output for each well model.

		Turbine Power (KW_e)				$\Delta W/W_{dry}$ (%)		
Depth (km)	Temperature Gradient (°C/km)	Dry CO_2	CO_2 Solution Proxy	Solution Density Approximation	T2Well	CO_2 Solution Proxy	Solution Density Approximation	T2Well
2.5	20	226	270	319	225	19.48	41.21	-0.62
2.5	35	1344	1538	1557	1388	14.43	15.85	3.27
2.5	50	2798	3192	3115	-	14.08	11.33	-
3.5	20	665	781	840	697	17.55	26.44	4.91
3.5	35	2448	2985	2895	-	21.94	18.26	-
3.5	50	4608	5397	5235	-	17.12	13.61	-
5.0	20	1435	1791	1796	-	24.81	25.16	-
5.0	35	4381	5557	5351	-	26.84	22.14	-
5.0	50	7629	8905	8306	-	16.73	8.87	-

Table 6-4 shows that wet CO_2, with liquid water removal, generates 14% to 41% more turbine power in a CPG system than dry CO_2, because, as described before, the exothermic precipitation of water from solution in CO_2 generates heat, and thus increases wellhead pressure, that later increases power generation, even if the water is removed. This effect more than outweighs the reduction in power generation due to decreased fluid mass flow rates that result from removal of the liquid water before the turbine inlet. Additionally, we assume that the liquid water is removed using gravitational separation which incurs no power consumption or pressures losses. Thus, the difference in power generation tends to increase with reservoir depth and geologic temperature gradients, where increased reservoir temperatures result in higher fractions of dissolved water and therefore higher

wellhead temperatures. For example, the change in power output for the Solution *Density Approximation* method, relative to dry CO_2, increases from 16% for the 2.5 km deep geothermal reservoir to 22% for the 5 km deep geothermal reservoir, in both cases for a geothermal temperature gradient of 35 °C/km, resulting in reservoir temperatures of 102.5ºC and 190ºC.

We investigated only three cases with T2Well, due to the temperature limitation of the ECO2N module, described previously. The T2Well cases always have a smaller change in power production when changing from dry to wet CO_2, compared to the other models. For example, at a reservoir depth of 2.5 km and a geothermal temperature gradient of 35 °C/km, the T2Well results estimate a power increase from dry to wet CO_2 of 3.3%, while the *CO_2 Solution Proxy* and the *Solution Density Approximation* models increase power by 14.4% and 15.8%, respectively. Furthermore, the change in power of the T2Well 2.5 km deep, with a geothermal temperature gradient of 20 °C/km, case results in a negative (-0.6%) power increase when going from dry to wet CO_2, i.e. a power decrease. This is a unique result and is caused by a decreased production temperature compared with dry CO_2. This is due to the solubility model of T2Well neglecting enthalpy changes due to the precipitation of water. The T2Well cases provide very similar wellhead temperatures to those for dry CO_2 (Table 6-3), and therefore the power output changes by a proportionately small amount.

The power gain percentage tends to increase as the both the depth and geothermal temperature gradient increase, with the exceptions of the 2.5 km deep, and 20°C/km

geothermal temperature gradient and the 5.0 km deep, 50 °C/km geothermal temperature gradient cases for both the *CO_2 Solution Proxy* and *Density Solution Approximation* models. For the 2.5km deep, 20°C/km geothermal temperature gradient cases, the large percentage gains for the wet CO_2 models are a result of the limited power produced (by the dry CO_2) due to the limited temperature/pressure of the reservoir. For instance, the turbine back pressure is fixed at 6.03 MPa for all cases; thus, an increase in fluid production pressure from an unusually small turbine inlet pressure of 7.62 MPa (dry CO_2, 2.5 km, 20°C/km case) to 8.25 MPa (*Density Solution Approximation*, 2.5 km, 20°C/km case) increases the turbine pressure differential from 1.59 MPa to 2.22 MPa, which results in an increase in the turbine output by 41.2%. However, the new turbine power output is still only 319 kW_e. Conversely, the 5.0 km deep, 50°C/km cases have a decrease in the percentage power gain, due to the large initial power generated by the dry CO_2 (7629 kW) and the increased water fraction produced, and thus decreased CO_2 production for these cases. Thus, the percentage increase in power must be considered in addition to the absolute power values for any configuration.

Overall, the largest factor causing differences in turbine power output is the wellhead fluid temperature, which is affected by the enthalpy of precipitating water. Higher wellhead temperatures increase the enthalpy difference across the turbine, which increases the power output. Thus, neglecting this enthalpy change during modelling underestimates the power generation, as the T2Well results show. Furthermore, if only a reduction in fluid mass flow rate is assumed, the outcome of using a water-saturated CO_2 solution in the well is that

both the magnitude and the sign of the change in power output are incorrect (i.e. the result is an incorrect decrease in power output instead of an increase).

6.4 Conclusions

Modeling the fluid in the well as wet CO_2 (i.e. CO_2 with dissolved H_2O and free liquid water) instead of dry CO_2 has a significant influence on the fluid that is produced at the wellhead, which impacts the power generation of the CPG system. Our simulations allow the following conclusions:

The inclusion of H_2O in solution with the CO_2 leads to the production of free-phase liquid H_2O at the wellhead, due to the precipitation of the initially dissolved water during the upwards flow of the production fluid, experiencing a decrease in pressure and temperature, reducing the water-in-CO_2 saturation index. The downhole wet CO_2 contains up to 19.2% dissolved H_2O by mass, depending on the temperature and pressure of the reservoir. While the mass fraction of wellhead H_2O is small for the majority of cases considered (<2%), it can be as much as 4% when the reservoir temperature is 140 °C.

Wet CO_2 will nearly always produce a higher wellhead temperature than dry CO_2. When the enthalpy of precipitating water is considered, the wellhead temperature is between 1.3°C and 46.3°C higher than when dry CO_2 is assumed.

The T2Well simulator substantially underestimates the wellhead temperature because the T2Well model neglects the enthalpy change due to precipitation of water from CO_2. For the three cases tested, the T2Well wellhead temperature and pressure are within 3% of the dry CO_2 model. However, the wellhead temperatures and pressures for the other modeled wet CO_2 cases are always larger. For example, for the 3.5 km, 20 C/km case, the T2Well

pressure is 1.1% higher than for the dry CO_2. However, the *CO_2 Solution Proxy* and the *Solution Density Approximation* models yields values between 4.0% and 8.6%.

Including the enthalpy of precipitation when modeling H_2O coming out of solution is critical. When the dissolved H_2O is assumed to have the enthalpy of water vapor, large amounts of heat are given off as it comes out of solution, raising the fluid temperature, decreasing the density, decreasing the pressure difference across the wellbore element, and ultimately raising the wellhead pressure. Furthermore, we verify our enthalpy assumption using experimental data from Chen et al. [168].

Using wet CO_2 increases the turbine power output between 15% and 25% above when dry CO_2 is assumed. The higher wellhead temperatures and pressures produced when using wet CO_2 increases the enthalpy difference across the turbine. This increase is greater than the decrease in power due to the removal of produced liquid water, resulting in a net positive increase in power generated by the turbine.

Chapter 7: References

[1] Adams BM, Kuehn TH, Bielicki JM, Randolph JB, Saar MO. A comparison of electric power output of CO2 Plume Geothermal (CPG) and brine geothermal systems for varying reservoir conditions. Applied Energy 2015;140:365–77. doi:10.1016/j.apenergy.2014.11.043.

[2] Adams BM, Kuehn TH. The Complementary Nature of CO2-Plume Geothermal (CPG) Energy Production and Electrical Power Demand. Volume 6: Energy, Parts A and B, ASME; 2012, p. 1791. doi:10.1115/IMECE2012-88704.

[3] IPCC. Global warming of 1.5°C. 2018.

[4] IPCC. Climate Change 2014: Synthesis Report. Contribution of Working Groups I, II and III to the Fifth Assessment Report of the Intergovernmental Panel on Climate Change. Geneva, Switzerland: 2014.

[5] IPCC. Climate Change 2014: Mitigation of Climate Change. Contribution of Working Group III to the Fifth Assessment Report of the Intergovernmental Panel on Climate Change. Cambridge: Cambridge University Press; 2014. doi:10.1017/CBO9781107415416.

[6] Dlugokencky E, Tans P. ESRL Global Monitoring Division - Global Greenhouse Gas Reference Network. NOAA/ESRL https://www.esrl.noaa.gov/gmd/ccgg/trends/data.html (accessed April 8, 2018).

[7] GISTEMP Team. GISS Surface Temperature Analysis (GISTEMP). NASA Goddard Institute for Space Studies 2018. https://data.giss.nasa.gov/gistemp/ (accessed April 10, 2018).

[8] Hansen J, Ruedy R, Sato M, Lo K. GLOBAL SURFACE TEMPERATURE CHANGE. Reviews of Geophysics 2010;48:RG4004. doi:10.1029/2010RG000345.

[9] Millar RJ, Fuglestvedt JS, Friedlingstein P, Rogelj J, Grubb MJ, Matthews HD, et al. Emission budgets and pathways consistent with limiting warming to 1.5 °C. Nature Geoscience 2017;10:741–7. doi:10.1038/ngeo3031.

[10] IPCC. IPCC Special Report on Carbon Dioxide Capture and Storage. Cambridge, United Kingdom: Cambridge University Press; 2005.

[11] International Energy Agency. World Energy Outlook 2017. OECD; 2017. doi:10.1787/weo-2017-en.

[12] European Union. L 140. vol. 52. 2009.

[13] State of California. Senate Bill No. 350: SB-350 Clean Energy and Pollution Reduction Act of 2015. Senate; 2015.

[14] State of Hawaii. House Bill No. 623: HB623 A bill for an act related to renewable standards. House of Representatives; 2015.

[15] State of Minnesota. § 216B.1691 Renewable Energy Objectives. https://www.revisor.mn.gov/statutes/cite/216B.1691; 2018.

[16] Massachusetts Institute of Technology. The Future of Geothermal Energy: Impact of Enhanced Goethermal Systems (EGS) on the United States in the 21st Century: an Assessment. 2006.

[17] U.S. Energy Information Administration (EIA) - Total Energy Monthly Data https://www.eia.gov/totalenergy/data/monthly/index.php (accessed November 12, 2018).

[18] EIA. Monthly Energy Review - Energy Information Administration 2017. https://www.eia.gov/totalenergy/data/annual/index.php#electricity%0A (accessed April 30, 2017).

[19] EIA. Electric Power Monthly. Electric Power Monthly 2017. https://www.eia.gov/electricity/monthly/epm_table_grapher.php?t=epmt_6_07_b (accessed January 11, 2017).

[20] Wiser R, Mills A, Seel J, Levin T, Botterud A. Impacts of Variable Renewable Energy on Bulk Power System Assets, Pricing, and Costs. 2017.

[21] Welcome to the New Normal: Negative Electricity Prices. The Electricity Journal 2018;31:94. doi:10.1016/j.tej.2018.01.013.

[22] Hirth L. The benefits of flexibility: The value of wind energy with hydropower. Applied Energy 2016;181:210–23. doi:10.1016/j.apenergy.2016.07.039.

[23] Connolly D. The Integration of Fluctuating Renewable Energy Using Energy Storage (Doctoral dissertation). University of Limerick, 2010.

[24] Kubik ML, Coker PJ, Hunt C. The role of conventional generation in managing variability. Energy Policy 2012;50:253–61. doi:10.1016/j.enpol.2012.07.010.

[25] Cavallo AJ. Energy Storage Technologies for Utility Scale Intermittent Renewable Energy Systems. Journal of Solar Energy Engineering 2001;123:387.

doi:10.1115/1.1409556.

[26] Denholm P, Hand M. Grid flexibility and storage required to achieve very high penetration of variable renewable electricity. Energy Policy 2011;39:1817–30. doi:10.1016/j.enpol.2011.01.019.

[27] U.S. Energy Information Administration (EIA) - Data https://www.eia.gov/totalenergy/data/browser/?tbl=T01.02#/?f=A (accessed April 30, 2017).

[28] Azar C, Lindgren K, Obersteiner M, Riahi K, van Vuuren DP, den Elzen KMGJ, et al. The feasibility of low CO2 concentration targets and the role of bio-energy with carbon capture and storage (BECCS). Climatic Change 2010;100:195–202. doi:10.1007/s10584-010-9832-7.

[29] Pires JCM, Martins FG, Alvim-Ferraz MCM, Simões M. Recent developments on carbon capture and storage: An overview. Chemical Engineering Research and Design 2011;89:1446–60. doi:10.1016/j.cherd.2011.01.028.

[30] Midldeton RS, Levine JS, Bielicki JM, Stauffer PH. Industrial CO2 and Carbon Capture: Near-term Benefit, Long-term Necessity. Energy Procedia 2017;114:7601–5. doi:10.1016/j.egypro.2017.03.1892.

[31] Singer AM, Branham M, Hutchins MG, Welker J, Woodard DL, Badurek CA, et al. The role of CO2 emissions from large point sources in emissions totals, responsibility, and policy. Environmental Science & Policy 2014;44:190–200. doi:10.1016/j.envsci.2014.08.001.

[32] National Energy Technology Laboratory. Carbon Storage Atlas: Fifth Edition. 2015.

[33] Randolph JB, Saar MO. Coupling carbon dioxide sequestration with geothermal energy capture in naturally permeable, porous geologic formations: Implications for CO2 sequestration. Energy Procedia 2011;4:2206–13. doi:10.1016/j.egypro.2011.02.108.

[34] Randolph JB, Saar MO. Impact of reservoir permeability on the choice of subsurface geothermal heat exchange fluid : CO2 versus water and native brine. Transactions - Geothermal Resources Council, vol. 35, 2011, p. 521–6.

[35] Kong X-Z, Saar MO. Numerical study of the effects of permeability heterogeneity on density-driven convective mixing during CO2 dissolution storage. International Journal of Greenhouse Gas Control 2013;19:160–73. doi:10.1016/j.ijggc.2013.08.020.

[36] Xu T, Apps JA, Pruess K. Reactive geochemical transport simulation to study mineral trapping for CO2 disposal in deep arenaceous formations. Journal of Geophysical Research: Solid Earth 2003;108. doi:10.1029/2002JB001979.

[37] Xu T, Pruess K. Reactive transport modeling to study fluid-rock interactions in enhanced geothermal systems (EGS) with CO2 as working fluid. World Geothermal Congress 2010.

[38] Consoli CP, Havercroft I, Irlam L. Carbon Capture and Storage Readiness Index: Comparative Review of Global Progress towards Wide-scale Deployment. Energy Procedia 2017;114:7348–55. doi:10.1016/j.egypro.2017.03.1585.

[39] Large-scale CCS facilities | Global Carbon Capture and Storage Institute https://www.globalccsinstitute.com/projects/large-scale-ccs-projects (accessed April 13, 2018).

[40] Ringrose PS, Mathieson AS, Wright IW, Selama F, Hansen O, Bissell R, et al. The In Salah CO2 Storage Project: Lessons Learned and Knowledge Transfer. Energy Procedia 2013;37:6226–36. doi:10.1016/j.egypro.2013.06.551.

[41] Frailey SM, Damico J, Leetaru HE. Reservoir characterization of the Mt. Simon Sandstone, Illinois Basin, USA. Energy Procedia 2011;4:5487–94. doi:10.1016/j.egypro.2011.02.534.

[42] Bauer RA, Carney M, Finley RJ. Overview of microseismic response to CO2 injection into the Mt. Simon saline reservoir at the Illinois Basin-Decatur Project. International Journal of Greenhouse Gas Control 2016;54:378–88. doi:10.1016/j.ijggc.2015.12.015.

[43] Finley RJ. An overview of the Illinois Basin - Decatur Project. Greenhouse Gases: Science and Technology 2014;4:571–9. doi:10.1002/ghg.1433.

[44] Tollefson J. US government abandons carbon-capture demonstration. Nature 2015. doi:10.1038/nature.2015.16868.

[45] Herzog HJ. Scaling up carbon dioxide capture and storage: From megatons to gigatons. Energy Economics 2011;33:597–604. doi:10.1016/j.eneco.2010.11.004.

[46] Gough C, Vaughan N. E. Synthesising existing knowledge on the feasibility of BECCS. 2015.

[47] McCoy S, Bertsch J, Growitsch C, Lorenczik S, Nagl S, Volk D, et al. The Role of CCS in Power Systems with High Levels of Renewables Penetration. Energy Procedia 2013;37:2665–75. doi:10.1016/j.egypro.2013.06.151.

[48] L′Orange Seigo S, Dohle S, Siegrist M. Public perception of carbon capture and storage (CCS): A review. Renewable and Sustainable Energy Reviews 2014;38:848–63. doi:10.1016/j.rser.2014.07.017.

[49] Ashworth P, Bradbury J, Wade S, Ynke Feenstra CFJ, Greenberg S, Hund G, et al. What's in store: Lessons from implementing CCS. International Journal of Greenhouse Gas Control 2012;9:402–9. doi:10.1016/j.ijggc.2012.04.012.

[50] Huff G, Currier AB, Kaun BC, Rastler DM, Chen SB, Bradshaw DT, et al. DOE/EPRI 2013 electricity storage handbook in collaboration with NRECA. 2013.

[51] Kousksou T, Bruel P, Jamil A, El Rhafiki T, Zeraouli Y. Energy storage: Applications and challenges. Solar Energy Materials and Solar Cells 2014;120:59–80. doi:10.1016/j.solmat.2013.08.015.

[52] Cavallo A. Controllable and affordable utility-scale electricity from intermittent wind resources and compressed air energy storage (CAES). Energy 2007;32:120–7. doi:10.1016/j.energy.2006.03.018.

[53] Yang Z, Liu J, Baskaran S, Imhoff CH, Holladay JD. Enabling renewable energy—and the future grid—with advanced electricity storage. JOM 2010;62:14–23. doi:10.1007/s11837-010-0129-0.

[54] Sørensen B. Renewable Energy Conversion, Transmission and Storage. Elsevier; 2007. doi:10.1016/B978-0-12-374262-9.X5001-0.

[55] Rehman S, Al-Hadhrami LM, Alam MM. Pumped hydro energy storage system: A technological review. Renewable and Sustainable Energy Reviews 2015;44:586–98. doi:10.1016/j.rser.2014.12.040.

[56] Sørensen B. Solar energy storage. Elsevier; 2015.

[57] Yang C-J, Jackson RB. Opportunities and barriers to pumped-hydro energy storage in the United States. Renewable and Sustainable Energy Reviews 2011;15:839–44. doi:10.1016/j.rser.2010.09.020.

[58] Budt M, Wolf D, Span R, Yan J. A review on compressed air energy storage: Basic principles, past milestones and recent developments. Applied Energy 2016;170:250–68. doi:10.1016/j.apenergy.2016.02.108.

[59] King M, Moridis G, Apps J. Compressed Air Energy Storage: Matching the Earth to the Turbo-Machinery - No Small Task. Proceedings of the 2013 Electrical Energy Storage Applications & Technologies (EESAT) Biennial International Conference, 2013, p. 1–8.

[60] Wang J, Lu K, Ma L, Wang J, Dooner M, Miao S, et al. Overview of Compressed Air Energy Storage and Technology Development. Energies 2017;10:991. doi:10.3390/en10070991.

[61] Luo X, Wang J, Dooner M, Clarke J, Krupke C. Overview of Current Development in Compressed Air Energy Storage Technology. Energy Procedia 2014;62:603–11. doi:10.1016/j.egypro.2014.12.423.

[62] World Energy Council. World Energy Resources: 2013 survey. 2013.

[63] Banks D. An Introduction to Thermogeology: Ground Source Heating and Cooling. Oxford, UK: Blackwell Publishing, Ltd; 2008. doi:10.1002/9781444302677.

[64] Zhang D, Jackson JM, Zhao J, Sturhahn W, Alp EE, Hu MY, et al. Temperature of Earth's core constrained from melting of Fe and Fe0.9Ni0.1 at high pressures. Earth and Planetary Science Letters 2016;447:72–83. doi:10.1016/j.epsl.2016.04.026.

[65] DiPippo R. Geothermal Power Plants: Principles, Applications, Case Studies and Environmental Impact (4th Edition). Elsevier; 2016.

[66] Pollack HN, Hurter SJ, Johnson JR. Heat flow from the Earth's interior: Analysis of the global data set. Reviews of Geophysics 1993;31:267. doi:10.1029/93RG01249.

[67] Olasolo P, Juárez MC, Morales MP, D´Amico S, Liarte IA. Enhanced geothermal systems (EGS): A review. Renewable and Sustainable Energy Reviews 2016;56:133–44. doi:10.1016/j.rser.2015.11.031.

[68] Breeze P. Power Generation Technologies (2nd Edition). Elsevier; 2014.

[69] Lund J, Bjelm L, Bloomquist G, Mortensen A. Characteristics, development and utilization of geothermal resources - a Nordic perspective. Episodes 2008;31.

[70] Mitsubishi Hitachi Powe Systems Americas, INC. - J Series https://amer.mhps.com/j-series.html (accessed November 17, 2018).

[71] GWEC. Global Wind Report 2016. 2017.

[72] Geothermal Maps | Geospatial Data Science | NREL https://www.nrel.gov/gis/geothermal.html (accessed November 13, 2018).

[73] Brasz J, P Biederman B, Holdmann G. Power Production from a Moderate-

Temperature Geothermal Resource. Geothermal Resource (GRC) Transactions 2005;29.

[74] Potter R, Robinson E, Smith M. Method of extracting heat from dry geothermal reservoirs. US Patent 3,786,858, 1974.

[75] Brown DW. Hot dry rock geothermal energy: important lessons from Fenton Hill. PROCEEDINGS, Thirty-Fourth Workshop on Geothermal Reservoir Engineering, Palo Alto: 2009.

[76] He Z, Zhang Y, Feng J, Ding Q, Li P. An EGS Site Evaluation Method for Geothermal Resources Based on Geology, Engineering and Economic Considerations. PROCEEDINGS, 43rd Workshop on Geothermal Reservoir Engineering, Palo Alto: 2018.

[77] Ziagos J, Phillips BR, Boyd L, Jelacic A, Stillman G, Hass. E. A technology roadmap for strategic development of enhanced geothermal systems. Proceedings of the 38th Workshop on Geothermal Reservoir Engineering, Stanford, CA 2013.

[78] Bachmann CE, Wiemer S, Woessner J, Hainzl S. Statistical analysis of the induced Basel 2006 earthquake sequence: introducing a probability-based monitoring approach for Enhanced Geothermal Systems. Geophysical Journal International 2011;186:793–807. doi:10.1111/j.1365-246X.2011.05068.x.

[79] Boudet H, Clarke C, Bugden D, Maibach E, Roser-Renouf C, Leiserowitz A. “Fracking” controversy and communication: Using national survey data to understand public perceptions of hydraulic fracturing. Energy Policy 2014;65:57–67. doi:10.1016/j.enpol.2013.10.017.

[80] FORGE Home | Department of Energy https://www.energy.gov/eere/forge/forge-home (accessed November 21, 2018).

[81] Brown W. D. A Hot Dry Rock Geothermal Energy Concept Utilizing Supercritical CO2 Instead of Water. Proceedings of the wenty-Fifth Workshop on Geothermal Reservoir Engineering, Palo Alto, California: 2000, p. 1–6.

[82] Adams BM, Kuehn TH, Bielicki JM, Randolph JB, Saar MO. On the importance of the thermosiphon effect in CPG (CO2 plume geothermal) power systems. Energy 2014;69:409–18. doi:10.1016/j.energy.2014.03.032.

[83] Garapati N, Randolph JB, Saar MO. Brine displacement by CO2, energy extraction rates, and lifespan of a CO2-limited CO2-Plume Geothermal (CPG) system with a horizontal production well. Geothermics 2015;55:182–94. doi:10.1016/j.geothermics.2015.02.005.

[84] Pruess K. Enhanced geothermal systems (EGS) using CO2 as working fluid—A novel approach for generating renewable energy with simultaneous sequestration of carbon. Geothermics 2006;35:351–67. doi:10.1016/j.geothermics.2006.08.002.

[85] Pruess K, Azaroual M. On the feasibility of using supercritical CO2 as heat transmission fluid in an engineered hot dry rock geothermal system. PROCEEDINGS, Thirty-First Workshop on Geothermal Reservoir Engineering, Palo Alto, California: 2006.

[86] Pruess K. Enhanced geothermal systems (EGS): comparing water and CO2 as heat transmission fluids. Proceedings of the New Zealand geothermal workshop, Auckland, New Zealand: 2007, p. 1–13.

[87] Pruess K. On production behavior of enhanced geothermal systems with CO2 as working fluid. Energy Conversion and Management 2008;49:1446–54. doi:10.1016/j.enconman.2007.12.029.

[88] Pruess K, Spycher N. Enhanced Geothermal Systems (EGS) with CO2 as Heat Transmission Fluid - A Scheme for Combining Recovery of Renewable Energy with Geologic Storage of CO2. Proceedings World Geothermal Congress, Bali, Indonesia: 2010.

[89] Borgia A, Pruess K, Kneafsey TJ, Oldenburg CM, Pan L. Simulation of CO2-EGS in a Fractured Reservoir with Salt Precipitation. Energy Procedia 2013;37:6617–24. doi:10.1016/j.egypro.2013.06.594.

[90] Atrens AD, Gurgenci H, Rudolph V. CO2 Thermosiphon for Competitive Geothermal Power Generation. Energy & Fuels 2009;23:553–7. doi:10.1021/ef800601z.

[91] Atrens AD, Gurgenci H, Rudolph V. Electricity generation using a carbon-dioxide thermosiphon. Geothermics 2010;39:161–9. doi:10.1016/j.geothermics.2010.03.001.

[92] Carroll S, Stillman G. Assessment of Key Physical and Chemical Research Findings for the Use of CO2 as a Heat Exchanging Fluid for Geothermal Energy Production. PROCEEDINGS, Thirty-Ninth Workshop on Geothermal Reservoir Engineering, Palo Alto, California: 2014.

[93] Saar MO, Randolph JB, Kuehn TH. Carbon Dioxide-Based Geothermal Energy Generation Systems and Methods Related Thereto. US Patent 8316955 B2, 2012.

[94] Randolph JB, Saar MO. Coupling geothermal energy capture with carbon dioxide sequestration in naturally permeable, porous geologic formations: A comparison

with enhanced geothermal systems. Geothermal Resources Council Transactions, vol. 34, 2010.

[95] Randolph JB, Saar MO, Bielicki J. Geothermal Energy Production at Geologic CO2 Sequestration sites: Impact of Thermal Drawdown on Reservoir Pressure. Energy Procedia 2013;37:6625–35. doi:10.1016/j.egypro.2013.06.595.

[96] Randolph JB, Saar MO. Combining geothermal energy capture with geologic carbon dioxide sequestration. Geophysical Research Letters 2011;38. doi:10.1029/2011GL047265.

[97] Szulczewski ML, MacMinn CW, Herzog HJ, Juanes R. Lifetime of carbon capture and storage as a climate-change mitigation technology. Proceedings of the National Academy of Sciences 2012;109:5185–9. doi:10.1073/pnas.1115347109.

[98] Janke B, Kuehn T. Geothermal Power Cycle Analysis for Commercial Applicability Using Sequestered Supercritical CO2 as a Heat Transfer or Working Fluid. ASME 2011 5th International Conference on Energy Sustainability, Parts A, B, and C, ASME; 2011, p. 1237–44. doi:10.1115/ES2011-54397.

[99] Garapati N, Randolph JB, Saar MO. Total Heat Energy Output From, Thermal Energy Contributions To, and Reservoir Development of CO2 Plume Geothermal (CPG) Systems. Proceedings of the Thirty-Ninth Workshop on Geothermal Reservoir Engineering, 2014, p. 1–12.

[100] Adams BM. On the Power Performance and Integration of Carbon-dioxide Plume Geothermal (CPG) Electrical Energy Production (Doctoral dissertation). University of Minnesota, 2015.

[101] Freifeld BM, Pan L, Doughty C, Zakem S, Hart K, Hostler S. Demonstration of Geothermal Energy Production Using Carbon Dioxide as a Working Fluid at the SECARB Cranfield Site, Cranfield, Mississippi. Proceedings, 41st Workshop on Geothermal Reservoir Engineering, Palo Alto, California: 2016.

[102] Pan L, Doughty C, Freifeld B. How to sustain a CO2-thermosiphon in a partially saturated geothermal reservoir: Lessons learned from field experiment and numerical modeling. Geothermics 2018;71:274–93. doi:10.1016/j.geothermics.2017.10.004.

[103] Freifeld B, Zakim S, Pan L, Cutright B, Sheu M, Doughty C, et al. Geothermal Energy Production Coupled with CCS: a Field Demonstration at the SECARB Cranfield Site, Cranfield, Mississippi, USA. Energy Procedia 2013;37:6595–603. doi:10.1016/j.egypro.2013.06.592.

[104] Hovorka SD. Three-Million-Metric-Ton-Monitored Injection at the Secarb Cranfield Project—Project Update. Energy Procedia 2013;37:6412–23. doi:10.1016/j.egypro.2013.06.571.

[105] Buscheck TA, Bielicki JM, Randolph JB. CO2 Earth Storage: Enhanced Geothermal Energy and Water Recovery and Energy Storage. Energy Procedia 2017;114:6870–9. doi:10.1016/j.egypro.2017.03.1615.

[106] Buscheck TA, Bielicki JM, Edmunds TA, Hao Y, Sun Y, Randolph JB, et al. Multifluid geo-energy systems: Using geologic CO2 storage for geothermal energy production and grid-scale energy storage in sedimentary basins. Geosphere 2016;12:678–96. doi:10.1130/GES01207.1.

[107] Buscheck TA, Bielicki JM, Chen M, Sun Y, Hao Y, Edmunds TA, et al. Integrating CO2 Storage with Geothermal Resources for Dispatchable Renewable Electricity. Energy Procedia 2014;63:7619–30. doi:10.1016/j.egypro.2014.11.796.

[108] Ogland-Hand JD, Bielicki JM, Nelson ES, Adams BM, Buscheck TA, Saar MO, et al. Effects of Bulk Energy Storage in Sedimentary Basin Geothermal Resources on Transmission Constrained Electricity Systems. PROCEEDINGS, 43rd Workshop on Geothermal Reservoir Engineering, Stanford, CA, Palo Alto, California: 2018.

[109] Garapati N, Adams BM, Randolph JB, Kuehn TH, Saar MO. Auxiliary Heating of Geothermally Preheated Brine or CO2 to Boost Electricity Production. In Preparation

[110] Liu H, He Q, Borgia A, Pan L, Oldenburg CM. Thermodynamic analysis of a compressed carbon dioxide energy storage system using two saline aquifers at different depths as storage reservoirs. Energy Conversion and Management 2016;127:149–59. doi:10.1016/j.enconman.2016.08.096.

[111] United Nations Framework Convention on Climate Change. Paris Agreement. Paris: http://unfccc.int/resource/docs/2015/cop21/eng/l09r01.pdf; 2015.

[112] Bird L, Milligan M, Lew D. Integrating Variable Renewable Energy: Challenges and Solutions. 2013.

[113] Phuangpornpitak N, Tia S. Opportunities and Challenges of Integrating Renewable Energy in Smart Grid System. Energy Procedia 2013;34:282–90. doi:10.1016/j.egypro.2013.06.756.

[114] Koohi-Kamali S, Tyagi VV, Rahim NA, Panwar NL, Mokhlis H. Emergence of energy storage technologies as the solution for reliable operation of smart power systems: A review. Renewable and Sustainable Energy Reviews 2013;25:135–65.

doi:10.1016/j.rser.2013.03.056.

[115] EPRI-DOE Handbook of Energy Storage for Transmission & Distribution Applications. 2003.

[116] Shimada R, Mukai K. Load-leveling and electric energy storage. IEEJ Transactions on Electrical and Electronic Engineering 2007;2:33–8. doi:10.1002/tee.20106.

[117] Matek B, Gawell K. The Benefits of Baseload Renewables: A Misunderstood Energy Technology. The Electricity Journal 2015;28:101–12. doi:10.1016/j.tej.2015.02.001.

[118] Bielicki JM, Adams BM, Choi H, Jamiyansuren B, Saar MO, Taff SJ, et al. Sedimentary Basin Geothermal Resource for Cost-Effective Generation of Renewable Electricity from Sequestered Carbon Dioxide. Proceedings of the 41st Stanford Geothermal Workshop 2016.

[119] Garapati N, Randolph JB, Valencia JL, Saar MO. CO2-Plume Geothermal (CPG) Heat Extraction in Multi-layered Geologic Reservoirs. Energy Procedia 2014;63:7631–43. doi:10.1016/j.egypro.2014.11.797.

[120] Pruess K, Oldenburg CM, Moridis G. TOUGH2 User's Guide, Version 2. Report LBNL-43134, Lawrence Berkeley National Laboratory, California 1999.

[121] Pruess K. ECO2N: A TOUGH2 Fluid Property Module for Mixtures of Water, NaCl, and CO2. Report LBNL-57952 Lawrence Berkeley National Laboratory, California 2005.

[122] Klein SA, Alvarado F. Engineering Equation Solver. F-Chart Software 2002.

[123] The MathWorks Inc. Matlab 2016a 2016.

[124] Farshad FF, Garber JD, Rieke HH, Komaravelly SG. Predicting Corrosion in Pipelines, Oil Wells and Gas Wells; a Computer Modeling Approach. Scientia Iranica Transaction C: Chemistry and Chemical Engineering 2010;17:86–96.

[125] Span R, Wagner W. A New Equation of State for Carbon Dioxide Covering the Fluid Region from the Triple-Point Temperature to 1100 K at Pressures up to 800 MPa. Journal of Physical and Chemical Reference Data 1996;25:1509–96. doi:10.1063/1.555991.

[126] Garapati N, Adams BM, Bielicki JM, Schaedle P, Randolph JB, Kuehn TH, et al. A Hybrid Geothermal Energy Conversion Technology - A Potential Solution for

Production of Electricity from Shallow Geothermal Resources. Energy Procedia 2017;114:7107–17. doi:10.1016/j.egypro.2017.03.1852.

[127] MISO. Midcontinent Independent System Operator Market Reports 2016. https://www.misoenergy.org/Library/MarketReports/Pages/MarketReports.aspx (accessed May 4, 2016).

[128] Welch P, Boyle P. New turbines to Enable Efficient Geothermal Power Plants. Geothermal Resources Council Transactions 2009;33:8.

[129] Randolph JB, Adams BM, Kuehn TH, Saar MO. Wellbore Heat Transfer in CO2-based Geothermal Systems. Geothermal Resources Council Transactions, vol. 36, 2012.

[130] Farshad FF, Rieke HH. Surface Roughness Design Values for Modern Pipes. SPE Drilling & Completion 2006;21:212–5. doi:10.2118/89040-PA.

[131] Bai B, Li X, Wu H, Wang Y, Liu M. A methodology for designing maximum allowable wellhead pressure for CO2 injection: application to the Shenhua CCS demonstration project, China. Greenhouse Gases: Science and Technology 2017;7:158–81. doi:10.1002/ghg.1640.

[132] Hubbert MK, Willis DG. Mechanics of hydraulic fracturing. Transactions of Society of Petroleum Engineers of AIME, 1957, p. 153–66.

[133] Court B, Celia M a., Nordbotten JM, Elliot TR. Active and integrated management of water resources throughout CO2 capture and sequestration operations. Energy Procedia 2011;4:4221–9. doi:10.1016/j.egypro.2011.02.370.

[134] Buscheck TA, Sun Y, Chen M, Hao Y, Wolery TJ, Bourcier WL, et al. Active CO2 reservoir management for carbon storage: Analysis of operational strategies to relieve pressure buildup and improve injectivity. International Journal of Greenhouse Gas Control 2012;6:230–45. doi:10.1016/j.ijggc.2011.11.007.

[135] Buscheck TA, White JA, Chen M, Sun Y, Hao Y, Aines RD, et al. Pre-injection Brine Production for Managing Pressure in Compartmentalized CO2 Storage Reservoirs. Energy Procedia 2014;63:5333–40. doi:10.1016/j.egypro.2014.11.565.

[136] Bergmo PES, Grimstad A-A, Lindeberg E. Simultaneous CO2 injection and water production to optimise aquifer storage capacity. International Journal of Greenhouse Gas Control 2011;5:555–64. doi:10.1016/j.ijggc.2010.09.002.

[137] De Vos K. Negative Wholesale Electricity Prices in the German, French and Belgian Day-Ahead, Intra-Day and Real-Time Markets. The Electricity Journal

2015;28:36–50. doi:10.1016/j.tej.2015.04.001.

[138] Fanone E, Gamba A, Prokopczuk M. The case of negative day-ahead electricity prices. Energy Economics 2013;35:22–34. doi:10.1016/j.eneco.2011.12.006.

[139] Biagi J, Agarwal R, Zhang Z. Simulation and optimization of enhanced geothermal systems using CO2 as a working fluid. Energy 2015;86:627–37. doi:10.1016/j.energy.2015.04.020.

[140] Majer EL, Baria R, Stark M, Oates S, Bommer J, Smith B, et al. Induced seismicity associated with Enhanced Geothermal Systems. Geothermics 2007;36:185–222. doi:10.1016/j.geothermics.2007.03.003.

[141] Gibbins J, Chalmers H. Carbon capture and storage. Energy Policy 2008;36:4317–22. doi:10.1016/j.enpol.2008.09.058.

[142] Fu C, Gundersen T. Carbon Capture and Storage in the Power Industry: Challenges and Opportunities. Energy Procedia 2012;16:1806–12. doi:10.1016/j.egypro.2012.01.278.

[143] International Energy Agency (IEA). 20 Years of Carbon Capture and Storage - Accelerating Future Deployment. 2016.

[144] Moody LF. Friction factor for pipe flow. Transaction of the ASME 1944;66:671–84.

[145] DOE US. Geothermal Electricity Technology Evaluation Model | Department of Energy https://www.energy.gov/eere/geothermal/geothermal-electricity-technology-evaluation-model (accessed August 22, 2018).

[146] Environmental Protection Agency (EPA). Geologic CO2 sequestration technology and cost analysis. 2008.

[147] BAC. Baltimore Aircoil Company - Cooling Towers, Closed Circuit Cooling Towers, Evaporative Condensers, Aircoil Evaporators, Ice Thermal Storage Systems -- Baltimore Aircoil Company 2014. http://www.baltimoreaircoil.com/english/products/overview (accessed March 15, 2014).

[148] Internal Revenue Code. § 45Q. 2018.

[149] Irlam L. GLOBAL COSTS OF CARBON CAPTURE AND STORAGE: 2017 Update. 2017.

[150] Psarras PC, Comello S, Bains P, Charoensawadpong P, Reichelstein S, Wilcox J. Carbon Capture and Utilization in the Industrial Sector. Environmental Science & Technology 2017;51:11440–9. doi:10.1021/acs.est.7b01723.

[151] Lazard. Levelised Cost of Energy Analysis. 2017.

[152] FERC. FERC Order 841. 2018.

[153] Piri M, Prévost JH, Fuller R. Carbon Dioxide Sequestration in Saline Aquifers: Evaporation, Precipitation and Compressibility Effects. Fourth Annual Conference on Carbon Capture and Sequestration DOE/NETL, 2005.

[154] Michael K, Golab A, Shulakova V, Ennis-King J, Allinson G, Sharma S, et al. Geological storage of CO2 in saline aquifers—A review of the experience from existing storage operations. International Journal of Greenhouse Gas Control 2010;4:659–67. doi:10.1016/j.ijggc.2009.12.011.

[155] Tutolo BM, Kong X-Z, Seyfried WE, Saar MO. High performance reactive transport simulations examining the effects of thermal, hydraulic, and chemical (THC) gradients on fluid injectivity at carbonate CCUS reservoir scales. International Journal of Greenhouse Gas Control 2015;39:285–301. doi:10.1016/j.ijggc.2015.05.026.

[156] Tutolo BM, Luhmann AJ, Kong X-Z, Saar MO, Seyfried WE. Experimental Observation of Permeability Changes In Dolomite at CO2 Sequestration Conditions. Environmental Science & Technology 2014;48. doi:10.1021/es4036946.

[157] Luhmann AJ, Kong X-Z, Tutolo BM, Garapati N, Bagley BC, Saar MO, et al. Experimental dissolution of dolomite by CO2-charged brine at 100°C and 150bar: Evolution of porosity, permeability, and reactive surface area. Chemical Geology 2014;380:145–60. doi:10.1016/j.chemgeo.2014.05.001.

[158] Boch R, Mindszenty A, Szanyi J, Deák J, Leis A, Kluge T, et al. Growth dynamics of geothermal carbonate scales: Forensic studies based on high-resolution mineralogical & geochemical analyses. GeoTirol 2016 - Annual Meeting DGGV, Innsbruck, Austria: 2016.

[159] Boch R, Szanyi J, Leis A, Mindszenty A, Deák J, Kluge T, et al. Geothermal Carbonate Scaling: Forensic Studies Applying High-Resolution Geochemical Methods. Proceedings of the European Geothermal Congress, Strasbourg, France: 2016.

[160] Boch R, Leis A, Haslinger E, Goldbrunner JE, Mittermayr F, Fröschl H, et al.

Scale-fragment formation impairing geothermal energy production: interacting H2S corrosion and CaCO3 crystal growth. Geothermal Energy 2017;5:4. doi:10.1186/s40517-017-0062-3.

[161] Bélteky L. Problems related to operating thermal wells subject to scaling in Hungary. Geothermics 1975;4:57–65. doi:10.1016/0375-6505(75)90009-7.

[162] Amann F, Gischig V, Evans K, Doetsch J, Jalali R, Valley B, et al. The seismo-hydromechanical behavior during deep geothermal reservoir stimulations: open questions tackled in a decameter-scale in situ stimulation experiment. Solid Earth 2018;9:115–37. doi:10.5194/se-9-115-2018.

[163] Spycher N, Pruess K, Ennis-King J. CO2-H2O mixtures in the geological sequestration of CO2. I. Assessment and calculation of mutual solubilities from 12 to 100°C and up to 600 bar. Geochimica et Cosmochimica Acta 2003;67:3015–31. doi:10.1016/S0016-7037(03)00273-4.

[164] Ahmad M, Casey M, Sürken N. Experimental assessment of droplet impact erosion resistance of steam turbine blade materials. Wear 2009;267:1605–18. doi:10.1016/j.wear.2009.06.012.

[165] Pan L, Oldenburg CM, Wu Y-S, Pruess K. T2Well/ECO2N Version 1.0: Multiphase and Non-Isothermal Model for Coupled Wellbore-Reservoir Flow of Carbon Dioxide and Variable Salinity Water. Report LBNL-4291E Berkeley National Laboratory, California 2011.

[166] Haar L, Gallagher JS, Kell GS, (U.S.) NSRDS, National Standard Reference Data System (U.S.). NBS/NRC steam tables : thermodynamic and transport properties and computer programs for vapor and liquid states of water in SI units. Washington [D.C.]: Hemisphere Pub. Corp.; 1984.

[167] Spycher N, Pruess K. CO2-H2O mixtures in the geological sequestration of CO2. II. Partitioning in chloride brines at 12–100°C and up to 600 bar. Geochimica et Cosmochimica Acta 2005;69:3309–20. doi:10.1016/j.gca.2005.01.015.

[168] Xuemin Chen, Gillespie SE, Oscarson JL, Izatt RM. Calorimetric determination of thermodynamic quantities for chemical reactions in the system CO2-NaOH-H2O from 225 to 325C. Journal of Solution Chemistry 1992;21:825–48. doi:10.1007/BF00651511.

[169] Spycher N, Pruess K. A Phase-Partitioning Model for CO2–Brine Mixtures at Elevated Temperatures and Pressures: Application to CO2-Enhanced Geothermal Systems. Transport in Porous Media 2010;82:173–96. doi:10.1007/s11242-009-9425-y.

[170] Pan L, Oldenburg CM, Wu Y-S, Pruess K. Wellbore flow model for carbon dioxide and brine. Energy Procedia 2009;1:71–8. doi:10.1016/j.egypro.2009.01.012.

Appendix: Copyright Reuse Permissions

This section contains the licenses and reprint permissions for the published chapters and external figures used in this dissertation.

IPCC Copyright for Figure 1-2
https://www.ipcc.ch/copyright/

ipcc REPORTS WORKING GROUPS ACTIVITIES NEWS CALENDAR

COPYRIGHT

Unless otherwise stated, the information available on this website, including text, logos, graphics, maps, images and electronic downloads is the property of the IPCC and is protected by intellectual property laws.

You may freely download and copy the material contained on this website for your personal, non-commercial use, without any right to resell or redistribute it or to compile or create derivative works there from, subject to more specific restrictions that may apply to specific materials.

Reproduction of limited number of figures or short excerpts of IPCC material is authorized free of charge and without formal written permission provided that the original source is properly acknowledged, with mention of the complete name of the report, the publisher and the numbering of the page(s) or the figure(s). Permission can only be granted to use the material exactly as it is in the report. Please be aware that figures cannot be altered in any way, including the full legend. For media use it is sufficient to cite the source while using the original graphic or figure. In line with established Internet usage, any external website may provide a hyperlink to the IPCC website or to any of its pages without requesting permission.

For any other use, permission is required. To obtain permission, please address your request to the Secretary of the IPCC in a signed letter with all relevant details using official letterhead and fax it to: +41 22 730 8025. All communications by mail should be addressed to:

IPCC Secretariat
World Meteorological Organization
7bis Avenue de la Paix, P.O. Box No. 2300
CH-1211 Geneva 2,
Switzerland

All e-mail communications should be addressed to Ms. Sophie Schlingemann, Legal Officer.

License for Figure 1-4 reused from Adams et al. 2015

ELSEVIER LICENSE
TERMS AND CONDITIONS

Dec 17, 2018

This Agreement between Mark Fleming ("You") and Elsevier ("Elsevier") consists of your license details and the terms and conditions provided by Elsevier and Copyright Clearance Center.

License Number	4490880604970
License date	Dec 16, 2018
Licensed Content Publisher	Elsevier
Licensed Content Publication	Applied Energy
Licensed Content Title	A comparison of electric power output of CO2 Plume Geothermal (CPG) and brine geothermal systems for varying reservoir conditions
Licensed Content Author	Benjamin M. Adams,Thomas H. Kuehn,Jeffrey M. Bielicki,Jimmy B. Randolph,Martin O. Saar
Licensed Content Date	Feb 15, 2015
Licensed Content Volume	140
Licensed Content Issue	n/a
Licensed Content Pages	13
Start Page	365
End Page	377
Type of Use	reuse in a thesis/dissertation
Portion	figures/tables/illustrations
Number of figures/tables /illustrations	1
Format	both print and electronic
Are you the author of this Elsevier article?	No
Will you be translating?	No
Original figure numbers	Figure 1
Title of your thesis/dissertation	The Performance of a Carbon-Dioxide Plume Geothermal Energy Storage System
Publisher of new work	University of Minnesota
Expected completion date	Jan 2019

License for Figure 1-5 reused from Buscheck et al. 2016

Order Details

Geosphere

Billing Status: **N/A**

Order detail ID:	71715846
ISSN:	1553-040X
Publication Type:	e-Journal
Volume:	
Issue:	
Start page:	
Publisher:	Geological Society of America
Author/Editor:	Geological Society of America

Permission Status: Granted

Permission type: Republish or display content

Type of use: Republish in a thesis/dissertation

Order 4487890620882

Requestor type	Academic institution
Format	Print, Electronic
Portion	chart/graph/table/figure
Number of charts/graphs/tables/figures	1
The requesting person/organization	Mark Fleming
Title or numeric reference of the portion(s)	Figure 2
Title of the article or chapter the portion is from	Multifluid geo-energy systems: Using geologic CO2 storage for geothermal energy production and grid-scale energy storage in sedimentary basins
Editor of portion(s)	N/A
Author of portion(s)	Thomas A. Buscheck, Jeffrey M. Bielicki, Thomas A. Edmunds, Yue Hao, Yunwei Sun, Jimmy B. Randolph, and Martin O. Saar
Volume of serial or monograph	12
Issue, if republishing an article from a serial	3
Page range of portion	678-696
Publication date of portion	May 5 2016
Rights for	Main product
Duration of use	Life of current edition
Creation of copies for the disabled	no
With minor editing privileges	no
For distribution to	Worldwide
In the following language(s)	Original language of publication
With incidental promotional use	no
Lifetime unit quantity of new product	Up to 14,999
Title	The Performance of a Carbon-Dioxide Plume Geothermal Energy Storage System
Institution name	University of Minnesota
Expected presentation date	Jan 2019

License for Figure 1-6 reused from Liu et al. 2016

ELSEVIER LICENSE
TERMS AND CONDITIONS

Dec 17, 2018

This Agreement between Mark Fleming ("You") and Elsevier ("Elsevier") consists of your license details and the terms and conditions provided by Elsevier and Copyright Clearance Center.

License Number	4487890939651
License date	Dec 14, 2018
Licensed Content Publisher	Elsevier
Licensed Content Publication	Energy Conversion and Management
Licensed Content Title	Thermodynamic analysis of a compressed carbon dioxide energy storage system using two saline aquifers at different depths as storage reservoirs
Licensed Content Author	Hui Liu,Qing He,Andrea Borgia,Lehua Pan,Curtis M. Oldenburg
Licensed Content Date	Nov 1, 2016
Licensed Content Volume	127
Licensed Content Issue	n/a
Licensed Content Pages	11
Start Page	149
End Page	159
Type of Use	reuse in a thesis/dissertation
Intended publisher of new work	other
Portion	figures/tables/illustrations
Number of figures/tables /illustrations	1
Format	both print and electronic
Are you the author of this Elsevier article?	No
Will you be translating?	No
Original figure numbers	Figure 2
Title of your thesis/dissertation	The Performance of a Carbon-Dioxide Plume Geothermal Energy Storage System
Publisher of new work	University of Minnesota
Expected completion date	Jan 2019

Reprint permission for Fleming et al. 2018

Mark Fleming <flemi311@umn.edu>

Permission to Reprint

Roland N Horne <horne@stanford.edu> Sun, Dec 16, 2018 at 5:32 PM
To: Mark Fleming <flemi311@umn.edu>

Yes, we grant you permission to reuse the paper as requested.

Roland N. Horne

Professor of Energy Resources Engineering

Stanford University

From: Mark Fleming [mailto:flemi311@umn.edu]
Sent: Sunday, December 16, 2018 2:59 PM
To: geothermal@se3mail.stanford.edu
Subject: Permission to Reprint

To whom it may concern,

I am writing to acquire the permission to reprint/reuse a published proceedings paper (where I am the primary author) for the use in my PhD thesis/dissertation.

The paper that I am requesting the reuse privileges is:

Title: High Efficiency and Large-Scale Subsurface Energy Storage with CO2

Authors: Mark R. Fleming, Benjamin M. Adams, Jimmy B. Randolph, Jonathan D Ogland-Hand, Thomas H Kuehn, Thomas A. Buscheck, Jeffrey M Bielicki, and Martin O. Saar. 2018.

Linked Source: https://pangea.stanford.edu/ERE/pdf/IGAstandard/SGW/2018/Fleming.pdf

Intended Reuse:

Reuse portion: Entire paper

Is an author of requested paper: Yes, I am the primary author (Mark Fleming)

Type of reuse: PhD Thesis/Dissertation

Thesis Title: The Performance of a Carbon-Dioxide Plume Geothermal Energy Storage System

Publisher: University of Minnesota

Expected Completion date: January 2019

Publication type: both print and electronic

Please let me know if you have any questions or require any additional information.

Thank you,

Mark Fleming